VOLUME 77 MAY 10, 1973 NUMBER 10

JPCHAx

THE JOURNAL OF PHYSICAL CHEMISTRY

PUBLISHED BIWEEKLY BY THE AMERICAN CHEMICAL SOCIETY

THE JOURNAL OF

PHYSICAL CHEMISTRY

AMERICAN CHEMICAL SOCIETY, *1155 Sixteenth St., N.W., Washington, D. C. 20036*

Books and Journals Division

JOHN K CRUM *Director*
RUTH REYNARD *Assistant to the Director*

CHARLES R. BERTSCH *Head, Editorial Processing Department*
D. H. MICHAEL BOWEN *Head, Journals Department*
BACIL GUILEY *Head, Graphics and Production Department*
SELDON W. TERRANT *Head, Research and Development Department*

 Published biweekly by the American Chemical Society at 20th and Northampton Sts., Easton, Pa. 18042. Second-class postage paid at Washington, D. C., and at additional mailing offices.

All manuscripts should be sent to *The Journal of Physical Chemistry*, Department of Chemistry, University of Minnesota, Minneapolis, Minn. 55455.

Additions and Corrections are published once yearly in the final issue. See Volume 76, Number 26 for the proper form.

Extensive or unusual alterations in an article after it has been set in type are made at the author's expense, and it is understood that by requesting such alterations the author agrees to defray the cost thereof.

The American Chemical Society and the Editor of *The Journal of Physical Chemistry* assume no responsibility for the statements and opinions advanced by contributors.

Correspondence regarding accepted copy, proofs, and reprints should be directed to Editorial Processing Department, American Chemical Society, 20th and Northampton Sts., Easton, Pa. 18042. Head: CHARLES R. BERTSCH. Assistant Editor: EDWARD A. BORGER. Editorial Assistant: JOSEPH E. YURVATI.

Advertising Office: Centcom, Ltd., 142 East Avenue, Norwalk, Conn. 06851.

Business and Subscription Information

Send all new and renewal subscriptions *with payment* to: Office of the Controller, 1155 16th Street, N.W., Washington, D. C. 20036. Subscriptions should be renewed promptly to avoid a break in your series. All correspondence and telephone calls regarding changes of address, claims for missing issues, subscription service, the status of records, and accounts should be directed to Manager, Membership and Subscription Services, American Chemical Society, P.O. Box 3337, Columbus, Ohio 43210. Telephone (614) 421-7230.

On changes of address, include both old and new addresses with ZIP code numbers, accompanied by mailing label from a recent issue. Allow four weeks for change to become effective.

Claims for missing numbers will not be allowed (1) if loss was due to failure of notice of change in address to be received before the date specified, (2) if received more than sixty days from date of issue plus time normally required for postal delivery of journal and claim, or (3) if the reason for the claim is "issue missing from files."

Subscription rates (1973): members of the American Chemical Society, $20.00 for 1 year; to nonmembers, $60.00 for 1 year. Those interested in becoming members should write to the Admissions Department, American Chemical Society, 1155 Sixteenth St., N.W., Washington, D. C. 20036. Postage to Canada and countries in the Pan-American Union, $5.00; all other countries, $6.00. Single copies for current year: $3.00. Rates for back issues from Volume 56 to date are available from the Special Issues Sales Department, 1155 Sixteenth St., N.W., Washington, D. C. 20036.

Subscriptions to this and the other ACS periodical publications are available on microfilm. Supplementary material not printed in this journal is now available in microfiche form on a current subscription basis. For information on microfilm or microfiche subscriptions, write Special Issues Sales Department at the address above.

Notice to Authors last printed in the issue of November 23, 1972

THE JOURNAL OF

PHYSICAL CHEMISTRY

Volume 77, Number 10 May 10, 1973

JPCHAx 77(10) 1193–1318 (1973)

COMMUNICATIONS TO THE EDITOR

AUTHOR INDEX

In papers with more than one author the name of the author to whom inquiries about the paper should be addressed is marked with an asterisk in the by-line.

THE JOURNAL OF
PHYSICAL CHEMISTRY

VOLUME 77, NUMBER 10 MAY 10, 1973

Relative Rates of Fluorination of Fluorinated Ethylenes

Ruby Foon* and G. P. Reid

School of Chemistry, The University of New South Wales, Kensington, N.S.W., 2033, Australia *(Received December 18, 1972)*

The relative rate constants for the gas-phase reaction of fluorine with fluoroethylene, 1,1-difluoroethylene, and tetrafluoroethylene have been measured from 203 to 353°K by a static competitive technique for the reaction F + >C=C< → >C(F)-C< and are given by $k(CH_2{=}CF_2)/k(CH_2{=}CHF) = 0.77 \pm 0.15 \exp(35 \pm 80)/RT]$ and $k(CF_2{=}CF_2)/k(CH_2{=}CF_2) = 0.51 \pm 0.07 \exp[(100 \pm 90)/RT]$. At 291°K, the rate constants are in the ratio $k(CH_2{=}CHF):k(CH_2{=}CF_2):k(CF_2{=}CF_2) = 1.00:0.85:0.76$. The order of reactivity is discussed in terms of the variation in A factor and the ease of forming activated complexes for the substituted fluoroethylenes.

Introduction

Competitive photochlorination studies[1] of the rate of addition of atomic chlorine to various chloroethylenes have shown the differences in reactivity to be small and comparable to the experimental error. On the other hand, the activation energies for the addition of atomic oxygen to chlorofluoroethylenes,[2] having no hydrogen substituents, are reported to correlate with the olefin ionization potentials while for the addition to fluoroethylenes,[3] a minimum activation energy is obtained at $CH_2{=}CF_2$ as the hydrogens in ethylene are successively replaced. This behavior has also been reported for the partly fluorinated butenes and propenes.[4] Such an effect is explicable in terms of the inductive and mesomeric effects described for fluorine attached to carbon atoms forming a double bond.[5] The rate of molecular fluorine addition to the fluoroethylenes, $CH_2{=}CHF$, $CH_2{=}CF_2$, and $CF_2{=}CF_2$, has been investigated in the present work by the competitive technique[6] used for the determination of small differences in Arrhenius parameters, in order to study the effect of fluorine substitution on olefin reactivity. The absolute kinetics of the addition of fluorine to fully halogenated 2-butenes have been studied by Rodgers[7] who has elucidated the main features of the mechanism. The only other study of the addition of fluorine to olefins[8] reports a decrease in reactivity as the hydrogens in ethylene are successively replaced by chlorine. The present work indicates a similar decrease with increase in fluorine substitution in fluoroethylenes.

Experimental Section and Results

Fluoroethylene and 1,1-difluoroethylene (Matheson Gas Co.) were purified by bulb-to-bulb distillation and found to be chromatographically pure. Tetrafluoroethylene was prepared from Teflon turnings by the method of Lewis and Naylor.[9] Gas chromatographic analysis revealed a trace of impurity which was not susceptible to fluorination.

The packed reaction vessel, preparation and handling of fluorine, gas chromatography system, and static competitive technique were all as described earlier[10] except that the consumption method had to be used to determine the relative rate constants since the initial fluorine addition

(1) (a) P. B. Ayscough, A. J. Cocker, F. G. Dainton, and S. Hirst, *Trans. Faraday Soc.*, **58**, 318 (1962); (b) P. B. Ayscough, F. S. Dainton, and B. E. Fleischfresser, *Trans. Faraday Soc.*, **62**, 1838 (1966).
(2) W. J. R. Tyerman, *Trans. Faraday Soc.*, **65**, 163 (1969).
(3) S. J. Moss, *Trans. Faraoay Soc.*, **67**, 3503 (1971).
(4) S. J. Moss and K. R. Jennings, *Trans. Faraday Soc.*, **64**, 686 (1968); **65**, 415 (1969).
(5) D. T. Clark, J. N. Murrell, and J. M. Tedder, *J. Chem. Soc.*, 1250 (1963).
(6) (a) G. C. Fettis and J. H. Knox, *Progr. React. Kinet.*, **2**, 1 (1964); (b) R. Foon and K. B. Tait, *J. Chem. Soc., Faraday Trans.*, **1**, 68, 1121 (1972).
(7) (a) A. S. Rodgers, *J. Phys. Chem.*, **67**, 2799 (1963); (b) *ibid.*, 69, 254 (1965).
(8) G. A. Kapralova, L. Yu Rusin, A. M. Chaikin, and A. E. Shilov, *Dokl. Akad. Nauk. SSSR*, **150**, 1282 (1963).
(9) E. E. Lewis and M. A. Naylor, *J. Amer. Chem. Soc.*, **69**, 1968 (1947).
(10) R. Foon and N. A. McAskill, *Trans. Faraday Soc.*, **65**, 3005 (1969).

product underwent secondary fluorine substitution as described below. Pressures of fluorine were varied from 5 to 10 Torr and total pressures in the reaction vessel were of the order of 600 Torr.

For the $CH_2{=}CF_2 + CF_2{=}CF_2$ competitions, carried out between 283 and 373°K, 35 mixtures in which the molar ratio, $CF_2{=}CF_2{:}CH_2{=}CF_2$, was varied from 0.66 to 1.20 were treated with gaseous fluorine diluted 40 to 100 times with nitrogen such that the molar ratio of total olefin to fluorine varied between 20 and 50. A gas chromatography column of 12 ft of 20% dinonyl phthalate followed by 12 ft of 20% diethyl phthalate both on Celite at 273°K was used. A least-squares analysis of the results gave $k(CF_2{=}CF_2)/k(CH_2{=}CF_2) = 0.51 \pm 0.07 \exp[(110 \pm 90)/RT]$ where the errors are standard errors and R = 1.987 cal mol^{-1}. At 291°K, $k(CF_2{=}CF_2)/k(CH_2{=}CF_2) = 0.91 \pm 0.02$, the mean and standard error of 23 values.

For the $CH_2{=}CF_2 + CH_2{=}CHF$ competitions, 64 fluorinations were carried out from 245 to 373°K in which the molar ratio, $CH_2{=}CF_2{:}CH_2{=}CHF$, was varied from 1.48 to 0.96 and that of the total olefins to fluorine from 20 to 50. Gas chromatographic analysis was made with the same columns as before except that they were cooled to 258°K. A least-squares analysis gave $k(CH_2{=}CF_2)/k(CH_2{=}CHF) = 0.77 \pm 0.15 \exp[(35 \pm 80)/RT]$ where the errors and R are as stated before. At 291°K, $k(CH_2{=}CF_2)/k(CH_2{=}CHF) = 0.85 \pm 0.05$, the mean and standard error of 12 values. The rate constants therefore can be arranged in the following order at 291°K: $k(CH_2{=}CHF)$: $k(CH_2{=}CF_2){:}k(CF_2{=}CF_2)$ = 1.00:0.85:0.76.

As a check on the extent of fluorine substitution occurring, the products from the $F_2 + CH_2{=}CF_2$ reaction were investigated using fluorination conditions similar to those used for kinetic measurements. Analysis of the total products by mass spectrometry indicated the presence of $C_2H_2F_4$, C_2HF_5, and C_2F_6, while gas chromatography showed C_2HF_5 to be the major product, the other products being $C_2H_2F_4$ together with C_2F_6 in the lesser amount, the ratio being $C_2H_2F_4{:}C_2HF_5{:}C_2F_6$ = 1:4:0.8. This is consistent with the addition of fluorine occurring first according to the reaction

$$CH_2{=}CF_2 + F_2 \longrightarrow CH_2FCF_3 \qquad (1)$$

followed by the secondary hydrogen abstraction reactions

$$CH_2FCF_3 + F_2 \longrightarrow CHF_2CF_3 + HF \qquad (2)$$

$$CHF_2CF_3 + F_2 \longrightarrow C_2F_6 + HF \qquad (3)$$

Hydrogen abstraction from CH_2FCF_3 should be much faster than from C_2HF_5 since it has been observed that CH_2F_2 readily fluorinates whereas CHF_3 does not react at all under similar conditions.[11] This order of reactivity could explain why C_2HF_5 is the major product.

Discussion

The mechanism for fluorine addition reaction 1 is probably the same as that first proposed by Miller and Dittman[12] and confirmed by Rodgers[7] for the addition to perhalo-2-butenes

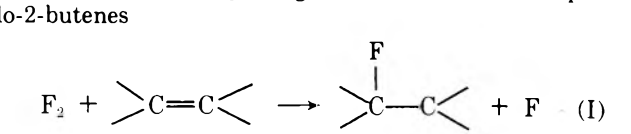

(I)

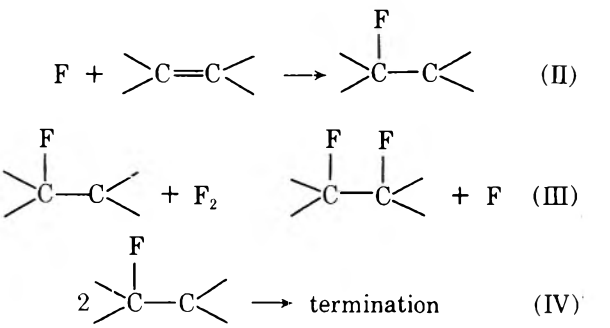

(II)

(III)

(IV)

Under steady-state conditions for this mechanism, the relative rate constants reported here refer to reaction II of the above mechanism, F + >C=C< → >C(F)C<. The fluoroalkyl radical formed in reaction I probably has the fluorine attached to the less fluorinated carbon atom, since this is the radical preferentially formed in the addition of near thermal ^{18}F atoms to partly fluorinated ethylenes.[13] Stabilization of the excited radical formed in **II** has been achieved by the nitrogen diluent present since no decomposition product was detected. Similar radical-chain mechanisms have been proposed for the fluorination[8] and bromination[14] of ethylene.

From the values of each rate constant ratio measured directly at 291°K, the following order is obtained: $CH_2{=}CHF > CH_2{=}CF_2 > CF_2{=}CF_2$. This order correlates with the A factors for these compounds, *viz.*, $A(CH_2{=}CHF){:}A(CH_2{=}CF_2){:}A(CF_2{=}CF_2)$ = 1.00:0.77:0.39. Since the differences in activation energy are small and indistinguishable from experimental error, the difference in reactivity has been attributed to this A factor variation. It can be explained in terms of a steric influence which results in the less crowded activated complexes being more readily formed. This favors the less substituted ethylenes. The A factor variation has been interpreted in this way for the reaction of difluoroamino radicals with various olefins.[15] This ionization potential determined by Lifshitz and Long[16] for $CF_2{=}CF_2$ is less than that for $CH_2{=}CHF$[16] so that it cannot be a decisive factor in determining the relative reactivity since $CF_2{=}CF_2$ is less reactive than $CH_2{=}CHF$. The comparative study of the reaction of fluorine with chloroethylenes[8] showed an order of reactivity $C_2H_4 > C_2H_3Cl > C_2H_2Cl_2 > C_2HCl_3 > C_2Cl_4$ for the surface reaction between the solidified olefin and adsorbed fluorine at 87°K. This result, which was obtained by measuring directly the pressure change during the reaction, provides independent confirmation of the substituent effect noted in the present work.

Acknowledgments. The authors wish to thank I.C.I.A.N.Z. Ltd. for the loan of a fluorine generator. G. P. R. acknowledges the award of a Commonwealth University Scholarship.

(11) R. Foon and N. A. McAskill, unpublished work.
(12) W. T. Miller and A. L. Dittman, *J. Amer. Chem. Soc.*, **78**, 2793 (1956); W. T. Miller, S. D. Koch, and F. W. McLafferty, *ibid.*, **78**, 4992 (1956); W. T. Miller and S. D. Koch, *ibid.*, **79**, 3084 (1957).
(13) T. Smail, R. Subramonia Iyer, and F. S. Rowland, *J. Amer. Chem. Soc.*, **94**, 1041 (1972).
(14) T. Berces and Z. G. Szabo, *Z. Phys. Chem.*, **56**, 39 (1967).
(15) A. J. Dijkstra, J. A. Kerr, and A. F. Trotman-Dickenson, *J. Chem. Soc. A*, 105 (1967).
(16) C. Lifshitz and F. A. Long, *J. Phys Chem.*, **67**, 2463 (1963).

Photolysis of Hydrazoic Acid in Aqueous Solution

D. Shapira and A. Treinin*

Department of Physical Chemistry, Hebrew University, Jerusalem, Israel *(Received November 14, 1972)*

The photolysis of HN_3 in aqueous solution was studied at 2139 and 2537 Å. Up to 0.1 *M* HN_3 the photolysis obeys the simple stoichiometry $HN_3 + H_2O \rightarrow N_2 + NH_2OH$ ($h\nu$) with a quantum yield $\phi = 1.00 \pm 0.05$. A stepwise nitrene mechanism is proposed and supported by studying the effects of Cl^- and allyl alcohol on the photolysis. The effects of these scavengers on the photolysis of N_3^- were also investigated and the results lead to the conclusion that the generation of NH_2OH from HN_3 and N_3^- involve two different precursors. Their nature is discussed. The use of the azide system as a convenient actinometer is described.

The photochemistry of HN_3 in the gas phase has been extensively studied.[1] It is now well established that reaction 1 is the major primary process in the photolysis. It is energetically more favorable than other possible reactions, even with the extra energy required to produce NH in its excited singlet state. There is some evidence that reaction 2 is also induced by vacuum uv,[2] but that at longer wavelengths reaction 1 triggers all subsequent reactions, whereby N_3 and NH_2 are also produced.[3]

$$HN_3 \xrightarrow{h\nu} NH + N_2 \quad (1)$$

$$HN_3 \longrightarrow H + N_3 \quad (2)$$

There are few reports on the photolysis of HN_3 in aqueous solution. In an early work Gleu[4] found that the main features of the photolysis at 254 nm can be explained by a mechanism consisting of reactions 1 and 3. In addition to N_2 and NH_2OH a low yield of NH_3 but no hydrazine was reported. Quantum yields were not determined. This was done more recently by Koch,[5] who claimed that the quantum yield $\phi(N_2)$ was concentration dependent, approaching a maximum value ~2 at high azide concentration and falling considerably below 1 at $[HN_3] \leq 0.1$ *M*. Ammonium azide was found to be one of the main products. These results were considered to imply that reaction 1 is insignificant in solutions and that the primary process is a reaction between excited and ground state HN_3 molecules. Similar features were observed with methyl azide and the contrast between these results and those displayed by the gas photolysis was suggested to be due to some stabilization of the excited azide molecule by hydroxylic solvents.[6]

$$NH + H_2O \longrightarrow NH_2OH \quad (3)$$

Here we present some new results on the photolysis of aqueous HN_3 at 2139 and 2537 Å. These wavelengths lie within the two first absorption bands of HN_3 (λ_{max} ~260 nm, ϵ_{max} ~47 M^{-1} cm^{-1}; λ_{max} ~197 nm, ϵ_{max} ~600 M^{-1} cm^{-1})[7] (see also Figure 1). Our findings appear to support the mechanism of Gleu[4] and to provide some information on the reactivity of NH in aqueous solution. The possibility that the same intermediate plays a role in the photolysis of N_3^- [8] was also investigated.

Experimental Section

Materials and Solutions. NaN_3 (CP) was twice recrystallized from water–ethanol solutions. Further recrystallizations proved to have no effect on the yields of the photolysis. Allyl alcohol (CP Merck) was subjected to several vacuum distillations. Water was triply distilled and all other materials were of AnalaR grade.

Procedure. Fresh solutions of HN_3 were prepared just before irradiation by adding $HClO_4$ to solutions of NaN_3. Under these conditions the analytical tests did not reveal any thermal decomposition in blank solutions. When the yield of N_2 was not measured, air-containing solutions were irradiated in stoppered vessels, since air was found to have no effect on the photolysis. For gas analysis, the NaN_3 and $HClO_4$ solutions were separately degassed before mixing in the irradiation system which was equipped with two bulbs. During irradiation the temperature was kept at 23 ± 1°.

The evacuation and determination of N_2, azide, NH_2OH, and NH_3 were conducted as described elsewhere.[9] The gaseous products were also subjected to mass spectrometric and gas chromatographic analysis using appropriate blanks. HN_3 and allyl alcohol, which interfere with the determination of NH_2OH, were evaporated under vacuum before analysis. $HClO_4$ was found to somewhat affect the phenol–hypochlorite method for determining NH_3 by enhancing the interference of NH_2OH. Therefore, care was taken to check against blank solutions with the same concentrations of NH_2OH and $HClO_4$.

Light Sources and Actinometry. Zn Lamp. For irradiation at 2139 Å a 25-W Philips zinc spectral lamp no. 93106 was used with 0.5-cm layer of water as a filter.

When solutions of 10^{-3} *M* were irradiated only the strong 2139-Å line and the weak 2062- and 2025-Å lines were absorbed. Actinometry was conducted with a solution of 2.2×10^{-4} *M* NaN_3 at pH 7.7 (with a borate buffer), the azide depletion being determined from the drop in its absorption at 235 nm taking $\phi(-N_3^-) = 0.32$.[10] The

(1) (a) R. A. Abramovitch and B. A. Davis, *Chem. Rev.*, **64**, 149 (1969); (b) A. Reiser and H. M. Wagner in "The Chemistry of the Azido Group," S. Patai, Ed., Interscience, London, 1971, p 441.
(2) (a) D. A. Milligan and M. E. Jacox, *J. Chem. Phys.*, **41**, 2838 (1964); (b) K. H. Welge, *ibid.*, **45**, 4373 (1965).
(3) B. A. Thrush, *Proc. Roy. Soc., Ser. A.*, **235**, 143 (1956).
(4) K. Gleu, *Berichte*, **61**, 702 (1928).
(5) E. Koch, *Tetrahedron*, **23**, 1747 (1967).
(6) R. A. Abramovitch and E. P. Kyba, ref 1b, p 221.
(7) J. R. McDonald, J. W. Rabelais, and S. P. McGlynn, *J. Chem. Phys.*, **52**, 1332 (1970).
(8) H. Okabe, *J. Chem. Phys.*, **49**, 2726 (1968).
(9) (a) I. Burak and A. Treinin, *J. Amer. Chem. Soc.*, **87**, 4031 (1965); (b) I. Burak, D. Shapira, and A. Treinin, *J. Phys. Chem.*, **74**, 568 (1970).
(10) D. Behar, D. Shapira, and A. Treinin, *J. Phys. Chem.*, **76**, 180 (1972).

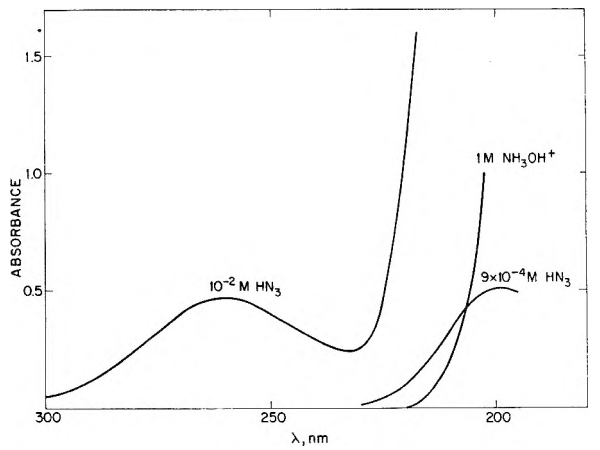

Figure 1. Electronic spectra of HN_3 and NH_3OH^+ in water. (The latter was obtained by measuring the spectrum of 0.5 *M* $(NH_2OH)_2 \cdot H_2SO_4$ against 0.5 *M* Na_2SO_4.)

light absorption by HN_3 and the actinometer at 2139 Å was the same but not total (at 2062 and 2025 Å total absorption prevailed). The time of irradiation of the actinometer was adjusted so that is final absorption at 2139 Å matched that of the HN_3 solution after its irradiation. Thus no correction for partial absorption was required.

At 10^{-2}–10^{-1} *M* HN_3 the 2139-Å line was totally absorbed. To reduce the effect of longer wavelengths a 0.5-cm layer of 1 *M* aqueous solution of acetone was used as a filter.[11] It transmits *ca.* 50% of the light at 2139 Å but it is somewhat affected by irradiation. Therefore care was taken to change the filter before each run and to irradiate the actinometer (in this case 10^{-3} *M* NaN_3 solution) for the same time. This filter cuts off light in the region 235–294 nm. The effect of longer wavelengths was determined by using a solution of 1 *M* acetone–8 *M* acetic acid as a filter which cuts off all light below 294 nm. The correction for this effect was negligible at 10^{-2} *M* HN_3 but reached 14% at 0.1 *M* HN_3.

To avoid light absorption by allyl alcohol in studying its effect as a scavenger, its solutions with 0.1 *M* HN_3 were irradiated through 0.5-cm layer of acetic acid as a filter. Under these conditions the photolysis was induced by wavelengths within the 260-nm band of HN_3, mainly the relatively strong Zn lines close to 280 nm.

Hg Lamp. Most of the experiments on the effect of Cl^- (which absorbs at 2139 Å) on the photolysis of HN_3 and N_3^- were carried out at 2537 Å. A low-pressure Hg lamp (Thermal Syndicate) was used for this purpose, with a 1-cm layer of 0.2 *M* KCl to cut off the 1849-Å line. A solution of 2×10^{-2} *M* NaN_3 served as a chemical actinometer; $\phi(-N_3^-) = 0.31$ was measured against uranyl oxalate.

Results and Discussion

HN_3 in Absence of Foreign Scavengers. Under all conditions employed the photolysis obeyed the simple stoichiometry

$$HN_3 + H_2O \xrightarrow{h\nu} N_2 + NH_2OH \qquad (4)$$

with quantum yields $\phi(N_2) = \phi(NH_2OH) = \phi(-N_3^-) = 1.00 \pm 0.05$. This is shown in Tables I and II. The following products could not be detected: NH_3, N_2H_4, H_2, and nitrogen oxides. Under total light absorption the yield varied linearly with time of irradiation. Light intensity was found to have no effect on the quantum yields in the range 8.4×10^{-8}–4.0×10^{-7} einstein $l.^{-1}$ sec^{-1}.

TABLE I: Yields of Products and Depletion of HN_3 at 214 nm[a]

Composition	pH	Yields, 10^{-5} *M* N_2	NH_2OH	$-\Delta(HN_3)$
10^{-3} *M* NaN_3	2.35	24.0	24.2	24.9
7×10^{-3} *M* $HClO_4$		24.0	23.6	24.1
		24.5	24.7	26.7
10^{-2} *M* NaN_3	1.4	33.4	33.5	
10^{-1} *M* $HClO_4$		61.5	63.9	

[a] Results of several runs are recorded.

These results are at variance with those of Koch[5] and rule out his mechanism for $[HN_3] \leq 0.1$ *M*. They also show that reaction 2 does not play a significant role, which is in keeping with a previous report that N_3 could not be detected on flash photolysis of HN_3.[12] They are consistent with Gleu's nitrene mechanism[4] but they do not rule out a concerted mechanism which involves direct interaction between excited HN_3 and water

$$HN_3^* + H_2O \longrightarrow NH_2OH + N_2 \qquad (5)$$

The uv spectrum of HN_3 displays a rich vibrational structure[7,8] and therefore in the gas phase reaction 1 probably proceeds by predissociation. Thus in solution HN_3* may live long enough to react with the solvent before dissociating.

The observed quantum yield $\phi = 1$ for reaction 4 is in keeping with both mechanisms, if HN_3* does not undergo deactivation before reacting with water (concerted mechanism) or before dissociating (stepwise mechanism). In the latter case NH and N_2 cannot undergo cage recombination and contrary to the gas photolysis, the fast reaction of NH with water prevents its reaction with HN_3, at least up to 0.1 *M*. This reaction should lead to the production of NH_4N_3[13] (*i.e.*, NH_4^+ in solution), which could not be detected.

Flash photolysis of HN_3 revealed no transient absorption which lives longer than 10 μsec,[12] but this does not rule out the nitrene mechanism since the lifetime of NH in water is presumably much shorter. Thus at this stage the two possible mechanisms are indistinguishable (see later).

Our results establish aqueous HN_3 as a useful chemical actinometer for the range ~200–260 nm. Its advantages are the following. (a) The quantum yield equals 1, independent of wavelength or concentration (up to 0.1 *M*). (b) By proper adjustment of concentration its response can be confined to the 2139-Å line of the Zn lamp with little interference from longer wavelengths. Therefore it is more convenient and accurate than the uranyl actinometers, which involve a differential method when applied to this wavelength region.[14] (c) The actinometer is easily prepared by acidifying aqueous NaN_3 before irradiation, and either the yield of NH_2OH is measured or (with dilute solutions) the depletion of HN_3. The latter can be readily determined by measuring the change in optical absorption, since the absorption of NH_3OH^+ at $\lambda > 200$ nm is relatively low[10] (Figure 1).

(11) For a similar filter see B. Muel and C. Malpiece, *Photochem. Photobiol.*, **10**, 283 (1969).
(12) A. Treinin and E. Hayon, *J. Chem. Phys.*, **50**, 538 (1969).
(13) A. O. Beckman and R. G. Dickinson, *J. Amer. Chem. Soc.*, **50**, 1870 (1928); **52**, 124 (1930).
(14) J. Jortner, M. Ottolenghi, and G. Stein, *J. Amer. Chem. Soc.*, **85**, 2712 (1963).

TABLE II: Quantum Yields of NH_2OH from the Photolysis of HN_3[a]

$[NaN_3]$, *M*	10^{-3}	10^{-2}	10^{-2}	10^{-2}	10^{-1}	2×10^{-2}
$[HClO_4]$, *M*	7×10^{-3}	4×10^{-1}	10^{-1}	2×10^{-2}	2×10^{-1}	10^{-1}
pH	2.35	0.80	1.40	2.15	1.20	1.5
λ, nm	214	214	214	214	214	254
$\phi(NH_2OH)$	1.02, 1.02	0.97, 0.97	0.98, 0.96	0.93	0.95, 1.02	1.00
	1.00	1.01	0.99	1.02	1.01, 1.01	

[a] See footnote to Table I.

A related actinometer which is even more conveniently employed is aqueous N_3^-. It also has the advantage that it can be used for the 229-nm line of the Cd lamp or the 254-nm line of the Hg lamp (see Experimental Section). However, its quantum yield is lower, somewhat depending on concentration, and the equality $\phi(-N_3^-) = \phi(NH_2OH)$ being valid only at $[N_3^-] \lesssim 10^{-3}$ *M*, $\lambda \gtrsim 220$ nm.[9]

HN_3 in Presence of Foreign Scavengers. The chemical reactivity of the precursor of hydroxylamine was examined by a simple competition technique. The choice of scavengers was limited by the requirements of low light absorption and of thermal stability. Cl^- and allyl alcohol were chosen to represent nucleophilic and unsaturated reagents, respectively.

High concentrations of NaCl and allyl alcohol were required in order to observe appreciable effects on the photolysis. $\phi(N_2)$ was not affected but the yield of NH_2OH was reduced. This indicates that the effect is not due to physical quenching of the excited state but to chemical reaction with the precursor of NH_2OH. A simple scheme that accounts for the results is

$$HN_3 \xrightarrow{h\nu} X \quad (6)$$

$$X + H_2O \longrightarrow NH_2OH \quad (7)$$

$$X + S \longrightarrow \quad (8)$$

where X and S are the precursor and scavenger, respectively. (Only the species pertaining to the discussion are represented.) This scheme leads to

$$\frac{\phi - \varphi}{\varphi} = \frac{k_8[S]}{k_7[H_2O]} \quad (9)$$

where ϕ and φ are the quantum yields of hydroxylamine in absence and presence of foreign scavenger, respectively. The validity of eq 9 is shown in Figure 2. (The concentrations of H_2O were determined from the densities of the solutions.)

The two scavengers hardly differ in their effect (Figure 2). The relative rate constant for Cl^- was calculated from such plots at several pH values in range 0.5–2.5 and was found to be nearly constant, $k_8/k_7 = 8 \pm 1$. Thus it appears that only a fraction of the collisions of X with H_2O are chemically effective. If X is an excited molecule, the chemically ineffective collisions are likely to bring about its deactivation and so ϕ is expected to be less than 1. Therefore our finding that $\phi = 1$ suggests that X is not an excited HN_3 molecule but the radical NH.

The effect of Cl^- on the photolysis of HN_3 was first discovered by Gleu[4] and was ascribed to the reaction $NH + H^+ + Cl^- \rightarrow NH_2Cl$. In strong HCl solutions NH_2Cl was claimed to produce Cl_2, which oxidizes NH_2OH to N_2O. In our experiments N_2O could not be detected, and moreover the effect of Cl^- on the yield of NH_2OH from HN_3 was found to be independent of pH (see also next section).

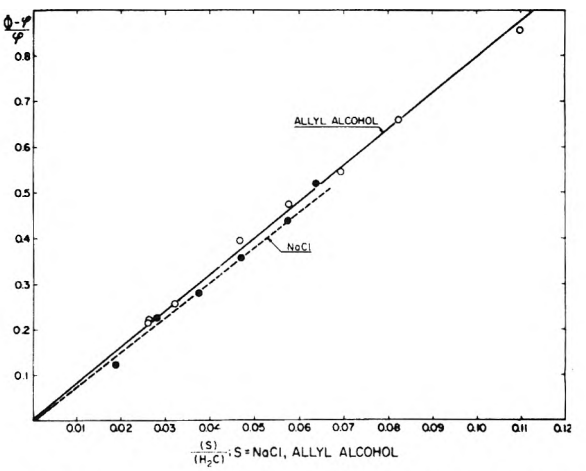

Figure 2. Effects of Cl^- and allyl alcohol on the yield of NH_2OH from the photolysis of 0.1 *M* HN_3: Cl^- pH 0.5, λ 2537 Å; allyl alcohol pH 1.2, λ ~280 nm (see Experimental Section).

N_3^- in Presence of Foreign Scavengers. The photolysis of N_3^- in water[9] bears close resemblance to that of HN_3. Therefore it was of special interest to check if in both cases the generation of NH_2OH involves the same precursor. For this purpose the study of the effect of scavengers was extended to higher pH values.

The following reactions should be considered for the precursor X′ in N_3^- solution.

$$X' + H_2O \longrightarrow NH_2OH \quad (10)$$

$$X' + S \longrightarrow \quad (11)$$

$$X' + N_3^- \longrightarrow \quad (12)$$

This scheme leads to

$$\frac{\phi' - \varphi'}{\varphi'}\left(1 + \frac{k_{12}[N_3^-]}{k_{10}[H_2O]}\right) = \frac{k_{11}[S]}{k_{10}[H_2O]} \quad (13)$$

where ϕ' and φ' are the yields of NH_2OH in absence and presence of scavenger, respectively. With $k_{12}/k_{10} = 285$ [9a] and $[N_3^-] = 2 \times 10^{-2}$ *M*, the following should be applicable

$$1.1\frac{\phi' - \varphi'}{\varphi'} = \frac{k_{11}[S]}{k_{10}[H_2O]} \quad (14)$$

The validity of eq 14 for Cl^- at pH 7.8 is shown in Figure 3, from which we derive $k_{11}/k_{10} = 680 \pm 20$. The same ratio was obtained at pH 6.9.

The effect of allyl alcohol was found to be much smaller but it displayed deviations from eq 14, as if k_{11}/k_{10} depends on [S], increasing from 40 to 90 on increasing the concentration of allyl alcohol from 0.5 to 1.8 *M*. Allyl alcohol clearly reacts with X′ much slower than Cl^-. A possible explanation for the change of its reactivity with concentration is that in this concentration range it can also react with the precursor of X′.

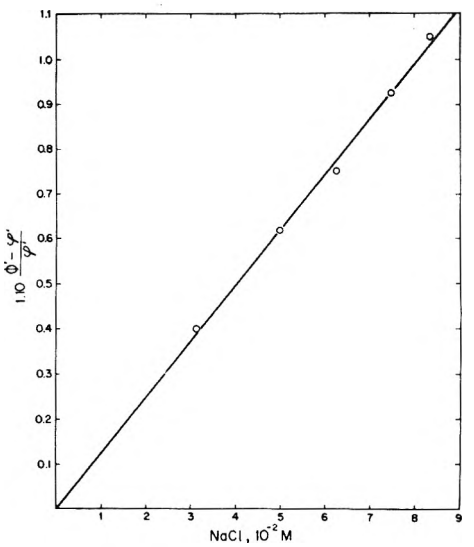

Figure 3. Effect of Cl^- on the yield of NH_2OH from the photolysis of 2×10^{-2} *M* N_3^- at 2537 Å, pH 7.8.

Here we summarize the available data on k_{11}/k_{10} for various scavengers: Cl^-, 680; N_3^-, 285;[9a] allyl alcohol, $\lesssim$40; NH_3, 18;[9a] H_2O, 1. Comparing this sequence with our results concerning the intermediate X, it becomes evident that we are dealing with two different species. X′ is much more selective; its insertion reactions[9a] with NH_3 and H_2O to form N_2H_4 and NH_2OH are relatively slow. Since k_{11} (Cl^-) cannot be appreciably higher than 10^{10} M^{-1} sec^{-1}, an upper limit of $\sim 10^7$ M^{-1} sec^{-1} can be estimated for k_{10} (H_2O).

The difference between X′ and X has not yet been resolved. Two possibilities to be considered are the following.

(a) X′ and X are the basic and acidic forms of the same intermediate, *e.g.*, N^- and NH or NH and NH_2^+, etc. To examine this possibility we studied more closely the effect of pH on the scavenging by Cl^-. From our previous analysis it appears that the reactivities of X′ and X do not vary with pH in the regions 7.8–6.9 and 2.5–0.5. In the intermediate pH region the system consists of a mixture of N_3^- and HN_3 (pK = 4.7). Still the yield of NH_2OH in presence of Cl^- could be calculated (within ±10% from the experimental values) by assuming that its precursor is a mixture of X and X′, which are produced from HN_3 and N_3^-, respectively, and react independently according to reactions 7, 8, 10, 11, and 12. Thus it appears that pH affects the photolysis only through the equilibrium $HN_3 \rightleftarrows H^+ + N_3^-$, which determines the amounts of X and X′ produced. However, these results do not rule out the possibility that X and X′ is an acid–base couple, but that this had no manifestation in our experiments since their reactions with water were much faster than the rate of acid–base equilibration.

(b) X and X′ are two different electronic states of NH. The photodissociation of HN_3 has been shown to yield the radical in its excited singlet state ($^1\Pi$ or $^1\Delta$).[2b,8] Its deactivation to the ground state $^3\Sigma^-$ is orbitally and spin forbidden and therefore may proceed more slowly than its reactions with water or the scavenger. Being relatively rich in energy it is likely to display little chemical selectivity; in particular, singlet NH (like singlet CH_2 and O, which are isoelectronic) is known to undergo fast insertion reactions,[1] reacting with NH_3 at each collision.[15] Thus the identification of X with singlet NH seems reasonable. On the other hand, there is little evidence for insertion of NH($^3\Sigma$) into the C–H bond,[1b] and when thermalized, its reaction with NH_3 is slow.[15] The possibility that X′ is NH($^3\Sigma^-$) should be further examined. (The flash photolysis of N_3^- has revealed some transient absorptions which have not yet been identified.[12] The excited N_3^- ions may undergo intersystem crossing to form their triplets, which then react with water, or the mechanism may involve the N^- radicals.

(15) M. Clerc, M. Schmidt, J. Hagege-Temman, and J. Belloni, *J. Phys. Chem.*, **75**, 2908 (1971).

Flash Photolysis. II. Photoreduction of Orotic Acid in Aqueous Medium

M. A. Herbert and H. E. Johns*

The Ontario Cancer Institute, Toronto 5, Canada *(Received May 15, 1972)*

Publication costs assisted by The Ontario Cancer Institute

The long-lived transient observed in the flash photolysis of orotic acid has been identified as the hydrogen adduct radical. This radical arises from a biphotonic process in which the first photon is required to produce an orotic acid triplet, while the second photon is absorbed by this triplet. This highly excited molecule then abstracts a hydrogen atom from a water molecule adding the hydrogen atom to the carbonyl oxygen. This adduct may then dissociate ($pK \sim 4$) leaving the same radical as the electron adduct. The absorption spectrum is the same as the electron adduct spectrum with a peak absorption at 325 nm. The variation of yield with pH has been measured and is higher at neutral pH than at acid pH. The second-order decay rate of the radical has been measured. Possible decay mechanisms have been suggested.

The uv photochemistry of orotic acid (uracil-6-carboxylic acid) has been extensively studied in aqueous solution using steady-state[1-9] and flash photolysis[10-13] techniques. It has been shown that the dimerization of orotic acid (OA) occurs when an OA molecule in the triplet state interacts with a ground-state molecule. The reaction rates for the dimerization and radiationless deactivation of the triplet state molecule, its energy level, triplet absorption spectrum, the quantum yield for intersystem crossing, and the rate constants for various quenching reactions have been measured.

In our flash photolysis studies we have observed a long-lived transient absorption in OA under high-intensity flashes.[12] A similar species has also been seen by Godfrey and Boag.[10] In this paper we will show that the transient species is produced when a triplet orotic acid molecule absorbs a second photon, exciting it to a higher lying energy state. This highly excited molecule can react with a water molecule, abstracting a hydrogen atom, leaving an ·OH radical. The ·OH radical may then attack a ground-state orotic acid molecule, adding to it to form the ·OH adduct. The absorption signal detected is from both these species. In this paper we present our observations on the properties of the long-lived transient, and the formation and decay of the radicals.

Experimental Section

The flash photolysis system used has an output of approximately 6×10^{17} photons (1 μeinstein) in the wavelength range 200–350 nm. The width of the exciting flash is 1.2 μsec at half peak height and is 99.9% complete in less than 4 μsec. We are able to detect absorption signals as small as 3×10^{-4} using a 45-cm path length (three passes of a 15-cm cell) and a pulsed xenon analyzing lamp. The system is described in greater detail elsewhere.[14,15]

The orotic acid was from Cyclo Chemical (Grade I) or Mann Research Labs, while the [6-^{14}C]orotic acid was from Amersham Searle Co. Identical experimental results were obtained using the OA in either the stock or recrystallized form. Solutions were mixed freshly for each experiment using water distilled four times in our quartz still. The solutions were deoxygenated by bubbling "prepurified grade" nitrogen (Gas Dynamics, Canadian Anaesthetic Gases) through them for at least 40 min prior to the experiment, and then were forced into the cell under a nitrogen atmosphere and sealed off under a positive nitrogen pressure. Unbuffered solutions had pH values from 4.3 to 5.0 for the concentrations of orotic acid used. Adjustments of the pH were made using $HClO_4$ or KOH (Analar Grade, BDH).

Thin layer chromatography (TLC) was carried out on thin layer cellulose plates (Machery Nagel and Co.) in a solvent system of 1-propanol–water (70:30 v/v). The chromatograms were then autoradiographed on Kodak No-screen X-ray film for 4 days. The chromatograms were cut up and counted in a Nuclear Chicago liquid scintillation counter using PPO and $(CH_3)_2$POPOP[16] in *p*-dioxane fluid. A cold dihydroorotic acid marker was run on the chromatograms and detected using Fink's reagent test.[17a] This test involves spraying the chromatogram with 0.5 *M* NaOH, drying, and then spraying with a solution of 1 g of *p*-dimethylaminobenzaldehyde in 100 ml of ethanol and 10 ml of concentrated HCl. Compounds with a saturated 5,6 bond react with the sprays to produce a yellow spot on the chromatogram. Uracil, barbituric acid, and isobar-

(1) A. Haug and P. Douzou, *Z. Naturforsch. B*, **20**, 509 (1965).
(2) A. Haug, *J. Amer. Chem. Soc.*, **86**, 3381 (1964).
(3) E. Sztumpf-Kulikowska, D. Shugar, and J. W. Boag, *Photochem. Photobiol.*, **6**, 41 (1967).
(4) D. W. Whillans and H. E. Johns, *Photochem. Photobiol.*, **9**, 323 (1969).
(5) D. W. Whillans, M.S. Thesis, University of Toronto, 1968.
(6) M. Charlier and C. Hélène, *Photochem. Photobiol.*, **6**, 501 (1967).
(7) C. L. Greenstock, I. H. Brown, J. W. Hunt, and H. E. Johns, *Biochem. Biophys. Res. Commun.*, **27**, 431 (1967).
(8) E. Sztumpf and D. Shugar, *Photochem. Photobiol.*, **4**, 719 (1965).
(9) C. Hélène and F. Brun, *Photochem. Photobiol.*, **11**, 77 (1970).
(10) T. Godfrey and J. Boag, personal communication.
(11) M. A. Herbert, J. W. Hunt, and H. E. Johns, *Biochem. Biophys. Res. Commun.*, **33**, 643 (1968).
(12) M. A. Herbert and H. E. Johns, *Photochem. Photobiol.*, **14**, 693 (1971).
(13) R. W. Yip, W. D. Riddell, and A. G. Szabo, *Can. J. Chem.*, **48**, 987 (1970).
(14) (a) W. B. Taylor, J. C. LeBlanc, D. W. Whillans, M. A. Herbert, and H. E. Johns, *Rev. Sci. Instrum.*, **43**, 1797 (1972); (b) J. C. LeBlanc, M. A. Herbert, D. W. Whillans, and H. E. Johns, *Rev. Sci. Instrum.*, **43**, 1814 (1972)).
(15) (a) D. W. Whillans, M. A. Herbert, J. W. Hunt, and H. E. Johns, *Biochem. Biophys. Res. Commun.*, **36**, 912 (1969); (b) M. A. Herbert, Ph.D. Thesis, University of Toronto, 1972.
(16) PPO and $(CH_3)_2$POPOP are scintillators. PPO is 2,5-diphenyloxazole and $(CH_3)_2$POPOP is *p*-bis[2-(4-methyl-5-phenyloxazolyl)]benzene.
(17) (a) R. M. Fink, R. E. Clive, C. McGaughey, and K. Fink, *Anal. Chem.*, **28**, 4, (1956); (b) C. L. Greenstock, *Trans. Faraday Soc.*, **66**, 2541 (1970).

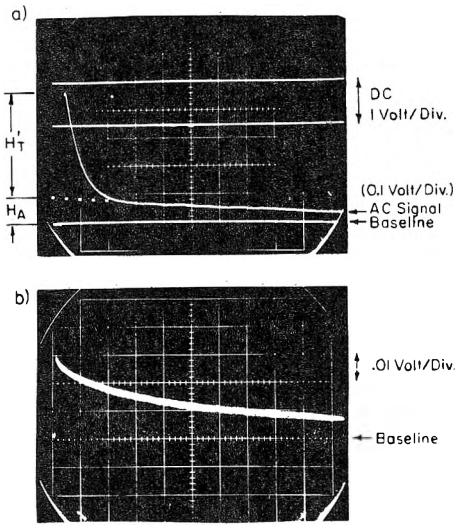

Figure 1. (a) Absorption signal from a solution of 3×10^{-5} *M* orotic acid displayed at a sweep speed of 50 μsec/division. The signal is ac coupled to the oscilloscope (vertical gain = 0.1 V/division, λ 340 nm). (b) Dc coupled adduct signal shown at 1 msec/division. This corresponds to the slow decay in a which appears as a straight line (vertical gain = 0.01 V/division, λ 340 nm).

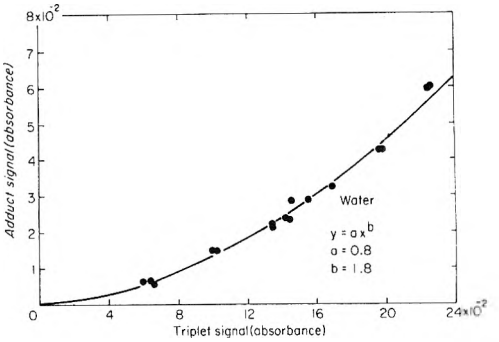

Figure 2. Variation of adduct signal (H_A) with total triplet signal ($H_A + H_T'$) for 3×10^{-5} *M* orotic acid solution measured at 340 nm. The total triplet signal is used as a measure of flash intensity. The solid line is the regression fit for $y = aX^b$ with $a = 0.8$ and $b = 1.8$. This shows a dependence on the square of the flash intensity.

bituric acid were detected by their uv absorption under a mineralight.

Decay of the Transient Signal. Figure 1a shows the transient signal observed at a sweep rate of 50 μsec/division in an unbuffered aqueous solution of 3×10^{-5} *M* orotic acid. The transient absorption consists of a large fast decaying signal from the triplet[12] followed by a smaller slower decaying signal from the adduct. The decay of the triplet is fast enough (lifetime is ~15 μsec) that the ac coupling time constant of the system (1 msec) has little effect on it. However, the slower decaying signal is badly distorted since its lifetime is longer than this time constant. To observe the proper decay of the adduct, we used a Tektronix 1A5 differential amplifier with the internal reference voltage adjusted to cancel out the dc level. The signal was then dc coupled into the oscilloscope. Figure 1b is the dc coupled signal shown with a sweep rate of 1 msec/division. Comparison of this trace to that in Figure 1a shows that the effect of the ac time constant is to increase the apparent rate of decay of the signal. (Note that the signal is displayed with a vertical gain of 0.1 V/division in Figure 1a and 0.01 V/division in Figure 1b.) All adduct decay rates were measured from dc coupled traces.

Measurement of Triplet Signal. From the traces given in Figure 1a, we can calculate the peak signal due to the triplet and that due to the adduct. H_T', the peak signal above the sloping base line, is a first approximation to the triplet signal. It does not include those triplets which were converted to adduct during the flash. The corrected triplet signal H_T is given by

$$H_T = H_T' + \frac{\epsilon_T}{\epsilon_A} H_A \qquad (1)$$

where ϵ_T and ϵ_A are the extinction coefficients of the triplet and adduct, respectively, and H_A (Figure 1a) is the absorption due to the adduct. The adduct extinction ϵ_A is the sum of the extinctions of the electron adduct (or protonated electron adduct) and the ·OH adduct. At pH 4.5, the value of ϵ_A is about 10^4 M^{-1} cm^{-1},[17b] while ϵ_T is 1.2×10^4 M^{-1} cm^{-1} if we assume that the triplets present are an equal mix of anion and neutral molecules (triplet p*K* is 4.5).[12] Equation 1 now is

$$H_T = H_T' + 1.2H_A \qquad (2)$$

We can approximate H_T by the sum $(H_T' + H_A)$. This approximation reduces the value of H_T by less than 5%, an error less than the normal experimental errors encountered.

Results

(*a*) *Intensity Dependence.* Figure 2 shows the variation of the adduct signal H_A with flash intensity. Since we are unable to measure the flash intensity directly, we have used the total triplet signal $(H_T' + H_A)$ as a measure of the flash intensity.

The solid line is the regression fit to the experimental points using the equation

$$y = aX^b \qquad (3)$$

with $a = 0.8$ and $b = 1.8$. Thus within experimental error (±15%) the yield of adduct depends on the square of the flash intensity and requires (i) either the absorption of two photons, or (ii) a triplet-triplet reaction for the production of an adduct molecule. To separate possibilities i and ii, we measured the relative yield of adduct signal as a function of triplet lifetime. Increasing amounts of the triplet quencher manganese sulfate[18] ($MnSO_4$) were added to a solution of 2.4×10^{-5} *M* orotic acid. This increased the triplet decay rate from a value of 3.4×10^4 sec^{-1} (30-μsec lifetime) with no added quencher to 11.5×10^4 sec^{-1} (8.7 μsec) at a quencher concentration of 1.4×10^{-4} *M*. The results are shown in Figure 3.

There is no change in the relative adduct signal size when $MnSO_4$ is added as a triplet quencher up to a concentration of 1.4×10^{-4} *M* in $MnSO_4$. Thus the production of adduct must be by mechanism i, that is, a biphotonic absorption. If the adduct were produced through a triplet-triplet reaction the yield would drop by a factor of 2 for each doubling of the decay rate of the triplet.

Because the excited singlet lifetime for orotic acid in solution is 5×10^{-11} sec,[19a] and the triplet lifetime is greater than 5×10^{-6} sec, the probability of absorbing a

(18) We have measured a rate constant of 5×10^8 M^{-1} sec^{-1} for the quenching of orotic acid triplet signal by $MnSO_4$.

(19) (a) J. Eisinger and A. A. Lamola, *Biochim. Biophys. Acta*, **240**, 299 (1971); (b) M. Charlier, C. Hélène, and M. Dourlant, *J. Chem. Phys.*, **66**, 700 (1969).

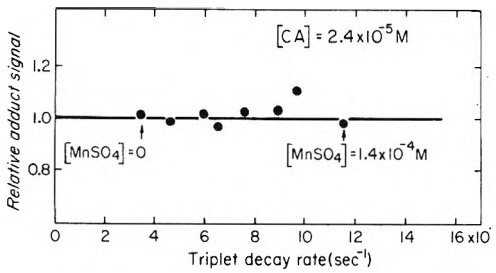

Figure 3. Variation of relative adduct signal with the triplet decay rate. Increasing amounts of the triplet quencher $MnSO_4$ were added to quench the triplet (λ 340 nm).

second photon during a triplet lifetime is more than 10^5 times greater than that for absorption during the excited singlet lifetime. Thus the second photon must be absorbed by the orotic acid molecule in its triplet state. The triplet state energy of orotic acid has been calculated as 2.7 eV from energy transfer[13] and phosphorescence measurements,[1,6,19b] and the absorption of a second photon from the flash would produce an excited molecule with about 6–9 eV of energy.

(*b*) *Absorption Spectra.* To obtain reproducible absorption spectra, it was necessary to use an internal monitor to correct for pulse to pulse variations in the flash intensity. A beam splitter directs part of the analyzing light to a second monochromator–photomultiplier detector which is set at a fixed wavelength providing a reference signal for each flash. The measured signals are then normalized to a constant reference signal correcting for any flash output variation.

Figure 4 shows the absorption spectrum of the long-lived transient measured 150 μsec after the flash in a solution of 5×10^{-5} *M* orotic acid at pH 1, 4.5, and 8.2. The spectra from the flash photolysis experiments are the result of duplicate points taken every 5 nm and are normalized at their peaks. Although the points are not shown for clarity, they rarely differ by more than ±5%. The solid line is Greenstock's spectrum[17b] of the solvated electron (e_{aq}^-) adduct to orotic acid measured at neutral pH using pulse radiolysis. This spectrum is very similar to that measured by Hayon[20] for the electron adduct. This spectrum has also been normalized to the adduct spectral peak.

The spectra shown are very similar, peaking at 325 nm. At pH 1, the spectrum has a distinct shoulder at 355 nm while at pH 4.5 and 8 there is only a slight shoulder at 345 nm. The similarity of the flash photolysis absorption spectra to the electron adduct spectrum in pulse radiolysis suggests that we have formed a radical with a structure similar to the OA electron adduct. We suggest that we are observing the OA C_4 carbonyl radical formed by hydrogen abstraction from a water molecule by the doubly excited OA molecule. When the OA triplet absorbs a second photon it will have about 6–9 eV, sufficient energy to break an H–OH bond in water, an endothermic reaction requiring 5.1 eV.[21] The OA molecule adds on the hydrogen atom producing the H· adduct radical and leaving an ·OH radical in the solution. This ·OH radical will attack ground state orotic acid molecules adding to form ·OH adducts to OA with a rate constant of 5.2×10^9 M^{-1} sec^{-1}.[17b] At an orotic acid concentration of 5×10^{-5} *M*, 63% of the ·OH radicals will have reacted with the orotic acid within 3.8 μsec, thus the build-in of the ·OH adduct absorption will be hidden under the first part of the triplet decay.

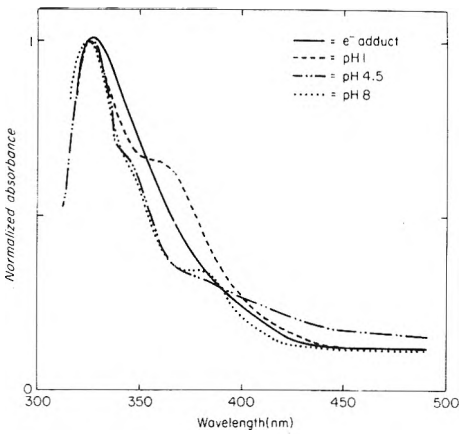

Figure 4. Adduct absorption spectra measured at pH 1, 4.5, and 8. The solid line is the electron adduct spectrum measured by Greenstock[17b] at neutral pH by pulse radiolysis.

At neutral pH, the shoulder on the spectrum at 345 nm is the result of the absorption of the ·OH adduct produced. At acid pH, a new shoulder is observed at 355 nm. This absorption may be from the carbonyl radical formed on the carboxyl group. At acid pH the carboxyl group is uncharged[4,22] and may abstract an H· from water to form a carbonyl radical which absorbs at 355 nm. At neutral pH, this group is negatively charged and probably does not abstract. Thus, no shoulder is observed at 355 nm.

The similarity of the flash spectra to the electron adduct spectrum suggests that the H· addition to OA occurs at a carbonyl group, probably the C_4 position.[20] Addition of an H· to either the C_5 or C_6 position produces a spectrum peaking at 345 nm.[17b] The addition of H· to the C_4 carbonyl produces a radical which undergoes deprotonation with a p*K* of about 4.[17b] The deprotonated form is then identical with the electron adduct. This species has a peak absorption coincident with our observed spectra as seen in Figure 4.

It has been shown in observations on thymine[23] and orotic acid[17b] that the peak absorptions of both the electron adduct and the protonated electron adduct occur at the same wavelength. This observation accounts for the same observed peak position of the spectra measured at pH 1, 4.5, and 8. There is, however, a decrease of about a factor of 2.5 in the peak extinction of the orotic acid electron adduct as it protonates with a p*K* of about 4.[17b] Thymine shows a similar sized decrease upon protonation.[23]

(*c*) *pH Dependence.* In Figure 5 the adduct signal (H_A) observed at 340 nm is plotted against pH from pH 0.5 to 9.5 for a solution of 4×10^{-5} *M* orotic acid. As the pH is increased from 0.5, H_A decreases from an initial value of 0.06 to a minimum of 0.025 at pH 2.4, then rises to a plateau value of 0.13 above pH 6. The general shape of the curve can be explained as follows.

The initial drop occurs as the ground-state orotic acid molecule ionizes from the neutral to anionic form with a p*K* of 1.8.[4,22] (Overlapping p*K* curves cause an apparent shift of the midpoint of the decreasing curve back to a pH of about 1.) As the ground-state molecule ionizes, the in-

(20) E. Hayon, *J. Chem. Phys.*, **51**, 4881 (1969).
(21) J. A. Ghormley and C. J. Hochanadel, *J. Phys. Chem.*, **75**, 40 (1971).
(22) E. M. Woolley, R. W. Wilton, and L. G. Hepler, *Can. J. Chem.*, **48**, 3249 (1970).
(23) (a) L. M. Theard, F. C. Peterson, and L. S. Myers, Jr., *J. Phys. Chem.*, **75**, 3815 (1971); (b) L. M. Theard, F. C. Peterson, and R. L. Voigt, Gulf General Atomic Report No. GA-10208 (1970).

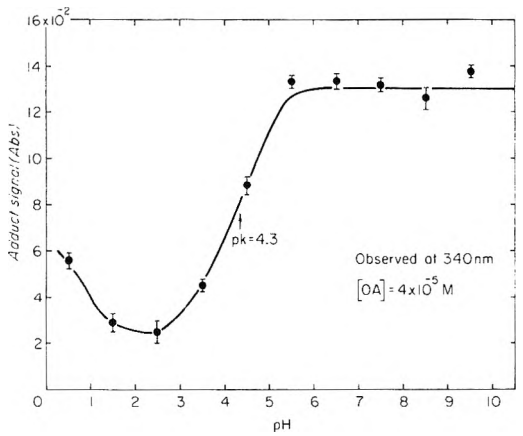

Figure 5. Variation of adduct signal H_A with pH. The error bars represent the range of values measured (λ 340 nm).

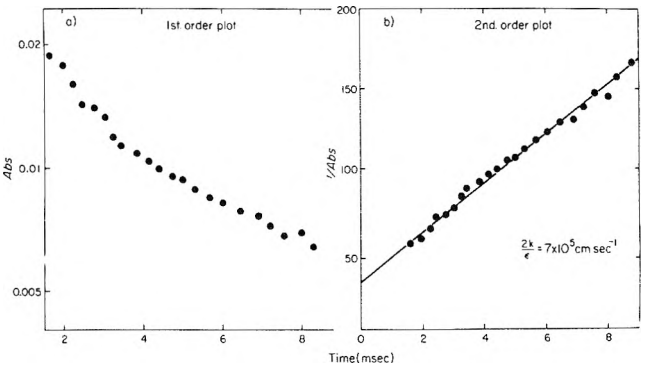

Figure 6. Decay of the adduct signal at 340 nm. (a) First-order plot of log of absorbance *vs.* time. The points do not lie on a straight line. (b) Second-order plot of 1/absorbance *vs.* time. These data are the same as in part a. The points lie on a straight line of slope $2k/\epsilon = 7 \times 10^5$ cm sec^{-1}.

tersystem crossing decreases by a factor of 2,[4] resulting in only one-half the number of triplets, which can absorb a second photon (to form adducts).

As the pH is further increased, the signal H_A increases approximately fivefold with the midpoint of the increase at a pH of 4.3. This increase can be explained by the following two factors.

(i) When the triplet absorption spectrum is multiplied by the flash output spectrum and the product integrated, it can be seen that a given number of anion triplets (the triplet has a pK of 4.5)[12] will absorb twice as many photons as will an equal number of neutral triplet molecules of orotic acid. Thus, there is a factor of 2 increase in triplet absorption as the triplet ionizes in going from below to above its pK. If we assume that after biphotonic absorption the formation of an adduct is 100% efficient, the yield of adducts will also increase by a factor of 2.

(ii) The additional 2.5-fold increase occurs as the adduct undergoes dissociation of a proton with a pK of about 4.[17b] The extinction of the dissociated form is greater than that of the protonated form by a factor of 2.5. Together these factors can account for the observed change.

(*d*) *Decay of the Transient.* Figure 6a is a first-order plot (log of absorbance *vs.* time) of the decay of the long-lived transient observed at 340 nm in an unbuffered solution of 4×10^{-5} M orotic acid. Figure 6b is a second-order plot (1/absorbance *vs.* time) of the same data. The points were measured on a photograph of a dc coupled transient signal such as shown in Figure 1b. The first-order plot (Figure 6a) is concave upward and cannot be represented by a good straight line. The second-order plot (Figure 6b) is a good straight line.

The second-order decay rate constants ($2k/\epsilon$) for orotic acid at pH 2, 4.5, and 8 are listed in Table I. The results were measured at wavelengths of 340 and 390 nm, and are the average of at least five measurements while the error shows the range of values obtained. The extinction coefficient is calculated from the absorption spectra assuming a peak extinction of 1.0×10^4 M^{-1} cm^{-1} for pH 8[17b] and 5.1×10^3 M^{-1} cm^{-1} for pH 2 (protonated form) and a mix of 50% protonated and 50% dissociated adduct for pH 4.5 giving an adduct extinction of 7.6×10^3 M^{-1} cm^{-1}. Based on these values, the decay rate constant, $2k$, has been calculated. The observed decay rate constant at 390 nm for all pH values and at 340 nm (pH 2) is 1.4×10^9 M^{-1} sec^{-1}. Greenstock[17b] measured a decay rate of 2×10^8 M^{-1} sec^{-1} for the ·OH adduct to orotic acid, while

TABLE I: Second-Order Decay Rate Constants ($2k$) of the Orotic Acid Adduct Signal

λ, nm	pH	$\epsilon_\lambda \times 10^3$, M^{-1} cm^{-1}	$2k/\epsilon \times 10^5$, cm sec^{-1}	$2k \times 10^9$, M^{-1} sec^{-1}
340	2.0	4.0	(3.4 ± 0.3)	(1.4 ± 0.2)
	4.5	5.2	(3.2 ± 0.9)	(1.7 ± 0.4)
	8.0	7.0	(2.5 ± 0.9)	(1.7 ± 0.5)
390	2.0	1.8	(7.8 ± 3)	(1.4 ± 0.4)
	4.5	2.2	(6.5 ± 2)	(1.4 ± 0.4)
	8.0	3.0	(4.8 ± 2)	(1.4 ± 0.5)

Theard, *et al.*,[23] measured decay rate constants of about 10^9 M^{-1} sec^{-1} for most pyrimidine ·OH and e_{aq}^- adducts.

(*e*) *Chromatography.* Thin layer chromatography was carried out in an attempt to isolate permanent products produced by the decay of these adducts. Solutions of 8×10^{-5} M [6-^{14}C]orotic acid were mixed at pH 4.5 (unbuffered) and 1. Samples were irradiated in the flash photolysis apparatus for 0, 5, 10, and 20 flashes and one sample was irradiated in a monochromator at 280 nm by steady-state methods. 100-μl volumes were spotted on the chromatograms and run in 1-PrOH–H_2O (70:30 v/v) and then autoradiographed for 4 days. Several compounds were spotted as markers, and their R_f values (±0.05) measured in this solvent system: dihydroorotic acid (R_f = 0.48), uracil (0.62), barbituric acid (0.32), isobarbituric acid (0.50). Orotic acid and orotic acid dimers were observed with R_f values of 0.41 and 0.19, respectively.

In the unbuffered solutions, a spot running with an R_f of 0.33 increased to a value of 0.41% of the spotted material after 20 flashes, while a small amount of a product with an R_f of about 0.6 was also visible. The product with an R_f of 0.6 was probably uracil caused either by a spontaneous decarboxylation of the orotic acid or a radiation-induced decarboxylation.[24] The product running with an R_f of 0.33 may be barbituric acid or possibly orotic acid glycol. Since there is no marker for the glycol, its presence can not be ruled out. The glycol is an expected product from the radical decay of the orotic acid OH adducts.

Despite repeated attempts the chromatography results with the pH 1 samples were very poor. To avoid dissolving the emulsion on the plate, it was necessary to neutralize the acid before spotting. This left a solution containing

(24) D. W. Whillans, personal communication, 1972.

0.1 M salt and even repeated desalting procedures could not prevent severe streaking and running of the spots.

(*f*) *Effect of N_2O, $MnSO_4$, and O_2 on Yields.* Saturation of the orotic acid solution with N_2O (by bubbling) had no effect on either the triplet or adduct signals observed. This means that no significant fraction of the observed adduct absorption is produced by the attack of solvated electrons on the orotic acid, ruling out the possibility that we are observing ionization of the orotic acid. Ionization would produce a solvated electron which would attack a ground-state orotic acid, producing an adduct with an extinction of 8500 M^{-1} cm^{-1} [17b] with a peak absorption at 330 nm. The observed signal would then be the sum of the absorption from the ionized molecule plus the absorption of the electron adduct. The addition of N_2O to the solution would block this reaction, reducing the adduct signal seen.

The use of a 10^{-2} M $MnSO_4$ solution as an optical filter to absorb photons of wavelengths less than 240 nm did not change the ratio of adduct to triplet signal observed. This means we are not observing a reaction of orotic acid molecules excited by the flash directly from the ground state, S_0, to the second excited singlet state, S_2.

The adduct signal was very sensitive to the presence of oxygen in the solution. Bubbling the solution with a mixture of 0.5% oxygen and 99.5% nitrogen reduced the lifetime of the adduct to under 50 μsec, after which point the transient due to the adduct could not be separated from the triplet signal accurately. This corresponds to an oxygen quenching rate of about 3×10^9 M^{-1} sec^{-1} in agreement with other measured rates for O_2 attack with orotic acid radicals.[17b]

Discussion and Conclusions

The following equations summarize the reactions occurring in the production of the adducts.

$$OA \xrightarrow{h\nu} OA^s \quad (4)$$

$$OA^s \xrightarrow{\Phi_{isc}} OA^t \quad (5)$$

$$OA^s \longrightarrow OA \quad (6)$$

$$OA^t \xrightarrow{h\nu} OA^{**} \quad (7)$$

$$OA^{**} + H_2O \longrightarrow OAH\cdot + \cdot OH \quad (8)$$

$$\cdot OH + OA \xrightarrow{5.2 \times 10^9\ M^{-1}\text{sec}^{-1}} OAOH\cdot \quad (9)$$

A ground-state orotic acid molecule, OA, absorbs a photon in the flash exciting it to an excited singlet state OA^s (eq 4). From the excited singlet state, a fraction of these molecules (Φ_{isc}) undergo intersystem crossing to become triplets, OA^t (eq 5), while the rest decay back to the ground state (eq 6). During the flash, a fraction of the triplets absorb a second photon, producing a highly excited molecule OA** (eq 7) which may have up to about 9 eV of excitation energy above the ground-state level. This molecule now interacts with a water molecule to abstract a hydrogen atom forming the H· adduct (eq 8) and leaving a hydroxyl radical (·OH) which can attack a ground-state orotic acid molecule to form the ·OH adduct (eq 9).

The hydrogen abstraction results in the addition of the hydrogen atom to a ketyl oxygen of the orotic acid, probably at the C_4 position,[20] resulting in structure 1, which has a pK of about 4[17b] and dissociates to structure 2 at pH values above this pK. Structure 2 is the same as the

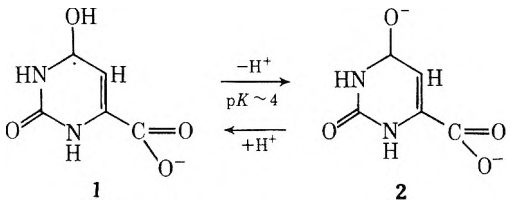

1 2

electron adduct produced in pulse radiolysis at neutral pH and explains why the spectra of the adduct made in the flash and the pulse radiolysis electron adduct are the same. The extra electron of the adduct is likely delocalized through the C_5, C_6, and carboxyl group positions as shown by resonant structure 3. Adams[25] has shown that in

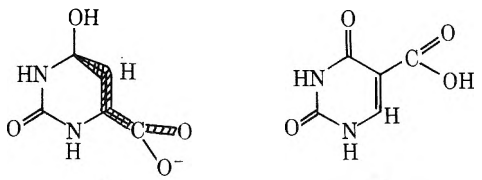

3 4

isoorotic acid, structure 4, the extinction coefficient of the electron adduct is considerably less than that for orotic acid. Since isoorotic has less resonant structure than orotic acid, he concludes that the higher extinction in the orotic acid radical indicates a larger degree of resonance for the orotic acid electron adduct radical. Delocalization of the unpaired electron onto the carboxyl or carbonyl group in orotic acid has been suggested to explain observed esr (electron spin resonance) signals.[26] In the uracil anion it has been suggested that the delocalization is onto the C_2 carbonyl group.[26] Esr studies of the free radicals produced by H· and ·OH attack on uracil and thymine[27,28] indicate that there is conjugation between at least two resonant forms of the radical. The study of γ-irradiated 5-nitro-6-methyluracil crystals[29] shows that the H· has added on to the oxygen on position 4 and the free electron is conjugated between the C_6 position and the C_4 position. Hüttermann reports esr evidence for resonant structures in orotic acid similar to 3. He has also detected the addition of an H· on the oxygen in the carboxyl group.[30]

The hydroxyl radical produced (eq 8) attacks at the 5 or 6 position. This produces a spectrum peaking around 345 nm[17b] which is added to the electron adduct spectrum producing the shoulder observed at 355 nm.

The decay mechanism of the observed radical species can only be suggested at this time. At neutral pH, the reaction of the electron adduct with an ·OH adduct might eliminate an OH^- and leave two ground-state orotic acid molecules. The reaction of two ·OH adducts could disproportionate to produce orotic acid glycol and orotic acid. This product may be the spot observed with an R_f of 0.33. At acid pH, the reaction of two protonated electron adducts could eliminate hydrogen, leaving two orotic acid molecules, while the reaction of the H· adduct with an ·OH adduct could eliminate a molecule of water, leaving two orotic acid molecules.

(25) G. E. Adams, C. L. Greenstock, J. J. van Hemmen, and R. L. Wilson, *Radiat. Res.*, **49**, 85 (1972).
(26) J. K. Dohrmann and R. Livingston, *J. Amer Chem. Soc.*, **93**, 5363 (1971).
(27) J. N. Herak and W. Gordy, *Proc. Nat. Acad. Sci. U.S.*, **54**, 1287 (1965).
(28) C. Nicolau, M. McMillan and R. O. C. Norman, *Biochim. Biophys Acta*, **174**, 413 (1969).
(29) W. Snipes and B. Benson *J. Chem. Phys.*, **48**, 4666 (1968).
(30) J. Hüttermann, J. F. Ward, and L. S. Myers, Jr., *J. Phys. Chem.*, **74**, 4022 (1970).

It has been reported that an excited orotic acid reacts with acrylonitrile to form the acrylonitrile radical.[9] The first step is almost surely a hydrogen abstraction reaction, but the authors report that they could not observe dihydroorotic acid, the expected product from disproportionation of two H· adducts, when the H· adduct is formed at the 5, 6 bond positions. This would suggest that in their system, the hydrogen abstraction does not add a hydrogen atom to the C_5 or C_6 positions, but rather to a carbonyl oxygen as we suggest.

Acknowledgments. The authors take pleasure in acknowledging the financial support of the Medical Research Council of Canada and the National Cancer Institute of Canada. We are indebted to Drs. J. W. Hunt, T. Penner, and D. W. Whillans for helpful discussions.

Excited State Chemistry of Indigoid Dyes. II. The Interaction of Thio- and Selenoindigo Dyes with Hydroxylic Compounds and Its Implications on the Photostability of Indigo[1]

George M. Wyman* and Bizhan M. Zarnegar

Department of Chemistry, University of North Carolina, Chapel Hill, North Carolina 27514 *(Received November 6, 1972)*

Publication costs assisted by the U.S. Army Research Office—Durham

The fluorescence and the photoisomerization of *trans*-thioindigo is quenched by phenol and *p*-nitrophenol at the diffusion-controlled rate. The effectiveness of ethanol, α-trifluoroethanol, and α,α'-hexafluoro-2-propanol as fluorescence quenchers ranges from 2.5 to 58% of the diffusion-limited value and increases with increasing acidity of the alcohol. The fluorescence quenching rates of selenoindigo and several dyes related to thioindigo with one or more of these hydroxy compounds were also determined. The results support the idea that an intramolecular proton transfer in the excited (S_1) state is responsible for the unique photostability and lack of fluorescence exhibited by indigo and its ring-substituted derivatives.

It is now generally recognized that indigo (Ia) and its ring-substituted derivatives exist only as the trans isomers[2,3] and that, in contrast with other indigoid dyes,[4,5] they will not undergo photochemical trans → cis isomerization,[2,6] nor do they exhibit any appreciable fluorescence.[7] When it was observed that the *N,N'*-dimethyl-[8,9] and *N,N'*-diacetyl derivatives[2,10] undergo photoisomerization, the photostability of the parent compound was attributed to hydrogen bonding.[2] Although the existence of hydrogen bonds in indigo in its ground state is now firmly established from crystallographic data,[3] this does not provide a wholly satisfactory explanation for the photostability, since the energy required for exciting the molecule to its S_1 state (*ca.* 48 kcal) is far greater than the stabilization that may be expected from the formation of two typical hydrogen bonds (*ca.* 10 kcal).

In a recent communication an alternative explanation was proposed by one of us for this remarkable photostability,[11] suggesting that a fast proton transfer occurs in the S_1 state (as represented by eq 1) and that this takes precedence over the other excited state processes (fluorescence and cis–trans isomerization) normally encountered in molecules of this type. The greatly enhanced (*ca.* 10^6-fold) acidity of Ar–NH groups and the similarly increased basicity of Ar–CO functions in the S_1 state is well known[12] and such intramolecular proton transfer phenomena have been reported for other compounds that are hydrogen bonded in the ground state, *e.g.*, derivatives of salicylic acid,[13] o-hydroxyazines,[14] and some hydroxybenzazoles.[15]

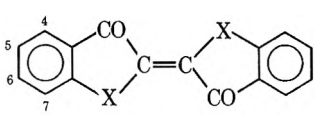

I

Ia, X = NH
Ib, X = S
Ic, X = S, 6,6'-diethoxy-
Id, X = S, 6,6'-di-*n*-hexoxy-
Ie, X = Se

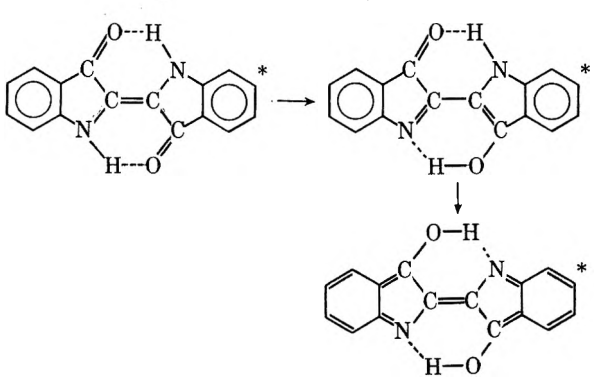

(1)

(1) Presented in part at the VI International Conference on Photochemistry, Bordeaux, Sept. 1971.
(2) W. R. Brode, E. G. Pearson, and G. M. Wyman, *J. Amer. Chem. Soc.*, **76**, 1034 (1954).
(3) H. v. Eller, *Bull. Soc. Chim. Fr.*, **106**, 1444 (1955); E. A. Gribova, *Kristallografiya*, **1**, 53 (1956).
(4) G. M. Wyman and W. R. Brode, *J. Amer. Chem. Soc.*, **73**, 1487 (1951).

The previous communication[11] contained preliminary results of the interaction of excited *trans*-thioindigo (Ib) as the prototype for "protonless indigo"[16] with phenol and *p*-nitrophenol. The present paper reports an extension of this study to ethanol and to two fluorinated alcohols; in addition the excited state interactions of several dyes related to thioindigo (Ic, Id, Ie, and II) with some of these

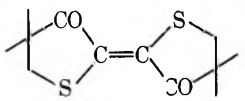

II

hydroxy compounds is also reported. Reexamination of the data reported earlier disclosed that the uniquely high rate found for the inhibition of the trans → cis isomerization of Ib by *p*-nitrophenol was due to an experimental artifact and the correct rate for this reaction was determined.

Experimental Section

(a) Materials. Indigo (Ia), thioindigo (Ib), and 6,6′-diethoxythioindigo (Ic) were research samples obtained from Allied Chemical Corp., the DuPont Co., and Ciba-Geigy S. A., respectively. A sample of resublimed indigo (Ia) and 3,3′-dioxo-4,4,4′,4′-tetramethyl-2,2′-bithioanylidene (II) were provided through the courtesy of Professor W. Luettke (University of Goettingen). The samples of selenoindigo (Ie) and 6,6′-di-*n*-hexoxythioindigo (Id) were made available to us by Dr. D. L. Ross (RCA Laboratories). Reagent grade phenol was used and the *p*-nitrophenol was recrystallized from benzene before utilization. Spectroscopic grade benzene was used for all measurements.

(b) Fluorescence Quenching. Solutions of the dyes in spectroscopic grade benzene were preirradiated for 5 (or more) min in the apparatus described previously[10] to obtain the photostationary state enriched with respect to the trans isomer. The exciting light was filtered either through a Corning blue filter (usually No. 5-60) or a Jena-Glas interference filter with a transmission peak at 459 nm. Irradiation was carried out through a rectangular water bath in order to eliminate heat effects. After irradiation the quencher solution was added (in the dark) and the fluorescence measured on a Hitachi Perkin-Elmer MPF-2A fluorescence spectrometer.

(c) Cis-Trans Isomerization. (1) Photostationary State Measurements. Appropriate mixtures of Ib and phenol (in benzene solution), contained in a 1-cm quartz absorption cell, were irradiated with light from a 300-W projection lamp through a Jena-Glas interference filter (λ_{max} 552 nm) to obtain a cis-rich photostationary state. The dye concentration was kept constant within each series of measurements.

(2) Kinetic Studies. Appropriate mixtures of Ib and *p*-nitrophenol (in benzene) were irradiated in an optical bench, using the projection lamp and interference filter described above, for identical periods of time (*ca.* 1 min) to bring about 4–8% conversion to the cis isomer. Correction for the reverse reaction was calculated from the equation developed by Lamola and Hammond.[17]

The relative concentrations of the trans isomer were determined spectroscopically by means of a Cary Model 17 spectrophotometer, using 565 nm as the analytical wavelength and the recently reported absorption curves for thioindigo in benzene.[18] Correction was made for the weak absorption due to the cis isomer at this wavelength; however, this was only necessary for the photostationary state measurements (at 565 nm ϵ_t 6220, ϵ_c 160).

Results

(a) Fluorescence Quenching. The fluorescence quenching results, based on Stern–Volmer treatment[19] of the fluorescence intensities as a function of quencher concentration, are tabulated in Table I. It should be noted that the fluorescence of these dyes is unaffected by the addition of anisole or *p*-nitroanisole, indicating that the quenching is neither due to electron transfer, nor to interaction of the dye with the nitro group. A comparison of the data in the first two lines of Table I with the corresponding results reported in ref 11 shows a downward revision of the quenching constants (from 9.3 to 8.2). Since both phenols quench at the same rate, we believe that this is the correct diffusion-controlled rate, although it is almost 20% lower than the value of 1.1×10^{10} obtained from the Debye equation.[20] Refinement of these measurements was probably due to the availability of the Cary 17 instrument, the high sensitivity of which permits the accurate measurement of the spectral absorption of the weakly absorbing solutions that are necessary for fluorescence measurements.

(b) Cis-Trans Isomerization. The Stern–Volmer-type plots of the photostationary state concentrations obtained on the thioindigo–phenol and thioindigo–*p*-nitrophenol systems using orange cut-off filters for the irradiation resulted in straight lines with slopes of 131 and 192.5, respectively.[11] However, when the absorption curves were computed for each isomer in the quencher-containing solutions by the method of Blanc and Ross,[21] it was found that *p*-nitrophenol enhances the intensity of absorption of the cis isomer at wavelengths greater than 500 nm. Thus the high (greater than diffusion controlled!) Stern–Volmer slope found for this system was due to this artifact and not to an interaction of the quencher with a second, lower-lying excited state, as had been thought. In order to eliminate this difficulty, the Ib–*p*-nitrophenol system was reinvestigated by a kinetic technique, where the low conversions make the results independent of the absorption intensity of the cis isomer. Moreover, the Ib–phenol system was also measured again with the use of an interference filter to provide a narrower range of wavelengths for excitation and, of course, the Cary 17 instrument. The re-

(5) R. Pummerer and G. Marondel, *Chem. Ber.*, **93**, 2834 (1960).
(6) Attempted photoisomerization of indigo in a degassed benzene solution by means of a flash photolysis apparatus with a 10-μsec lifetime was unsuccessful. (D. G. Whitten, personal communication.)
(7) A weak fluorescence has been found (near 625 nm) in some samples of indigo in benzene. However, a resublimed sample showed essentially no fluorescence.
(8) J. Weinstein and G. M. Wyman, *J. Amer. Chem. Soc.*, **78**, 4007 (1956).
(9) C. R. Giuliano, L. D. Hess, and J. D. Margerum, *J. Amer. Chem. Soc.*, **90**, 587 (1968).
(10) G. M. Wyman and A. F. Zenhaeusern, *J. Org. Chem.*, **30**, 2348 (1956).
(11) G. M. Wyman, *Chem. Commun.*, 1332 (1971).
(12) *Cf.* A. Weller, *Discuss. Faraday Soc.*, 183 (1965).
(13) A. Weller, *Z. Elektrochem.*, **60**, 1144 (1956).
(14) A. Weller and H. Wolf, *Justus Liebigs Ann. Chem.*, **657**, 64 (1962).
(15) D. L. Williams and A. Heller, *J. Phys. Chem.*, **74**, 4473 (1970).
(16) It has already been reported that the conjugate acid cation obtained by dissolving thioindigo in concentrated sulfuric acid behaves very much like indigo does in inert solvents, hence this selection appears well justified (*cf.* W. R. Brode and G. M. Wyman, *J. Amer. Chem. Soc.*, **73**, 4267 (1951)).
(17) A. A. Lamola and G. S. Hammond, *J. Chem. Phys.*, **43**, 2129 (1965).
(18) G. M. Wyman and B. M. Zarnegar, *J. Phys. Chem.*, **77**, 831 (1973).
(19) O. Stern and M. Volmer, *Z. Phys.*, **20**, 183 (1919).
(20) *Cf.* J. G. Calvert and J. N. Pitts, "Photochemistry," Wiley, New York, N. Y., 1966, p 627.
(21) J. Blanc and D. L. Ross, *J. Phys. Chem.*, **72**, 2817 (1968).

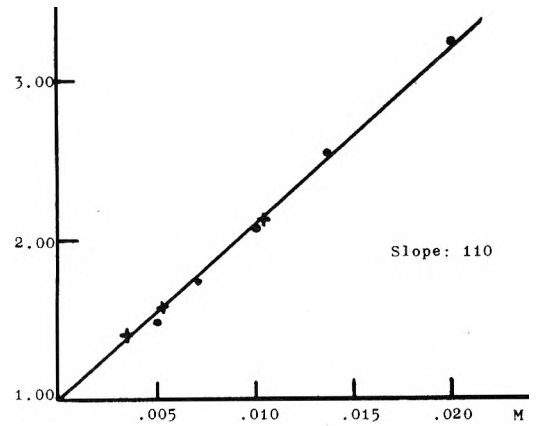

Figure 1. Stern–Volmer type plots of the inhibition of the trans → cis isomerization of thioindigo by phenol and *p*-nitrophenol (solvent benzene): ●, $(c/t)^0/(c/t)_q$ at the photostationary state *vs.* phenol concentration; ×, $(\text{rate})^0/(\text{rate})_q$ at 4–8% trans → cis conversion *vs.* *p*-nitrophenol concentration.

sults obtained are plotted by the Stern–Volmer approach in Figure 1. The slope of the single straight line is in very good agreement with the corresponding values obtained from the fluorescence-quenching measurements for these two systems (*cf.* Table I).

Discussion of Results

The excellent agreement between the fluorescence quenching constants in Table I and the rates of the inhibition of the trans → cis isomerization (Figure 1) for the Ib–phenol and Ib–*p*-nitrophenol systems clearly demonstrates that there is a very fast, diffusion-limited interaction between the excited (S_1) trans isomer and the phenol molecule. Furthermore, the phenols interact neither with the excited cis form, nor with the twisted intermediate that is almost certainly involved in the isomerization process. On the other hand, the possibility of a triplet intermediate is still not rigorously excluded, even though it has not been possible to detect such a precursor by flash photolytic techniques.[18,22]

The data in Table I also indicate that for the same dye there is a correlation between the quenching rate constants and the acidity of the quencher. This is especially apparent in the series of alcohols used; in contrast with ethanol, the two fluorinated alcohols are weak acids (pK_a of CF_3CH_2OH = 12.4, $(CF_3)_2CHOH$ = 9.3)[23] and the differences observed in the quenching rates strongly suggest acid–base interactions. At first glance phenol (pK_a = 10.0) appears to be anomalous in this respect; however, the relative acidities in benzene may well be somewhat different than in aqueous solution where the pK_a values have been determined. While *p*-nitrophenol had been selected as one of the quenchers, because it is more acidic than phenol, it only helped to confirm that the rate of the Ib–phenol interaction is diffusion limited. Dye II was surprising in two respects: first it was not expected to exhibit fluorescence at room temperature[18] and, second, it was not expected to be as strongly basic in the excited state as its aromatic analogs, due to the lack of conjugation between the carbonyl groups and benzene rings. However, there is no doubt that in the excited (S_1) state it is also interacting with phenol at the diffusion-controlled rate. Thus it appears that conjugation of the carbonyl groups with the sulfur atoms within the "basic chromophore" responsible for its indigoid character (absorption in the visible, fluorescence and cis–trans isomerization)[18,24] is sufficient to enhance the basicity of the carbonyl groups in the excited (S_1) state.

TABLE I: Stern–Volmer Rate Constants and Excited State Lifetimes

Dye	Quencher	τ, nsec	$k_q\tau$ [c]	$k_q \times 10^9$
Ib	Phenol	13.4[a]	110 ± 2	8.2
Ib	*p*-Nitrophenol		112 ± 2	8.3
Ib	CF_3CH_2OH		22 ± 1	1.6
Ib	$(CF_3)_2CHOH$		65 ± 1	4.9
Ib	C_2H_5OH		2.6 ± 0.1	0.19
Ic	Phenol	0.9 ± 0.3[a]	8.4 ± 0.1	9.3[d]
Id	Phenol	0.9[b]	7.4 ± 0.1	8.2
Ie	Phenol	2.3[b]	19.0 ± 0.3	8.2
Ie	*p*-Nitrophenol		18.5 ± 0.1	8.1
II	Phenol	0.7 ± 0.3[a]	7.6 ± 0.2	10.8[d]
II	CF_3CH_2OH		4.1 ± 0.1	5.9

[a] Determined through the kindness of Professor W. R. Ware by the single photon counting technique (in air). [b] Determined indirectly by assuming quenching at the diffusion-controlled rate of 8.2×10^9. [c] Least-squares analysis. [d] These values are probably too high; they are based on the value of τ indicated in the table, but which is subject to considerable uncertainty (as shown).

While these results do not prove that an intramolecular proton transfer occurs when indigo (or one of its ring-substituted derivatives) is excited to its S_1 state, nonetheless they are completely consistent with that concept. The observed very fast reaction of each prototype dye in its excited singlet state with phenol (and, whenever attempted, with *p*-nitrophenol) and the apparent acidity dependence of the rate of this interaction attests to the strong basicity of excited indigoid molecules. In view of what is known of the enhanced basicity of aromatic carbonyl compounds in the excited singlet state,[12] it is reasonable to assume that in indigo dyes the basicity is largely localized in the carbonyl groups. This work has also demonstrated that, once a donor–acceptor complex is formed between the excited dye and the hydroxy compound, the adduct will neither isomerize nor fluoresce.

Since in indigo the potentially acidic protons are held in the close proximity of the potentially basic carbonyl groups by means of hydrogen bonding in the ground state, the occurrence of such an intramolecular proton transfer would seem to be exceedingly likely on excitation. Recent quantum-mechanical calculations have also indicated an appreciable increase in the electron density of the carbonyl groups and a corresponding decrease on the nitrogen atoms when indigo is excited to its S_1 state;[25] there is little doubt that such a redistribution of the electron cloud in the molecule would favor, if not require, the proposed proton transfer. By analogy with the behavior of the systems studied in the present investigation, the product of such a proton transfer would not be expected to isomerize or to fluoresce, but to decay to the trans ground state by a radiationless process.[26] Thus one may conclude that, al-

(22) Thioindigo can be isomerized through a triplet intermediate by using an appropriate sensitizer. (Unpublished data of the authors.)
(23) R. Filler and R. M. Schure, *J. Org. Chem.*, **32**, 1217 (1967).
(24) H. Herrmann and W. Luettke, *Chem. Ber.*, **101**, 1715 (1968).
(25) E. Wille and W. Luettke, *Angew. Chem., Int. Ed. Engl.*, **10**, 803 (1971).
(26) One of the referees pointed out that other molecules that contain intramolecular hydrogen bonds (*e.g.*, o-hydroxyazobenzenes[27] and o-hydroxybenzophenones[28]) have also been found to undergo fast radiationless deactivation to the ground state.
(27) D. Gegiou and E. Fischer, *Chem. Phys. Lett.*, **10**, 99 (1971).

though the photostability and lack of fluorescence exhibited by indigo may seem anomalous, when viewed from the standpoint of ground-state chemistry, this behavior is consistent with that shown by related systems in the excited state.

Acknowledgments. The authors are greatly indebted to Professors W. Luettke, W. R. Ware, A. Weller, and D. G. Whitten for many helpful discussions and to the Chemistry Department of Duke University and the Spectroscopy Department of the Max Planck Institute for Biophysical Chemistry for making their facilities available for carrying out some of this work. This research was supported by the U. S. Army Research Office—Durham.

(28) N. J. Turro in "Technique of Organic Chemistry," Vol. XIV, P. A. Leermakers and A. Weissberger, Ed., Interscience, New York, N. Y., 1969, p 223.

Quenching of Biphenyl Fluorescence by Inorganic Ions

A. R. Watkins

Max-Planck-Institut für Biophysikalische Chemie, 34 Göttingen-Nikolausberg, Germany *(Received June 13, 1972)*

Publication costs assisted by the Max-Planck-Institut für Biophysikalische Chemie, Göttingen

Examination of the quenching of biphenyl fluorescence by a series of inorganic salts shows that the measured rate constants, in comparison to earlier measurements for anthracene, are in most cases larger. This can be correlated with the more negative value of the excited state reduction potential on going from anthracene to biphenyl. However, electron-transfer fluorescence quenching, which would be expected in view of this behavior, is shown by flash photolysis not to occur for the systems biphenyl–NH_4CNS and biphenyl–$N(C_2H_5)_4Br$, although it may be operative to a limited extent for the system biphenyl–KI. A mechanism which accounts for these experimental observations is suggested.

The fluorescence of many organic compounds in solution is quenched by the addition of inorganic salts. The anion of the salt is generally regarded as the species responsible for the quenching process; the commonly accepted mechanism is formulated as a transfer of an electron from the anion to the electronically excited molecule, followed by a reverse electron-transfer reaction which leads to the system in its original unexcited state.[1,2]

$$\begin{array}{ccc} {}^1M^* + A^- & \longrightarrow & M^{\cdot -} + A^{\cdot} \\ \downarrow & & \downarrow \\ M + h\nu & & M + A^- \end{array} \qquad (1)$$

Recently, evidence has become available which appears to provide support for the mechanism outlined above. An investigation of the quenching of the fluorescence of a number of dyestuffs has shown that the quenching efficiency of inorganic anions shows a trend which parallels the trend in the oxidation potentials of the anions used as quenchers.[3] In addition, a semiquinone intermediate, apparently resulting from an oxidation-reduction process, has been identified in the quenching of benzhydroquinone fluorescence by the cobalticyanide anion.[4]

In some cases, however, doubt has been expressed as to whether electron-transfer mechanism 1 is generally applicable. The quenching action of iodide and bromide ions has been attributed to a heavy-atom enhancement of the intersystem crossing rate,[5,6] and an alternative general mechanism for fluorescence quenching by inorganic anions, in which an interaction depending on the polarizability of the inorganic anion leads to the disappearence of the fluorescing state, has been proposed.[7] On the other hand, the quenching of anthracene fluorescence by inorganic anions, including iodide and bromide, was recently shown not to occur by heavy atom perturbation of the spin–orbit coupling and it was postulated that fluorescence quenching takes place *via* an electron transfer mechanism.[8] In view of the confusion surrounding this topic, it seemed advisable to investigate the mechanistic details of this type of fluorescence quenching in more detail, focussing attention on polynuclear aromatics, the chemical and spectroscopic properties of which have been well characterized. This note reports the result of an investigation of the quenching of biphenyl fluorescence by inorganic anions.

Experimental Section

Biphenyl (Schuchardt) was recrystallized several times from ethanol and zone refined. Tetrahexylammonium

(1) Th. Forster, "Fluoreszenz Organischer Verbindungen," Vandenhoeck and Ruprecht, 1951.
(2) L. E. Orgel, *Quart. Rev., Chem. Soc.*, 422 (1954).
(3) D. K. Majumdar, *Z. Phys. Chem.*, **217**, 200 (1961).
(4) J. Feitelson and N. Shaklay, *J. Phys. Chem.*, **71**, 2582 (1967).
(5) A. R. Horrocks, T. Medinger, and F. Wilkinson, *Photochem. Photobiol.*, **6**, 21 (1967).
(6) H. Leonhardt and A. Weller in "Luminescence of Organic and Inorganic Materials," H. P. Kallman and G. M. Spruch, Ed., Wiley, New York, N. Y., 1962.
(7) J. Glowacki, *Bull. Acad. Pol. Sci.*, **11**, 487 (1963).
(8) R. Beer, K. M. C. Davis, and R. Hodgson, *Chem. Commun.*, 840 (1970).

chloride, tetrabutylammonium perchlorate, and tetrabutylammonium nitrate were purified by recrystallization from ethanol; tetraethylammonium bromide (Fluka purum) and ammonium thiocyanate (Merck pro analysi) were recrystallized several times from acetonitrile, and potassium iodide (Merck Suprapur) was used without further purification. The solvent used in this work, acetonitrile, was prepared from Merck Uvasol acetonitrile by distillation from P_2O_5. The experimental details relating to the fluorescence quenching and flash measurements have been described elsewhere;[9] the experimental arrangement used made possible the insertion of filter solutions or glass filters between the flash lamps and the sample, in order to ensure that the exciting light was absorbed exclusively by the fluorescer, in this case biphenyl. This was of considerable importance, as direct excitation of the inorganic anion led to electron ejection,[10] which resulted in the formation of biphenyl radical anions independently of the quenching process. This could be avoided in the flash experiment with $N(C_2H_5)_4Br$ as quencher only by using a relatively high concentration of biphenyl and could not be completely eliminated in the system biphenyl-KI. The biphenyl radical anions formed by flashing these systems without any cut-off filters were relatively stable, having lifetimes of ~0.3 msec. In all fluorescence quenching experiments excitation occurred at 315 nm, with the exception of nitrate, which was excited at 270 nm at a quencher concentration <0.02 *M*.

Results and Discussion

Table I shows the measured quenching constants for the quenching of biphenyl fluorescence in acetonitrile by a range of inorganic salts. The corresponding rate constants k have been calculated from the quenching data using a value of 16 nsec for the lifetime of the first excited singlet state of biphenyl.[11] In Table I are also shown values of k, taken from ref 8, for the quenching of anthracene fluorescence by inorganic anions in acetonitrile solution.

The fluorescence quenching efficiency, according to the reaction 1, will depend on the magnitude of the free energy change associated with the transfer of an electron from the anion to the electronically excited aromatic molecule. By analogy with the case where A is a neutral acceptor or donor, this will be given by

$$\Delta G_q = (E_{1/2}(A^-/A) - E_{1/2}(M^-/M)) - \Delta E \quad (2)$$

where $E_{1/2}(A^-/A)$ and $E_{1/2}(M^-/M)$ are the polarographic half-wave potentials corresponding to the one-electron reduction processes

$$M + e \longrightarrow M\cdot^- \quad \text{and} \quad A\cdot + e \longrightarrow A^- \quad (3)$$

respectively, and ΔE is the energy of the first excited singlet state. The quantity $E_{1/2}(A^-/A)$ is somewhat difficult to estimate for inorganic anions in acetonitrile and the establishment of a direct correlation between ΔG_q and k is for this reason not possible. However, the quantity $-E_{1/2}(M^-/M) - \Delta E$ (referred to hereafter as $\Delta G'$) can be used as a basis for comparison of the quenching data for the two fluorescing substances; values of −1.63 eV for biphenyl and −1.32 eV for anthracene are obtained. These values are a measure of the ability of the molecule in the excited state to accept an electron, *i.e.*, they represent the excited state reduction potentials of biphenyl and anthracene.

TABLE I: Fluorescence Quenching Constants K and Fluorescence Quenching Rate Constants k for Biphenyl and Anthracene in Acetonitrile

	Biphenyl		Anthracene
Salt	K,[a] M^{-1}	10^9k,[b] M^{-1} sec^{-1}	10^9k,[c] M^{-1} sec^{-1}
$N(C_4H_9)_4ClO_4$	2.6	0.16	
$N(C_6H_{13})_4Cl$	11.3	0.71	0.095
$N(C_4H_9)_4NO_3$	117	7.3	
$N(C_2H_5)_4Br$	80.4	5.0	1.9
NH_4SCN	138	8.6	3.5
KI	195	12.2	11

[a] Determined (with the exception of KI) in air-saturated solution and corrected for fluorescence quenching by O_2. [b] Calculated assuming τ = 16 nsec for the biphenyl first excited singlet state. [c] From ref 8.

Table I shows that there is, in fact, a correlation between k and the excited state reduction potential for all anions for which data are available, with the single exception of iodide. Fluorescence quenching by chloride, bromide, and thiocyanate occurs more efficiently for biphenyl than for anthracene, which, in view of the higher value of $\Delta G'$ for biphenyl than for anthracene, suggests that the electron-transfer step of reaction 1 determines the efficiency of the quenching process. The similar values of k for the iodide quenching of biphenyl and anthracene probably result from the fact that quenching is diffusion controlled in these two cases, which would mask a possible dependence on $\Delta G'$.

If mechanism 1 really is the process leading to fluorescence quenching, the radical anion of biphenyl can reasonably be expected to be identifiable as an intermediate. To this end we have determined, using conventional flash photolysis techniques, the transient absorption spectra of the systems biphenyl-KI, biphenyl-$N(C_2H_5)_4Br$, and biphenyl-NH_4SCN under pulsed light excitation; these are shown in Figures 1 and 2.[10,12,13] It should be noted that the quencher concentrations in these experiments were chosen to ensure that more than 90% of the primarily excited molecules disappeared *via* the quenching process. This requirement meant that analogous experiments with the less soluble salts $N(C_4H_9)_4NO_3$, $N(C_6H_{13})_4Cl$, and $N(C_4H_9)_4ClO_4$ could not be carried out.

The triplet-triplet absorption spectrum of biphenyl can, in all three cases, be identified as a component of the transient absorption spectrum.[14] Since the spectra have been obtained under conditions where the biphenyl fluorescence is almost completely quenched, the relatively high yields of triplets indicate that a major pathway for the quenching reaction is one leading to the formation of triplets. A surprising feature, however, is that no formation of the radical anion of biphenyl appears to take place for the systems with bromide and thiocyanate as quenchers. If this species were present, a sharp peak at 24.5 kK would

(9) K. H. Grellmann, A. R. Watkins, and A. Weller, *J. Phys. Chem.*, **76**, 469 (1972).
(10) J. Jortner, M. Ottolenghi, and G. Stein, *J. Phys. Chem.*, **68**, 247 (1964).
(11) I. B. Berlman, "Handbook of Fluorescence Spectra of Aromatic Molecules," Academic Press, New York, N. Y., 1971.
(12) D. Rehm and A. Weller, *Isr. J. Chem.*, **8**, 259 (1970).
(13) P. Balk, G. J. Hoijtink, and J. W. H. Schreurs, *Recl. Trav. Chim. Pays-Bas*, **76**, 813 (1957).
(14) We are unable to explain the shift to shorter wavelengths of the biphenyl triplet spectrum in the flash spectrum of the system biphenyl-tetraethylammonium bromide; this effect only appears at high concentrations of biphenyl.

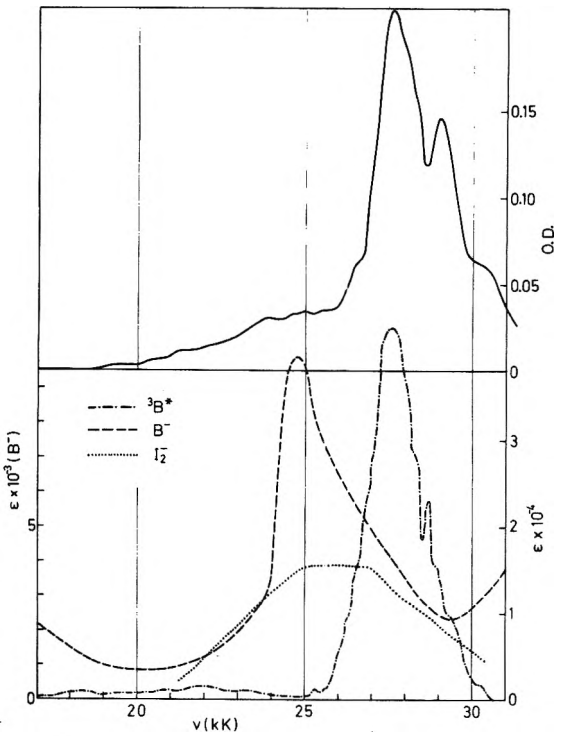

Figure 1. Transient absorption spectrum (upper half of diagram) obtained on flashing biphenyl (2.27×10^{-3} *M*) with KI (0.0475 *M*) in acetonitrile (filter solution: 0.5 *M* KI in H_2O). The sources for the spectra of the intermediates shown in the lower half of the diagram are as follows: biphenyl radical anion from ref 13, the I_2^- ion from ref 19.

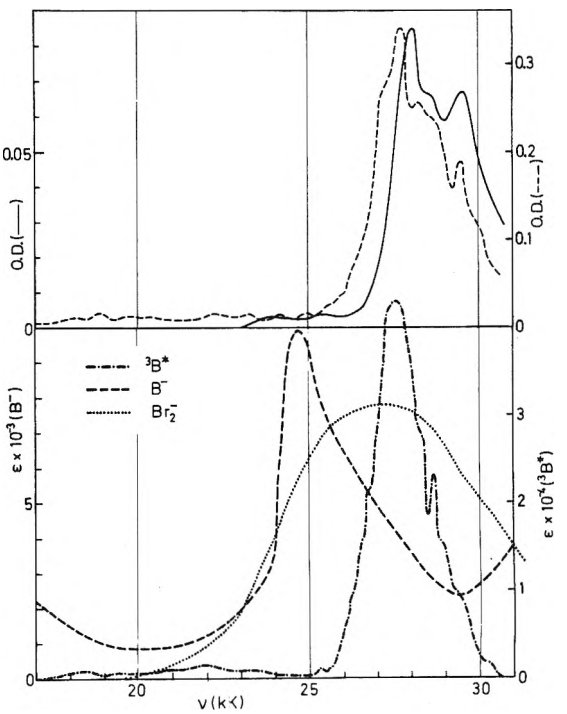

Figure 2. The upper half of the diagram shows transient absorption spectra obtained on flashing biphenyl (0.10 *M*) with tetraethylammonium bromide (5.00×10^{-2} *M*) in acetonitrile (solid curve, filter Schott WG 305); and on flashing biphenyl (2.00×10^{-3} *M*) with ammonium thiocyanate (0.20 *M*) in acetonitrile (dashed curve, 0.1 *M* NH_4CNS in EtOH as filter). The lower half of the diagram shows the spectra of possible intermediates; the Br_2^- spectrum is taken from ref 19.

be expected to be visible in the experimentally obtained transient spectrum; in fact, there is virtually no absorption in this region with the systems biphenyl-NH_4 CNS and biphenyl-$N(C_2H_5)_4Br$. The system biphenyl-KI shows a weak tail in this region, for which there are two possible explanations. One is to regard this broad absorption as being due to the I_2^- ion and (masked by the I_2^- absorption) the biphenyl radical anion, both resulting from an electron transfer in the excited state (reaction 1, subsequent reaction of the iodine atoms so produced with I^- forms I_2^-). However, this assignment is not unambiguous, and an alternative interpretation of this result would attribute the absorption to the difficulty of exciting biphenyl without simultaneously irradiating the iodide ion; this will presumably lead to the formation of I_2^- by electron ejection independently of the quenching process.[10]

$$I^- \longrightarrow I\cdot + e$$
$$I\cdot + I^- \longrightarrow I_2^- \qquad (4)$$

The lifetime of this broad absorption (~0.7 msec) is longer than those of the triplet (0.6 msec) and of the radical anion of biphenyl produced directly by electron ejection (0.3 msec), and agrees approximately with the lifetime of I_2^- (~0.8 msec) formed by electron ejection, suggesting that the species I_2^- is the main component of this absorption. The source of this absorption around 25 kK in the flash spectrum must therefore remain something of an open question. However, it is clear that radical ion formation is negligible in the systems biphenyl-NH_4CNS and biphenyl-$N(C_2H_5)_4Br$.

There are a number of reasons which could account for the failure to detect radical anion formation in the flash experiments with ammonium thiocyanate and tetraethylammonium bromide. One is the possible instability of the biphenyl radical anion under these experimental conditions; however, flashing the same sample without filters (see above) showed that the biphenyl radical anion decayed with a half-time which should have allowed its detection. Another explanation, also consistent with the electron transfer hypothesis, is that a rapid reverse electron transfer occurs after the initial electron transfer, before the two species have had time to diffuse apart. However, experiments with other systems[6,9] where ion formation from the quenching reaction is known to be energetically possible have shown that formation of the free ions from the initially formed ion pair does occur. There appears to be no way of reconciling these results with the electron-transfer mechanism previously proposed for this type of fluorescence quenching.[8] A mechanism based on heavy-atom perturbation, by the quenching ion, of the spin-orbit coupling in $^1M^*$ would explain why no biphenyl radical ions can be detected in the flash experiments, but offers no explanation of why a correlation between k and $\Delta G'$ is found, or why, for example, quenching in the system biphenyl-$N(C_4H_9)_4NO_3$ is more efficient than in the system biphenyl-$N(C_2H_5)_4Br$.

We would like to propose a third mechanism, which could provide a possible explanation of these results. The collision complex, which, regardless of the subsequent mechanism, will always be primarily formed, can be regarded as containing contributions from electron-transfer states such as $(M^- \cdots A\cdot)$. The extent of mixing of these states will be, by first-order perturbation theory,[15] in-

(15) H. F. Hameka, "Advanced Quantum Chemistry," Addison-Wesley, Reading, Mass., 1965.

versely proportional to the energy difference between the collision complex and the electron-transfer states being mixed in. This can be formulated as

$$\Psi(^1M...A^-) = \Psi^0(^1M...A^-) + \sum_i C_i\Psi_i(M\cdot^-...A\cdot)$$

where

$$C_i = \left(\frac{\langle\Psi_i(M\cdot^-...A\cdot)|H'|\Psi^0(^1M^*...A^-)\rangle}{E^0(^1M^*...A^-) - E_i(M\cdot^-...A\cdot)}\right)$$

where $E^0(^1M^*\cdots A^-)$ and $E_i(M\cdot^-\cdots A\cdot)$ are the energies of the collision complex (approximately the energy of $^1M^*$) and the higher lying electron-transfer states i, respectively, and H' is a perturbation operator. If it is assumed that mixing in of the states $\Psi_i(M\cdot^-\cdots A\cdot)$ brings about a coupling of the initial state (singlet) with the final state (triplet),[16] then the dependence of the quenching rate on $\Delta G'$ can be explained by the form of the denominator in the expression for C_i. This interpretation has close affinities with the mechanism proposed by Tsubomura and Mulliken[17] for fluorescence quenching by oxygen, and is supported by the observation of Tournon and El-Bayoumi[18] that interaction between the alkyl substituent and the aromatic ring in a series of phenylalkyl compounds leads to an enhancement of intersystem crossing having charge-transfer character. We are hoping to explore this problem further by investigating the range of validity of the correlation between the quenching efficiency and $\Delta G'$.

Acknowledgments. Thanks are due to Mrs. S. Reiche for valuable assistance with the experimental work, and to Dr. W. Kühnle for the purification of the solvent used in this work.

(16) J. N. Murrell, *Mol. Phys.*, **3**, 319 (1960).
(17) H. Tsubomura and R. S. Mulliken, *J. Amer. Chem. Soc.*, **82**, 5966 (1960).
(18) J. Tournon and M. A. El-Bayoumi, *J. Chem. Phys.*, **56**, 5128 (1972).
(19) L. I. Grossweiner and M. S. Matheson, *J. Phys. Chem.*, **61**, 1089 (1957).

Recoil Tritium Reactions with Cyclobutanone. A Test for Electronically Excited Products of the T-for-H Substitution Reaction[1]

G. Izawa, Edward K. C. Lee, and F. S. Rowland*

Department of Chemistry, University of California, Irvine, California 92664 *(Received September 27, 1972)*

Publication costs assisted by the Division of Research, United States Atomic Energy Commission

The possibility of the formation of electronically excited molecules in hot atom reactions has been evaluated for T-for-H substitution reactions with gas-phase cyclobutanone (c-C_3H_6CO). Measurements of relative yields *vs.* pressure show that highly excited c-$C_3H_5TCO^*$ molecules decompose by two separate mechanistic pathways, with the formation either of C_2H_3T plus CH_2CO or of c-$C_3H_5T^*$ plus CO. The yields of tritiated C_3 products are slightly larger than anticipated from the energetic decomposition of vibrationally excited ground state c-C_3H_5TCO, and an upper limit of 10% has been estimated for the fraction of c-C_3H_5TCO formed in any of the excited electronic states. The median vibrational energy is estimated to be 3–4 eV, somewhat less than the 5 eV estimated for T-for-H substitution reactions with c-C_4H_8. The chief other products from hot T* reactions with c-C_3H_6CO are HT and several radicals originating with ring-opening attack of T* on the ring C–C bonds. The ratio of HT/c-C_3H_5TCO is ~1.8 for cyclobutanone, leading to an estimate of ~95 kcal/mol for the average C–H bond dissociation energy in c-C_3H_6CO.

Introduction

Energetic tritium atoms from nuclear recoil[2] substitute into organic molecules by the replacement of H, as in (1),

$$T^* + RH \longrightarrow RT^* + H \qquad (1)$$

with the formation of highly excited parent molecules, RT*. These molecules are sufficiently excited to undergo secondary decomposition unless first stabilized by deexcitation in collisions with the other molecules of the medium. The primary decomposition mechanisms observed for such excited molecules are usually the same as those found for thermal excitation of the parent molecules, although additional decomposition pathways with higher excitation energies are also frequently to be found. In most instances, such recoil tritium experiments have provided no information as to which electronic states of the parent molecule are involved, and the assumption has frequently been made from the similarity in decomposition mechanisms—and for lack of any contradictory experimental evidence—that the excited recoil tritium product normally has high vibrational and/or rotational energy in

(1) This research was supported by Contract No. AT-(04-3)-34, Agreement No. 126, U. S. Atomic Energy Commission.
(2) For a recent general discussion of hot atom chemistry in recoil tritium systems, see F. S. Rowland in "Molecular Beams and Chemical Kinetics," C. Schlier, Ed., Academic Press, New York, N. Y., 1970, pp 108–137.

the ground electronic state. In an effort to get additional information about the possible formation of products in excited electronic states in these reactions, we have now studied the substitution of energetic tritium atoms into cyclobutanone, as in (2), together with the subsequent secondary decompositions. (Asterisks are used to designate tritium atoms with excess kinetic energy, and molecules with excess excitation energy without specification of the form of energy.)

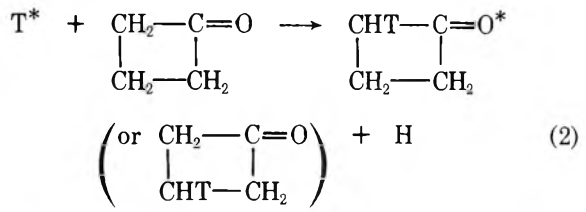

The thermal decomposition of cyclobutanone from the vibrationally hot ground electronic state (S_0*) has been shown to lead almost entirely to ethylene plus ketene (99.5%), plus the minor route through cyclopropane and CO (0.5%), as in (3) and (4).[3] In contrast, the decomposition from the first excited triplet state (T_1) leads only to the formation of hot cyclopropane, as in (4).[4] Unless first collisionally stabilized, the hot cyclopropane can then isomerize to propylene, as in (5).

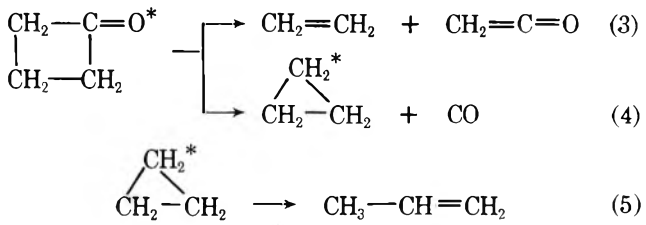

Decomposition from the vibrationally hot first excited singlet electronic state (S_1*) has been shown to give both (3) and (4) with a product ratio, $\Sigma C_3/(CH_2{=}CH_2)$, varying from 0.4 to 0.8 with increasing energy,[5] indicating semiquantitatively that an appreciable yield of C_3 can be anticipated if this state is involved. The mechanisms of the decompositions from the upper excited singlet states are complex,[6] but this should not seriously hamper the investigation of the possible presence of electronically excited molecules among the products from such recoil tritium substitution reactions, since both the lowest triplet and the lowest excited singlet states each give from 30 to 100% C_3 products. Basically, the only known mode of decomposition of cyclobutanone which fails to give a substantial yield of C_3 hydrocarbon products is the thermal pyrolysis of the ground-state singlet. While higher rotational/vibrational excitation of the ground state singlet does increase the C_3 yields, they remain relatively small, much less than from excited state decompositions.

Our positive observation of relatively small yields of such C_3 products, as described below, is approximately at the limits of error for our estimate of expected C_3 yields from ground-state singlet molecular reactions. Therefore, we are able to conclude that excited electronic states are of at most minor importance, but with an estimated upper limit on such participation that is not too restrictive ($\leq$ about 10%).

By analogy with other recoil systems,[2] the major additional reactions of energetic tritium atoms with cyclobutanone should include hydrogen abstraction (6) and substitution at the C–C bonds with ring opening to an excited radical. Smaller radicals and molecules should also be expected from decomposition of the excited radicals formed in the primary substitution reactions (7a) to (7d).

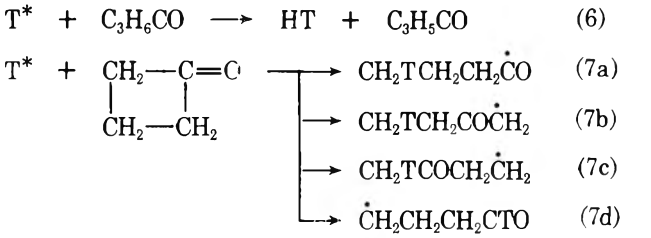

Experimental Section

Pressure Studies. Much of the information about secondary decomposition reactions in energetic tritium systems is usually obtained through examination of the variations in relative product yields with pressure.[2,7] Experimental complications arise for such studies with cyclobutanone because of its low vapor pressure at room temperature (38.3 Torr at 295.9°K).[5a] Nuclear reactor irradiations at higher temperatures are possible, but they introduce several complexities of other kinds. Accordingly, we have made our pressure-dependent studies with added concentrations of argon from 0 to 1400 Torr. These variable ratios of argon/cyclobutanone must also involve difficulties from the possible changes in the moderator characteristics of the systems, with consequent uncertainty in the tritium energy distributions being sampled from one pressure range to another. The range of available pressures is limited on the lower side by the necessity that sufficient material be present in the gas phase to dissipate the initially high energy of the tritium atoms from nuclear recoil.[8]

The experiments were carried out with energetic tritium atoms from the nuclear reaction $^3He(n, p)T$. Most of the procedures were routine,[9] and have been described in detail before. The particular experimental alterations for cyclobutanone systems are given below.

Chemicals. Cyclobutanone (Aldrich Chemical Co.) was purified by preparative gas chromatography using a 50-ft Carbowax 20-M column at 80°. The earliest samples contained ~1% acetone as an impurity, which was not present in the later samples; no difference was observed in the yields of products (except for the yield of acetone-*t*) between the acetone-free samples and the others.

Argon (Matheson), H_2S (Matheson), and O_2 were used without further purification. ^3He (Monsanto Research Co.) was free from radioactive impurities.

Sample Preparation. The pressure of cyclobutanone was maintained between 25 and 35 Torr because of its low vapor pressure. The other components always included ^3He (9–15 Torr) and O_2 (20–25 Torr). Pressures above 60 Torr were obtained by the addition of as much as 1400

(3) (a) M. N. Das, T. D. Coyle, and W. D. Walters, *J. Amer. Chem. Soc.*, **76**, 6271 (1954). $A = 3.6 \times 10^{14}$ sec^{-1}; $E_{act} = 52.0$ kcal/mol; (b) A. T. Blades, *Can. J. Chem.*, **47**, 615 (1969). For the C_3 pathway, $A \cong 2.3 \times 10^{14}$ sec^{-1} and $E_{act} = 58.0$ kcal/mol.
(4) H. O. Denschlag and E. K. C. Lee, *J. Amer. Chem. Soc.*, **90**, 3628 (1968).
(5) (a) G. B. Kistiakowsky and S. W. Benson, *J. Amer. Chem. Soc.*, **64**, 80 (1942); (b) N. E. Lee and E. K. C. Lee, *J. Chem. Phys.*, **50**, 2094 (1969), and references therein.
(6) (a) J. C. Hemminger, C. F. Rusbult, and E. K. C. Lee, *J. Amer. Chem. Soc.*, **93**, 1867 (1971); (b) J. C. Hemminger and E. K. C. Lee, *J. Chem. Phys.*, **56**, 5284 (1972); (c) R. Shortridge, Jr., W. Yang, and E. K. C. Lee, *Mol. Photochem.*, **1**, 325 (1969).
(7) (a) E. K. C. Lee and F. S. Rowland, *J. Amer. Chem. Soc.*, **85**, 897 (1963); (b) Y.-N. Tang and F. S. Rowland, *J. Phys. Chem.*, **72**, 707 (1968).
(8) J. W. Root and F. S. Rowland, *Radiochim. Acta*, **10**, 104 (1968).
(9) J. K. Lee, E. K. C. Lee, B. Musgrave, Y.-N. Tang, J. W. Root, and F. S. Rowland, *Anal. Chem.*, **34**, 741 (1962).

Torr of argon. The samples used for analysis of the location of tritium within propylene-*t* had higher than usual concentrations of ^{3}He (25 Torr) in order to increase the total amount of tritium available in the system.

Radiochemical Analysis. The separation of the various products and their assay for tritium activity was carried out by conventional radio gas chromatography with metal internal flow proportional counters. The entire radio gas chromatographic system from injection through counting was maintained at 80–100° by wrapping all of the components with heater tape. The metal counters used in this work showed a plateau more than 200 V long at 112°, with no quenching of counting during the passage of cyclobutanone or other oxygen-containing compounds under these experimental conditions.

A variety of chromatographic columns was used during this work. The oxygen-containing species were analyzed with the 50-ft Carbowax 20-M column at 80°, while most of the hydrocarbons were separated with dimethylsulfolane (60 ft at 23°) or acetonylactone (80 ft at 0°) columns. The C_2 hydrocarbons were separated from one another with a column of propylene carbonate on alumina (50 ft at 0°); HT from ^{41}Ar with 10-X molecular sieve (50 ft at 25°); and HT from CH_3T with activated charcoal (5 ft at 25°). The separation of the propylene-*t* into alkyl- and olefinically tritiated components was performed with a 400-ft silver nitrate–ethylene glycol column at 0°.[10]

Results and Discussion

Reaction Products. Recoil tritium atoms react with cyclobutanone to form the simple expected products (HT, cyclobutanone-*t*, c-C_3H_5T, propylene-*t*, CH_2=CHT), as well as many other tritiated compounds both in unscavenged systems and in the presence of either O_2 or H_2S as a scavenger molecule. The multiplicity of labeled products is illustrated in Figures 1 and 2. While most of the volatile compounds, especially the hydrocarbons, have been identified, a number of less-volatile tritium-labeled species, most of them probably oxygen-containing molecules, have not. It is quite apparent, then, that we have only a partial understanding of the full complexity of recoil tritium reactions with cyclobutanone.

The observed relative yields in several experiments are shown in Table I for the tritiated hydrocarbons and some known oxygenated species. Highly unsaturated products such as allene-*t* and acetylene-*t* are regularly found in low yield as the consequence of continued decomposition of the most highly excited labeled molecules formed in the system. The saturated products and C_5 or C_6 hydrocarbons which required radical combination reactions for formation are diverted by O_2 scavenger into other, unidentified but presumably oxygenated, species. The experiments with H_2S as scavenger showed the presence of C_3H_6T, CH_2TCH_2, and CH_2T radicals through the formation of the corresponding alkane-*t* molecules. These tritiated alkyl radicals can readily originate from the decomposition of the ring-opened radicals formed in (7a) to (7c), respectively.

Pressure Dependence of Product Yields. If the decomposition of excited cyclobutanone-*t* into (a) ethylene plus ketene, or (b) cyclopropane plus carbon monoxide occurs through any states with lifetimes of about 10^{-9} to 10^{-10} sec, then a complementary pressure dependence should be observed, with cyclobutanone-*t* increasing in yield with increased pressure and ethylene-*t* and the C_3H_5T molecules decreasing in yield. The pressure dependence of the

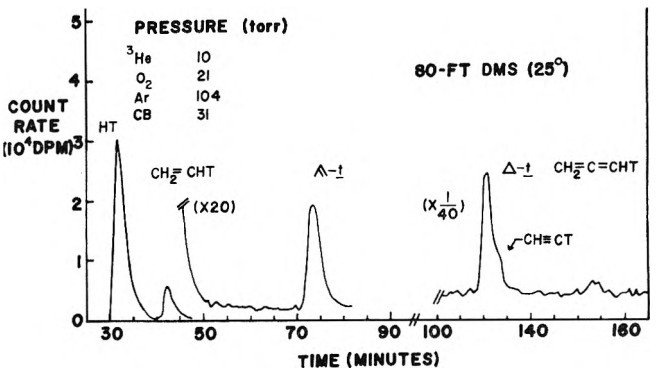

Figure 1. Radio gas chromatogram of tritiated hydrocarbon products on 80-ft DMS column at 25°.

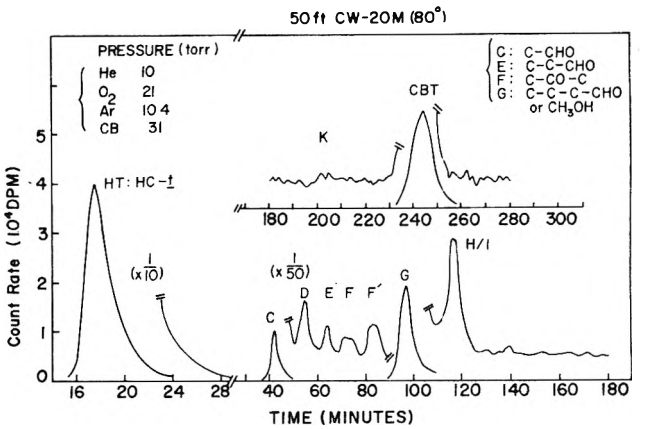

Figure 2. Radio gas chromatogram of tritiated oxygenated products on 50-ft carbowax-20M column at 80°.

product yields is shown in Figure 3 for the O_2-scavenged system. A small pressure dependence of the surviving cyclobutanone-*t* fraction $[S/(S + D)]$[11] is shown in Figure 4. In this graph, all of the cyclobutanone data have been plotted on the assumption that argon is only 0.25 times as efficient as cyclobutanone itself. The data for $S/(S + D)$ following the substitution of T-for-H in cyclobutane are also included on the graph for comparison.[7a]

The data have not been corrected for the yield of C_2H_3T from other reactions, *e.g.*, $CH_2TCH_2COCH_2^* \rightarrow CH_2TCH_2^* \rightarrow CHT{=}CH_2$. Such reactions are similar to those found with $CH_3CH_2CH{=}CD_2$ as the substrate through the sequence $CH_2TCH_2CH{=}CD_2 \rightarrow CH_2TCH_2^* \rightarrow CHT{=}CH_2$,[12] and the yields are assumed to be both (a) small; and (b) essentially pressure-independent.

The very large change in moderating conditions from pure cyclobutanone at 30 Torr to argon–cyclobutanone mixtures at 1400 Torr/30 Torr will not only substantially reduce the yields of all "hot" products[13] but may also decrease the average kinetic energy of the T atom at the time of substitution, and therefore the average excitation

(10) E. K. C. Lee and F. S. Rowland, *Anal. Chem.*, **36**, 218 (1964).
(11) S = stabilization = [cyclobutanone-*t*]. D = decomposition = $\frac{3}{2} \times [C_2H_3T]$. Since $\frac{1}{3}$ of the methylene groups in cyclobutanone are converted to ketene by reaction 3, the observed CH_2=CHT yield was multiplied by $\frac{1}{2}$ in estimating the fractional decomposition of the parent molecule through this pathway. The C_3 products were not originally included in this calculation; subsequent evaluation of their yields indicated only minor quantitative changes and no qualitative effects.
(12) E. K. C. Lee and F. S. Rowland, *J. Phys. Chem.*, **74**, 439 (1970).
(13) The "pure" cyclobutanone samples were already moderated slightly by the 10–15 Torr of ^{3}He added as the source of the tritium atoms. The moderating efficiency of ^{3}He is probably about 4 times that of ^{40}Ar.

TABLE I: Distribution of Radioactive Products Following Reactions of Recoil Tritium Atoms with Cyclobutanone[b]

		Gas[a] pressure, Torr			
^3He		10	12	9	15
CB		31	34	34	36
Ar		187	207	103	180
O_2		21	23	0	0
H_2S		0	0	26	0
Yields of Tritium-Labeled Products (Parent-*t* = 100)					
HT		457	457	~1450	
CH_3T		...	...	190	884
Ethane-*t*		...	...	17	
Ethylene-*t*		86	87	107	
Propane-*t*		...	...	7	68
Propylene-*t*		18	17	32	28
n-Butane-*t*		...	...	...	30
Cyclopropane-*t*		15	11[c]	15[c]	20
Acetylene-*t*		...	4	2	
1-Butene-*t*		...	...	...	13
Allene-*t*		1	1	...	11
n-Pentane-*t*		...	...	...	3
1-Pentene-*t*		...	...	...	7
Isopentane-*t*		...	...	...	2
1,5-Hexadiene-*t*	B	...	...	...	10
Acetaldehyde-*t*	C	17	16	~20	15
	D	7	6	...	2
Propionaldehyde-*t*	E	2	3	...	9
Acetone-*t*	F	3	2	...	9
	F′	3	4	...	...
n-Butyraldehyde-*t* or CH_2TOH	G	51	51	...	13
	H	14	13	...	8
	I			...	4
	J	1	...	...	4
	K	2	1	...	3
	c-C_3H_5TCO	(100)	(100)	(100)	(100)
	M	...	...	...	15
$\Sigma_{Hydrocarbons}$		577	577	1820	1066
$\Sigma_{Oxygenated}$		200	196	120	192
Total		777	773	1940	1268

[a] One sample was analyzed for hydrocarbons; a second sample with essentially identical composition was analyzed for oxygenated products. [b] Unless specified otherwise, the hydrocarbon separation was carried out with the DMS column and the oxygenated molecules were separated on the Carbowax 20M column. [c] The 80-ft ACTN column was used to separate CH≡CT from c-C_3H_5T.

energy of the T-for-H product. At the highest pressure of argon, the fractional decomposition of cyclobutanone-*t* could thus be anticipated to be at a minimum for two reasons: (i) shorter time prior to collision and stabilization for excited molecules and/or (ii) lower average excitation energy following the primary substitution reaction.

The small magnitude of the pressure dependence, however, suggests that the average residual excitation energy of cyclobutanone-*t* is changed slightly, if at all, by the variation in argon/cyclobutanone ratio from zero to more than 45. In similar argon moderation studies, the absolute hot yields of HT and CH_3T from recoil tritium reactions with CH_4 are reduced by about a factor of 20, while the HT/CH_3T ratio is varied by only about 30%.[14] It is likely that the energy ranges for possible reaction, as well as the distribution of reactions over these ranges, are quite different for the formation of HT and CH_3T. Consequently, if hot reactions of such different character are affected

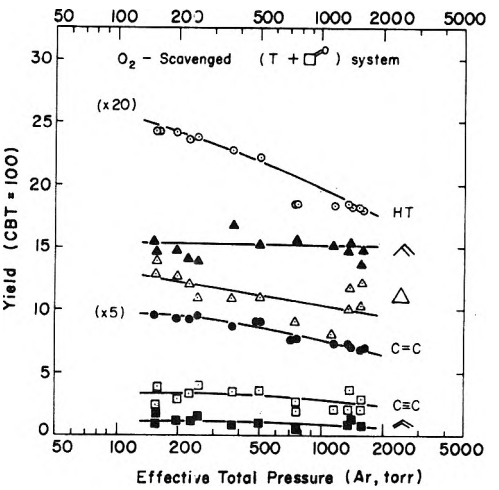

Figure 3. Pressure dependence of tritiated products in O_2-scavenged cyclobutanone: O, HT (reduced by 20); O, C_2H_3T (reduced by 5); ▲, propylene-*t*; △, c-C_3H_5T; □, CH≡CT; ■, CH_2=C=CHT.

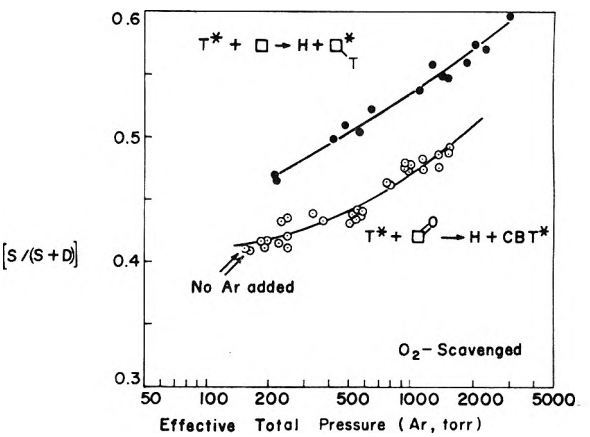

Figure 4. Fractional stabilization *vs.* pressure for cyclobutane-*t* and cyclobutanone-*t* (expressed in equivalent pressure of argon; relative collision efficiencies: Ar, 0.25; c-C_4H_8, 1.0; c-C_3H_6CO, 1.0.); ●, c-C_4H_7T; O, c-C_3H_5TCO.

only by 30% in relative yield, it is a quite plausible hypothesis that the *median* energy for formation of CH_3T by substitution—and by inference, cyclobutanone-*t*—will hardly be affected by the change in moderating conditions. Put alternatively, it seems easier to moderate hot tritium atoms completely to thermal energies, avoiding all hot reactions, than to alter appreciably the relative distribution of excitation energies from those T-for-H substitution reactions which actually occur.

The vibrationally hot cyclopropane-*t* formed by decomposition of an electronically excited cyclobutanone-*t* might also be expected to show a complementary pressure dependence for cyclopropane-*t* and propylene-*t*, as in (5). However, as illustrated in Figure 5,[15] the relative yield of these two products is essentially independent of pressure over the wide range investigated. The significance of the numerical value for the ratio of yields for the two C_3 molecules, and of the constancy of this ratio with pressure, is partially clouded by the expectation that some propylene-

(14) D. Seewald and R. Wolfgang, *J. Chem. Phys.*, **47**, 143 (1967).
(15) Deactivating efficiencies of He, O_2, Ar, and cyclobutanone were taken to be 0.05, 0.25, 0.25 and 1.0, respectively, per unit pressure. Data were taken from ref 5b and from unpublished work by J. Metcalfe, H. A. J. Carless, and E. K. C. Lee.

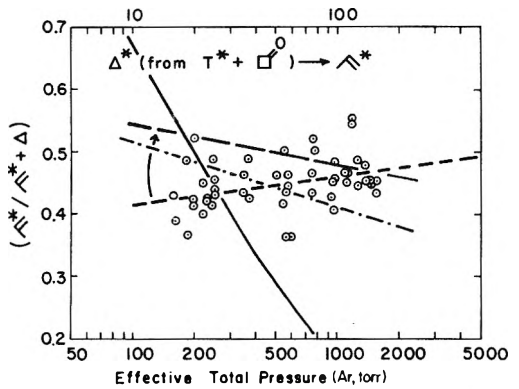

Figure 5. Yield ratio as function of pressure for propylene-*t* vs. ΣC_3 products: O, observed ratios; - - -, approximate fit to experimental data; – –, approximate fit adjusted for C_3 products "lost" at low pressure; —, pressure dependence for decomposition of monoenergetic molecules; —·—·, typical pressure dependence for broad distribution of excitation energies.

TABLE II: Intramolecular Distribution of Tritium in Propylene-*t* from T* + Cyclobutanone

Pressure[a] of Ar, Torr	(Alkyl-*t*/olefinic-*t*)	% Alkyl-*t*	% Propylene-*t*[b] from c-C_3H_5T decomp
0	1.9_2	66	59
0	1.8_5	65	60
80	1.7_5	64	63
400	1.9_5	66	58
400	1.7_4	64	63
400	1.8_9	65	60
800	1.7_7	64	62
1100	1.9_2	66	59
Average	1.85 ± 0.06	65 ± 1	61 ± 2

[a] Samples contained (Torr in parentheses) in addition to argon: ^3He (10–15), cyclobutanone (30–35), O_2 (10–20). [b] The propylene-*t* from c-C_3H_5T decomposition is assumed to be 42% alkyl-*t* and 58% olefinic-*t*.[15] All other propylene-*t* is assumed to be $CH_2TCH{=}CH_2$ from reactions such as (9b).

t should also be formed by the sequence (8) and (9b) following (7a). Decomposition of $CH_2TCH_2CH_2$* radicals by the lower activation energy path (9a) can also be expected and probably contributes to the CH_2T radical yield identified through the H_2S scavenger experiments (Table I).

$$CH_2TCH_2CH_2CO^* \longrightarrow CH_2TCH_2CH_2^* + CO \quad (8)$$

$$CH_2TCH_2CH_2^* \longrightarrow CH_2T^* + CH_2{=}CH_2 \quad (9a)$$

$$\longrightarrow CH_2TCH{=}CH_2 + H \quad (9b)$$

"Hot radical" decompositions, as in (9b), normally show negligible pressure dependence of yields in recoil tritium systems. Moreover, the propylene-*t* from (9b) always carries the tritium label in the alkyl position, while that originating from the isomerization of c-C_3H_5T* should be only 42% alkyl-tritiated.[16] Measurement of the per cent alkyl tritium in propylene-*t* is essentially pressure independent at 65 ± 1%, as shown in Table II. This per cent alkyl can originate from a mixture of 61% propylene-*t* from the isomerization of c-C_3H_5T* plus 39% $CH_2TCH_2CH_2$ from the direct ring-opening pathway shown in eq 8 and 9b. Since the 39% propylene-*t* from (9b) is pressure independent, there is still no marked pressure dependence of the yields of c-C_3H_5T* and its propylene-*t* isomerization product in the data of Figure 5.

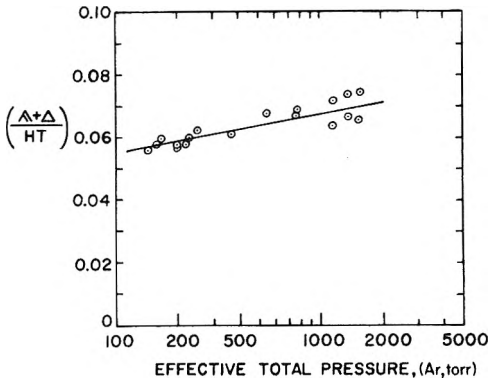

Figure 6. Relative yield *vs.* HT of summed yields of c-C_3H_5T + propylene-*t* as a function of equivalent pressure of argon.

The solid line in Figure 5 illustrates the typical ratio changes expected for a narrow band of c-C_3H_5T* excitation energies, as illustrated for a half-pressure of stabilization of 200 Torr; the data are clearly in disagreement with such an hypothesis for any half-pressure.

The HT yields in O_2-scavenged recoil tritium systems are known to be largely independent of pressure.[2] However, the observed yield ratio of (propylene-*t* + c-C_3H_5T)/(HT) increased from a value of 0.057 at 150 Torr total pressure to 0.070 at 1500 Torr total pressure, an increase of ~20%, as shown in Figure 6. This increase with pressure is probably indicative of further hot decomposition of C_3 products at low pressures, with the formation of molecules not recovered as identifiable chromatographic peaks. Decomposition of propylene-*t* *via* allylic H-elimination, as in (10), is quite feasible, if the excitation energy is greater than ~100 kcal/mol, and may well be the most important reaction involved in this low-pressure depletion of C_3 product yields.

$$CH_3CH{=}CHT^* \longrightarrow H + CH_2{=}{=}CH{=}{=}CHT \quad (10)$$

If the data of Figure 6 are used for estimating a correction for "unmeasured C_3 products" in Figure 5, *i.e.*, bringing the total C_3 yield up to 0.070 at all pressures, *and* if all of this "missing" C_3 yield is assumed to be propylene-*t* which has undergone further decomposition, then the lower pressure data points would all be shifted upward, more or less as shown for the "average" behavior symbolized by the two dotted lines. This "correction" to the observed data is, however, no more than a plausible suggestion, and is supported neither by identification of the allylic type products suggested by eq 10 nor by demonstration that such products, if found, would necessarily be obtained only by the decomposition of propylene-*t*.

The scatter in Figure 5 is large enough to conceal the moderate pressure dependence anticipated if the c-C_3H_5T* molecules were formed with a wide range of excitation energies, such as in the distributions usually found for molecules directly excited in recoil tritium substitution reactions.[2] Such a broad distribution (c-C_4H_7T* decomposition followed T-for-H in c-C_4H_8) is illustrated in Figure 5 and roughly parallels the "corrected" curve; a broad distribution shifted somewhat toward shorter lifetimes can obviously be made to fit within the limited accuracy of the data. This data scatter is larger than expected from statistical considerations alone and is also rather larger than is usually found for the ratios of randomly

(16) F. S. Rowland, C. McKnight, and E. K. C. Lee, *Ber. Bunsenges. Phys. Chem.*, **72**, 236 (1968).

chosen pairs of products in such experiments. More than usual amounts of radiation damage were done to the organic components of samples containing a high concentration of argon and a low concentration of the parent molecule. The experimental perturbations related to such radiation damage may well have contributed some additional scatter in relative yields, but we do not believe that we yet know a complete explanation for the sources of scatter in the data.

The failure to observe any appreciable pressure dependence of the relative C_3 yields over an approximately 10-fold change in collisional stabilization range must indicate that at most a small fraction of c-C_3H_5T* molecules have excitation energies corresponding to molecular lifetimes in the 10^{-9} to 10^{-10} sec range. This observation is consistent with the assumption of a very broad distribution of excitation energies, and broad distributions *are* obtained in photochemical decomposition systems, even with essentially monoenergetic excitation of the carbonyl precursor.[17] A badly skewed distribution of excitation energies would also be a possibility, but this is not a particularly persuasive rationalization. Alternatively, the observation of an approximately constant ratio of c-C_3H_5T/propylene-*t* could also be explained through the postulate of a common precursor for both. There appears to be no other experimental evidence in support of the latter speculation.

A satisfactory quantitative mechanistic explanation of the relative yields of the various C_3 products is not yet available. The evidence in Table II of substantial fractions of both alkyl- and olefinically labeled tritium in propylene-*t* indicates at least two mechanisms operative in propylene-*t* formation. The olefinically bound tritium by itself requires at least one "scrambling" mechanism, of which the c-C_3H_5T* isomerization is an important possibility. If some other mechanism—*e.g.*, a trimethylene-*t* intermediate—were also involved, then the assignment in Table II of percentage contributions of the two reaction mechanisms would, of course, be in error.

In the following section, the sum of the yields of propylene-*t* plus c-C_3H_5T is used as a diagnostic probe for the presence of c-C_3H_5TCO in either the S_1* or T_1* excited states. The uncertainties in the mechanisms of formation of the two C_3H_5T products naturally carries over into these estimates of excited electronic state participation. It should be noted, however, that we have assumed that all of the observed C_3H_5T yields should be assigned as though formed solely by reactions 4 and 5. If this assignment is incorrect, then we have overestimated the C_3H_5T yield from these reactions, and therefore of the importance of electronically excited states as products of the T-for-H reaction. As will be seen below, rather low upper limits are placed upon the importance of these electronically excited states in these reactions, and any overestimate of the C_3H_5T yields would, upon subsequent correction, only reduce these already low upper limits.

Energy Deposition in Cyclobutanone-t. The decomposition of cyclobutanone has been thoroughly studied by pyrolysis,[3] photolysis,[5,6] and photosensitization.[4] The thermal studies show an activation energy of 52.0 kcal/mol toward decomposition to ethylene plus ketene, with an *A* factor of $10^{14.56}$ sec^{-1}. Using these data,[3,5b] an RRKM calculation of decomposition rates from the vibrationally excited ground state was carried out, with the results shown in Figure 7. This calculation shows that the stabilized molecules must, at the pressures of our experiments, have been excited with less than 5 eV internal excitation

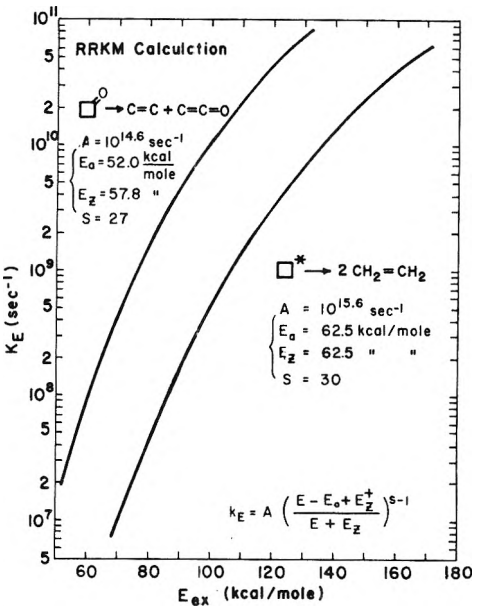

Figure 7. Calculated RRKM rate constant for decomposition of c-C_3H_6CO* to C_2H_4 + CH_2CO. Shown for comparison, decomposition of c-C_4H_8* to $2C_2H_4$. Not shown: decomposition of c-C_3H_5CO* to C_3H_6 + CO.

energy. With fractional stabilization in the 0.4–0.5 range, the median excitation energy for T-for-H substitution in cyclobutanone appears to be about 3–4 eV, somewhat lower than the value of ~5 eV found in the earlier studies of energy deposition in c-C_4H_8[7a] and c-C_4D_8.[18] Any errors in these RRKM calculations are of course carried over into such comparisons of average excitation energies between two different systems. However, with such similar molecules as c-C_4H_8 and c-C_3H_6CO, many of the uncertainties arising from the RRKM calculations are common to both systems and would tend to cancel the effects of such errors. We conclude that the dynamics of T-for-H substitutions into cyclobutanone appear to be slightly altered from that found with cyclobutane, presumably influenced by the difference between C=O and CH_2 substituent groups in adjacent parts of the molecules.

The RRKM calculations also indicate that the minor (0.5%) thermal decomposition path into CO and cyclopropane certainly becomes progressively more important with increasing vibrational energy in the hot ground electronic state.[3b] For example, ~9% of the excited molecules are calculated to decompose by this C_3 mode at 80 kcal/mol excitation energy, with an increasingly larger fraction at higher energies, rising to about 20% at 140 kcal/mol, as shown in Figure 8.[19] (See also Table III.)

Some corroboration of this RRKM prediction of the increased importance of the C_3 route at higher energies can be found in the experiments of Dorer, *et al.*, who have

(17) (a) R. J. Campbell, E. W. Schlag, and B. W. Ristow, *J. Amer. Chem. Soc.*, **89**, 5098 (1967); (b) R. J. Campbell and E. W. Schlag, *ibid.*, **89**, 5103 (1967).

(18) A. Hosaka and F. S. Rowland, *J. Phys. Chem.*, **75**, 3781 (1971).

(19) Notice in Figure 8 that ~5% of the molecules are calculated to decompose at 60 kcal/mol excitation energy *via* loss of CO, although in thermolysis only 0.7% of cyclobutanone is observed to decompose by this route at 393° (E_{act} = 58.0 kcal/mol). Since the temperature dependence of the cyclopropane yield is not accurately known, the calculated percentage yields of C_3 products could easily be off by a factor of 2 at high excitation energies. Thus the branching ratio between the C_2 path and the C_3 path may vary from about 12 to about 6 overall in the excitation range between 60 and 140 kcal/mol. The experimentally observed value is C_2/C_3 = 130/26 = 5 (Table III).

TABLE III: Comparison of Relative Yields of HT and RT* in O_2-Scavenged Cyclobutanone and Cyclobutane Systems

Cyclobutanone (200 Torr)		Cyclobutane (94 Torr)	
HT	457	HT	304
C_2H_3T	(½ × 87)[a] = 130	C_2H_3T	101
Propylene-*t*	(17 − 6)[b] = 11	*c*-C_4H_7T	(100)
c-C_3H_5T	15		
$CH_2{=}C{=}CHT$	1	RT	201
c-C_3H_5TCO	(100)		
RT	257		
HT/RT	1.78 ± 0.1	HT/RT	1.51 ± 0.04

[a] Correction for decomposition to C_2H_4 + CHTCO. [b] Correction for attack on cyclobutanone with ring opening, as in (8) plus (9b).

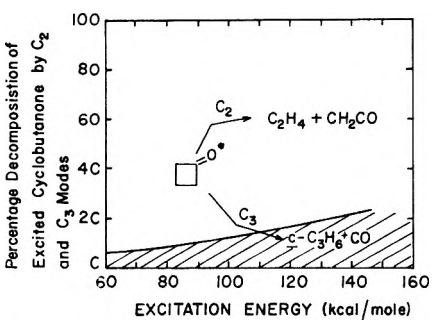

Figure 8. RRKM-calculated percentage decomposition of *c*-$C_3H_6CO^*$ by C_2 and C_3 pathways as function of excitation energy.

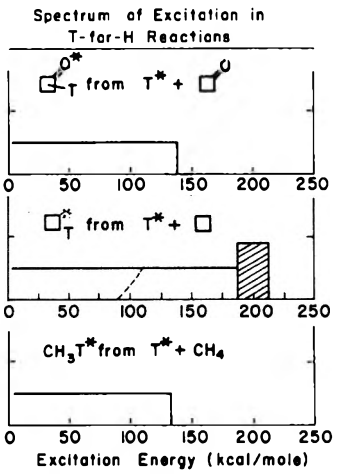

Figure 9. Typical inferred probability distributions of excitation energies from pressure dependence of parent molecules in recoil tritium reactions. Bottom: CH_3T from T* + CH_4 (ref 7); middle: *c*-C_4H_7T from T* + *c*-C_4H_8; one possible fit for *c*-C_3H_5TCO from T* + *c*-C_3H_6CO.

found 7 ± 1% decomposition through this mode following the insertion reaction into cyclobutanone of $^1CH_2$ from photolysis of diazomethane.[20] The energy for the excited 2-methylcyclobutanone molecules in these experiments has been estimated as 103 kcal/mol, and the loss of CO is accompanied in this case by the formation of methylcyclopropane and the corresponding C_4 olefinic isomerization products.

A broad distribution of excitation energies can be postulated to fit the observed decomposition patterns *vs.* pressure for cyclobutanone-*t* molecules, in analogy with the distributions inferred earlier for *c*-$C_4H_7T^*$ and CH_3T^* molecules formed by T-for-H substitution. Such a distribution is illustrated in Figure 9, as calculated exclusively for the decomposition into C_2H_3T plus ketene. By combining this spectrum with the RRKM calculation of Figure 7, an excitation energy-averaged fractional C_3 yield of 0.10 can be calculated for the cyclobutanone-*t* decomposition. The inclusion of this fraction of C_3 products together with the C_2 products will then lead to a second spectrum shifted slightly toward higher excitation energies than that of Figure 9, and the calculation can then be repeated. This iterative procedure will rapidly converge to a C_3 fraction between 0.10 and 0.15. Neither the RRKM calculation nor the inferred excitation spectra are exact enough to justify such a detailed calculation.[21]

Relative Unimportance of Electronic Excitation in Cyclobutanone-t. The data presented in Table III show that the ratio of C_3 products (propylene-*t* + *c*-C_3H_5T) to the C_2 products (multiplied by ½ to correct for loss of tritium to CHTCO) is 0.20 from recoil tritium reactions with cyclobutanone. With a smooth distribution of excitation energies such as shown in Figure 9, greater than 90% of the C_2 fraction at 200 Torr Ar pressure arises from the decomposition of cyclobutanone-*t* with excitation energies in the 80–145 kcal/mol. Since the calculated C_3/C_2 ratio varies from 0.10 to 0.20 in this energy range (Figure 8), a reasonable average estimate would be 0.15, and the excess C_3 yield beyond that expected from decomposition of the hot ground state (~0.20 − 0.15) is an approximate measure of the importance of electronically excited cyclobutanone-*t* molecules in the product spectrum. The C_3/C_2 ratio from photochemically excited singlet cyclobutanones gradually increases from 0.40 to ~1.0 in the excitation range from 90 to 140 kcal/mol,[5b,6c] with an interpolated value of ~0.7 at 115 kcal/mol. Therefore, the fraction of decomposition products attributable to electronically excited (S_1^*) cyclobutanone-*t* present in the recoil tritium system can be estimated crudely as ~12%, *i.e.*, 0.05 × (1.7/0.7) = 0.12. Since the yields of cyclobutanone-*t* and its decomposition products are about equal, this percentage should be reduced by a factor of 2 in the comparison to the sum of decomposition products plus cyclobutanone-*t*. Allowing for the uncertainties in these estimates, the upper limit on the formation of (S_1^*) electronically excited molecules of cyclobutanone-*t* can be placed as about

(20) R. H. Wollenberg, P. B. Do, and F. H. Dorer, private communication.

(21) None of the actual experimental measurements are capable of differentiating among excitation energies less than about 4 eV, since all molecules with 3 or 0.3 eV excitation energy are completely stabilized at all experimental pressures. The flat distributions below 3 eV in Figure 9 have no significance and could just as well be represented by equal areas representing energies in the range, for example, from 3 to 4 eV instead of 0–4 eV. Experiments with the isomerization of CH_2TNC^* indicate that excitation energies less than 3 eV have a negligible probability in that system [C. T. Ting and F. S. Rowland, *J. Phys. Chem.*, **74**, 4080 (1970)].

10% of the T-for-H substitution yield; with moderate changes in assumptions and/or numerical estimates, all of the C_3 products could probably be accounted for without the necessity for a postulate of the participation of electronically excited primary substitution products.

The estimated upper limit on (T_1*) decomposition, leading essentially completely to C_3 products, is correspondingly lower—about 5% of the product yields. These upper limits are not additive, moreover, but rather are either/or: less than 10% (S_1*) or 5% (T_1*), or some intermediate percentage between 5 and 10% for various possible mixtures of (S_1*) and (T_1*).

During the course of these experiments, concurrent investigations with cyclobutanone and some of its alkyl-substituted homologs have demonstrated that the C_3 products are somewhat less sharply diagnostic for electronically excited products than we had believed when the recoil experiments were initiated. Therefore, our chief conclusion is a general, semiquantitative statement that electronically excited products do not appear to play an important role in recoil tritium systems, at least for the reactions of T* with cyclobutanone.

In retrospect, the finding that there is no more than a small probability for the production of electronically excited cyclobutanone-*t* in the T* + cyclobutanone system is not too surprising. The first excited singlet electronic state of cyclobutanone is formed by an n-π* transition involving promotion of an electron in molecular orbitals primarily localized in the C=O chromophore. It should be relatively difficult to accomplish this electronic excitation during the replacement by the recoil tritium atom of an α- or β-H atom bonded to the carbon atoms at some distance from the chromophore. The high-energy electronic transitions involving the molecular orbitals localized near the substitution sites for T-for-H must lie far above 150 kcal/mol excitation.[22] If some electronically excited cyclobutanone-*t* molecules were produced at these much higher energies, we would not expect to detect them through any complementary pressure dependence of the yields of cyclobutanone-*t* and its decomposition products, since stabilization would be an unlikely event. Moreover, we have no assurance that decomposition from such high-lying excited states would lead to the formation of the C_3 products used as diagnostic indicators of electronic excitation in these experiments. In the present circumstances, however, we have no evidence that suggests the participation in any important way of such highly excited electronic states.

Labeled Radicals. The experiments carried out in the presence of H_2S show very substantial yields of CH_3T, indicative of CH_2T radicals in yields approximately twice that of cyclobutanone-*t*. The source of these CH_2T radicals is almost certainly the decomposition of ring-opened radicals. Although we have no means (without the use of partially deuterated parent molecules) for identifying the source of the CH_2T radicals, we believe that the chief source is the decomposition of $CH_2TCH_2CH_2CO$ radicals into $CH_2T + C_2H_4 + CO$. No comparable yield of ring-opened products was observed in the recoil experiments with cyclobutane, but still larger yields have been found with alkyl-substituted cyclopropanes.[23] The implication is strong for the 4-membered ring compounds that attack on a C-CH_2 bonding system is generally less successful than on a C—C=O system, with C-T formation to the carbon atom adjacent to the carbonyl system.

Bond Dissociation Energies. The "hot" HT/RT ratios obtained from the T* + cyclobutanone system and from the T* + cyclobutane system, as shown in Table III, reflect the relative efficiencies of reactions 1 and 2 for these two 4-membered ring molecules. The average HT/RT ratio for the two types of C-H bonds in cyclobutanone (α and β carbons) is 0.27 unit higher than that in cyclobutane. This increase corresponds to ~1 kcal/mol weaker C-H bond in cyclobutanone compared to that in cyclobutane,[2,7,17] assuming no bond energy dependence in the T-for-H substitution reaction. From the published correlations of HT yields with bond dissociation energies,[2] the average bond dissociation energy in cyclobutanone can be estimated as 95 kcal/mol.

(22) (a) A. Udvarhazi and M. A. El-Sayed, *J. Chem. Phys.*, **42**, 3335 (1965); (b) W. C. Johnson Jr., and W. T. Simpson, *ibid.*, **48**, 2168 (1968); (c) R. F. Whitlock and A. B. F. Duncan, *ibid.*, **55**, 218 (1971).

(23) Y. N. Tang and F. S. Rowland, *J. Phys. Chem.*, **69**, 4297 (1965).

Pulse Radiolytic Study of the Site of OH· Radical Attack on Aliphatic Alcohols in Aqueous Solution

K.-D. Asmus,* H. Möckel, and A. Henglein

Hahn-Meitner-Institut für Kernforschung Berlin GmbH, Sektor Strahlenchemie, 1 Berlin 39, West Germany

(Received December 27, 1972)

Publication costs assisted by Hahn-Meitner Institut GmbH Berlin

The formation of reducing and oxidizing radicals has been investigated in the reaction of hydroxyl radicals with formate, alcohols, and diols in pulse-irradiated aqueous solutions. Reducing radicals (CO_2^- and α-alcohol radicals) were identified by their reaction with tetranitromethane, oxidizing alkoxy radicals by their reaction with iodide. The reaction of hydroxyl radicals with formate and ethylene glycol exclusively leads to a radical with reducing properties. The principal reducing radical from methanol, CH_2OH, is formed from only 93% of the reacting hydroxyl radicals. The remaining 7% are accounted for by methoxy radicals formed in the reaction $OH\cdot + CH_3OH \rightarrow H_2O + CH_3O\cdot$. Relative probabilities for hydrogen atom abstraction from the α position, from the OH group, and from other positions of alcohols and diols by OH radicals are derived from the experimental data.

Introduction

The hydroxyl radical is known to react with aliphatic alcohols *via* abstraction of a hydrogen atom from a C-H bond.[1] The reaction

$$OH\cdot + CH_3OH \rightarrow H_2O + \dot{C}H_2OH \qquad (1)$$

for example, leads to the formation of a hydroxymethyl radical. In case of higher alcohols abstraction can occur at any carbon atom to give α-alcohol radicals ($R_2\dot{C}OH$), β-alcohol radicals ($-\dot{C}R-CR_2OH$), radicals with the unpaired electron even further away from the α-carbon atom (R = organic residue or H), though abstraction of an H atom from the α position seems in general to be preferred. Optical spectra, pK values, esr spectra, and the polarographic behavior of a number of α-alcohol radicals have been investigated.[2-6] They can easily be distinguished from β-alcohol radicals (or γ-, δ- etc., radicals) by their physical and chemical properties. α-Alcohol radicals, for example, readily transfer an electron to acceptors such as nitrobenzene,[7] hexacyanoferrate(III),[8] and tetranitromethane,[9,10] while β-alcohol radicals (etc.) do not undergo such reactions. Two pulse radiolytic studies have been reported where the extent of α-hydrogen atom abstraction from various aliphatic alcohols by hydroxyl radicals was investigated.[7,8] These studies were carried out with N_2O saturated (2×10^{-2} M) aqueous solutions at high alcohol concentrations (10^{-2} to 1 M), and *ca.* 5×10^{-4} M of either nitrobenzene or hexacyanoferrate(III) as an electron acceptor. Under these conditions the hydrated electrons formed during the irradiation were converted to OH radicals ($N_2O + e_{aq}^- \rightarrow N_2 + OH^- + OH\cdot$), and both OH· and H· rapidly attacked the alcohol to form the various types of alcohol radicals. The electron acceptors were subsequently reduced exclusively by the α-alcohol radicals thereby producing $C_6H_5\dot{N}O_2^-$ or $Fe(CN)_6^{4-}$. The yields of these electron transfer reactions could easily be determined from the large changes in absorption resulting from these reactions. The results are listed in Table I. In both cases, it was assumed that the reaction of OH· with methanol exclusively occurs *via* eq 1; *i.e.*, the relative yield of reduction was taken as 100% for methanol. Less reduction occurs when higher alcohols are used as OH radical scavengers, and the relative yields obtained were interpreted as relative probabilities of hydrogen atom abstraction from the α-carbon atom of these alcohols. The data of the two independent investigations are seen to agree well.

Burchill and Ginns,[11] however, recently derived relative abstraction probabilities from kinetic data on radiation-induced oxidation of several alcohols by hydrogen peroxide in aqueous solution which are lower than those given in Table I. They found that α-hydrogen abstraction by OH radicals occurs to only 90 and 86% from ethanol and 2-propanol, respectively. Walling and Kato[12] in their study on the oxidation of 2-propanol by Fenton's reagent also found a lower yield (85%) of α abstraction. The values derived from the hydrogen peroxide experiments are also seen to be internally consistent, and the observed discrepancies between these and the pulse radiolysis data may be attributed to a different interpretation of the results. In a private communication, Dr. Burchill pointed out that methanol in its reaction with OH radicals might not exclusively produce $\dot{C}H_2OH$ radicals. This would mean that all the relative yields given in Table I are too

(1) See, for example: (a) M. S. Matheson and L. M. Dorfman in "Pulse Radiolysis," The MIT Press, Cambridge, Mass., 1969; (b) A. Henglein, W. Schnabel, and J. Wendenburg in "Einführung in die Strahlenchemie," Verlag Chemie, Weinheim, 1969.
(2) I. A. Taub and L. M. Dorfman, *J. Amer. Chem. Soc.*, **84**, 4053 (1962).
(3) K.-D. Asmus, A. Henglein, A. Wigger, and G. Beck, *Ber. Bunsenges. Phys. Chem.*, **70**, 756 (1966).
(4) M. Simic, P. Neta, and E. Hayon, *J. Phys. Chem.*, **73**, 3794 (1969).
(5) R. Livingston and H. Zeldes, *J. Chem. Phys.*, **44**, 1245 (1966).
(6) M. Grätzel, A. Henglein, J. Lilie, and M. Scheffler, *Ber. Bunsenges. Phys. Chem.*, **76**, 67 (1972).
(7) K.-D. Asmus, A. Wigger, and A. Henglein, *Ber. Bunsenges. Phys. Chem.*, **70**, 862 (1966).
(8) G. E. Adams and R. L. Willson, *Trans. Faraday Soc.*, 65, 2981 (1969).
(9) K.-D. Asmus, A. Henglein, M. Ebert, and J. P. Keene, *Ber. Bunsenges. Phys. Chem.*, **68**, 657 (1964).
(10) J. Rabani, W. A. Mulac, and M. S. Matheson, *J. Phys. Chem.*, **69**, 53 (1965).
(11) C. E. Burchill and I. S. Ginns, *Can. J. Chem.*, **48**, 1232, 2628 (1970).
(12) C. Walling and S. Kato, *J. Amer. Chem. Soc.*, **93**, 4275 (1971).

TABLE I: Percentage of H Atom Abstraction from the α-Carbon Atom of Various Alcohols According to Earlier Pulse Radiolytic Investigations[a]

Alcohol	% Abstraction: Nitrobenzene method	% Abstraction: Hexacyanoferrate(III) method
Methanol	100	100
Ethanol	97	97
1-Propanol	68	61; 65
2-Propanol	96	89; 95
1-Butanol	35	34

[a] See ref 7 and 8.

high. There are, in fact, earlier observations which could cast some doubt on the role of methanol as the "100% α-abstraction standard"; it was observed that the CO_2^- radical anion formed by attack of OH radicals on formate reduces tetranitromethane[13] and hexacyanoferrate(III)[14] with a somewhat higher yield than the products of the OH radical reaction with methanol.

The present pulse radiolysis study, therefore, has been undertaken to redetermine the yield of reducing species in the reaction of hydroxyl radicals with various alcohols and formate. As an electron acceptor tetranitromethane was used which is known to react with α-alcohol radicals and CO_2^- *via*[9,10,13]

$$>COH + C(NO_2)_4 \longrightarrow C(NO_2)_3^- + NO_2 + H^+ + >CO \quad (2)$$

and

$$\cdot CO_2^- + C(NO_2)_4 \rightarrow C(NO_2)_3^- + NO_2 + CO_2 \quad (3)$$

The stable nitroform anion was detected by its strong absorption at 350 nm (ϵ 1.50×10^4 M^{-1} cm^{-1}).

Experiments were also carried out to determine whether or not methoxy radicals are produced as a second possible species in the reaction of hydroxyl radicals with methanol *via*

$$OH\cdot + CH_3OH \rightarrow CH_3O\cdot + H_2O \quad (4)$$

For identification of methoxy radicals the oxidation of iodide ions[15,16]

$$CH_3O\cdot + I^- \xrightarrow{I^-} CH_3O^- + I_2^- \quad (5)$$

was used. Similar experiments were also carried out with higher alcohols.

Finally, it should be mentioned that hydrogen atoms which are produced during the irradiation of aqueous solutions can also abstract H atoms from the various positions of an alcohol. The yield of hydrogen atoms in N_2O saturated solutions is much lower, however, than the yield of hydroxyl radicals (G(H) = 0.6; G(OH) = 5.5).[1] The data reported in this paper, therefore, represent abstraction probabilities by a 9:1 radical mixture of OH· and H·, but even if the relative reactivities of hydroxyl radicals and hydrogen atoms were different with respect to the position of the attacked hydrogen atom in the alcohol molecule, the figures would still reflect in the main the reaction probabilities of the OH radical owing to its much higher concentration in the radical mixture.

Experimental Section

The technique and equipment of pulse radiolysis have already been described.[1b,17] Electron pulses of 0.3–1.0 μsec duration (200–700 rads) were generally used. The dose was monitored with a secondary emission foil. The chemical standard was an aqueous solution saturated with N_2O (*ca.* 2×10^{-2} *M*), and containing 2×10^{-1} *M* HCOONa and 1.2×10^{-4} *M* $C(NO_2)_4$. Tetranitromethane in such a solution is reduced to nitroform *via* reaction 4 with $G = G(e_{aq}^- + OH\cdot + H\cdot) = 6.1$ (G = number of species/100 eV of absorbed energy).

The solutions were prepared from triply distilled water. Alcohols, sodium formate, and potassium iodide were of reagent grade. Traces of oxygen in nitrous oxide were removed by passing the N_2O through a column filled with aqueous Cr^{2+} solution. Tetranitromethane was purified by washing several times with triply distilled water. A saturated solution of $C(NO_2)_4$ (6×10^{-3} *M*) served as a stock solution. The water was generally deaerated with argon prior to saturating with N_2O and/or addition of other solutes (which had been deaerated separately). All experiments were performed at room temperature (*ca.* 20°).

Evaluation of Data

The calculation of radiation chemical yields is based on the generally accepted values on the formation of primary species in aqueous solutions: $G(e_{aq}^-) = 2.7$, $G(OH\cdot) = 2.8$, and $G(H\cdot) = 0.6$. Hydrated electrons were converted to hydroxyl radicals by N_2O. Thus in N_2O saturated solutions a total of $G(OH\cdot) = 5.5$ and $G(H\cdot) = 0.6$ were available.[1]

The individual error for an optical single pulse experiment is *ca.* ±10%, mainly given by the uncertainty in the monitored dose. A much higher accuracy is necessary for the correct interpretation of our data. Therefore, every result reported here is a mean of some 20 to 30 individual experiments. For the comparison of relative yields of $C(NO_2)_4$ reduction by several radicals, it is a prerequisite that always the same fraction of radicals react with tetranitromethane. Therefore, concentrations were chosen to ensure that the product of rate constant and scavenger concentration remained practically constant for all reactions involved. Further, direct comparisons were made only between results obtained at the same dose. Taking all the uncertainties into account, the total error limits can be given with ±2% for the $C(NO_2)_4$ reduction and ±10% for the I^- oxidation results.

Results and Discussion

Relative Yields of Reducing Species. Figure 1 shows the optical absorption at 350 nm as a function of time observed in pulse irradiated solutions containing 2×10^{-2} *M* nitrous oxide and 1.2×10^{-4} *M* tetranitromethane plus, respectively, 2×10^{-1} *M* of sodium formate (Figure 1a), ethanol (Figure 1b), and 1-propanol (Figure 1c). Under these conditions the conversion of the hydrated electrons by N_2O and the reaction of hydroxyl radicals (and hydrogen atoms) with formate or alcohols go to completion during the 1-μsec pulse. The subsequent reaction of CO_2^- and α-alcohol radicals with tetranitromethane occurs with rate constants of the order of 10^9–10^{10} M^{-1} sec^{-1}[9,10,13]

(13) A. Fojtik, G. Czapski, and A. Henglein, *J. Phys. Chem.*, **74**, 3204 (1970).
(14) G. E. Adams, private communication.
(15) F. S. Dainton, I. V. Janovsky, and G. A. Salmon, *J. Chem. Soc. D*, 335 (1969); *Proc. Roy. Soc., Ser. A*, **327**, 305 (1972).
(16) D. H. Ellison, G. A. Salmon, and F. Wilkinson, *Proc. Roy. Soc. Ser. A*, **328**, 23 (1972).
(17) A. Henglein, *Allg. Prakt. Chem.*, **17**, 296 (1966).

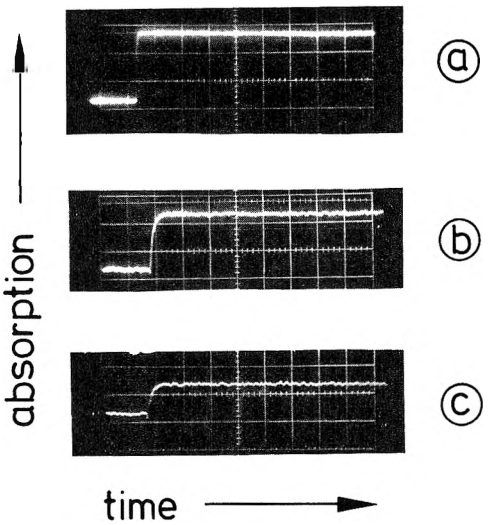

Figure 1. Formation of nitroform in pulse-irradiated aqueous solutions containing N_2O (2×10^{-2} *M*), $C(NO_2)_4$ (1.2×10^{-4} *M*), and OH· radical scavengers: a, HCOONa (2×10^{-1} *M*); b, C_2H_5OH (2×10^{-1} *M*); c, *n*-C_3H_7OH (2×10^{-1} *M*). Pulse length, 1 μsec (*ca.* 700 rads); time scale, 50 μsec/large division.

TABLE II: Relative Yields of H · Abstraction from the α Position, from the OH Groups, and from β (or γ, δ, etc.) Positions of Various Alcohols

Alcohol (or formate)	α Abstraction	OH abstraction	β (γ, δ etc.) abstraction
$HCOO^-$	100		
CH_3OH	93.0	7.0	
C_2H_5OH	84.3	2.5	13.2
n-C_3H_7OH	53.4	<0.5	46.0
$(CH_3)_2CHOH$	85.5	1.2	13.3
n-C_4H_9OH	41.0	<0.5	58.5
tert-C_4H_9OH		4.3	95.7
$(CH_2OH)_2$	100	<0.1	
$CH_2OH-CHOH-CH_3$	79.2	<0.1	20.7
$CH_3-CH_2OH-CH_2OH-CH_3$	71.0	<0.1	29

The formation of the nitroform anion in these reactions is therefore practically complete within a few microseconds after which the optical absorption remains constant.

It can be seen in Figure 1 that the largest increase in absorption is obtained for solutions containing formate, giving $G(C(NO_2)_3^-) = 6.1$, *i.e.*, as expected the sum of $G(OH\cdot) + G(H\cdot) + G(e_{aq}^-)$. This yield, therefore, will be taken as 100%. A lower relative yield of 84% is observed for ethanol solutions. This implies that 16% of the hydroxyl radicals did not form the reducing α radical, $CH_3\dot{C}HOH$. In the case of 1-propanol the yield of nitroform, *i.e.*, of α radicals, is as low as 53%.

A summary of the results obtained for formate, various alcohols, and diols is given in the second column of Table II. From all the OH radical scavengers only formate and ethylene glycol form reducing radicals with a yield of 100%.

It should be mentioned that the reduction of tetranitromethane by α radicals formed from diols takes place with somewhat lower rate constants than the corresponding reactions of α-alcohol radicals.[9] The following rate constants were determined from the kinetic analysis of the pseudo-first-order increase of nitroform absorption in pulsed solutions of diols (*ca.* 2×10^{-1} *M*) and relatively low tetranitromethane (TNM) concentrations (10^{-5} to 10^{-4} *M*): *k*(TNM + ethylene glycol radical) = 1.7×10^9 M^{-1} sec^{-1}, *k*(TNM + 1,2-propanediol radical) = 3.2×10^9 M^{-1} sec^{-1}, and *k*(TNM + 2,3-butanediol radical) = 3.3×10^9 M^{-1} sec^{-1}. Accordingly, the tetranitromethane concentrations in the diol and formate reference solutions were adjusted to ensure an equally high product of TNM concentration and rate constant for the evaluation of the relative reduction yields.

The figures given in Table II are lower than those listed in Table I. The relative yield for 2-propanol is now quite close to that measured by Burchill and Ginns.[11] The most interesting result, however, appears to be that for methanol. Only 93% of the hydroxyl radicals are found to produce CH_2OH radicals in their reaction with CH_3OH, while the remaining 7% must be accounted for by some other reaction, the most logical of which is the formation of methoxy radicals as a second product *via* reaction 4.

This is supported by the results for a solution containing 1.2×10^{-4} *M* tetranitromethane, 2 *M* CH_3OH, and 5×10^{-2} *M* $(CH_3)_2CHOH$, where the relative yield of $C(NO_2)_3^-$ absorption increased to 100%, although hydroxyl radicals are still scavenged directly by the methanol. Probably the $CH_3O\cdot$ radical undergoes an abstraction reaction

$$CH_3O\cdot + (CH_3)_2CHOH \rightarrow CH_3OH + (CH_3)_2\dot{C}OH \quad (6)$$

forming a reducing 2-propanol radical. The corresponding reaction with methanol

$$CH_3O\cdot + CH_3OH \rightarrow CH_3OH + \dot{C}H_2OH \quad (7)$$

is apparently not fast enough in aqueous solution to compete with other deactivation reactions of the methoxy radical.

Relative Yields of Oxidizing Species. The methoxy radical has already been postulated as an intermediate in the radiolysis of pure methanol.[15,16] It was identified by its reaction with the iodide according to eq 5. In the present investigation aqueous N_2O saturated solutions containing 5×10^{-4} *M* I^- and various concentrations of CH_3OH were pulsed. In the absence of methanol I^- is oxidized by hydroxyl radicals

$$OH\cdot + I^- \rightarrow OH^- + I \quad (8)$$

and the iodine atom adds to another I^- ion to form the strongly absorbing I_2^- complex[18]

$$I^- + I \rightleftarrows I_2^- \quad (9)$$

This equilibrium lies well to the right at the I^- concentration used. Under the present condition, reaction 8 and the forward reaction of eq 9 are complete within less than 1 μsec, and the I_2^- absorption (370 nm) can be measured immediately after the pulse. Upon addition of methanol the yield of I_2^- should decrease owing to the competition between reactions 1 and 8.

Figure 2a shows a plot of the observed I_2^- extinction (normalized for dose) as a function of CH_3OH concentration (dashed curve). At low alcohol concentrations the experimental points are a good fit with the solid curve which describes the direct competition between reactions 1 and

(18) (a) J. K. Thomas, *Trans. Faraday Soc.*, **61**, 702 (1965); (b) G. E. Adams, J. W. Boag, and B. D. Michael, *Trans. Faraday Soc.*, **61**, 1674 (1965); (c) J. H. Baxendale, P. L. T. Bevan, and D. A. Stott, *Trans. Faraday Soc.* **64**, 2389 (1968).

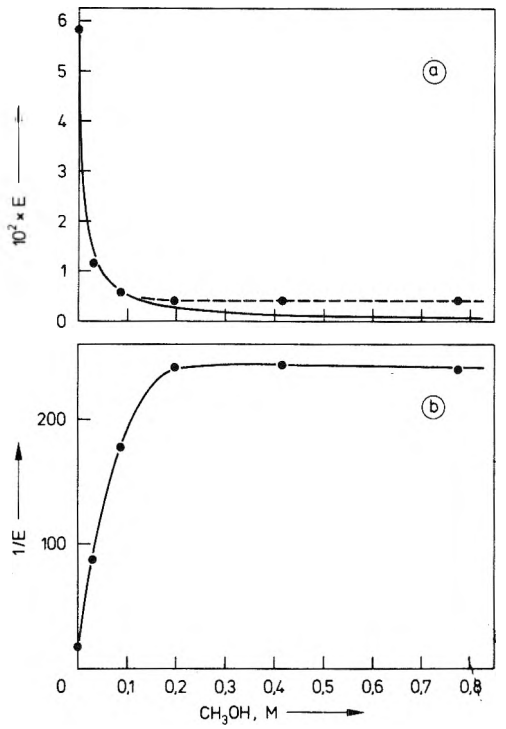

Figure 2. a, Yields of I_2^- ions in pulse-irradiated solutions containing N_2O (2×10^{-2} *M*) and I^- (5×10^{-4} *M*) as a function of CH_3OH concentration. Dashed curve, experimental values; solid curve, calculated for simple competition between CH_3OH and I^- for hydroxyl radicals. b, Plot of $1/E(I_2^-)$ against CH_3OH concentration. Yields are normalized for dose.

8 according to

$$\frac{1}{E} = \frac{1}{E_0}\left(1 + \frac{k_1[CH_3OH]}{k_8[I^-]}\right) \qquad (10)$$

(E_0 is the extinction of I_2^- in solutions without methanol, and k_1 and k_8 are the known rate constants[19] for the reaction of OH with methanol (4.5×10^8 M^{-1} sec^{-1}) and iodide (9×10^9 M^{-1} sec^{-1}), respectively.) At higher alcohol concentrations the experimental curve reaches a plateau which is higher than expected for the pure competition indicating the formation of an oxidizing $CH_3O\cdot$ radical in the reaction of OH radicals with methanol.

For quantitative analysis $1/E$ is plotted *vs.* $[CH_3OH]$ in Figure 2b. At low methanol concentrations a straight line is obtained as expected from eq 10. At higher alcohol concentrations $1/E$ reaches a plateau at 243. Since $1/E_0 = 17.2$ the ratio $E_{plateau}/E_0 = 0.071$. This means that methanol suppresses only 93% of the extinction E_0 obtained in its absence. The remaining 7% is in good agreement with the percentage value of hydroxyl radicals that react with methanol without forming the reducing CH_2OH radicals (see column 2 of Table II). It should be mentioned that E_0 results solely from the reaction of hydroxyl radicals with iodide. The oxidizing $CH_3O\cdot$ species, responsible for the $E_{plateau}$, might be produced by hydrogen atoms ($G(H\cdot) = 0.6$) as well as by hydroxyl radicals ($G(OH) = 5.5$) in their reaction with methanol. Depending on this as yet unknown hydrogen atom contribution our result has an uncertainty up to 10%.

Similar experiments were carried out with iodide–methanol solutions at pH >13 where the basic form O^- of the hydroxyl radical exists. The results were the same within the limits of error indicating that O^- forms $\dot{C}H_2OH$ and $CH_3O\cdot$ in its reaction with methanol with the same relative probabilities as OH radicals.

A compilation of alkoxy radical yields from several alcohols and diols measured by the iodide method is listed in the third column of Table II. The highest yields were observed for methanol and 2-methyl-2-propanol, *i.e.*, compounds carrying exclusively CH_3 groups. The formation of alkoxy radicals becomes less important with increasing number of secondary and tertiary hydrogen atoms in the alcohol molecules.

The fourth column of Table II contains the difference between 100% and the sum of the percentages given in columns 2 and 3. This difference has to be attributed to the relative yield of hydrogen atom abstraction by hydroxyl radicals from carbon atoms in the β, γ, etc. positions.

(19) M. Anbar and P. Neta, *Int. J. Appl. Radiat. Isotopes*, **18**, 493 (1963).

Electron Spin Resonance Investigation of the Disappearance of Trapped Hydrogen Atoms in γ-Irradiated Sulfuric Acid Glasses

E. D. Sprague and D. Schulte-Frohlinde*

Abteilung Strahlenchemie, Max-Planck-Institut für Kohlenforschung, D-4330 Mülheim a. d. Ruhr, West Germany
(Received September 14, 1972)

Publication costs assisted by Abteilung Strahlenchemie, Max-Planck-Institut für Kohlenforschung

Esr measurements of the decay at low temperatures of hydrogen atoms produced by γ irradiation of 6 *M* H_2SO_4 glasses, with and without small concentrations of added 2-propanol, are reported. An analysis of the satellite lines present in the spectrum shows that the environment of the hydrogen atoms changes during the course of the reaction, and it is also observed that the saturation behavior is altered. The kinetic behavior is interpreted as a redistribution of the hydrogen atoms into deeper and deeper traps, in competition with irreversible decay reactions with other hydrogen atoms, 2-propanol molecules, or other reactive species present in the matrix. It is shown that these results are not adequately explained in terms of the presently existing theory of diffusion-controlled reactions.

Introduction

It is well established that γ irradiation of acidic glasses at 77°K yields trapped hydrogen atoms,[1] which, when released from their traps by warming, combine to form molecular hydrogen[2,3] or react with organic additives.[4,5] The complex kinetic behavior of hydrogen atoms in glassy 6 *M* H_2SO_4 has been interpreted[6,7] in terms of the theory of diffusion-controlled reactions,[8] and isotope-effect measurements[9] have shown that the activation energy of the actual chemical reaction does not control the kinetics.

We present here new results on these systems which cannot be explained with the diffusion-kinetic treatment. These results are better interpreted in terms of a redistribution of the hydrogen atoms among a variety of traps in the matrix.

Experimental Section

Reagent grade chemicals and triply distilled water were used to prepare a series of solutions of 6 *M* sulfuric acid containing from 0.0000 to 0.0653 *M* 2-propanol.

The sample tubes were constructed from 5-cm lengths of Teflon tubing (3 mm i.d., 4 mm o.d.). Each tube was sealed at one end with a Pyrex ball and fitted at the other end with a short length of 3-mm o.d. Pyrex tubing. Tubes containing the various solutions were sealed off in air, quenched to 77°K, and irradiated at 77°K with ^{60}Co γ rays to a total dose of approximately 0.40 Mrad at a dose rate of 0.54 Mrad/hr. This dose produces an initial concentration of trapped hydrogen atoms of approximately 0.001 *M*.[4] All samples were clear glasses. Parallel experiments with empty sample tubes showed the absence of detectable amounts of hydrogen atoms in or on the surface of the Teflon after irradiation.

Esr spectra were obtained using a Varian E-9 X-band spectrometer with a Varian V-4532 dual-sample cavity equipped with low-impedance modulation coils appropriate to the E-line machine. The sample and reference cavities were modulated at frequencies of 100 and 10 kHz, respectively. All measurements were made with the sulfuric acid samples immersed in either liquid nitrogen or liquid argon in the standard esr dewar. Corrections for day-to-day variations in machine conditions were made, using the signal from a sample of DPPH–sodium chloride mixture in the reference cavity at room temperature as the standard. Absolute concentration measurements were not made. Microwave power levels were read from the built-in scale on the microwave bridge, and thus may be in error by a constant factor. This has no effect on the conclusions reached in this paper. The kinetic measurements were made at a nominal power level of 0.01 mW to avoid problems due to power saturation.

Some spectra were digitalized by means of a Hewlett-Packard 2402-A integrating digital voltmeter connected to a Kienzle D 44 printer. These spectra and the kinetic data were analyzed on a PDP-10 computer using a least-squares curve-fitting program.[10]

Results

The hydrogen atom decay curves obtained at 77°K for samples of 6 *M* H_2SO_4 containing various concentrations of 2-propanol are presented in Figure 1. Similar curves resulted for 2-propanol concentrations of 0.0026, 0.0052, 0.0157, and 0.0418 *M*. The outstanding characteristic of these decay plots is the initial period of rapid decay followed by much slower decay. Behavior similar to this is often observed in reactions of species produced in solids by ionizing radiation, and is usually explained in terms of (1) initial nonrandom spatial distributions of the reacting species or (2) initial distribution of the reacting species among traps with a variety of depths.[11] A further possibil-

(1) R. Livingston, H. Zeldes, and E. H. Taylor, *Phys. Rev.*, **94**, 725 (1954).
(2) R. Livingston, H. Zeldes, and E. H. Taylor, *Discuss. Faraday Soc.*, **19**, 166 (1955).
(3) R. Livingston and A. J. Weinberger, *J. Chem. Phys.*, **33**, 499 (1960).
(4) W. Kohnlein and D. Schulte-Frohlinde, *Radiat. Res.*, **38**, 173 (1969).
(5) D. E. Holmes and N. B. Nazhat, *Int. J. Radiat. Phys. Chem.*, **3**, 251 (1971).
(6) K. Vacek and D. Schulte-Frohlinde, *J. Phys. Chem.*, **72**, 2686 (1968).
(7) K. Vacek, *Progr. Probl. Contemp. Radiat. Chem., Proc. Czech. Annu. Meet. Radiat. Chem., 10th, 1970*, 367 (1971).
(8) T. R. Waite, *J. Chem. Phys.*, **32**, 21 (1960).
(9) K. Vacek and C. von Sonntag, *Chem. Commun.*, 1256 (1969).
(10) J. L. Dye and V. A. Nicely, *J. Chem. Educ.*, **48**, 443 (1971).
(11) J. M. Flournoy, L. H. Baum, and S. Siegel, *J. Chem. Phys.*, **36**, 2229 (1962).

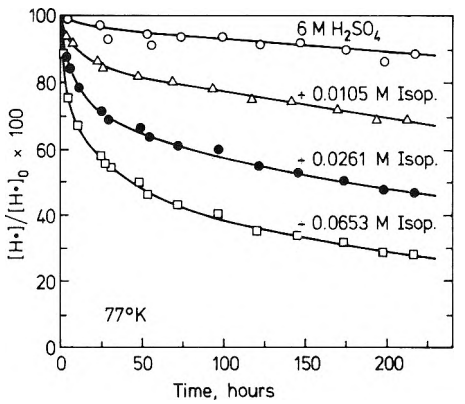

Figure 1. Decay curves obtained at 77°K for hydrogen atoms in γ-irradiated 6 *M* H_2SO_4 glasses containing various amounts of 2-propanol.

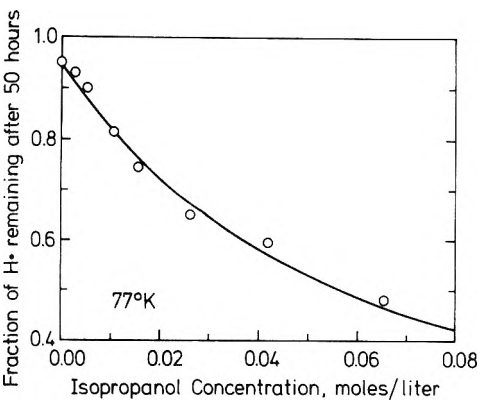

Figure 2. Fraction of hydrogen atoms remaining in γ-irradiated samples of 6 *M* H_2SO_4 after 50 hr at 77°K as a function of added 2-propanol concentration.

ity is (3) the treatment given for diffusion-controlled reactions in condensed media.[8]

For hydrogen atoms in acidic glasses, the first possibility may be eliminated, since relaxation measurements[12,13] have shown that the hydrogen atoms are distributed uniformly throughout the matrix. In addition, identical kinetic behavior is observed for hydrogen atoms produced in identical systems either by γ irradiation or photochemically from 0.01 *M* Fe^{2+} present in the matrix.[7]

An initial distribution of the hydrogen atoms among a variety of traps would result in decay curves formed from the superposition of first-order contributions from the various traps. The decay curves obtained here can be well represented by assuming the existence of two types of traps. Such an analysis, however, yields the initial concentrations of hydrogen atoms in the two types of traps, as well as the two rate constants, and it was found that the percentage of hydrogen atoms initially in deep traps varied from about 60% for the sample containing 0.0653 *M* 2-propanol to almost 100% for the sample containing no 2-propanol. It seems highly improbable that such small concentrations of 2-propanol could be responsible for such dramatic changes in the sulfuric acid matrix with respect to the possible traps available for hydrogen atoms. Evidence against this possibility is presented later in this paper.

This behavior can be better explained as follows. Immediately after irradiation, almost all hydrogen atoms are located in shallow traps which are present in large numbers. They move from trap to trap through the matrix until they encounter some reactive species, such as other hydrogen atoms, other free radicals formed during irradiation, dissolved oxygen,[14] or dissolved 2-propanol, with which they react and thus disappear, or until they encounter a relatively deep trap, from which they are not able to escape quickly. The overall process is a competition for the hydrogen atoms between reactive species and deep traps.

To test this hypothesis, the fraction of hydrogen atoms remaining after 50 hr at 77°K as a function of the 2-propanol concentration (Figure 2) was calculated under the following assumptions. First, the cross sections for trapping and for reaction are presumed equal. The experiments using deuterated and nondeuterated 2-propanol as additives showed that reaction occurs upon almost every encounter,[9] and it is assumed that every encounter of a hydrogen atom with a deep trap leads to trapping. Second, the fact that the hydrogen atoms do not remain permanently trapped is ignored. The error introduced in this way is minimized by calculating the result of the competition at the time roughly dividing the initial, fast stage of the reaction from the final, slower stage. The time chosen was t = 50 hr. As seen in Figure 1, the amount of decay between t = 50 and t = 100 hr is small. Therefore, most hydrogen atoms occupy traps at t = 50 hr from which they cannot escape in 50 hr, and the error caused by this assumption is not large.

In Figure 2, reaction with species other than 2-propanol is indicated by the 5% decay in 6 *M* H_2SO_4 alone. If a concentration is assumed for the deep traps, the expected result of the competition can be calculated. It should be noted that this concentration is not that of traps with a particular depth, but rather the sum of the concentrations of all traps with depths greater than a certain minimum value. These are the traps from which the hydrogen atoms would have a very small probability of escape during a time period of 50 hr at 77°K. The solid line in Figure 2 was calculated from eq 1, in which a deep trap concentra-

$$\text{Fraction of H atoms remaining after 50 hr at 77°K} = \frac{0.063}{0.063 + [\text{2-propanol}]} 0.95 \quad (1)$$

tion of 0.063 *M* was used. The factor 0.95 in eq 1 is an approximate correction for the reaction in the absence of 2-propanol. The calculation is not sensitive to the particular method of making this correction. The agreement seen in Figure 2 supports the above hypothesis.

An interesting conclusion is that the traps occupied by the hydrogen atoms in 6 *M* H_2SO_4, 50 hr or more after γ irradiation, are qualitatively different from those occupied immediately after irradiation, although very little decay has occurred. We now show that it is possible to physically demonstrate this difference.

The esr signal of hydrogen atoms in acid glasses shows satellite lines which result from simultaneous spin flips of neighboring protons.[15] Determination of the intensity of the satellite lines with respect to the main transition allows calculation of the average distance between the trapped hydrogen atoms and the neighboring protons.[16] The experimental observations and calculations have been extended to two and three simultaneously flipping pro-

(12) J. Zimbrick and L. Kevan, *J. Chem. Phys.*, **47**, 5000 (1967).
(13) B. G. Ershov, G. P. Chernova, O. Ya. Grinberg, and Ya. S. Lebedev, *Izv. Akad. Nauk SSSR, Ser. Khim.*, 2439 (1968).
(14) D. E. Holmes, N. B. Nazhat, and J. J. Weiss, *J. Phys. Chem.*, **74**, 1622 (1970).
(15) H. Zeldes and R. Livingston, *Phys. Rev.*, **96**, 1702 (1954).
(16) G. T. Trammell, H. Zeldes, and R. Livingston, *Phys. Rev.*, **110**, 630 (1958).

TABLE I: Average Distances between Trapped Hydrogen Atoms and Neighboring Protons undergoing Simultaneous Spin Transitions in γ-Irradiated 6 *M* H_2SO_4

r_1, Å	r_2, Å	r_3, Å	Remarks
1.82	1.82	1.87	This work, t = 0
1.87	1.88	>1.98	This work, t = 100 hr
1.79	1.80	1.85	Reference 17

tons.[17] Since it was deemed possible that energetically deeper traps would be characterized by larger separations between the trapped hydrogen atoms and the neighboring protons, the above experiment was carried out twice for 6 *M* H_2SO_4. The first measurements were made shortly after completion of γ irradiation and were followed by an identical set approximately 100 hr later. The analysis used was essentially the same as that applied earlier.[17]

A least-squares curve-fitting program[10] was used to separate the high-field line into singlet, doublet, triplet, and quartet components, corresponding to the main transition and the various satellite lines. Plotting the sets of intensities obtained in this way at a series of power levels allowed corrections to be made for the effects of power saturation. The relative intensities were converted to distances using the formulas given previously,[17] and the results are presented in Table I. The distances r_1, r_2, and r_3 are the average distances between the trapped hydrogen atoms and the neighboring protons undergoing simultaneous spin transitions with the unpaired electron, one, two, and three at a time, respectively. A comparison of the first and third lines in Table I shows that the present study yielded values in good agreement with those previously reported.[17]

The most significant result in Table I is the clear difference observed for the same sample at the two different times. At t = 100 hr it was difficult to establish the value of r_3 because of the very low intensity of the corresponding satellite lines. It can only be said that it is apparently greater than 1.98 Å.

Also in agreement with the conclusion that the distances are greater at t = 100 hr is the observation that the main signal saturated noticeably more easily. The greater distances imply smaller interactions, resulting in longer relaxation times and easier saturation of the esr signal.

A further piece of evidence was obtained by transferring all of the samples used for kinetic measurements into liquid argon (87°K) at the end of the time period shown in Figure 1. After about 28.5 hr at 87°K, the samples were returned to 77°K. As expected, the points at 87°K gave curves similar to those at 77°K, except for greatly differing time scales. This is interpreted as a further redistribution of the hydrogen atoms into still deeper traps, in competition with additional decay. That this is correct is shown most clearly in Figure 3, where logarithmic plots of the hydrogen atom signal intensities at 77°K in two of the samples are given for the 150-hr time periods immediately preceding and immediately following the treatment at 87°K. It is seen from Figure 3 that the decay of the hydrogen atoms remaining after the treatment at 87°K is too slow to be observed on this time scale. This observation was made in all the samples and leads to the conclusion that these hydrogen atoms occupy very deep traps.

In order to test the possibility that raising the temperature to 87°K alters the nature of the sulfuric acid matrix itself, the following experiment was carried out. Two samples of 6 *M* H_2SO_4 were quenched to 77°K and then stored at 87°K for 100 hr. At the end of this time period two additional samples were quenched to 77°K, and all four samples were irradiated and immediately measured at 77°K. From the peak-to-peak distances directly measurable in the spectrum, the intensity ratio of the first satellite to the main transition was determined at each of five different microwave power levels for each sample. These measurements were repeated after 100 hr of storage at 77°K. In analogy with the results from the detailed analysis described above, the intensity ratios changed significantly over this time period. More importantly, however, the data from the four samples were indistinguishable from each other, both at t = 0 and at t = 100 hr. This shows conclusively that, at least with respect to the traps available for hydrogen atoms, no change in the 6 *M* H_2SO_4 matrix occurs on warming to 87°K.

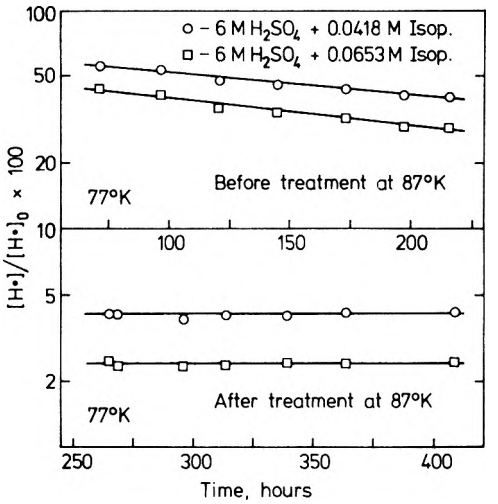

Figure 3. First-order decay plots at 77°K for γ-irradiated 6 *M* H_2SO_4 + 2-propanol samples before and after 28.5 hr at 87°K.

A comparison of the final slope of the decay curve in Figure 3 at 77°K before the treatment at 87°K with the initial slope of the decay curve at 87°K yields an estimate of the activation energy for the reaction, which should correspond to the average depth of the traps occupied by the hydrogen atoms at this point in the reaction. This can be carried out relatively accurately only for those samples containing at least 0.01 *M* 2-propanol, where the apparent rates are somewhat larger and, therefore, more easily measured. Values of 5.79 ± 0.12 kcal/mol were obtained from these samples, and the other samples gave values within 0.4 kcal/mol of this value. It is important to emphasize that the activation energy is not dependent on the 2-propanol concentration. This is good evidence against the possible argument mentioned above that the 2-propanol significantly alters the distribution of possible traps available for the hydrogen atoms in the sulfuric acid matrix.

It is also interesting to estimate a value for the Arrhenius frequency factor for the reaction at this point. If the pseudo-first-order rate constants obtained from the initial slopes of the decay curves at 87°K are corrected for the small amount of decay in the sample without 2-propanol, and are then divided by the respective 2-propanol concentrations, the second-order rate constant for this reaction is obtained. A value of 0.0011 ± 0.0003 M^{-1} sec^{-1} at 87°K was found. Combining this with the observed activation

(17) W. Kohnlein and J. H. Venable, Jr., *Nature (London)*, **215**, 618 (1967).

energy of 5.79 kcal/mol yields the reasonable value of 2.4 $\times 10^{11} M^{-1}$ sec^{-1} for the frequency factor.

Discussion

Two arguments were given previously to justify the use of the diffusion-kinetic treatment.[7] The first was the fact that hydrogen atoms react nonspecifically in sulfuric acid glasses at low temperatures.[9] This only shows, however, that the activation energy of the actual reaction is not the controlling factor. It is just as well explained when it is assumed that the activation energy of trap release controls the reaction kinetics.

The second argument was based on eq 2, which is obtained by substituting the Arrhenius equation into the

$$\ln\left(\ln\frac{[H]_0}{[H]}\right) = \ln A - \frac{E}{RT} + \ln t \qquad (2)$$

first-order kinetic equation.[7] A is the Arrhenius frequency factor, E is the activation energy, R is the gas constant, T is the absolute temperature, and t is the time. If a linear relationship is observed between the logarithm of the time required for a certain fraction of decay and the reciprocal of the temperature, this indicates that the activation energy is constant over this fraction of the reaction. It was shown that such linear relationships were observed for 30 and 60% decay in 6 M H_2SO_4 containing 0.03 M 2-propanol.[7] Examination of Figure 2, however, reveals that this is not a definitive test. In a sample containing 0.03 M 2-propanol, at least 35% of the hydrogen atoms disappear in the fast, initial stage of the reaction. This experiment, therefore, gives primarily an indication of the rate at which the hydrogen atoms are released from the traps which they occupy immediately after irradiation. From the slope of the lines obtained from eq 2,[7] we estimate an activation energy of 4.1 kcal/mol. Comparing this with the value of 5.79 kcal/mol from the present study approximately 200 hr after irradiation provides confirmation of the idea that the hydrogen atoms are redistributed into deeper traps as the reaction proceeds.

It has been demonstrated in the present study that the diffusion of the hydrogen atoms results in a significant alteration of their average microscopic environment. Since existing diffusion-kinetic theory assumes that the average microscopic environment of reacting particles remains constant and does not include a consideration of the detailed structure of the matrix, it is not able to explain such an effect. The effect is, however, a logical consequence of the interpretation given here.

Some comment should be made on the recent report concerning hydrogen atom decay in γ-irradiated, 0.13 mol fraction perchloric acid at low temperatures.[18] The kinetic results were interpreted in terms of simultaneous, first-order decays of two groups of hydrogen atoms, those located in shallow traps and those located in deep traps. As shown here, however, this simple model is not able to explain the effect of adding small amounts of 2-propanol to the system. In addition, we believe that it is much more reasonable to assume the existence of a wide, continuous distribution of types of traps in the matrix, rather than just two discrete types. In this paper the existence of at least three types of traps has been demonstrated: the shallow traps occupied immediately after irradiation, the deeper traps occupied after the initial, rapid decay, and the very deep traps occupied after the treatment at 87°K.

Acknowledgment. The authors wish to thank Professor T. F. Williams for pointing out an error in the proton-distance calculations.

(18) C. J. Ultee and C. R. Kepford, *J. Chem. Phys.*, **52**, 3462 (1970).

Dielectric Behavior of the Ternary System Benzene–Cyclohexane–Dioxane

Ralph D. Nelson, Jr.,* Marcia Mungenast, and John X. Sierant

Department of Chemistry, West Virginia University, Morgantown, West Virginia 26506 *(Received November 27, 1972)*

The dielectric constants, far-infrared refractive indices, and sodium D line refractive indices are discussed for the ternary mixture benzene–cyclohexane–dioxane. Small deviations from linear additivity of molar polarization contributions are discussed in terms of molecular interactions. The system is essentially ideal, and the fluxional character of the dioxane molecule prevents any significant interaction with the benzene π electrons.

Introduction

Molecular interactions are often considered to be the result of local electric fields created by molecular dipole moments (or higher multipoles) or of orbital overlap interactions. In the gas phase such interactions between pairs of molecules may be studied by measuring the properties of a binary system as a function of temperature and partial pressures over a wide range of conditions.[1] Measurements in the liquid phase are restricted to a much nar-

(1) R. D. Nelson, Jr., and R. H. Cole, *J. Chem. Phys.*, **54**, 4033 (1970).

rower range of easily attainable conditions, and reducing the concentrations of the two species to low values may be accomplished only by introducing a third component. The use of ternary systems thus provides an opportunity to investigate molecular interactions with the same flexibility as gas-phase measurements, and it also allows adjustment of one parameter, such as density, so that a wide variety of solution compositions may be prepared and tested at the same density to see how strongly dependent on molecular composition other properties are, exclusive of density variations.

Ternary solutions are not a common subject for study because they require numerous measurements to establish the shape of the constant value contours on a ternary diagram. The system studied was chosen because it involves nonpolar molecules with the properties of fairly complete inertness (cyclohexane), aromatic character (benzene), and strong local electric fields (dioxane). Besides this, the molecules are completely intermiscible, are in common use, and have similar physical properties.

Experimental Section

All the pure liquids were reagent quality materials which had been dried over molecular sieves and distilled shortly before use. Physical properties for the pure liquids were comparable to the literature values. The dielectric permittivities were measured at 1 kHz in a Balsbaugh Laboratories 20 TNLV cell with a General Radio 1620A ratio arm capacitance bridge. The far-infrared refractive index was determined at 30 cm^{-1} with an HCN laser apparatus previously described.[2] We should like to note a correction in the equation for offset correction reported earlier. Equation 3 of ref 2 should read as follows

$$FG_{lig} - FG_{air} = h \tan\left[\sin^{-1}\left(\frac{n_{lig}}{n_{air}} \sin 2\Theta_c\right)\right] - h \tan 2\Theta_c$$

The refractive index at the sodium D line was measured with a Bausch and Lomb Model 33-45-58 refractometer. Densities were determined using a 10-ml Ostwald-Sprenger pycnometer and included buoyancy corrections. Nineteen solutions were measured. To compute the deviations from linear additivity of polarizations or molar volume, the following equations were used.[3]

$$V_{obsd} = \Sigma X_i M_i / d_{obsd} \quad (1)$$

$$V_{lin} = \Sigma(X_i M_i / d_i) \equiv \Sigma X_i V_i \quad (2)$$

$$S_{obsd} = (\epsilon - 1)/(\epsilon + 2) \quad (3)$$

$$S_{lin} = P_{lin}/V_{lin} \quad (4)$$

$$P_{obsd} = S_{obsd} V_{obsd} \quad (5)$$

$$P_{lin} = \Sigma(X_i M_i / d_i)(\epsilon_i - 1)/(\epsilon_i + 2) \equiv \Sigma X_i P_i \quad (6)$$

Equations 3-6 may be used for molar refraction R instead of P if the square of the refractive index is used in place of ϵ. These can be rearranged to solve for d, ϵ, or n^2. Here V stands for molar volume, P for molar polarization, X for mole fraction, d for density, ϵ for dielectric permittivity relative to a vacuum, n for refractive index, S for specific polarization, and M for molecular weight (*i.e.*, molar mass). The equations giving the values which would be obtained if linear additivity held true are

$$d_{lin} = \Sigma X_i V_i / \Sigma X_i M_i \quad (7)$$

$$\epsilon_{lin} = (2S_{lin} + 1)/(1 - S_{lin}) \quad (8)$$

Results were computed using the West Virginia University Computing Center's IBM 360/75 computer. The NEPROP subroutine package was appended to propagate estimated errors through for a more complete data analysis.[4] The sources of uncertainty result in approximately the same error for each solution, so the absolute uncertainties given apply to each of the 19 solutions measured. The uncertainty estimates refer to one standard deviation for the various experimental quantities and are 0.07% for density, 0.02% for visible refractive index, 0.2% for far-infrared refractive index, 0.02% for dielectric permittivity, 0.1° for T, and 0.0005 for mole fraction. The data are summarized in Table I.

Results and Discussion

Except for a few mixtures, the molar quantities were additive to within the experimental error. The exceptions were the benzene-cyclohexane mixture, with a positive deviation of 0.5 cm^3/mol in V for a 1:1 mixture; the cyclohexane-dioxane mixture, with a negative deviation of 0.6 cm^3/mol in V; and the ternary mixture R_D values, where variations in the dispersion of light as a function of concentration gave positive deviations of as much as 1.7 cm^3/mol for the 1:1:2 mixture of benzene-cyclohexane-dioxane. If these deviations in R_D had been due to variations in P_E as concentrations changed, then R_{FIR} and P should show deviations parallel to those in R_D. Since parallel behavior was not observed, the deviations may be attributed to changes in the dispersion (variation of refractive index with frequency of the measuring radiation near an absorption line) of the mixtures.

For some years it has been known that the benzene-cyclohexane system is not completely ideal.[5] Vapor-pressure studies have shown deviations ascribed to a general aliphatic-aromatic interaction with a heat of mixing at 25° of 810 J/mol and an excess volume of 0.66 cm^3/mol for a 1:1 mixture.[6] The second virial coefficients for cyclohexane, benzene, and a mixed pair are −910, −814, and −918 cm^3/mol, respectively.[7] Our measurements confirm the excess volume, but show that there is no anomaly in the refraction and polarization behavior of this mixture. That is, while the molecular interaction causes a mixture of 1 mol of benzene and 1 mol of cyclohexane to have a volume greater than the sum of the volumes before mixing, the polarizability of the molecules is not significantly affected by the interaction. Application of the Kramers-Kronig relation[8] then requires that the sum of the integrated intensities for the absorption bands in the system is the same for the unmixed as the mixed systems, *i.e.*, the shifts in absorption band location are either negligible or are offset by compensating changes in the absorption coefficients.[9]

One might well expect significant interactions in the benzene-dioxane system, since benzene has highly polari-

(2) R. D. Nelson, Jr., and C. E. White, *J. Phys. Chem.*, **73**, 3439 (1969).
(3) N. E. Hill, W. E. Vaughan, A. H. Price, and M. Davies, "Dielectric Properties and Molecular Behavior," Van Nostrand, New York, N. Y., 1969, Chapters 3 and 4.
(4) R. D. Nelson, Jr., and M. R. Ellenberger, *J. Chem. Educ.*, **44**, 678 (1972).
(5) G. Scatchard, S. E. Wood, and J. M. Mochel, *J. Chem. Phys.*, **43**, 119 (1939).
(6) J. S. Rowlinson, "Liquids and Liquid Mixtures," 2nd ed, Plenum Press, London, 1969, Chapter 4.
(7) J. S. Rowlinson, *Nature (London)*, **194**, 470 (1962).
(8) V. V. Daniel, "Dielectric Relaxation," Academic Press, London, 1967, Chapter 5.
(9) K. H. Illinger and C. P. Smyth, *J. Chem. Phys.*, **35**, 392 (1961).

TABLE I: Summary of Results for (Air Saturated) Liquids at 25°

	Benzene	(Lit.)	Cyclohexane	(Lit.)	Dioxane	(Lit.)	Uncertainty
Density, g/ml	0.8701	(0.8736)[a]	0.7668	(0.7737)[a]	1.0280	(1.0336)[c]	0.0006
n_D^2	2.243	(2.244)[a]	2.026	(2.026)[a]	2.017	(2.023)[c]	0.001
n_{HCN}^2	2.262	(2.284)[a]	2.000	(2.014)[a]	2.150	(2.160)[e]	0.01
ϵ_0	2.272	(2.274)[b]	2.016	(2.015)[b]	2.235	(2.209)[b]	0.001
M, g/mol	78.11		84.16		88.11		
V, cm³/mol	89.771		109.755		85.710		0.07
R_D, cm³/mol	26.30		27.98		21.69		0.02
R_{FIR}, cm³/mol	26.6		27.4		23.7		0.2
P, cm³/mol	26.80		27.77		25.00		0.02

[a] "Selected Values of Properties of Hydrocarbons and Related Compounds," American Petroleum Institute Research Project 44 (1968) for liquids with the air removed. [b] A. A. Maryott and E. R. Smith, "Table of Dielectric Constants of Pure Liquids," NBS Circular No. 514, U. S. Government Printing Office, Washington, D. C., 1951. [c] 20° values from the "Handbook of Chemistry and Physics," 47th ed, Chemical Rubber Publishing Co., Cleveland, Ohio, 1966. [d] J. E. Chamberlain, E. B. C. Weaver, H. A. Gebbie, and W. Slough, *Trans. Faraday Soc.*, **63**, 2605 (1967). [e] Reference 13.

zable electron clouds, and dioxane provides strong electric fields to affect the distribution of electrons in the region near the carbon–oxygen bonds. But the data showed no such effect, indicating that the benzene–dioxane interaction does not significantly affect either the predominantly chair conformation of dioxane, the packing in solution, or specific interactions with the energy levels of benzene. It seems that the rapid chair–boat–reversed chair motion[10] precludes such effects. Dilution of a 50:50 mixture of benzene and dioxane with cyclohexane produces data which show only the excess volume due to the benzene–cyclohexane interaction.

The mixtures of cyclohexane with dioxane are quite ideal in both refraction and polarization behavior, supporting and extending earlier work on this pair.[11] The small negative deviation in molar volume may be due to packing of the dioxane into the looser structure of cyclohexane.

The polarization measurements were carried out at three frequencies chosen because they fairly well separate the effects of electronic, vibrational, and rotational polarization. Most of the polarization is due to the electron cloud distortion produced in the presence of an electric field. Note that if the visible refraction is taken close to an absorption line in the ultraviolet and is not extrapolated to zero frequency (by making several measurements in the visible, assuming a line shape, and solving for the extrapolated value), the value measured will be somewhat larger than the true electronic polarization.[3] If the electronic band has a large absorbance and the vibrational contribution to R_{FIR} is small, R_D may be greater than R_{FIR} or P. This effect makes the visible polarization of cyclohexane larger than the far-infrared or audio values. This also explains the deviations from linear additivity that are observed for R_D of the ternary mixtures. Corrections could be applied to R_D using empirical formulas and more extensive measurements in the visible region, but this would not produce a significant increase in information about molecular interactions.

The far-infrared and the audio values should be identical if there are no (a) permanent dipole moments, (b) polar conformations for predominantly nonpolar species, (c) polar impurities, and (d) collision-induced moments with a duration of 1 psec or more. The far-infrared values were not as precise as the audio values, but served as a check for nontrivial contributions from the above sources of polarity. Only in the case of 1,4-dioxane and its solutions was there a difference between the two values beyond experimental uncertainty. This compound is known to exist in several conformations: the nonpolar oxygen chair, the somewhat polar carbon boat (dipole moment calculated to be 0.76 D, where 1 D = 10^{-18} esu cm), and the polar oxygen boat (dipole moment calculated to be 1.62 D). The calculations are based on the geometric additivity of the C–O–C group moment of 1.15 D from diethyl ether.[12] The observed polarizations indicate a dipole moment of 0.25 D for the mixture of conformers under the experimental conditions.

The fraction of molecules in a nonpolar conformation may be computed as $1 - (\mu_{obsd}/\mu_{polar})^2$ if there is only one polar conformation possible. Here there are two, so only limits may be set, and these are that between 90 and 98% of the dioxane is in the nonpolar conformation. This polarity is not immediately evident from dielectric relaxation work at microwave frequencies because the lifetime of the polar conformers is quite short. Relaxation here occurs predominantly by the fluxional path of polar–nonpolar–polar (oppositely directed) path rather than by the slower (for this molecule) path of overall rotation. This mechanism produces a broad absorption band in the far infrared whose characterization in terms of process frequency and band shape are not firmly based[13] on theory. Relaxation work for dioxane, thioxane, and dithiane supports this view,[14] and several other systems have been shown to exhibit fluxional relaxation.[2,15]

Our conclusions for the ternary system benzene–cyclohexane–dioxane may be summarized as follows.

(1) The benzene–cyclohexane interaction does not significantly affect the charge distributions or energy levels of the molecules in the mixture compared to the pure liquids. The excess heat of mixing must arise from some other source.

(2) Rapid conformational changes in dioxane prevent the expected changes in charge distribution due to bond dipoles interacting with the π electron cloud of benzene.

(3) As expected, the cyclohexane–dioxane interaction is essentially ideal, a slight negative deviation in volume being perhaps due to packing.

(10) W. B. Smith and B. A. Shculders, *J. Phys. Chem.*, **69**, 579 (1965).
(11) A. Vierk, *Z. Anorg. Chem.*, **261**, 283 (1950).
(12) R. D. Nelson, Jr., D. R. Lide, Jr., and A. A. Maryott, *Nat. Stand. Ref. Data Ser., Nat. Bur. Stand.*, **No. 10** (1967).
(13) M. Davies, G. W. F. Pardoe, J. Chamberlain, and H. A. Gebbie, *Trans. Faraday Soc.*, **66**, 273 (1970).
(14) J. Crossley, A. Holt, and S. Walker, *Tetrahedron*, **21**, 3141 (1965).
(15) R. D. Nelson, Jr., and C. P. Smyth, *J. Phys. Chem.*, **69**, 1006 (1965).

(4) Dioxane is at least 90 and probably over 98% nonpolar conformer, but is best viewed as a fluxional molecule with frequency of maximum conversion between conformers somewhat above 5 cm^{-1} (1.5×10^{11} Hz).

(5) The ternary system here may be used as a solvent system having variable amounts of π electron cloud character, but *not* for varying amounts of local electric field.

Acknowledgments. This note includes work submitted to Middlebury College, Middlebury, VT, in partial fulfillment of the requirements for the degrees of Bachelor of Arts for M. M. and of Master of Science for J. X. S. The work was supported by Grant No. GP-22829 from the National Science Foundation and by West Virginia University.

Determination of Rotational Barriers in Four Thioamides[1]

R. F. Hobson, L. W. Reeves,* and K. N. Shaw

The Chemistry Department, University of Waterloo, Waterloo, Ontario, Canada *(Received August 25, 1972)*

Publication costs assisted by the National Research Council of Canada

The hindered rotation barriers of four thioamides have been determined using the best techniques available. The proton magnetic resonance (nmr) spectra of *N,N*-dimethylthiocarbamyl cyanide reveals long-range intermethyl couplings $^4J_{HH}$. The rotation barrier in terms of the free energy of activation is high in this molecule (23.5 ± 0.5 kcal/mol) and this suggests that the π electron density at the nitrogen contributes to the spin coupling. On reexamination of another amido-type molecule, *N,N*-dimethylnitrosamine, also with a high barrier (22.5 ± 0.5 kcal/mol) the hitherto unreported $^4J_{HH}$ coupling is confirmed. It is suggested that this long-range coupling will correlate well with energy barriers in amides. The complete line shape fits were accomplished using both eight-site and two-site formulations. Because the coupling to chemical shift ratios are so small, the error in use of the two-site approximation is negligible. Reinvestigation of *N,N*-dimethylthiocarbamyl chloride gives kinetic parameters essentially in agreement with previous studies. Long-range coupling $^4J_{HH}$ occurs in *N,N*-dimethylthiocarbamyl fluoride and assists in the assignment of the methyl peaks. The compound *N,N*-dimethylthiourea has a much lower barrier to rotation (13.9 ± 0.2 kcal/mol). The energy barriers are explained in terms of valance bond theory. In general the thio compounds have an energy barrier approximately 2 kcal/mol higher than corresponding amides. Using the present study of the thiourea, our previous study of *N,N*-dimethylselenourea, and valence bond structures, the hindered barrier in *N,N*-dimethylurea is estimated. This estimate agrees well with a value 2 kcal/mol lower than the measured thiourea barrier. The failure to detect the estimated barrier of 11 kcal/mol in the urea compound is ascribed to chemical shift degeneracy.

Introduction

There have been many studies of amides and amido-type molecules by nuclear magnetic resonance (nmr)[2-4] but because of the difficulties in properly measuring the rates of hindered rotation about the N-C bond, there exists only a small quantity of reliable data on these energy barriers. These data are not organized well enough to cover related structural series of amido-type systems, enabling separation of the contributing factors which determine the energy barriers experimentally or theoretically.[5-9] In our laboratory we have adopted the point of view that amide rotation rates provide a stringent test of the capabilities of the techniques of measurement of rate processes *via* the contributions to transverse nuclear spin relaxation and the effect on nmr line shapes.[10] In general the chemical shifts are small between *N*-methyl groups and long-range coupling,[11] which has largely been ignored hitherto, must be included in the theoretical analysis as well as many other precautions.[5-7,12] The measurement of ΔG^* is not, in general, sufficient, nor accessible, by simple coalescence temperature measurements in multisite exchange involving unknown chemical reaction mechanisms and it is to this end that the power of the nmr technique can be used to greatest effect.[13,14]

The almost complete absence of studies of a series of related amides is a serious drawback in any analysis of the

(1) Research supported by the National Research Council of Canada in grants to L. W. R.
(2) (a) H. Kessler, *Agnew. Chem., Int. Ed. Engl.*, **9**, 219 (1970); (b) W. E. Stewart and T. H. Siddall, III, *Chem. Rev.*, **70**, 517 (1970).
(3) T. H. Siddall and W. E. Stewart, *Progr. Nucl. Magn. Resonance Spectros.*, **5**, 33 (1969).
(4) G. Binsch, *Top. Stereochem.*, **3**, 97 (1968).
(5) L. W. Reeves and K. N. Shaw, *Can. J. Chem.*, **49**, 3671 (1971).
(6) L. W. Reeves, R. C. Shaddick, and K. N. Shaw, *Can. J. Chem.*, **49**, 3683 (1971).
(7) P. T. Inglefield, E. Krakower, L. W. Reeves, and R. Stewart, *Mol. Phys.*, **15**, 65 (1968).
(8) M. T. Rogers and J. C. Woodbrey, *J. Phys. Chem.*, **66**, 540 (1962).
(9) M. Rabinovitz and A. Pines, *J. Amer. Chem. Soc.*, **91**, 1585 (1969).
(10) A. Allerhand, H. S. Gutowsky, J. Jonas, and R. A. Meinzer, *J. Amer. Chem. Soc.*, **88**, 3185 (1966).
(11) V. J. Kowalewski and D. G. Kowalewski, *J. Chem. Phys.*, **33**, 1794 (1960).
(12) L. W. Reeves and K. N. Shaw, *Can. J. Chem.*, **23**, 3641 (1970).
(13) S. O. Shan and L. W. Reeves, *J. Amer. Chem. Soc.*, in press.
(14) S. O. Shan and L. W. Reeves, *J. Amer. Chem. Soc.*, in press.

factors which influence the hindered rotation (HR). Now, having the necessary techniques to make reliable measurements, we propose to study a carefully selected series and to attempt an analysis of contributing factors at several levels of sophistication.[15,16] In this present work the emphasis is on the determination of activation parameters for HR in related thioamides. Previous work on these compounds has not been extensive in varying the molecular structure in a regular manner.[17-22] One isolated measurement has been made on a selenourea compound.[23]

Experimental Section

It is convenient to refer to amide-type molecules by a short-hand notation. Let the molecule $(CH_3)_2NC(X)=Y$, be described by a function x in the following way: Yx(X). In this notation, for example, *N,N*-dimethylthiocarbamyl fluoride may be written Sx(F).

(i) Preparation of Compounds. (A) N,N-Dimethylthiocarbamyl fluoride was prepared by adding 18 g of powdered silver fluoride (Alfa Inorganics) in small portions over 10 min to 13.9 g of bis(dimethylthiocarbamyl) disulfide (Eastman Kodak Co.) dissolved in 100 ml of acetonitrile at 30–40°. The mixture was stirred continuously, and as the reaction is instantaneous it is important to prepare the AgF in the form of fine granules since a layer of Ag_2S on the surface of the AgF rapidly hinders the reaction. The formation of Sx(F) was completed on stirring for an additional 20 min. The basis for this preparation has been described by Goshorn, *et al.*[24] After the acetonitrile was removed using a rotary evaporator the residue was washed thoroughly with ether, the ether was also removed, and then the viscous residue was vacuum distilled. The final product boiling point was 31° at 1.5 ± 1 Torr. The Sx(F) was classified by ir and nmr spectroscopy and was found to be unstable at temperatures above 30°. It should be noted that the reaction of SbF_3 with Sx(Cl), under the conditions suggested by Schrader[25] and Metzger and Wilson[26] was particularly violent and Sx(F) could not be isolated from the reaction mixture.

The sample used for nmr kinetic study consisted of an 18.2 mol % solution of Sx(F) in tetrachloroethane (TCE) with 4.6 and 1.1 mol % of dioxane and hexamethyldisiloxane (HMDS), respectively, sealed in a medium-walled sample tube under N_2 at a pressure of about 500 Torr.

(B) N,N-Dimethylthiocarbamyl chloride was obtained from the Aldrich Chemical Co., and was purified by double recrystallization from pentane. This compound may also be prepared by a method described by Goshorn[24] for the corresponding diethylthiocarbamyl chloride. The nmr sample was a 20.4 mol % solution of Sx(Cl) in CCl_4 with dioxane and HMDS as for Sx(F) above.

(C) N,N-Dimethylthiourea was prepared by a method similar to that proposed by Bennett, *et al.*,[27] for unsymmetrical ureas. A mixture of 10 g of dimethyl cyanamide (K & K Laboratories), 20.2 ml of concentrated ammonium hydroxide, and 6.8 ml of H_2O was stirred in a round-bottom three-necked flask while H_2S was bubbled slowly through the mixture for 90 min. during which time the temperature was controlled between 20 and 30°. The temperature of the bath was then reduced to 5–10° and the solution was stirred for an additional 2 hr while a white precipitate formed. The precipitate was filtered cold and washed with ice-cold aqueous ethanol. The product was further purified by recrystallization from benzene as fine white needles. The final yield was greater than 35%.

The nmr sample was prepared and sealed under vacuum in a medium-walled tube as a 3.6 mol % solution of $Sx(NH_2)$ in TCE. At this concentration $Sx(NH_2)$ formed a near-saturated solution. 1.5 and 0.9 mol % of dioxane and HMDS, respectively, were also added to the sample.

(D) N,N-Dimethylthiocarbamyl bromide, Sx(Br), could not be isolated from a solution of Sx(Cl) in acetonitrile saturated with HBr in a manner analogous to the preparation of Ox(Br).[15] Bubbling HBr into the Sx(Cl) solution appeared to cause immediate decomposition. A second preparation was attempted by allowing 15 g of bis(dimethylthiocarbamyl) disulfide dissolved in 125 ml of acetonitrile to react with 5 ml of Br_2 in the same solvent. Although a rapid reaction took place and a yellow precipitate formed, the required product again could not be isolated.

(E) A sample of N,N-dimethylthiocarbamyl cyanide was kindly provided by Professor Jan Sandström. This was used without further purification as a 3 mol % solution in TCE containing 1.2 mol % HMDS. The nmr tube was of medium thickness and sealed under N_2 at a pressure of about 500 Torr.

(F) N,N-Dimethylthiocarbamyl azide was prepared by a method previously described for the corresponding carbamyl azide.[15] A mixture of 100 ml of acetonitrile, 11.2 g of sodium azide, and 20 g of Sx(Cl) was stirred at 40° for 28 hr and a bright yellow solid formed. The acetonitrile was taken off in a rotary evaporator and the resultant slurry was taken up in benzene at 45°, filtered, and again separated. However, a vacuum distillation (135–145°, 4–6 Torr) caused some decomposition. A sample was prepared as a 20 mol % solution in CCl_4 but further decomposition prevented a reliable kinetic study.

(ii) Methods. All studies of exchange modified ^1H nmr spectra were made using an HA-100 spectrometer and total line shape analyses as already described.[6,12,15] The computer program GPLONK was used for iterative line shape fitting of digitized experimental data. It is now well recognized that total line shape analyses give the most reliable rate constants, and hence activation parameters, from nmr studies but some additional comments are probably in order. Standard regressional techniques[5] are used to determine the "best fit" Arrhenius plot and thus error estimates of the slope and intercept based upon the data scatter are available. However, it is of some concern to know that these statistical errors are representative of the real errors in derived activation parameters. If rate constants arbitrarily close to the true values, as determined by a minimum line shape fit deviation, are available it is not necessary to weight the ordinate Arrhenius plot points. Similarly, if temperature control is adequate, abscissa error bounds may be neglected. Now by varying the position of specific points in an Arrhenius

(15) E. A. Allan, R. F. Hobson, L. W. Reeves, and K. N. Shaw, *J. Amer. Chem. Soc.*, **94**, 6604 (1972).
(16) R. F. Hobson and L. W. Reeves, *J. Magn. Resonance*, in press.
(17) A. Lowenstein, A. Melera, P. Rigny, and W. Walter, *J. Phys. Chem.*, **68**, 1597 (1964).
(18) R. C. Neuman, Jr., and L. B. Young, *J. Phys. Chem.*, **69**, 2570 (1965).
(19) G. Isaksson and J. Sandstrom, *Acta Chem. Scand.*, **21**, 1605 (1967).
(20) J. Sandstrom, *J. Phys. Chem.*, **71**, 2318 (1967).
(21) C. E. Holloway and M. H. Gitlitz, *Can. J. Chem.*, **45**, 2659 (1967).
(22) T. H. Siddall, III, and W. E. Stewart, *J. Org. Chem.*, **32**, 3261 (1967).
(23) L. W. Reeves, R. C. Shaddick, and K. N. Shaw, *J. Phys. Chem.*, **75**, 3372 (1971).
(24) R. H. Goshorn, W. W. Levis, Jr., E. Jaul, and E. J. Ritter, *Org. Syn.*, **35**, 55 (1955).
(25) G. Schrader, "British Intelligence Objectives Subcommittee," Final Report No. 714 B.I.O.S., Information Section, London, 1945.
(26) H. P. Metzger and I. B. Wilson, *J. Biol. Chem.*, **238**, 3432 (1963).
(27) F. Bennett and R. Zingaro, *Org. Syn.*, **36**, 23 (1956).

plot the sensitivity of the final activation parameters to possible errors may be considered, as outlined recently by Becker, *et al.*[28] Systematic errors in temperature tend to cause a translation of the line accompanied by a small rotation, while errors caused by incorrect chemical shifts and line widths in the absence of exchange or field inhomogeneity line shape distortions are reflected as a rotation of the plot about a point slightly above that corresponding to the coalescence temperature. It appears that fluctuations in temperature up to 1° are almost insignificant so far as the free energy of activation ΔG^* is concerned (over a large temperature range) but may be an order of magnitude more significant for the entropy of activation ΔS^*. An ideal situation with temperature-independent chemical shifts and equivalent line widths in the absence of exchange, measurable from a nonexchanging symmetrical resonance line with a natural line width of 0.3 Hz or less, permits an estimate of ΔG^* to within 0.1 kcal/mol; but ΔS^* is still an order of magnitude more sensitive to systematic errors. Therefore, in general, the regressional error quoted for ΔG^* is representative of the true error while such an error is less significant for ΔS^*. This has also been illustrated by a survey of all available data for the hindered rotation in *N,N*-dimethylcarbamyl chloride.[15]

Since the entropy of activation is very sensitive to experimental errors this parameter may be used as a check for internal reliability. That is, if the upper and lower bounds for ΔS^* can be independently obtained for a specific type of kinetic (exchange) process, and the interval so defined is sufficiently small, these bounds may be directly compared with those derived from an Arrhenius plot. In this manner, once the reliability of the overall experimental method has been established, other exchange systems which are not expected to have ΔS^* values within the prescribed interval may be studied with some confidence. The activation energy for HR in simple amides and thioamides is largely determined by changes in the bonding forces while the entropy of activation reflects changes in the freedom of atomic motion.[29] Also, as only about 12 normal vibrational modes are involved and the major structural change on entering the transition state is the lengthening of the N–C bond which is compensated for by a shortening of the C=S bond, the internal rotation to first order is a simple statistical function. Since the amides can rotate about the N–C bond in two distinct directions it may be assumed that the upper bond for ΔS^* is $R \ln 2 \simeq 1.4$ cal deg^{-1} mol^{-1} with a lower bound of zero. This relatively small interval corresponds to an error in ΔG^* of 0.1 kcal/mol. Furthermore, as there are two possible transition states for amides[2b] with very different dipolar characteristics, ΔS^* may be positive or negative depending upon the solvation structure involved for a thioamide in solution. Therefore, if the maximum allowable error in ΔG^* is 0.5 kcal/mol, the corresponding error in ΔS^* is about 4 cal deg^{-1} mol^{-1} and hence the experimentally determined value is considered to be acceptable if it is in the range from −4.0 to 4.0 cal deg^{-1} mol^{-1}. These entropy bounds may be compared with $\Delta S^* = 3.6$ cal deg^{-1} mol^{-1} as measured for the inversion of cyclohexane.[30]

Results

N,N-Dimethylthiocarbamyl Cyanide. This compound has previously been studied by Sandström,[20] who used o-dichlorobenzene as a solvent with a concentration of Sx(CN) of 33.3 mol %. The chemical shift between the *N*-methyl protons was reported as 0.2 ppm while the activation parameters agree satisfactorily with those reported here. In the present work we have used a less polar solvent and found unexpected but interesting spin-coupling features in the spectrum, which require at least a test of the validity of using only two sites to describe the exchange.[12] In TCE the spectrum of Sx(CN) shows two chemically shifted quartets (slow exchange limit).

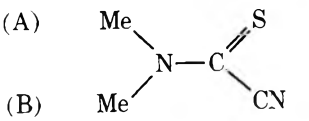

The long-range coupling, referred to the above canonical structure, arises from inter-methyl spin–spin interactions. This is the first reported case of H–C–N–C–H $^4J_{HH}$ splitting. In view of the previously known high barrier in Sx(CN)[20] it seems reasonable that the unusually high electron density in the N–C bond might, at the nitrogen, provide a coupling mechanism for the methyl proton spins. If this premise were true, then other amido-type molecules with a high barrier should also show intermethyl proton spin coupling under appropriate conditions. This led us to reinvestigate the spectrum of *N,N*-dimethylnitrosamine (DMN). We observed intermethyl coupling in this compound at a concentration of 92 mol % in tetrabromoethane. The spin coupling constants seem to depend on solvent, temperature, and concentration in a somewhat unpredictable way. The values of $^4J_{HH}$ are both in the range 0.25 ± 0.05 Hz. We have known for some time that the resolution of the cis and trans couplings in Ox(H) depends on the solvent[31] and since the barrier in this compound is also high ($\Delta G^* \simeq 21$ kcal/mol) the apparent loss of resolution in the spectrum may be connected with the appearance of unresolved long-range inter-methyl proton–proton spin–spin coupling. Now that techniques of Fourier Transform Carr-Purcell "J" spectra are available to measure extremely small couplings (down to ≃0.01 Hz),[32] these results suggest a study of these long-range couplings as a function of ΔG^* for the HR.

The *N*-methyl proton chemical shifts of Sx(CN) displayed a slight linear dependence upon temperature variation. The low-field feature was most sensitive with their separation ranging from 0.178 ppm at 130.2° to 0.108 ppm at 171.0°. We predict from this and other unpublished results[33] that $\Delta\omega < 0$ or the methyl protons cis to sulfur appear at low field. This is opposite to our findings for the compound Ox(CN) and indicates that, when compared with CN, sulfur has a more diamagnetic effect than oxygen.

N,N-Dimethylthiocarbamyl Fluoride. This compound has not previously been examined and the spectrum in the slow exchange limit reveals long-range couplings to both *N*-methyl groups from the fluorine nucleus. At room temperature $J_{trans} = 2.5 \pm 0.05$ Hz but a small variation in temperature of these couplings can be detected. At the highest temperature used (139.2°) the couplings extrapo-

(28) R. R. Shoup, E. D. Becker, and M. L. McNeel, *J. Phys. Chem.*, **76**, 71 (1972).
(29) A. Streitwieser, Jr., "Molecular Orbital Theory for Organic Chemists," Wiley, New York, N. Y., 1961, p 311.
(30) F. A. L. Anet and A. J. R. Bourn, *J. Amer. Chem. Soc.*, **89**, 760 (1967).
(31) V. J. Kowelewski, private communication.
(32) R. L. Vold and S. O. Chan, *J. Magn. Resonance*, **4**, 208 (1971); R. Freeman and D. W. Hill, *J. Chem. Phys.*, **54**, 301 (1971); R. L. Vold and R. R. Shoup, *ibid.*, **56**, 4787 (1972).
(33) R. F. Hobson, Ph.D. Thesis, The University of Waterloo, 1972.

TABLE I: Summary of Kinetic Results

Compd	Mol %	Solvent	E_a, kcal/mol	$\Delta H^*(25°)$, kcal/mol	ΔS^*, cal deg^{-1} mol^{-1}	$\Delta G^*(25°)$, kcal/mol	Temp range, °C
Sx(CN)	1.9	TCE	25.2 ± 0.5	24.6 ± 0.5	3.8 ± 1.1	23.5 ± 0.5	130–171
Sx(F)	18.2	TCE	21.4 ± 0.5	20.8 ± 0.5	0.2 ± 1.2	20.7 ± 0.5	51–140
Sx(Cl)	20.0	CCl_4	18.3 ± 0.3	17.7 ± 0.3	−3.3 ± 0.9	18.7 ± 0.3	40–98
Sx(NH_2)	3.6	TCE	13.7 ± 0.2	13.1 ± 0.2	−2.8 ± 0.8	13.9 ± 0.2	−29–70

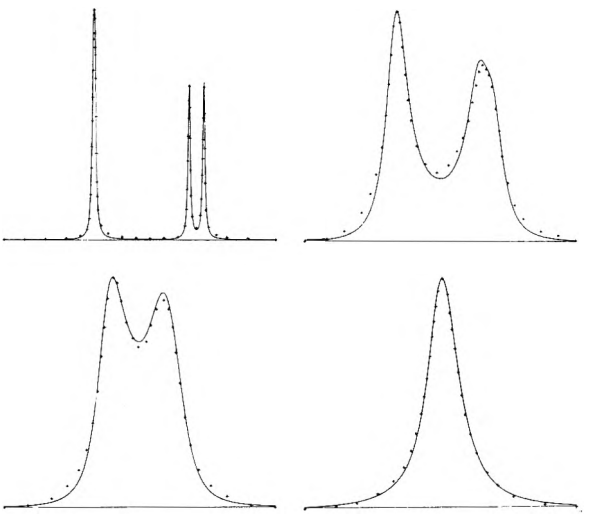

Figure 1. Fitted spectra for Sx(F) (experimental crosses over computer-simulated spectrum): top left k = 0.07 sec^{-1}, T = 50.9°, width = 39.05 Hz; top right k = 13.1 sec^{-1}, T = 109.1°, width = 47.00 Hz; bottom left k = 28.2 sec^{-1}, T = 120.4°, width = 34.01 Hz; bottom right k = 94.9 sec^{-1}, T = 139.2°, width = 25.28 Hz.

late to J_{trans} = 2.1 ± 0.05 Hz and J_{cis} = 0.23 ± 0.05 Hz. Because of the small magnitude of the cis coupling a relative sign determination using the methods of multisite exchange was not possible.[5] The couplings were assumed to be of the same sign, consistent with previous determinations of relative signs in amides.[5-7,34] A set of representative line shape fits are included in Figure 1 while the activation and rate data appear in Table I.

There is a strong linear dependence of the internal chemical shift $\Delta\omega$ upon temperature variation. At 51° $|\Delta\omega|$ = 0.190 ppm. This variation is manifest mainly by the high-field methyl feature, which also displays the largest scalar coupling. These data indicate that $\Delta\omega > 0$, oposite to Sx(CN). The parent compound, Ox(F), was reported to have a chemical shift $|\Delta\omega| \simeq +0.01$ ppm while the larger scalar coupling, also appearing at high field, was given as J_{trans} = 0.8 Hz, and J_{cis} = 0.3 Hz. Since the cis and trans π couplings are expected to be similar,[35] the large differences between trans couplings in Ox(F) and Sx(F) are thought to be effects brought on by increased asymmetry in the ground-state wave function due to the presence of sulfur. Thus the changes caused by substitution indicate that $\Delta\omega$ may be allied to J_{trans} (in mechanism) while J_{cis} derives from a somewhat substituent independent effect, or effects which largely cancel one another.

N,N-Dimethylthiocarbamyl Chloride. Sx(Cl) has previously been studied. Newman, *et al.*,[36] found ΔG^* = 19.0 kcal/mol at 266°K while Sandström[20] reports 19.1 kcal/mol at 250.2°K. The solvent for the former study was 94 mol % CCl_4 while the latter used 73 mol % *o*-dichlorobenzene. Both of these numbers appear slightly high. The kinetic data for this simple two-site case appears in Table I.

There is a small nonlinear dependence of $\Delta\omega$ upon temperature, varying from 2.1 Hz at 30° to 1.8 Hz at 95°. We have estimated $\Delta\omega > 0$, curiously similar in sign and magnitude to $\Delta\omega$ for Ox(F)[5] suggesting that the d orbital contributions to the magnetic anisotropy at the *N*-methyls by sulfur and chlorine are similar in magnitude but differ in sign. The free energies of activation for these compounds are also the same within experimental error. A possible trend is now apparent, namely, that ΔG^* and $\Delta\omega$ will be similar in the series Ox(F), Sx(Br), Sex(Br); Ox(Cl), Sx(Br), Sex(I); etc. A consequence is that $\Delta\omega$ for Ox(Br) and Sx(Br) is almost degenerate,[33] a prediction which should be experimentally tested once Sx(Br) is isolated.

N,N-Dimethylthiourea. This compound displays a large internal chemical shift, $|\Delta\omega|$, varying linearly from 0.313 ppm at −29° to 0.234 ppm at +70°. The low-field methyl feature is most sensitive implying $\Delta\omega < 0$. The kinetic results are summarized in Table I.

Discussion

The present study extends considerably the reliable energy barrier determinations for thioamides. The free energies of activation (in kcal/mol at 25°) for the present work are Sx(CN), 23.5 ± 0.5; Sx(F), 20.7 ± 0.5; Sx(Cl), 18.7 ± 0.3; and Sx(NH_2), 13.9 ± 0.2. The corresponding ΔG^* values for the simple amides are Ox(CN), 21.4 ± 0.6;[16] Ox(F), 18.1 ± 0.6;[5] Ox(Cl), 16.5 ± 0.5;[16] and an estimated barrier of approximately 5.0 for Ox(NH_2).[2b] The estimate for Ox(NH_2) was not made from nmr data quantitatively but was suggested as upper limits, set because the variation with temperature of the spectrum showed no effects attributable to decrease in exchange rate.[2b] As was pointed out in a recent note[23] the barriers in thioamides are generally about 2 kcal/mol higher than in corresponding oxyamides while selenoamides possess barriers about 1 kcal/mol higher again. The regularity of trends thus makes the hitherto estimated barrier for Ox(NH_2) quite incongruous.

The increase in the energy barrier for this compound is connected, in valence bond terms, with a greater contribution from canonical structure II because the C=S bond has less double bond character than the C=O bond. The

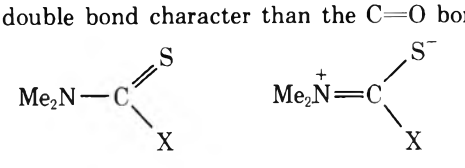

I II

(34) A. J. R. Bourn and E. W. Randall, *Mol. Phys.*, **8**, 567 (1964).
(35) J. A. Pople, W. G. Schneider, and H. J. Bernstein, "High-Resolution Nuclear Magnetic Resonance," McGraw-Hill, New York, N. Y., 1959, p 35.
(36) R. C. Newman, Jr., D. N. Roark, and V. Jonas, *J. Amer. Chem. Soc.*, **89**, 3412 (1967).

barrier appears to be a similar function of the substituent X in both amides and thioamides. The sharing of delocalized π energy in related urea structures leads to a much lower energy barrier. Major contributing canonical valence bond structures for $Ox(NH_2)$ can be written in three forms (III-V).

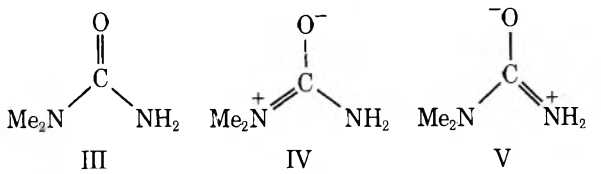

Ignoring the small effect of methyl substitution (in place of hydrogen) on nitrogen, the N-C bond π electron density in $Ox(NH_2)$ will be approximately one-half of that in the simple amide Ox(H). Thus, taking $\Delta G^* = 21 \pm 0.5$ kcal/mol for Ox(H),[2b] the estimated ΔG^* in $Ox(NH_2)$ becomes 10.5 kcal/mol. This value agrees quite well with an estimated 11.9 kcal/mol that can be obtained by using a figure of 2 kcal/mol less than the thiourea $Sx(NH_2)$. The reason that research workers have failed to detect a barrier to rotation in $Ox(NH_2)$ is most rationally explained by a small internal chemical shift which approaches zero (and then changes sign) at temperatures which are low enough to slow down the rotation significantly.

Surface Acidity of Transition Metal Modified Aluminas. Infrared and Nuclear Magnetic Resonance Investigation of Adsorbed Pyridine

F. E. Kiviat and Leonidas Petrakis*

Gulf Research & Development Company, Pittsburgh, Pennsylvania 15230 *(Received December 15, 1972)*

Publication costs assisted by Gulf Research & Development Company

The surface acidity of transition metal modified aluminas was investigated by means of pyridine adsorption. Both infrared and wide-line nmr spectroscopy of adsorbed pyridine were studied. It was observed that alumina and both Co and Ni impregnated alumina contained only Lewis acid surface sites, whereas alumina impregnated with Mo, either in the presence or absence of Co or Ni, contained both Lewis and Brønsted surface acid sites. Relationships between the ratio of the various types of Lewis to Brønsted surface acid sites and integrated infrared absorption bands were derived. The Lewis to Brønsted acid site ratios were approximately the same with calcined and reduced modified aluminas. Wide-line nmr spectra indicate that the physically adsorbed pyridine on both calcined and reduced modified aluminas has considerable mobility, while chemisorbed pyridine shows much broader spectra.

Introduction

Spectroscopic investigations of surfaces have received considerable attention in recent years because they can provide information about the interaction between adsorbed species and the surface. Surface acidity is one property that has received particular attention for it can play a significant role in determining the behavior of solid surfaces.[1] A variety of probe molecules has been utilized to both qualitatively ascertain the acidity as well as provide a measure of the distribution and strength of the acid sites.

Pyridine, which is both a Lewis and Brønsted base, has been used successfully as a probe to characterize the acidity of oxide surfaces.[1-10] The ability to distinguish Lewis and Brønsted surface acidity using a pyridine probe has resulted in studies of the following surfaces, *inter alia:* η-Al_2O_3,[2] γ-Al_2O_3,[3] δ-Al_2O_3,[4] silica-alumina,[5,6] zeolites,[7-9] and chromia.[10] Recent compilations of surfaces studies are given by Tanabe[1a] and Basila.[1b]

The surface properties of the above oxides are significantly altered by incorporation of a second metal oxide. The manner in which the surface acidity is modified upon such an addition is the subject of this investigation.

Parry[2] showed that pyridine adsorbed on either Lewis or Brønsted acid sites of an oxide surface will produce sharp bands in the infrared spectral region 1400-1650 cm^{-1}.

(1) (a) K. Tanabe, "Solid Acids and Bases," Academic Press, New York, N. Y., 1970; (b) M. R. Basila, *Appl. Soectrosc. Rev.*, **1**, 289 (1968).
(2) E. P. Parry, *J. Catal.*, **2**, 317 (1963).
(3) (a) T. R. Hughes and H. M. White, *J. Phys. Chem.*, **71**, 2192 (1967); (b) T. R. Hughes, H. M. White, and R. J. White, *J. Catal.*, **13**, 58 (1969).
(4) (a) H. Knozinger and H. Stolz, *Fortschr. Kolloid. Polym.*, **55**, 16 (1971); (b) H. Stolz and H. Knozinger, *Kolloid-Z. Z. Polym.*, **243**, 71 (1971).
(5) M. R. Basila, T. R. Kantner, and K. H. Rhee, *J. Phys. Chem.*, **68**, 3197 (1964); M. R. Basila and T. R. Kantner, *ibid.*, **70**, 1681 (1966).
(6) P. Pichat, M. V. Mathieu, and B. Imelik, *Bull. Soc. Chim. Fr.*, 2611 (1969).
(7) J. W. Ward and R. C. Hansford, *J. Catal.*, **13**, 154 (1969), and references therein.
(8) M. Lefrancois and G. Malbois, *J. Catal.*, **20**, 353 (1971), and references therein.
(9) L. G. Christner, B. V. Liengme, and W. K. Hall, *Trans. Faraday Soc.*, **64**, 1679 (1968).
(10) A. Zecchina, *et al.*, *J. Phys. Chem.*, **76**, 571 (1972).

These absorption frequencies and the species responsible for the absorptions are as follows: 1450, 1490, 1580, and 1600–1630 cm^{-1} for pyridine chemisorbed to a Lewis acid surface site; 1490, 1540, 1620, and 1640 cm^{-1} for pyridine chemisorbed to a Brønsted acid surface site, *i.e.*, an adsorbed pyridinium ion.[2] The actual values of these frequencies are dependent upon the particular oxide surface studied as well as the temperatures employed for both the oxide pretreatment and the adsorption–desorption of pyridine. The normal vibrational modes giving rise to these absorptions, except for the 1540-cm^{-1} pyridinium absorption, are primarily pyridine in-plane ring deformations. The 1540-cm^{-1} absorption of the pyridinium ion arises primarily from the in-plane NH^+ deformation.[2,5]

Pyridine adsorbed on the following modified aluminas was studied in order to elucidate the nature of the acidic sites: 2% MoO_3/η-Al_2O_3, 6% MoO_3/η-Al_2O_3, 9% MoO_3/η-Al_2O_3, 10% MoO_3/γ-Al_2O_3, 2% Co–10% MoO_3/η-Al_2O_3, 2% Ni–10% MoO_3/η-Al_2O_3. The percentages indicate the weight per cent of the transition metal relative to the weight of the entire catalyst. Also investigated, to aid in the above elucidation, was the conversion of chemisorbed pyridine on η-Al_2O_3 to adsorbed pyridinium ion *via* the addition of HCl. The structural implications of the measurements of acidity reported here will also briefly be discussed.

Experimental Procedure

A. Materials. The modified aluminas were prepared by standard impregnation techniques. MoO_3 was impregnated on the base alumina (either η or γ) from an aqueous solution of ammonium paramolybdate. CoO and NiO were incorporated using aqueous solutions of $Co(NO_3)_2$ and $Ni(NO_3)_3$, respectively. The preparations were dried at 100° for 2 hr, then calcined at 500° for 18 hr in a current of dry air.

B. Spectroscopic Procedures. For ir investigation, samples were ground into a fine powder and that portion which passed through a 44-μ sieve was used to prepare thin wafers. The wafers, which were 1 in. in diameter, were obtained by pressing ~100 mg of material at a pressure of ~8000 psi for a time period ranging from 0.5 to 1 min. All treatments of the wafers were carried out after the wafer was mounted in the infrared cell. The cell was attached to a standard vacuum system in which the ultimate pressure achieved, with pumping, was $\sim 10^{-6}$ Torr. The infrared cells used were similar to those described by Basila.[5]

Initially, the wafer was evacuated at 500° for 16 hr. Reduction of the wafer was accomplished by flowing H_2 at a rate of ~20 cc/min at 500° for a period of 4 hr. This was immediately followed by further evacuation at 500° for 4 hr.

Pyridine was added to the wafer surface by exposure to 12 Torr of vapor at 150° for 1 hr, followed by 2 hr of evacuation at the same temperature. The spectrum usually indicated hydrogen-bonded pyridine, which is characterized by absorptions in the region 1440–1450 cm^{-1} and at 1600 cm^{-1}.[2] The wafer was then further evacuated at 150° for 16 hr. Spectra recorded after this treatment indicated only chemisorbed pyridine. Other evacuation temperatures and time periods were used, and these are specified in the text. The addition of HCl, the purpose of which was to convert adsorbed pyridine to adsorbed pyridinium ion, was accomplished by exposing the catalyst containing adsorbed pyridine to ~2 Torr at room temperature, and then isolating the infrared cell from the vacuum line. Spectra were recorded with the catalyst in the HCl atmosphere.

All spectra were recorded at ambient temperature on a Beckman IR-12 infrared spectrophotometer, which was continually flushed with dry air. The cell was positioned in the instrument for at least 2 hr prior to the recording of a spectrum. The spectrophotometer was frequently calibrated using a polystyrene film, and all frequencies presented are accurate to within 2 cm^{-1}. The spectral slit width was 4 cm^{-1} throughout the entire spectrum. The reference beam was attenuated using either a wedge or wire screen.

The integrated band intensities were obtained with a planimeter. Each integrated band intensity was generally reproducible to within a relative error of less than 1%. In a few unfavorable cases, this relative error was at most less than 2%. The integrated band intensities obtained from the spectra of a wafer undergoing various treatments were normalized to an integrated band intensity from the same sample within the same series of treatments.

The values of parameters obtained from integrated band intensity ratios are the average values determined from at least two series of spectra. Each series of spectra was from a different wafer preparation of the same material, subjected to identical treatment.

The absolute values of the integrated band intensities due to absorptions of chemisorbed pyridine did change during a time interval of 8 hr to 4 days. However, the ratios of integrated band intensities were within 4% of each other. The values of ratios reported were those obtained within 8 hr of the last wafer treatment.

Nuclear magnetic resonance experiments were carried out with standard Varian V-4200A nmr spectrometer equipped with Fieldial for magnetic field scanning. The first derivative of the resonance absorption was recorded at 11.09 MHz using 40-Hz audiomodulation of the field with sufficiently low peak-to-peak amplitude to prevent artificial broadening. Intensities were obtained from the peak-to-peak line width and amplitude of the first-derivative curves, and they were normalized to the intensity of a standard sample run under identical conditions.

Results and Discussion

A. Pyridine Adsorbed on η-Al_2O_3 and γ-Al_2O_3. Figures 1A, 1B, and 1C present the spectra of pyridine adsorbed on calcined η-Al_2O_3 and Table I the observed absorption maxima. The absence of absorption bands in the spectral region from ~1430 to ~1450 cm^{-1} and at ~1600 cm^{-1} in these spectra indicates that no detectable hydrogen-bonded pyridine is present on the η-Al_2O_3 surface.[2]

A comparison of the two spectra presented in Figures 1A and 1B shows that evacuation at 500° for 1 hr results in the disappearance of the 1618-cm^{-1} absorption band and a shift of that at 1453 to 1457 cm^{-1}. This effect is attributed to the presence of two distinct chemisorbed species upon the η-Al_2O_3 surface. The adsorbed species more strongly bonded to the surface has characteristic absorption maxima at 1625, 1578, 1496, and 1457 cm^{-1}, whereas these occur at 1618, 1578, 1496, and 1453 cm^{-1} for the more labile adsorbed species. These results are consistent with those reported by Parry.[2]

The existence of two adsorbed species demonstrates that there are two distinct types of Lewis acid sites on the

TABLE I: Observed Infrared Spectra of Chemisorbed Pyridine in the Region 1400–1650 cm^{-1}

Sample	Treatment[a]	Observed frequencies, cm^{-1} [b]							Chemisorbed species present[c]
1. Alumina									
Calcined η-Al_2O_3	B	1453	1496		1578	1618	1625		LPY(I), LPY(II)
	C	1457	1496		1578		1625		LPY(II)
	D	1453(+)	1489	1539		1612		1638	BPY (+, residual LPY)
Reduced η-Al_2O_3	B	1453	1496		1578	1618	1625		LPY(I), LPY(II)
γ-Al_2O_3	B	1456	1495		1574		1623		LPY
	C	1458	1497		1574		1626		LPY
2. Modified alumina									
2% MoO_3/η-Al_2O_3	B	1453	1495		1578	1618(sh)	1623		LPY(I), LPY(II)
	C	1457	1497		1576		1626		LPY(II)
6% MoO_3/η-Al_2O_3	B	1455	1495	1543	1578		1623	1640	LPY(I), BPY[e]
	C	1457	1497		1578		1625		LPY(I)
9% MoO_3/η-Al_2O_3	B	1456	1491	1543	1578	1614	1625	1640	LPY(I), BPY[e]
Reduced 9% MoO_3/η-Al_2O_3	B	1455	1491	1543	1578	1614	1623	1640	LPY(I), BPY[e]
9% Co/η-Al_2O_3	B	1454	1495		1578	1619(sh)	1624		LPY(I), LPY(II)
2% Co–10% MoO_3/η-Al_2O_3	A	1453	1492	1543	1578	1613	1624	1640	LPY(I), LPY(II), BPY
	B	1453	1492	1543	1578	1613	1625	1640	LPY(I), LPY(II), BPY
2% Ni–10% MoO_3/η-Al_2O_3	A	1453	1491	1543	1578	1612	1625	1640	LPY(I), LPY(II), BPY
10% MoO_3/γ-Al_2O_3	A	1453	1493	1542	1578	1620	1625	1640	LPY, BPY
	B	1456	1493	1543	1578	1620	1625	1640	LPY, BPY
	C	1458					1626[d]		LPY

[a] All catalysts are calcined only unless reduction is specified. The catalysts were exposed to 12 Torr of pyridine at 150° for 1 hr followed by A, evacuation for 2 hr at 150°; B, evacuation for 16 hr at 150°; C, evacuation for 1 hr at 500°; D, addition for 2 Torr of HCl. [b] The symbol (sh) refers to a distinct shoulder. [c] LPY(I), LPY(II), and BPY refer to pyridine chemisorbed to Lewis acid I, Lewis acid II, and Brønsted acid surface sites, respectively. LPY refers to chemisorption at an unspecified Lewis acid site. [d] The spectrum obtained was too weak to unequivocally ascertain the remainder of the absorption maxima. [e] Observed spectra indicate that a small amount of LPY(I) is present.

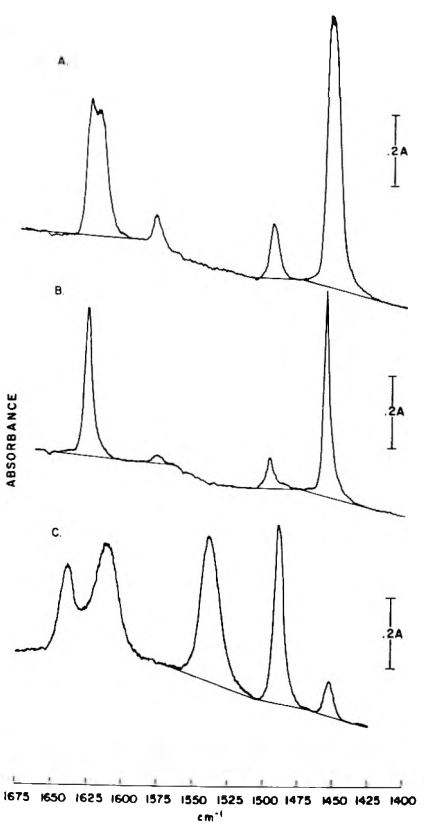

Figure 1. Infrared spectra of chemisorbed pyridine on η-Al_2O_3: (A) LPY(I) and LPY(II), η-Al_2O_3 exposed to 12 Torr of pyridine for 1 hr at 150° followed by evacuation at 150° for 16 hr; (B) LPY(II), sample yielding spectrum A, but followed by evacuation at 500° for 1 hr; (C) BPY, same treatment as A, but followed by the addition of 2 Torr of HCl at room temperature.

η-Al_2O_3 surface. The difference in lability of the two chemisorbed species furthermore indicates that the two surface Lewis acid sites are of different acidic strength. The more labile chemisorbed species, hereafter referred to as LPY(I), possesses band maxima at 1618, 1578, 1496, and 1453 cm^{-1} and is bonded at the weaker type of site, hereafter referred to as Lewis acid site I. The type of site of greater Lewis acid strength will be referred to as Lewis acid site II, with pyridine chemisorbed to this site referred to as LPY(II).

The only previous spectroscopic interpretations of the chemisorption of pyridine to alumina surfaces, other than Parry's,[2] are those of Hughes and coworkers,[3] Knözinger and Stolz,[4] and Pichat, *et al.*[6]

The spectrum reported by Hughes, *et al.*,[3a] of pyridine chemisorbed to γ-Al_2O_3 contained absorption bands at 1453, 1492, 1575, and 1615 cm^{-1}. These were interpreted as being due to pyridine chemisorbed to one type of Lewis site. There was no evidence for a doublet in the 1615-cm^{-1} region, although a weak broad absorption was observed at ~1600 cm^{-1}. The above results were confirmed by adsorbing pyridine on γ-Al_2O_3 under identical conditions as used for η-Al_2O_3. After 16 hr of evacuation at 150°, absorption bands were observed at 1456, 1495, 1574, and 1623 cm^{-1}. The absorption band at 1623 cm^{-1} was broad, but no evidence existed for a doublet. Upon further heating and evacuation at 500° for 1 hr, the 1456-cm^{-1} absorption band shifted to 1458 cm^{-1}, and the 1623-cm^{-1} band to 1626 cm^{-1}. Two alternative explanations exist for these observations. First, it could be that the γ-Al_2O_3 surface contains only one type of Lewis acid site. However, this does not explain the observed shifts upon evacuation at 500°. Alternatively, two Lewis acid surface sites may exist. Then the vibrational frequencies of the chemisorbed

pyridine to these sites would be for all intents accidentally degenerate. This degeneracy could be ascribed to approximate equal acidic strengths of the two sites.

Knözinger and Stolz[4] studied the adsorption of pyridine on a δ-Al_2O_3 surface. They observed four distinct types of Lewis acid surface sites, and where each site gives rise to characteristic vibrational frequencies of adsorbed pyridine in the region 1400–1700 cm^{-1}. The relative amount of each type of site present on a given surface was shown to be dependent upon both the calcination temperature and the temperature at which pyridine was adsorbed. When the δ-Al_2O_3 was calcined at 500° and the pyridine adsorbed at 200°, absorption bands were observed at 1449, 1490, 1576, 1614, and 1624 cm^{-1}, and also a shoulder at 1617 cm^{-1}. Our findings are consistent with these results, although we did not observe a shoulder on the 1618-cm^{-1} band. This is undoubtedly due to the differences in the aluminas used (as, for example, the differences in behavior between the γ- and η-Al_2O_3).

Pichat, *et al.*, reported the spectrum of pyridine adsorbed on a P Degussa Al_2O_3.[6] However, these authors did not consider the distribution of Lewis acid surface sites among several types, as did Parry,[2] Knözinger and Stolz,[4] and ourselves.

Figure 1C presents the spectrum of adsorbed pyridinium ion, hereafter referred to as BPY. The characteristic absorptions of BPY at 1489, 1539, 1612, and 1639 cm^{-1} are well developed. The weak absorption at 1453 cm^{-1} is due to residual LPY(I) and LPY(II).

A comparison of the spectra in Figure 1 shows that the 1539-cm^{-1} absorption of BPY is free from interference due to LPY(I) and LPY(II), and hence can be used to evaluate the amount of BPY. Similarly, absorption bands due to LPY(I) and LPY(II) are free from BPY interference at 1453 cm^{-1}. All three species absorb at ~1490 cm^{-1} and have overlapping bands in the interval 1600–1650 cm^{-1}.

The spectrum of the chemisorbed pyridine on an H_2 reduced η-Al_2O_3 contained identical absorption maxima as that obtained from an unreduced wafer (*i.e.*, Figure 1A). The only difference in these spectra was that the ratio of the absorbances (*i.e.*, peak intensities or heights) of the 1618-cm^{-1} absorption band to that at 1625 cm^{-1} had a value of 0.93 for the reduced η-Al_2O_3, and a value of 1.08 for the unreduced wafer. All other absorbances normalized to the absorbance of the 1453-cm^{-1} absorption band were identical in both spectra. This slight difference in these ratios indicates that H_2 reduction, relative to an absence of reduction, does not significantly alter the relative amounts of Lewis acid sites I and II on the η-Al_2O_3 surface.

The remaining chemisorbed pyridine after evacuation at 500° for 1 hr on the reduced η-Al_2O_3 yielded a duplicate spectrum to that of the unreduced η-Al_2O_3 (*i.e.*, Figure 1B). This indicates that, in a qualitative sense, reduction does not affect the relative strengths of Lewis acid sites I and II.

B. Pyridine Adsorbed on Modified η-Al_2O_3. Nmr Results. The nmr spectra of a series of molybdena (9%) modified alumina that either have been calcined at 500° only or subsequently reduced with H_2 also for 2 hr at the same temperature were recorded in the manner discussed in the Experimental Section. The pretreatment was followed by exposure to pyridine vapor at its room temperature vapor pressure. Both reduced and calcined samples when exposed to pyridine for the same periods adsorbed comparable amounts (Table II). The observed signals due to pyridine were narrow with a line width of ~0.1 G. Care was taken in the recording of the spectra so as not to artifically overmodulate and broaden the observed resonances. The narrow signals observed show that the pyridine adsorbed under the conditions indicated is in a liquid-like state exhibiting considerable mobility on the surface. Upon pumping the system at room temperature, the signal intensity becomes lower and the signal broadens.

TABLE II: Comparison of Nmr Parameters of Physically Adsorbed and Chemisorbed Pyridine on Calcined and Reduced Mo-Al_2O_3

	Prior to any pumping		After pumping at Rt for 2 hr		After pumping at 150° for 2 hr	
	Relative intensity[a]	ΔH[b]	Relative intensity[a]	ΔH[b]	Relative intensity[a]	ΔH[b]
Calcined	0.4	0.08	~0.2	0.24	<0.1	~3
Reduced	0.4	0.14	~0.3	0.24	0.1	~3

[a] Relative intensities expressed as a fraction of the intensity of a standard alumina run under identical conditions. [b] Peak-to-peak line width in gauss.

This behavior is consistent with Karagounis'[11] observation and phenomenological explanation that the monolayer closest to the surface is more under the influence of the substrate than the additional layers. Two hours of pumping removed some 30% of the initial pyridine from the reduced material while the same amount of pumping removed some 60% of the physically absorbed pyridine from the calcined material. This would indicate a slightly stronger binding of the physically adsorbed pyridine on the reduced material than on the corresponding calcined. Further corroborative evidence for this is offered by the behavior of pyridine upon subsequent pumping at 150° for 2 hr. Such pumping presumably should remove all of the physically adsorbed pyridine. In the case of the reduced material, the narrow signal disappears completely and a much broader one now is detected (~3 G) of an intensity which is about 30% that of the originally adsorbed pyridine. In the calcined sample again the narrow signal due to the physically adsorbed material is eliminated completely upon pumping at 150° for 2 hr, but unlike the reduced sample no broad signal is observed with a single scan of the appropriate spectral region. However, when a time average computer is used to scan the region, then a broad signal quite similar to that from the reduced sample is also obtained. These results, as summarized in Table II, indicate the following. There is no fundamental qualitative difference between the behavior of reduced and calcined molybdena modified η-Al_2O_3. Rather the difference is one of degree. The amount of pyridine adsorbed initially is approximately the same, but the calcined material loses its physically adsorbed pyridine somewhat more readily. The physically adsorbed pyridine gives a very narrow liquid-like signal while the chemisorbed has considerable immobility as evidenced by the far broader signal. Finally, the intensity of the chemisorbed pyridine on the calcined samples is less than that of the reduced ones requiring time averaging for its observation. Further evacuation of the samples at 500° removes most of this broad and weak signal that was observed after evacuation at 150°. This indicates that the physically adsorbed pyri-

(11) G. Karagounis, *Nature (London)*, **201**, 604 (1964).

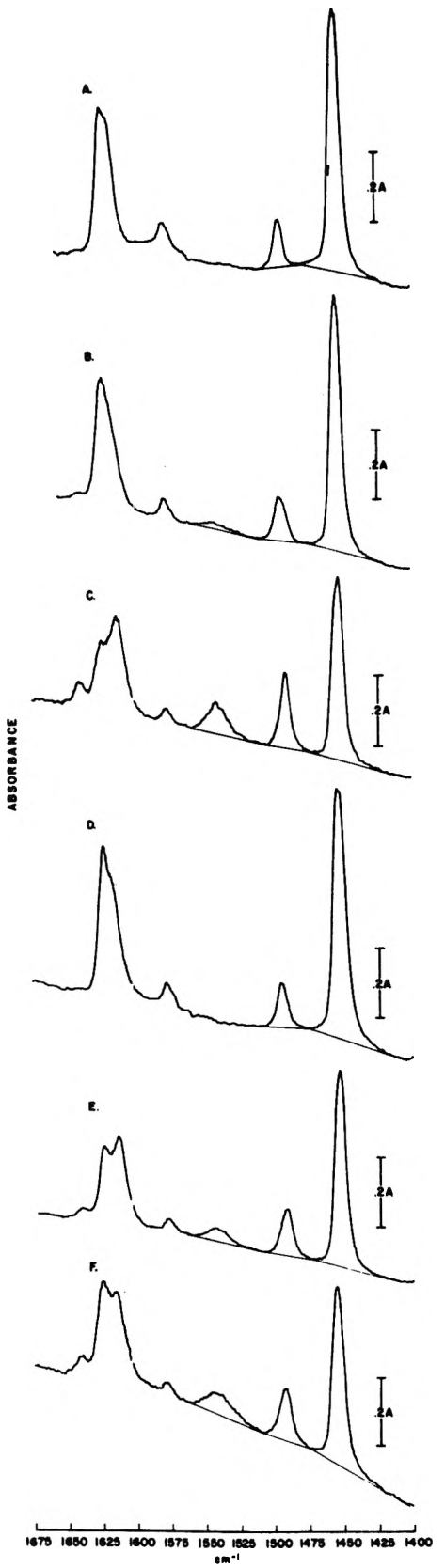

Figure 2. Infrared spectra of chemisorbed pyridine on modified alumina (all samples are calcined and were treated by exposure to 12 Torr of pyridine for 1 hr at 150° followed by evacuation at 150° for 16 hr): A, 2% MoO_3/η-Al_2O_3; B, 6% MoO_3/η-Al_2O_3; C, 9% MoO_3/η-Al_2O_3; D, 9% Co/η-Al_2O_3; E, 2% Co–10% MoO_3/η-Al_2O_3; F, 10% MoO_3/γ-Al_2O_3.

dine is completely removed upon pumping at 150°, whereas the chemisorbed is not.

C. Pyridine Adsorbed on Modified η-Al_2O_3. Ir Results. Table I presents the observed absorption maxima and Figure 2A–F presents the spectra of pyridine chemisorbed on the following modified η-aluminas: 2% MoO_3/η-Al_2O_3; 6% MoO_3/η-Al_2O_3; 9% MoO_3/η-Al_2O_3; 9% Co/η-Al_2O_3; 2% Co–10% MoO_3/η-Al_2O_3; 10% MoO_3/γ-Al_2O_3. Although not shown, the spectra of chemisorbed pyridine on a 9% Ni/η-Al_2O_3 and 2% Ni–10% MoO_3/η-Al_2O_3 were identical with those for the Co-containing aluminas.

Those catalysts containing 9% MoO_3 have a distinctly well-developed absorption band at $\sim$1543 cm^{-1}; the 6% MoO_3/η-Al_2O_3 catalyst has a weak absorption at this wave number. These absorptions demonstrate the presence of surface Brønsted acidic sites. The 2% MoO_3/η-Al_2O_3 catalyst does not show Brønsted surface acidity. This difference in behavior between the 2% and 6% MoO_3/η-Al_2O_3 catalysts is most probably due to a concentration effect.

A sample of 25% MoO_3/η-Al_2O_3 was prepared and treated identically as the 9% Mo-containing samples. Inspection of the spectra indicates a much larger amount of BPY relative to both types of LPY than for the 9% Mo-containing catalysts. This is consistent with the difference between the 2 and 6% catalysts being attributed to a Mo concentration effect.

The spectra of the 2% MoO_3/η-Al_2O_3 and 9% Co/η-Al_2O_3 catalysts with chemisorbed pyridine (Figure 2A, D) are the only modified aluminas with an absorption at 1618 cm^{-1}. The absorption occurs as a distinct shoulder and is not resolved into a doublet as in the spectrum of η-Al_2O_3. This absorption, as well as the strong absorption occurring at 1453 cm^{-1} in these spectra, indicates the presence of LPY(I) and LPY(II) upon these surfaces.

The remainder of the modified aluminas' spectra contains absorptions at 1543 cm^{-1} due to BPY. Interference due to the 1612-cm^{-1} BPY absorption band can obscure a shoulder at 1618 cm^{-1}; therefore, the presence or absence of LPY(I) must be determined from the position of the absorption band in the 1453–1457-cm^{-1} region. An absorption band at 1453 cm^{-1} (or 1454 cm^{-1}) indicates the presence of either LPY(I) or LPY(I) and LPY(II), whereas absorption at 1457 cm^{-1} (or 1456 cm^{-1}) indicates the presence of only LPY(II). The presence of an absorption band at 1455 cm^{-1} is indicative of both LPY(I) and LPY(II), but where the amount of LPY(I) relative to LPY(II) is significantly less than that present on η-Al_2O_3.

The above assignments for chemisorbed pyridine on the modified aluminas are presented in Table I. They are, as implied in the above discussion, based upon analogy with the spectrum obtained upon chemisorption of pyridine to an η-Al_2O_3 surface. The implied assumption is that the detectable chemisorbed pyridine on the modified aluminas is bonded to the substrate. This assumption is reasonable as indicated by the observation that the 1453-cm^{-1} (or 1454-cm^{-1}) absorption band, where present, is approximately of the same intensity for catalysts of different Mo and Co concentration upon identical treatment.

Further support of this assumption was obtained by the following experiment. KBr wafers of both η-Al_2O_3 and MoO_3 were prepared, and where the Al and Mo were present at 10% by weight of the pellet. The wafers were subjected to the following treatment: heating at 100° for 16 hr with evacuation; exposure to 15 Torr of pyridine at

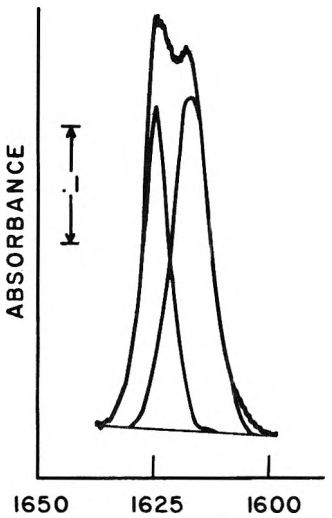

Figure 3. Resolved 1618-, 1625-cm^{-1} doublet of chemisorbed pyridine on η-Al_2O_3.

100° for 0.5 hr; heating at 100° for 2 hr with evacuation. Chemisorption of pyridine upon η-Al_2O_3 was observed, but no adsorption on MoO_3 was detected. The implication is that pyridine chemisorbs solely to the Al_2O_3, and the MoO_3 serves as a proton source, either as an individual unit or synergistically through the substrate.

D. Determination of the Relative Amounts of LPY and BPY on Modified η-Al_2O_3 Surfaces. Basila has reported an infrared spectroscopic procedure for evaluating the amount of pyridine bonded to Lewis acid sites relative to that bonded to Brønsted acid sites on silica–alumina catalysts.[5] This method utilizes the absorbances (peak heights) of the 1450- and 1490-cm^{-1} absorption bands which are due to pyridine bonded to a Lewis acid site, and to Lewis and Brønsted acid sites, respectively.

The procedure adopted herein to evaluate the relative amounts of pyridine bonded to Lewis and Brønsted acid sites is a modification of Basila's. It differs in that integrated band intensities are utilized instead of absorbances. This is necessary because the frequencies of the observed band maxima in the 1450- and 1490-cm^{-1} regions are dependent upon the relative concentrations of adsorbed pyridine on the two Lewis and Brønsted acid sites. As previously mentioned, the former varies from 1453 to 1457 cm^{-1} and the latter from 1489 to 1496 cm^{-1}. The absorptivity of each vibrational mode varies with frequency; consequently, the use of absorptivities would introduce large and indeterminate errors if an observed band maximum were used to determine concentrations. Also, the use of integrated band intensities is preferable to absorbances since a relatively large spectral slit width is used.[12] The integrated band intensities are determined relative to baselines which are constructed according to the usual tangent baseline method,[12] and are shown in the spectra.

Application of Beer's law, in integrated form, for the observed absorptions in the 1450-, 1490-, and 1543-cm^{-1} spectral regions of pyridine adsorbed on a modified η-Al_2O_3 surface yields the following relationships.

$$\int_{1475}^{1412^{1}/_{2}} A_{1450}\,d\nu = \alpha_{1450}{}'bc' + \alpha_{1450}{}''bc'' \qquad (1)$$

$$\int_{1512^{1}/_{2}}^{1475} A_{1490}\,d\nu = \alpha_{1490}{}'bc' + \alpha_{1490}{}''bc'' + \alpha_{1490}{}^{B}bc^{B} \qquad (2)$$

$$\int_{1567^{1}/_{2}}^{1512^{1}/_{2}} A_{1540}\,d\nu = \alpha_{1540}{}^{B}bc^{B} \qquad (3)$$

The observed integrated band intensity in the above is given by $\int_e^f A_\nu\,d\nu$ where the limits of integration e and f correspond to the endpoints of the baseline, $\alpha_\nu{}^i$ is the apparent integrated absorptivity for the ith adsorbed species in the spectral region ν, defined by the appropriate limits of integration, b is the optical path length, and c^i is the concentration of the ith adsorbed species, *i.e.*, c^B is identical to BPY, etc. The actual integration limits, to within ± 5 cm^{-1}, utilized herein are included.

Upon division of eq 1 and 2 by eq 3, and rearrangement of the results, the following are obtained.

$$\frac{\mathrm{LPY(I)}}{\mathrm{BPY}} = \frac{\left(\frac{\alpha_{1490}''}{\alpha_{1540}{}^{B}}\right)\left\{\frac{\int A_{1450}\,d\nu}{\int A_{1540}\,d\nu}\right\} - \left(\frac{\alpha_{1450}''}{\alpha_{1540}{}^{B}}\right)\left\{\left(\frac{\int A_{1490}\,d\nu}{\int A_{1540}\,d\nu}\right) - \left(\frac{\alpha_{1490}{}^{B}}{\alpha_{1540}{}^{B}}\right)\right\}}{\left(\frac{\alpha_{1490}''}{\alpha_{1540}{}^{B}}\right)\left(\frac{\alpha_{1450}'}{\alpha_{1540}{}^{B}}\right) - \left(\frac{\alpha_{1450}''}{\alpha_{1540}{}^{B}}\right)\left(\frac{\alpha_{1490}'}{\alpha_{1540}{}^{B}}\right)} \qquad (4)$$

$$\frac{\mathrm{LPY(II)}}{\mathrm{BPY}} = \frac{\left(\frac{\alpha_{1490}'}{\alpha_{1540}{}^{B}}\right)\left\{\frac{\int A_{1450}\,d\nu}{\int A_{1540}\,d\nu}\right\} - \left(\frac{\alpha_{1450}'}{\alpha_{1540}{}^{B}}\right)\left\{\left(\frac{\int A_{1490}\,d\nu}{\int A_{1540}\,d\nu}\right) - \left(\frac{\alpha_{1490}{}^{B}}{\alpha_{1540}{}^{B}}\right)\right\}}{\left(\frac{\alpha_{1490}'}{\alpha_{1540}{}^{B}}\right)\left(\frac{\alpha_{1450}''}{\alpha_{1540}{}^{B}}\right) - \left(\frac{\alpha_{1450}'}{\alpha_{1540}{}^{B}}\right)\left(\frac{\alpha_{1490}''}{\alpha_{1540}{}^{B}}\right)} \qquad (5)$$

The above gives the ratio of pyridine adsorbed on either Lewis acid sites I or Lewis acid sites II to that adsorbed on Brønsted acid sites on a modified η-Al_2O_3 surface.

1. Determination of Relative Integrated Absorptivity Coefficients. The values of the relative integrated absorptivities are obtained from the differences in integrated band intensities resulting from the conversion of pyridine adsorbed on to Lewis acid sites on an η-Al_2O_3 surface to adsorbed pyridinium ions. This approach was initially promulgated by Basila, *et al.*, where it was used to obtain relative absorptivities for pyridine adsorbed on silica–alumina surfaces.[5] The conversion of pyridine chemisorbed on Lewis acid sites to pyridinium ions was affected by the addition of HCl as previously described. Attempts to effect this conversion by the addition of water were not successful, which agrees with previous reports.[3b]

All integrated band intensities are utilized in ratios; therefore, the instrumentally caused distortion (*i.e.*, the observed band contour can be expressed as a product of the true band profile and an instrument function) is partially cancelled.[13] This cancellation is not complete because the instrumental function is frequency dependent, and the procedure used herein normalizes one spectral region with respect to another. However, the normalization procedure does minimize the deviation of the observed LPY/BPY values from the average value, the maximum relative deviation being 20%.

The values for the relative integrated absorptivities are obtained from spectra as described below. Figures 1A, 1B, and 1C are representative of the spectra from which the

(12) W. J. Potts, Jr., "Chemical Infrared Spectroscopy, Vol. 1: Techniques," Wiley, New York, N. Y., 1963.
(13) K. S. Seshadri and R. N. Jones, *Spectrochim. Acta*, **19**, 1013 (1963).

TABLE III: Ratio of Lewis to Brønsted Acid Surface Sites on Modified γ-Aluminas[a]

Modified alumina	2-hr evacuation at 150°				16-hr evacuation at 150°			
	LPY(I)/BPY	LPY(II)/BPY	LPY(I)/LPY(II)	LPY/BPY	LPY(I)/BPY	LPY(II)/BPY	LPY(I)/LPY(II)	LPY/BPY
9% MoO_3/η-Al_2O_3	0(*A*)	3.4 ± 0.5	0	3.4	0.2 ± 0.1	3.7 ± 0.1	0	4
Reduced 9% MoO_3/η-Al_2O_3	0(*A*)	3.0 ± 0.5	0	3.0	0(*A*)	2.4	0	2.4
2% Co–10% MoO_3/η-Al_2O_3	6.3 ± 0.7	3.4 ± 0.7	1.9	9.9	2.5 ± 0.5	5.3 ± 0.7	0.5	7.8
2% Ni–10% MoO_3/η-Al_2O_3	2.2 ± 0.4	4.7 ± 0.9	0.5	6.9				

[a] The following notation s used: LPY(I), LPY(II), and BPY; amount of pyridine chemisorbed to Lewis acid I, Lewis acid II, and Brønsted acid surface sites, respectively; (*A*), a value which was within the experimental deviation was determined, and was set equal to zero.

relative integrated absorptivities are extracted. The frequencies of absorption maxima, as well as relative integrated band intensities and absorbances, are repeatable for different wafers of the same composition subjected to identical treatments.

The relative integrated absorptivities ($\alpha_{1450}''/\alpha_{1540}^{B}$) and ($\alpha_{1490}''/\alpha_{1540}^{B}$) are evaluated from the changes in the 1450-, 1490-, and 1540-cm^{-1} integrated band intensities when LPY(II) is converted to BPY *via* the addition of HCl. Figures 1B and 1C illustrate the nature of these spectral changes. These changes are described by eq 1–3 when written in incremental form similar to that of Basila, *et al.*[5] The values of ($\alpha_{1450}''/\alpha_{1540}^{B}$) and ($\alpha_{1490}''/\alpha_{1540}^{B}$) thusly determined are 1.00 ± 0.04 and 0.192 ± 0.013, respectively.

Other parameters characteristic of LPY(II) that will prove necessary for ensuing calculations are ($\alpha_{1450}''/\epsilon_{1625}''$) and ($\alpha_{1490}''/\epsilon_{1625}''$). These parameters are obtained from the spectrum presented in Figure 1B, and are the quotients of the appropriate integrated band intensity divided by the absorbance at 1625 cm^{-1}. The values of ($\alpha_{1450}''/\epsilon_{1625}''$) and ($\alpha_{1490}''/\epsilon_{1625}''$) are 0.52 ± 0.01 and 0.098 ± 0.003, respectively.

The relative integrated absorptivity ($\alpha_{1490}^{B}/\alpha_{1540}^{B}$) is the ratio of the 1490-cm^{-1} integrated band intensity to that of the 1540-cm^{-1} absorption band when the pyridinium ion is the only adsorbed species present. An η-Al_2O_3 surface containing only adsorbed pyridinium ions can be obtained by exposing a surface containing both LPY(I) and/or LPY(II) to HCl and Figure 1C presents such a spectrum. The value of ($\alpha_{1490}^{B}/\alpha_{1540}^{B}$) is 0.63 ± 0.02, and where a correction has been made for the presence of LPY as indicated by the weak band at 1450 cm^{-1}.

The relative integrated absorptivity ($\alpha_{1450}'/\alpha_{1490}'$), which is necessary for evaluating the remaining absorptivities, can be obtained from the spectrum of an η-Al_2O_3 surface containing both LPY(I) and LPY(II) and no BPY (Figure 1A). Although the absorption bands of LPY(I) and LPY(II) in the 1450- and 1490-cm^{-1} spectral regions are not resolvable, the 1625-cm^{-1} absorption maximum in the spectrum of LPY(II) is resolved from that at 1618 cm^{-1} of LPY(I).

Resolution of the band contours was effected using a Du Pont curve resolver. Two function channels were used. The combinations of functions tried were as follows: both Gaussian, both Lorentzian, and one Gaussian with one Lorentzian. The best visual match for the resolved band contour with the observed were obtained when the LPY(II) 1625-cm^{-1} absorption band was represented by a Lorentzian function and the LPY(I) 1618-cm^{-1} band was represented by either a Lorentzian or Gaussian function. In both cases, the absorbances of the resolved 1625-cm^{-1} LPY(II) absorption band were identical. Figure 3 presents the resolved band contours where both functions are Lorentzian.

LPY(II)'s contribution to the total observed integrated band intensities in the spectral regions 1450 and 1490 cm^{-1} is the product of the absorbance of the resolved 1625-cm^{-1} absorption band and either the parameter ($\alpha_{1450}''/\epsilon_{1625}''$) or ($\alpha_{1490}''/\epsilon_{1625}''$), respectively. The values of these parameters were previously determined. Upon subtraction of these corrections to the observed integrated band intensities in the spectral region 1453 and 1490 cm^{-1}, the integrated band intensities in these regions due to LPY(I) are obtained. The ratio of the integrated band intensity due to LPY(I) at 1453 cm^{-1} to that at 1490 cm^{-1} is ($\alpha_{1450}'/\alpha_{1490}'$), and its value is 8.8 ± 0.8.

The relative integrated absorptivities ($\alpha_{1450}'/\alpha_{1540}^{B}$) and ($\alpha_{1490}'/\alpha_{1540}^{B}$) are evaluated by exposing an η-Al_2O_3 surface containing LPY(I) and LPY(II) to HCl, resulting in the formation of BPY from both LPY species. Absorption bands at 1450, 1578, 1618, and 1625 cm^{-1} either disappear completely or are drastically weakened, and absorption bands develop at 1540, 1615, and 1640 cm^{-1} while the 1490-cm^{-1} absorption band increases in intensity.

These spectral changes are described by eq 1–3 expressed in incremental form similar to those presented by Basila,[5] and where the gain in pyridinium ion concentration upon acidification is equal to the loss of both LPY(I) and LPY(II) concentrations. The use of these relationships with the identity ($\alpha_{1450}'/\alpha_{1490}'$) $\equiv$ ($\alpha_{1450}'/\alpha_{1540}^{B}$)/($\alpha_{1490}'/\alpha_{1540}^{B}$) yields a system of simultaneous equations solvable for ($\alpha_{1450}'/\alpha_{1540}^{B}$) and ($\alpha_{1490}'/\alpha_{1540}^{B}$). The values determined are 1.40 ± 0.04 and 0.16 ± 0.01, respectively.

2. Calculated Results for Lewis to Brønsted Acidity Ratios on Modified η-Al_2O_3. Substituting the values for the relative integrated absorptivities into eq 4 and 5, the following relationships for the relative amounts of LPY(I), LPY(II), and BPY on a modified η-Al_2O_3 surface are obtained.

$$\frac{\text{LPY(I)}}{\text{BPY}} = 1.8\left\{\frac{\int_{1475}^{1412^{1}/_{2}} A_{1450}\,d\nu}{\int_{1512^{1}/_{2}}^{1567^{1}/_{2}} A_{1540}\,d\nu}\right\} - 9.2\left\{\frac{\int_{1512^{1}/_{2}}^{1475} A_{1490}\,d\nu}{\int_{1512^{1}/_{2}}^{1567^{1}/_{2}} A_{1540}\,d\nu}\right\} + 5.8 \quad (6)$$

$$\frac{\text{LPY(II)}}{\text{BPY}} = 12.8\left\{\frac{\int_{1512^1/_2}^{1475} A_{1490}\,d\nu}{\int_{1567^1/_2}^{1512^1/_2} A_{1540}\,d\nu}\right\} - 1.5\left\{\frac{\int_{1475}^{1512^1/_2} A_{1450}\,d\nu}{\int_{1567^1/_2}^{1512^1/_2} A_{1540}\,d\nu}\right\} - 8.1 \quad (7)$$

The concentration ratios LPY(I)/BPY and LPY(II)/BPY also represent the relative number of acid sites upon the surface that are of sufficient strength to interact with pyridine.

The results obtained for the modified aluminas are presented in Table III. The deviation of the observed values of a ratio from the average value is given in the table. The ratio [LPY(I)/LPY(II)] is obtained upon division of [LPY(I)/BPY] by [LPY(II)/BPY].

The relative error in the ratios [LPY(I)/BPY] and [LPY(II)/BPY], upon consideration of the uncertainties in the values obtained for the relative integrated absorptivities, is 40%. The numerical results then obtained from eq 6 and 7 are really semiquantitative in nature.

The ratios of integrated absorptivities obtained herein apply to pyridine chemisorbed to an η-Al_2O_3 surface. It is not presently known if these values are valid for pyridine chemisorbed to other aluminas, *e.g.*, γ-Al_2O_3. It is known that the apparent absolute integrated absorptivities can vary by a factor of at least 2 from surface to surface.[3b]

Conclusions

The behavior of η-Al_2O_3 observed is consistent with that previously reported.[2] The η-Al_2O_3 contains two Lewis acid sites which chemisorb pyridine, and where the sites differ in acidic strength (as reflected by the difference in the lability of chemisorbed pyridine from each site with respect to increasing temperature). No Brønsted acid sites are present upon the surface. Reduction with H_2 does not significantly affect the relative amounts of pyridine chemisorbed to these acidic sites.

The major observations pertaining to the behavior of the modified aluminas are as follows. Modification of the η-Al_2O_3 by impregnation with MoO_3, where the weight per cent Mo is at least 6%, results in the formation of Brønsted acid sites on the surface. There is also a redistribution of the relative amount of pyridine chemisorbed to the various Lewis acid sites. This behavior is similar to that produced by adsorbing pyridine upon aluminas that have been pretreated at successively higher temperatures.[4] The stronger Lewis acid site predominates at both increased pretreatment temperature and in the presence of impregnated MoO_3. This would tend to indicate that the impregnated MoO_3 occupies specific sites upon the alumina surface. Speculation as to the nature of alumina sites occupied by the impregnated MoO_3 in terms of Peri's model[14] is at present premature, because the precise form of the molybdenum oxide is still not known.[15,16] Surprisingly, there also appears to be no significant difference in the surface acidity, as measured by pyridine chemisorption, between MoO_3 impregnated aluminas that are "only" calcined and reduced.

Impregnation of the η-Al_2O_3 with NiO or CoO did not yield Brønsted surface acidic sites. Also, the relative amounts of pyridine adsorbed to Lewis I and Lewis II acid sites are not significantly altered relative to that upon the surface of η-Al_2O_3. The addition of either of these oxides with MoO_3 resulted in a different distribution of Lewis acid sites upon the surface than when the surface was impregnated with MoO_3, as well as an increased Lewis/Brønsted surface acidic ratio. These results indicate, although by no means are they conclusive, that both the Ni and Co interact with the MoO_3, and that the resultant species occupies specific sites upon the η-Al_2O_3 surface. This interpretation is in agreement with that of Mitchell and coworkers in that these authors have suggested interaction between the Mo and Co oxides to yield a definite moiety.

(14) J. B. Peri, *J. Phys. Chem.* **69**, 220 (1965).
(15) J. H. Ashley and P. C. H. Mitchell, *J. Chem. Soc. A*, 2730 (1969).
(16) J. M. J. G. Lipsch and G. C. A. Shuit, *J. Catal.*, **15**, 174 (1969).

Characterization of Polycrystalline Solid Solutions of Cupric Oxide–Magnesium Oxide by Electron Spin Resonance Methods

D. Cordischi,*

Laboratorio Applicazioni in Agricoltura del C.N.E.N. Centro Studi Nucleari della Casaccia, Rome

F. Pepe, and M. Schiavello

Centro di Studio su "Struttura ed Attività Catalitica di Sistemi di Ossidi" del C.N.R. and Instituto di Chimica, Università di Roma, Rome, Italy *(Received July 26, 1972)*

Publication costs assisted by the Comitato Nazionale per l'Energia Nucleare

Polycrystalline solid solutions of CuO-MgO, with low copper content (≤1 atomic %), were investigated by esr methods. Two signals were found: one due to Cu^{2+} ions in octahedral sites and the other to Cu^{2+} ions in an axial field. The first is assigned to Cu^{2+} in the bulk, the second to Cu^{2+} ions located on and possibly near to the surface. Quantitative evaluation of the concentration of the two Cu^{2+} species shows that, especially at lower total copper contents, accumulation of Cu^{2+} ions on the MgO surface occurs. The axial signal strongly decreases upon vacuum treatment between room temperature and 500° and it is slowly restored by contact with air or N_2O. The possible causes of this behavior and a correlation of the esr results with the catalytic activity for N_2O decomposition are discussed.

1. Introduction

Solid solutions of transition metal ions in magnesium oxide have received attention in this laboratory for their catalytic properties.[1] The physical characterization of the solid solutions, namely the homogeneity, oxidation state, and stability of the ion, is usually performed by using X-ray, magnetic susceptibility, and reflectance spectra measurements. These techniques are no longer adequate for the investigation of dilute systems, which also show interesting catalytic properties. A more sensitive technique for obtaining useful information, when applicable, is electron spin resonance (esr). The present paper deals with the CuO-MgO polycrystalline solid solutions. This system has previously been studied[2-4] by X-ray and optical spectroscopy methods over a large concentration range. Among esr studies on Cu^{2+}-containing systems, it may be recalled that MgO single crystals containing trace amounts of Cu^{2+} ions have been extensively studied by esr in order to clarify the presence of the Jahn-Teller effect.[5-9] The behavior of Cu^{2+} ions supported on alumina and zeolites[10-13] has also received much attention. For these systems the esr spectra are very complex and strongly dependent on the conditions of preparation and on the various treatments at temperatures between room temperature and 500°. This behavior suggests that, in this temperature range, Cu^{2+} ions may easily change the oxidation state and distribution on the surface, but the overall picture is not very clear because of the complexity of the spectra. The aim of this work is to give a picture of the features of the Cu^{2+} ions in the dilute CuO-MgO system under conditions similar to those used in the catalytic experiments[14] by the use of the esr technique.

2. Experimental Section

2.1. Materials. The specimens were prepared by impregnating MgO (obtained from basic $MgCO_3$, decomposed at 600° for 2 hr) with copper nitrate solution, drying at 110°, mixing and heating at 600° in air for 1 hr, grinding, and finally firing at 1200° (or at 1350°) in air for 6 hr. The samples fired at 1200° were annealed, while that fired at 1350° was quenched in air.

The samples are designated as MCu, or MCu Q if quenched. The number after the letters gives the nominal concentration of copper atoms with respect to 100 Mg atoms. A summary of the samples investigated and of their features is reported in Table I. Copper analyses were carried out by the atomic absorption method and surface area determinations by the BET method, using krypton as adsorbate (p_0 = 2.72 Torr, σ = 19.4 Å^2). X-Ray analysis did not show extra lines due to phases different from that of MgO.

2.2. Esr Procedure. Esr spectra were recorded at room temperature at X-band frequencies using a Hilger and Watts Microspin spectrometer equipped with a TE_{011} cylindrical cavity. The absolute concentration of Cu^{2+} was obtained from electronically integrated and/or first derivative spectra, by comparison with those of a single crystal of $CuSO_4 \cdot 5H_2O$ (see later for details). Several spectra were also recorded at liquid nitrogen temperature using a Varian X-band spectrometer.

(1) A. Cimino and F. Pepe, *J. Catal.*, **25**, 362 (1972), and references therein.
(2) F. H. Chapple and F. S. Stone, *Proc. Brit. Ceram. Soc.*, **45** (1964).
(3) (a) N. G. Schmahl and E. Minzl, *Z. Phys. Chem. (Frankfurt am Main)*, **41**, 66 (1964); (b) N. G. Schmahl, J. Barthel, and G. F. Eickerling, *Z. Anorg. Allg. Chem.*, **332**, 230 (1964).
(4) O. Schmitz Du Mont and H. Fendel, *Monatsh. Chem.*, **96**, 495 (1965).
(5) J. W. Orton, P. Auzin, J. H. E. Griffiths, and J. E. Wertz, *Proc. Phys. Soc.*, **78**, 554 (1951).
(6) W. Low and J. Suss, *Phys. Lett.*, **7**, 310 (1970).
(7) U. Höchli, K. A. Muller, and P. Wysling, *Phys. Lett.*, **15**, 5 (1965).
(8) R. E. Coffman, *J. Chem. Phys.*, **48**, 609 (1968).
(9) K. Zdánský, *Phys. Rev.*, **177**, 490 (1969).
(10) P. A. Berger and J. F. Roth, *J. Phys. Chem.*, **71**, 4307 (1967).
(11) H. Lumbeck and J. Voitlander, *J. Catal.*, **13**, 117 (1969).
(12) A. Nicula, D. Stamires, and J. Turkevich, *J. Chem. Phys.*, **42**, 3684 (1965).
(13) D. Mikheilkin, V. A. Shvets, and V. B. Kazanskii, *Kinet. Katal.*, **11**, 747 (1970).
(14) Unpublished results from this laboratory.

TABLE I

Sample	Cu analytical content, atoms/100 Mg atoms	Surface area m^2/g	Latt.[d] param, Å	Mag moment, B.M.
MCu 10	7.3	0.2	4.2138	1.77
MCu 5	3.7		4.2123	1.70
MCu 1	1.12	18	4.2117	1.70
MCu 0.5	0.49	48	4.2117	
MCu 0.1	0.12	41	4.2117	
MCu 0.05[a]	0.06	41	4.2117	
MCu 0.05 R[a]	0.06	38	4.2117	
MCu 0.1 J.M.[b]	0.26		4.2117	
MCu 1Q[c]	1.12	1.3	4.2117	1.70

[a] Two different preparations. [b] MgO Specpure from Johnson, Matthey and Co. Ltd. (London). [c] Fired at 1350° and quenched. [d] The lattice parameter for MgO is 4.2116 Å.

2.3. Treatments. A small portion (20–40 mg) of the sample was enclosed in a Pyrex tube and sealed to a vacuum system. After the desired thermal treatment the sample was detached by sealing off the glass under dynamic vacuum. Several experiments (treatment of the same specimen at different temperature under vacuum or in the presence of a given gas) were also carried out in an esr tube connected to the vacuum system *via* a ground joint and isolated by means of stopcocks.

3. Experimental Results

3.1. Characterization of Esr Spectra. The esr spectra at room temperature of MCu samples show two different signals attributed to Cu^{2+} ions (Figure 1).

(a) The first is a single symmetrical line whose shape was checked to be essentially Lorentzian, at $g = 2.190$. Its width and intensity generally increase with copper concentration. The line width shows a strong dependence on the recording temperature; at 77°K a narrowing by a factor of more than 2 occurs, and at this temperature and lower copper content, hyperfine structure is observed with $|A| = 19$ G (Figure 2). Evacuation, or oxidation in the range 20–500°, slightly affects this signal.

(b) The second signal is an asymmetrical signal analogous to those given by Cu^{2+} ions of axial symmetry in polycrystalline or amorphous samples.[10,11,13] Hyperfine structure of Cu^{2+} is clearly visible on this signal. The corresponding principal values of A and g tensors are: $g_\parallel = 2.352$, $|A_\parallel| = 120$ G; $g_\perp = 2.063$, $|A_\perp| = 27$ G. The shape of this signal does not change much at 77°K (Figure 2). For reasons reported later (see Discussion) this signal is attributed to Cu^{2+} ions located at, or near to, the surface ($Cu^{2+}_{surface}$). Both signals are not easily saturated by microwave power.

The absolute concentrations of Cu^{2+} ions have been determined using two different methods. (i) The total concentration of Cu^{2+} ions contributing to the esr spectrum (Cu^{2+}_{total}) was obtained from spectra electronically integrated over about 1500 G, centered at $g \simeq 2.2$, using the formula given by Poole[15] for computing the number of spins and $CuSO_4 \cdot 5H_2O$, as standard. (ii) The concentration of the Cu^{2+} in the bulk (Cu^{2+}_{bulk}) is found from first derivative spectra, evaluating the amplitude h and the width ΔH (peak to peak) of the symmetrical signal.[15] The determination of absolute concentration of Cu^{2+} ions in axial symmetry ($Cu^{2+}_{surface}$) is less easy and direct. In fact if the relative intensity is sufficiently large, the axial signal can be detected in the integrated spectrum and the ratio $Cu^{2+}_{surface}/Cu^{2+}_{bulk}$ can be evaluated accordingly. By contrast, when the relative intensity is small, the axial signal is no longer observable in the integrated spectrum, but it can still be observed in the first derivative spectrum. An analysis of several spectra of the former case gives the conversion factor which allows to estimate the absolute $Cu^{2+}_{surface}$ concentration from first derivative spectrum.

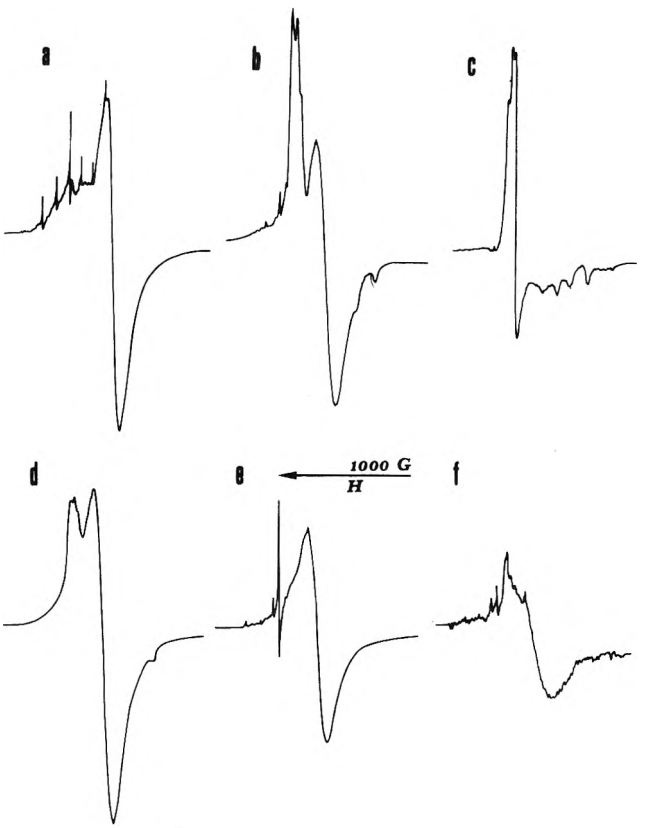

Figure 1. Esr spectra of MCu samples recorded at room temperature: a, MCu 1 Q; b, MCu 0.5; c, MCu 0.05; d, MCu 1; e, MCu 0.5 evacuated at 480°, 4 hr; f, MCu 0.05 evacuated at 480°, 4 hr. The scale of the spectra can be derived from the length of the arrow whose value in gauss is indicated. The spikes in 1a are due to Mn^{2+} and Cr^{3+} impurities. The Cr^{3+} signal is barely visible in 1b and 1e. In 1e and 1f the signal at $g = 2.004$ is also visible.

3.2. Esr Spectra of the Samples. 3.2.1. Untreated Samples. Table II shows results obtained for the samples of Table I before any special treatments (hereafter called untreated samples), together with those reported in section 3.2.2. The main features of the results are as follows. (i) the Cu^{2+}_{total} contents are generally in good agreement with the analytical one. At the highest contents, however, the values from esr are lower than expected (see below). (ii) The $Cu^{2+}_{surface}$ content of the 1200° samples differs considerably from the content of the 1350° one. The former exhibit a substantial constant $Cu^{2+}_{surface}$ concentration over the total copper contents while in the latter, the axial signal is barely observable. It should be noted that the 1350° sample shows a strong decrease in the surface area. (iii) The $Cu^{2+}_{surface}/Cu^{2+}_{total}$ ratio for the 1200° samples decreases with increasing total copper content. In

(15) G. P. Poole, Jr., "Electron Spin Resonance," Interscience, New York, N. Y., 1967, pp 554, 798.

TABLE II

Sample	Before treatments Cu^{2+} from esr[d]			Evac at 480° 4 hr Cu^{2+} from esr[d]			Oxidat. at 480° 1 hr Cu^{2+} from esr[d]			Oxidat. at r.t. 4 months Cu^{2+} from esr[d]		
	Total	Bulk	Surface	Total	Bulk	Surface	Total	Bulk	Surface	Total	Bulk	Surface
MCu 10	4.80	5.1	...									
MCu 5	3.20	3.8	...									
MCu 1	0.86	0.66	0.09	0.79	0.71	0.03	0.89	0.75	0.027		0.68	0.08
MCu 0.5	0.46	0.36	0.12	0.38	0.40	0.02				0.43	0.31	0.08
MCu 0.1	0.15	0.09	0.07	0.10	0.10	0.015	0.10	0.10	0.04	0.10	0.11	0.05
MCu 0.05	0.08	≤0.03	0.08	0.06	0.06	0.02	0.09	0.07	0.02	0.09	0.07	0.04
MCu 0.05 R	0.05	0.04	0.03	0.05	0.07	~0.01		0.07	0.02			
MCu 0.1 J.M.[a]	0.30	0.28	0.03	0.25	0.28	0.02		0.29	0.025	0.26	0.31	0.035
MCu 1 Q[b]	0.65	0.51	≤0.01	0.73	0.54	...	0.68	0.57	...			
MCu 5[c]	1.75	1.21	...									
MCu 1[c]	0.91	0.60	...									

[a] See Table I, footnote *b*. [b] Fired at 1350° and quenched. [c] Kindly supplied by Professor F. S. Stone; firing temperature: 1600°. [d] Atoms/100 Mg atoms.

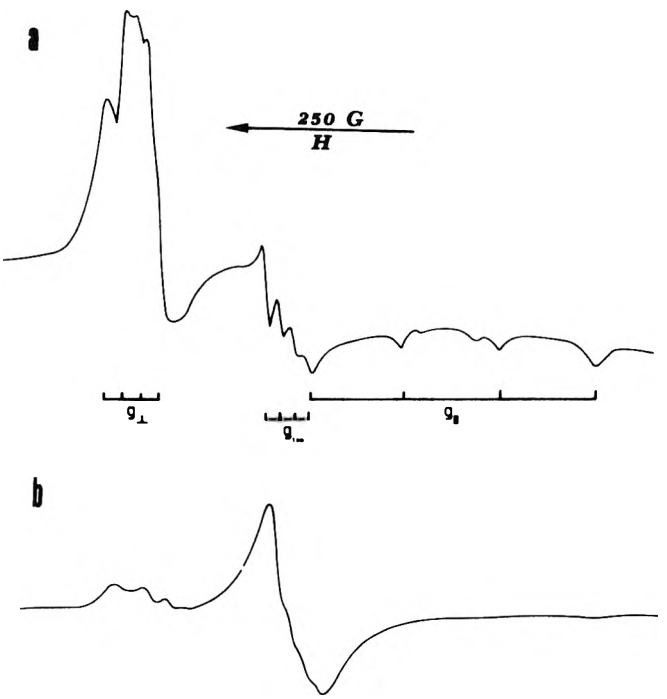

Figure 2. Esr spectra of MCu samples recorded at 77°K: a, MCu 0.05; b, MCu 0.5. The scale of the spectra can be derived from the length of the arrow whose value in gauss is indicated.

the MCu5 and MCu10 samples the axial signal is not more resolved because the symmetrical one dominates the spectrum and also considerable line broadening is present.

3.2.2. Treated Samples. (a) Outgassing at Various Temperatures. A preliminary outgassing on all the samples was carried out at 480° ($p \simeq 10^{-5}$ Torr, 4 hr), *i.e.*, under conditions usually adopted in the pretreatment for the catalytic experiments.[14] The axial signal after vacuum treatment is considerably reduced but does not disappear completely. The residual $Cu^{2+}_{surface}$ concentration is almost constant in all samples and seems not to depend on initial concentration. By contrast, the Cu^{2+}_{bulk} concentration shows a small increase and Cu^{2+}_{total} concentration a small decrease. These variations do not exceed 10–20%; *i.e.*, they are within the uncertainty of esr determinations, but since all figures quoted in Table II are the average of several spectra and sometimes of repeated vacuum treatments, the above variations may be significant. An example is shown by the spectra of MCu 0.05, reported in Figure 1, where the symmetrical signal clearly increases upon vacuum treatment.

In a further series of experiments, the dependence of the signal on the temperature of evacuation between room temperature and 500° was studied for some samples. The time of evacuation was 4 hr at each temperature. The samples selected were: MCu 0.1; MCu 0.05, (which showed a marked decrease upon vacuum treatment at 480°) and MCu 0.1 J.M. (which showed only a small effect). The results are reported in Figure 3. There was a continuous decrease of $Cu^{2+}_{surface}$ concentration until values about the same as in the experiments at 480° were observed. Similar small change as described before was observed in Cu^{2+}_{total} and Cu^{2+}_{bulk} concentrations.

(b) Oxidation at Various Temperatures. (i) Damp and Dry Air. All the samples first outgassed for 4 hr at 480° were heated for 1 hr at the same temperature in air. No change in the esr spectra was observed. The same specimens left in damp air at room temperature for 4 months showed a marked increase of the axial signal. The concentration of $Cu^{2+}_{surface}$ increases up to 50–90% of the initial values. These results are reported in Table II and in Figure 4. The difference between the results of short treatment at 480° in air and these of extended treatment at room temperature in air has induced us to study the kinetics of the axial signal increase, choosing a treatment temperature of 200°. The kinetics were carried out on two samples (MCu 0.5 and MCu 0.1) previously outgassed under vacuum at 480° for 4 hr. The samples were submitted to dry and damp air (air saturated with water at 25°) at 200° for different times up to a maximum of 50 hr. The results reported in Figure 5 show a slow but continuous increase of $Cu^{2+}_{surface}$ concentration with time. The effect of water is sensible for MCu 0.1 but not for MCu 0.5.

(ii) N_2O. The influence of N_2O was tested on the specimens MCu 0.1, MCu 0.05, and MCu 0.1 J.M. previously outgassed at various temperatures (see section 3.2.2. a). The treatments with N_2O (~60 Torr) were performed, at various temperatures, by allowing the samples to stand for 30 min in contact with N_2O. Between experiments samples were outgassed at 480° for 30 min. The results reported in Figure 3 indicate that N_2O also has little effect on the spectrum. Only for MCu 0.1 is a small increase of $Cu^{2+}_{surface}$ concentration observed. This sample, in con-

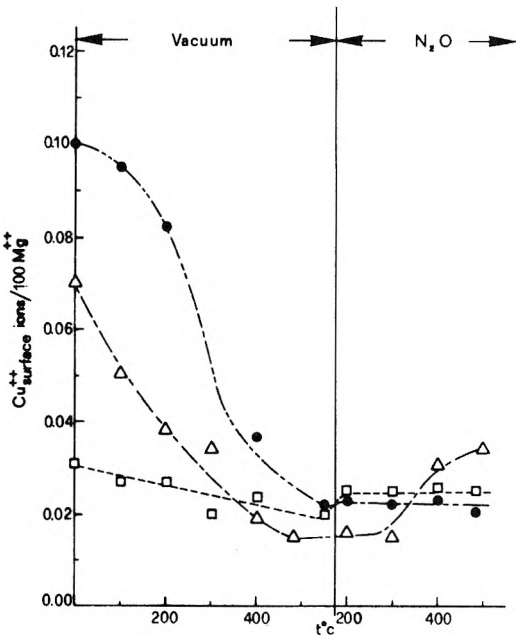

Figure 3. Dependence of $Cu^{2+}{}_{surface}$ concentration on treatment temperature *in vacuo* and in N_2O: ●, MCu 0.05; △, MCu 0.1; □, MCu 0.1 J.M. The time of evacuation was 4 hr for each temperature. The treatment with N_2O was done for 30 min.

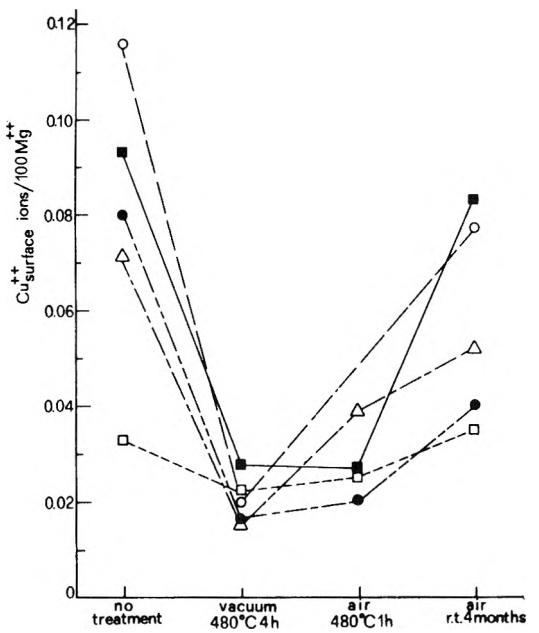

Figure 4. Variation of $Cu^{2+}{}_{surface}$ surface concentration upon various treatments: ●, MCu 0.05; △, MCu 0.1; □, MCu 0.1 J.M.; O, MCu 0.5; ■, MCu 1.

trast to the other ones, shows the same effect after being treated at 480° in air for 1 hr (Figure 4).

3.3. Esr Signal at g = 2.004. Beside the two signals described above, another signal develops upon vacuum treatment. It consists of a single slightly asymmetrical line at $g = 2.004$ with a width of about 6 G, which can easily be saturated by microwave power (Figure 1e). It is immediately destroyed by opening the specimen in air at room temperature, but subsequent vacuum treatment restores it with an intensity generally higher. The intensity of this signal increases with the temperature of vacuum treatment up to 500° and a further increase is observed upon treatment in the presence of N_2O up to 300°. However, the intensity of this signal shows rather poor reproducibility. The fact that its intensity increases in the presence of N_2O and in a second vacuum treatment, after treatment in air at 200°, would suggest that it is an oxygen species. However, an almost similar signal has been found in some cases[16] and assigned to carbon species. Further experiments are needed to identify the paramagnetic species responsible.

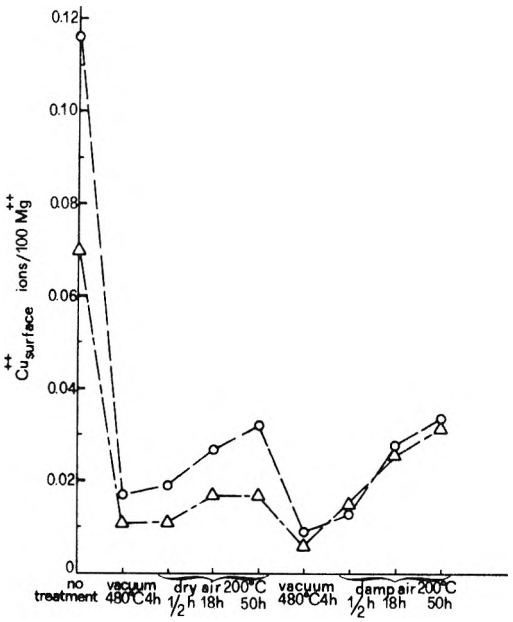

Figure 5. Dependence of $Cu^{2+}{}_{surface}$ concentration on treatment time at 200° in dry and damp air after evacuation: O, MCu 0.5; △, MCu 0.1.

4. Discussion

4.1. Assignment of the Esr Signals. The main results obtained in the present investigation can be summarized as follows: (a) two esr signals are present, one assignable to Cu^{2+} ions in octahedral sites and the other to Cu^{2+} ions in an axial field; (b) the axial signal is very sensitive to vacuum treatment.

The esr spectra of Cu^{2+} ions in octahedral sites in MgO have been discussed by several authors.[5-9] The symmetrical line at $g = 2.190$ ($Cu^{2+}{}_{bulk}$) arises from a dynamic Jahn-Teller effect. At 77°K, a hyperfine structure with $|A| = 18.6$ G appears[5,8] in single crystal or polycrystalline specimens. The strong line width temperature dependence is attributed to an Orbach relaxation mechanism[7] from which a J-T splitting of about 1100 cm^{-1} was evaluated. Consequently, the line width found in our specimens at room temperature does not allow resolution of any hyperfine structure which may be present. There are also other factors operating in our case which may increase the line width even further: dipolar interaction responsible for increase in the line width with increasing concentration, and possibly strains at the sites occupied by Cu^{2+} in the bulk.

Axial spectra, similar to that observed in our samples, although not reported previously for Cu^{2+} ions in MgO, are rather common for polycrystalline Cu^{2+} complexes. In these complexes the symmetry of Cu^{2+} can be octahedral (with an elongated tetragonal distortion), square planar, square pyramidal,[17] and similar spectra are found for

(16) D. J. Muller and D. Haneman, *Surface Sci.*, **24**, 369 (1971).

Cu^{2+} ions in ionic host crystals.[10,11,13] The principal values of the g and A tensors for all these types of complexes are not very different and consequently they do not allow identification of the copper coordination without information from other techniques. It is only possible to state that the axial spectrum in MgO arises from Cu^{2+} ions either associated with some defect or located on and close to the surface. In this way the J-T distortion is "frozen out" in a fixed direction also at room temperature.

The behavior of the axial spectrum with various treatments allows us to state that the axial crystal field is due to the proximity of Cu^{2+} ions to the surface. The high sensitivity of this signal to vacuum treatment and its reappearance in air (also at room temperature) find an easy explanation if it is assumed that the ions responsible for the signal are on, and possibly near to, the surface. It is not possible to evaluate down to what depth from the surface the Cu^{2+} ions give rise to the axial signal. Theoretical considerations based on point charge models give only rough approximation,[18] but assuming an r^{-3} dependence of the axial field,[18,19] where r is the distance from the surface, only Cu^{2+} ions in the first few layers can contribute the the axial spectrum.

Another explanation for the axial spectrum observed at room temperature could be the presence of clusters of Cu^{2+} ions on the surface or at grain boundaries of MgO. In this case the axial spectrum could arise from a cooperative distortion effect involving a change from a dynamic to a static J-T effect. This interpretation seems less likely for two reasons: (a) the ratio of the intensity of the axial spectrum to that of the symmetrical one should increase with total copper content, as in perovskites;[20] (b) the well resolved hyperfine structure in the axial spectrum indicates only small dipolar and exchange interaction and magnetically isolated copper ions.

4.2. Localization of $Cu^{2+}_{surface}$ Ions. The relatively high percentage of $Cu^{2+}_{surface}$ ions indicates large localization on the surface, especially at lower copper contents. In fact, for a sample with a surface area of 40 m^2/g, the sites in the, say, first four layers are 12% of the total sites, while we found a $Cu^{2+}_{surface}$ concentration up to 80% of the total copper (MCu 0.05).

The large difference between the sample fired at 1350° and those fired at 1200° is due mainly to the difference in surface area. This accumulation of Cu^{2+} ions near to the surface could be due to thermodynamic causes. Theoretical calculations[21] for impurities possessing an absolute charge value different from that of the ions of the host crystal show such accumulation of impurity ions at the surface, but no evaluation has been done for ions with the same charge. The presence of paramagnetic impurities in a MgO crystal causes distortion[22] and adding the tendency of Cu^{2+} ions to distort the octahedral by the J-T effect, the surface sites are probably energetically favorable for copper ions.

The decrease of the axial signal upon outgassing at 480° is due mainly to a reduction of Cu^{2+} ions to a lower oxidation state, probably Cu^+. The reduction to Cu^0 appears as less likely since it is known from the phase diagram[23] of the system CuO-Cu_2O-Cu, that Cu_2O is formed under vacuum at temperatures above 500°. Below this temperature, the reduction can be limited to the surface, but always leading to Cu^+ state. Moreover there is no suspicion of Cu^0 formation from the esr measurements. However, it must be emphasized that other causes different from chemical reduction may be responsible for the decrease of signal intensity. A change in symmetry or in distribution of some of the Cu^{2+} ions can transform the contribution of these ions to the Cu^{2+}_{bulk} spectrum. Some indication that this process may in fact occur comes from the slight but significant increase of the symmetrical signal upon outgassing at 480°. The assumption that the Cu^{2+} ions contributing to the axial spectrum are those on the surface as well as those immediately below at different depth from the surface explains the different behavior upon outgassing. Depending on the local situation a Cu^{2+} ion near to the surface can be reduced to Cu^+ or it can change its symmetry by small atomic (or vacancy) movements thus transforming to Cu^{2+}_{bulk}, or finally it can remain unchanged as it is shown by the residual axial signal which always is present after vacuum treatment (Table II). The slow restoration rate of the axial signal (Figures 3 and 4) in air or in N_2O at room temperature and 200° strongly contrasts with the rapid reduction of this signal under vacuum. This does not necessarily mean that the oxidation rate is low. In fact, experiments on pure or supported Cu_2O[24,25] show that Cu^+ is oxidized by O_2 in this temperature range at a much higher rate. The slowness of the increase in axial signal can be linked to topological requirements. Indeed, if some clustering of Cu^+ ions occurs during the vacuum treatment, when these ions are reoxidized they may escape detection by esr because of the strong interactions between them. After a rapid oxidation a slow migration of Cu^{2+} around the surface occurs and the initial conditions are restored. This process may be visualized as a sort of relaxation effect due to differences in coordination and ionic radius of copper ions in the two different oxidation states. The water probably plays some role in this process although our results are not conclusive.

A similar migration of Cu^{2+} ions on γ-alumina has been suggested by Berger and Roth[10] to explain the appearance, on air admission at room temperature to reduced samples, of a new esr signal of strongly interacting Cu^{2+} ions.

4.3. Correlation of the Esr Studies with the Catalytic Results. The catalytic results for the decomposition of N_2O over MCu catalysts show that: (a) all the samples studied exhibit an apparent activation energy (E_a) ranging from 22 to 25 kcal/mol; (b) the increase of copper content provokes an increase in activity. The E_a found for

TABLE III

Catalyst	Cu^+ after vacuum treatment[a]	k_{abs}, cm min^{-1}
MCu 0.1	1.8×10^{-2}	2×10^{-7}
MCu 0.5	2.8×10^{-2}	3×10^{-7}
MC 1	4.5×10^{-2}	7×10^{-7}

[a] Fraction of cationic surface sites.

(17) H. A. Kuska and N. T. Rogers in "Radical Ions," E. T. Kaiser and L. Kevan, Ed., Interscience, New York, N. Y., 1968, p 578.
(18) G. D. Watkins, *Phys. Rev.*, **113**, 79 (1959).
(19) B. W. Figgis "Introduction to Ligand Field" Interscience, New York, N. Y., 1964, p 41.
(20) C. Friebel and D. Reinen, *Z. Naturforsch.*, **24a**, 1518 (1969).
(21) K. L. Kliewer and S. J. Koehler, *Phys. Rev.* **140A**, 1226 (1965).
(22) M. Borg and D. K. Ray, *Phys. Rev.*, **1B**, 4144 (1970).
(23) J. Bloem, *Philips Res. Rep.*, **13** (1958).
(24) W. E. Garner, F. S. Stone, and P. F. Tiley, *Proc. Roy. Soc., Ser. A*, **211**, 472 (1952).
(25) M. O'Keeffe and F. S. Stone, *Proc. Roy. Soc., Ser. A*, **267**, 501 (1962).

Cu_2O is 23 kcal/mol while for CuO is 25 kcal/mol. This latter oxide is partly reduced to Cu_2O at least on the surface, due to the pretreatment adopted in catalysis (480°, 4 hr, 10^{-5} Torr). Consequently, its activity and its E_a are attributed to Cu^+.[14] On the other hand, the E_a values obtained for the MCu specimens clearly resemble that found on Cu_2O. In these specimens the Cu^+ content, formed during the outgassing treatment, can be evaluated by the esr methods only indirectly. In Table III an attempt to correlate the amount of Cu^+ formed and the catalytic activity of some MCu specimens is made. The table reports the fraction of surface sites occupied by Cu^+ ions, calculated from the decrease of $Cu^{2+}{}_{surface}$ per unit surface area together with the absolute rate constant (k_{abs}) at 350° for the N_2O decomposition. It may be noted that the amount of reduced Cu^+ formed parallels the increase in activity, thus suggesting that the main active sites in the N_2O decomposition can be identified as Cu^+ ions.

Acknowledgment. The Authors wish to thank Professor A. Cimino for valuable discussion and for critically reading the manuscript.

Theoretical Free Energy of Activation for Dehydration of Hydrated Ions in Solution

Sang Hyung Kim and B. T. Rubin*

Technological Institute, Northwestern University, Evanston, Illinois 60201 *(Received June 14, 1972)*

Publication costs assisted by the National Institutes of Health

The free energy of activation for dehyration of primary hydrated ions in the liquid was calculated from a statistical thermodynamic formulation. A quasicrystalline solid was assumed for the liquid structure wherein each particle is constrained to move within their own free volumes. In the activation process free water molecules are produced from the initial bound water molecules by rotating the water dipoles to the activated orientation such that ion-water bonds are broken. The introduction of the constant potential cage approximation for the free water molecules defines the condition for the activated state as well as accounting for the influence of the surrounding liquid. The stretching contribution of the ion-water bond to the dehydration process is neglected. The effective potential energy of an ion-water pair in the hydrated ion cluster was determined by the potential energy of one ion-water pair and a semiempirical factor obtained from gas-phase measurements. The potential energy of an ion-water pair includes ion-dipole, ion-quadrupole, ion-induced dipole, dispersion, and repulsion interactions. The calculated free energy of activation for dehydration of primary hydrated ions are in the relative order $Li^+ > Na^+ > K^+$ and $Cl^- > Br^- > I^-$ for the same degree of dehydration, *i.e.*, when each ion has lost the same number of bound water molecules. The calculated results are discussed in relation to measured relaxation times of bound water in the primary hydration shell, ionic permeability of biological membranes, and specific adsorption of ions at the metal-solution interphase.

Introduction

The dehydration of primary hydrated ions may play a major role in ionic diffusion through biological membranes,[1-4] porous networks, as well as in the specific adsorption of ions at the metal-solution interphase.[5,6] The calculation of the activation free energy of dehydration for various ions could contribute valuable information to the understanding of the above processes. In this paper we assume that the rotation of bound water molecules without the stretching of ion-water bonds constitutes the activation process of the dehydration reaction and calculate the free energy of activation as a function of degree of dehydration from a statistical thermodynamic formulation. The results for various ions are discussed in relation to measured relaxation times of bound water in the primary hydration shell, the diffusion through biological membranes, and adsorption in the electrical double layer. Limitations and improvements of the treatment are discussed.

General Formulation

The activation energy of dehydration of a primary hydrated ion in aqueous solution may be obtained by calculating the partition functions and potential energies of initial and activated states. The initial state consists of N_i ions with $N_{bw}{}^0$ bound waters with each bound water molecule maintained at its equilibrium separation distance from the ion and with its dipole oriented in the minimum energy position. In the ion field, such bound water molecules undergo internal vibrational, librational, and re-

(1) L. J. Mullins, *J. Gen. Physiol.*, **42**, 1013 (1959).
(2) B. Hille, *Proc. Nat. Acad. Sci. U.S.*, **68**, 280 (1971).
(3) P. Mueller and D. O. Rudin, "Current Topics in Bioenergetics," Vol. 3, D. R. Sanadi, Ed., Academic Press, New York, N. Y., 1969.
(4) F. F. Offner, *Biophys. J.*, **12**, 1583 (1972).
(5) J. O'M. Bockris and A. K. N. Reddy, "Modern Electrochemistry," Vol. 2, Plenum Press, New York, N. Y., 1970, Chapter 7.
(6) T. N. Andersen and J. O'M. Bockris, *Electrochim. Acta*, **9**, 347 (1964).

stricted translational motions. The activated state consists of N_i ions with N_{bw}* bound water molecules and N_{fw}* free water molecules. N_{bw}* bound water molecules are assumed subject to the same kind of motions as those in the initial state. N_{fw}* free water molecules are produced from bound water molecules by breaking ion–water bonds. In the activation process of dehydration an ion–water bond is broken by rotating the water dipole from its initial orientation to an activated orientation which corresponds to zero potential energy of interaction while keeping the center of mass of the water molecule essentially unaltered with respect to the ion. Such free water molecules in the activated state undergo internal librational as well as restricted translational motions within a potential cage consisting of surrounding inert secondary water molecules of the liquid. The internal vibrational motions of the water molecules are assumed to be unaltered in the field of ion.

The liquid is considered as a quasicrystalline solid in which each of the particles is constrained to move within their own free volumes of relatively constant potential energy.[7,8] In the general case for N_i ions moving within the volume v_f, N_{bw} bound water molecules, and N_{fw} free water molecules, the partition function for such an assembly may be written as

$$F = \frac{(N_{bw} + N_{fw} + N_i)!}{N_{bw}!\,N_{fw}!\,N_i!}(f_{bw})^{N_{bw}}(f_{fw})^{N_{fw}} \times \left\{\frac{(2\pi m_i kT)^{3/2}}{h^3} v_f\right\}^{N_i} \quad (1)$$

where f_{bw} and f_{fw} are the partition functions for a bound water molecule and a free water molecule. m_i is the mass of the ion. The partition function (eq 1) is similar to that employed by Eley and Evans[8] in their calculation of entropy change in ionic hydration. The partition function of the initial state (N_i ions and $N_{bw}{}^0$ bound waters) is

$$F^0 = \frac{(N_{bw}{}^0 + N_i)!}{N_{bw}{}^0!\,N_i!}(f_{bw}{}^0)^{N_{bw}{}^0}\left\{\frac{(2\pi m_i kT)^{3/2}}{h^3} v_f\right\}^{N_i} \quad (2)$$

Similarly, the partition function for the activated state (N_i ions, N_{bw}* bound waters and N_{fw}* free waters) is

$$F^* = \frac{(N_{bw}^* + N_{fw}^* + N_i)!}{N_{bw}^*!N_{fw}^*!N_i!}(f_{bw}^*)^{N_{bw}^*}(f_{fw}^*)^{N_{fw}^*} \times \left\{\frac{(2\pi m_i kT)^{3/2}}{h^3} v_f\right\}^{N_i} \quad (3)$$

The total number of water molecules are the same in both initial and activated states, *i.e.*, $N_{bw}{}^0 = N_{bw}^* + N_{fw}^*$. The equilibrium constant for the equilibrium between initial and activated states is

$$K^* = (F^*/F^0)(e^{-V_0/kT})^N \quad (4)$$

where V_0 is defined as the potential energy difference between the two states measured from the respective lowest vibrational energy levels at 0°K; *i.e.*, the activation energy barrier, and N is Avogadro's number. Introducing eq 2 and 3 into eq 4 with $N_j = n_j N$ we obtain

$$K^* = \frac{(n_{bw}{}^0 N)!}{(n_{bw}^* N)!(n_{fw}^* N)!}\frac{(f_{bw}^*)^{n_{bw}^* N}(f_{fw}^*)^{n_{fw}^* N}}{(f_{bw}{}^0)^{n_{bw}{}^0 N}}(e^{-V_0/kT})^N \quad (5)$$

Utilizing Stirling's approximation $x! = (x/e)^x$ eq 5 becomes

$$K^* = \frac{(f_{bw}^*/n_{bw}^*)^{n_{bw}^* N}(f_{fw}^*/n_{fw}^*)^{n_{fw}^* N}}{(f_{bw}{}^0/n_{bw}{}^0)^{n_{bw}{}^0 N}}(e^{-V_0/kT})^N \quad (6)$$

The standard free energy of activation for creating n_{fw}* waters from bound waters is $\Delta G^* = -kT \ln K^*$. Thus

$$\Delta G^* = -NkT \times \ln \frac{(f_{bw}^*/n_{bw}^*)^{n_{bw}^*}(f_{fw}^*/n_{fw}^*)^{n_{fw}^*}}{(f_{bw}{}^0/n_{bw}{}^0)^{n_{bw}{}^0}} + NV_0 \quad (7)$$

The potential energy barrier and partition functions in eq 7 are constructed as follows.

(1) Potential Energy Barrier V_0. The potential energy barrier V_0 is defined by the relation

$$V_0 = \epsilon^* - \epsilon^0 \quad (8)$$

where ϵ* is the total potential energy of the ion–water cluster in the activated state and ϵ^0 is the total potential energy of the ion–water cluster in the initial state. The zero of energy is chosen as the infinite separation of ion and water molecules at rest. Both ϵ* and ϵ^0 are constructed from the potential energy of interaction of one ion–water pair U_0 and the scaling factor λ_n which accounts for the variation in the potential energy of interaction of one ion–water pair as a function of the number of water molecules bound to the ion. This variation in potential energy arises in principle from lateral interaction effects as well as coupling between internal motions. λ_n is deduced from the stepwise enthalpies of ion hydration as measured in the gas phase,[9,10] *i.e.*

$$\lambda_n = \left(\frac{U_{T,n}}{n}\right)\Big/ U_{T,n=1} \quad (9)$$

where $U_{T,n}$ is the sum of the successive enthalpies of hydration defined as

$$U_{T,n} = \sum_{n=1}^{n} \Delta H_{n-1}{}^{\circ}{}_n \quad (10)$$

for the step-wise gas-phase reactions

$$X^Z(H_2O)_{n-1} + H_2O = X^Z(H_2O)_n \qquad \Delta H_{n-1}{}^{\circ}{}_n \quad (11)$$

X^Z represents a cation or anion carrying charge Z. The quantity $\lambda_n U_0$ specifies the average effective interaction energy of one ion–water pair $\bar{U}_n$ in a given ion–water cluster consisting of n_{bw} bound waters. Thus

$$\bar{U}_n = \lambda_n U_0 \quad (12)$$

The potential energy of interaction U_0 between one water molecule and the ion is obtained by considering the potential produced by the ion acting at the center of the water molecule.[11] In addition, we included the ion-induced dipole, dispersion, and repulsive interactions. Now, the total potential energy of interaction U_0 between the ion (i) and the axially symmetric water molecule about the z axis is

$$U_0 = -\frac{Ze\mu\cos\theta}{r^2} + \frac{Ze\Theta_z(3\cos^2\theta - 1)}{2r^3} - \frac{(Ze)^2\alpha_w}{2r^4} - \frac{3}{2}\frac{\alpha_i\alpha_w}{r^6}\frac{I_i I_w}{I_i + I_w} + Ar^{-12} \quad (13)$$

where Z is the sign of the ion; r is the distance between the center of the ion and that of the water molecule; θ is the angle between the z and the r axis; e, μ, Θ_z, α, and I

(7) E. A. Guggenheim, *Proc. Roy. Soc., Ser. A*, **135**, 181 (1932).
(8) D. D. Eley and M. G. Evans, *Trans. Faraday Soc.*, **34**, 1093 (1938).
(9) I. Dzidic and P. Kebarle, *J. Phys. Chem.*, **74**, 1466 (1970).
(10) M. Arshadi, R. Yamdigni, and P. Kebarle, *J. Phys. Chem.*, **74**, 1475 (1970).
(11) A. D. Buckingham, *Quart. Rev., Chem. Soc.*, **13**, 183 (1959).

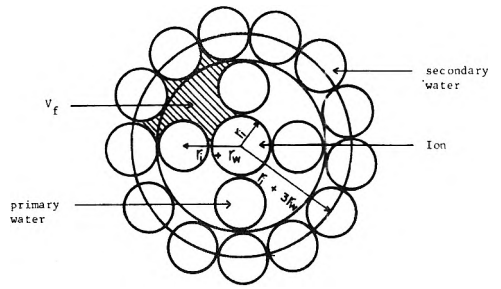

Figure 1. Calculation of free volume V_f. r_i and r_w are the radii of ion and water, respectively. This figure is a two-dimensional representation of the primary hydrated ion with secondary hydration shell in three dimensions.

are the electronic charge, dipole moment of water, quadrupole moment of water, isotropic polarizability, and ionization potential, respectively. Subscripts i and w indicate ion and water, respectively. The repulsive constant A was obtained from the equilibrium condition

$$\left(\frac{\partial U_0}{\partial r}\right)_{r=r_i+r_w} = 0$$

at $\theta = 0$ or π for the cation or anion, respectively.

Since the activated state is composed of n_{bw}^* bound waters and n_{fw}^* free waters, the potential energy barrier V_0 (eq 8) is now written as

$$V_0 = (\epsilon_{fw}^* + \epsilon_{bw}^*) - \epsilon^0 \quad (14)$$

In the activated state the total potential energies of interaction of free waters with other constituents in the cluster are assumed to be zero such that $\epsilon_{fw}^* = 0$. Thus V_0 becomes

$$V_0 = n_{bw}^* \lambda_{n_{bw}^*} U_0 - n_{bw}^0 \lambda_{n_{bw}^0} U_0 \quad (15)$$

where we have used eq 12 with $\epsilon_{bw}^* = n_{bw}^* \bar{U}_{n_{bw}^*}$ and $\epsilon^0 = n_{bw}^0 \bar{U}_{n_{bw}^0}$. The number of bound waters in the activated state n_{bw}^* determines the entire potential energy of the cluster since there is no potential energy contribution from the free water. Thus, the appropriate value of $\lambda_{n_{bw}^*}$ is that value of λ_n given by eq 9 corresponding to n_{bw}^*. Similar remarks hold for choosing $\lambda_{n_{bw}^0}$. The potential energy difference arising from structural deviations of the activated state from that of the corresponding equilibrium gas-phase configuration is assumed negligible.

In forming the free waters in the activated state it is assumed that the process occurs instantaneously for $n_{fw}^* > 1$ rather than in successive steps. This is consistent with the averaging procedure embodied in eq 9. Consequently, λ^* for free waters in the activated state is assumed to be independent of n_{fw}^* and thus $\lambda^* = \lambda_{n_{bw}^0}$ (see eq 27).

(2) Construction of the Partition Functions f_{bw}^0 and f_{bw}^*. The construction of the specific partition functions constituting f_{bw}^0 and f_{bw}^* relies upon the formulation of Eley and Evans.[8]

A bound water molecule is considered as a harmonic oscillator vibrating with frequency ν in the effective average potential field of the ion $\bar{U}_n$ (eq 12). The frequency ν was calculated by the relation

$$\nu = \frac{1}{2\pi}\sqrt{k/\mu_m}$$

where the force constant k was obtained by the formula

$$k = \left(\frac{\partial^2 \bar{U}_n}{\partial r^2}\right)_{r=r_i+r_w}$$

at $\theta = 0$ or π for cations and anions, respectively; μ_m is the reduced mass of a water–ion pair. The corresponding partition function is

$$f_{vib} = (1 - e^{-h\nu/kT})^{-1} \quad (16)$$

This vibrational mode of a bound water molecule has arisen from a restricted translation along the axis connecting the centers of the ion and the water molecule. The other two translational modes are restricted by the lateral interactions of the water molecule with the effective potential field produced by the surrounding primary waters. The water molecules are therefore considered moving in the free area A_f on the ion surface, which is given as (see Figure 1)

$$A_f = \frac{1}{n_w}\{4\pi(r_i + r_w)^2 - n_w \pi r_w^2\} \quad (17)$$

where n_w is the total number of water molecules in the primary shell. The resulting partition function is

$$f_{rest.\,tr.} = \frac{2\pi m_w kT}{h^2} A_f \quad (18)$$

where m_w is the mass of the water molecule. The bound water molecules were further assumed to undergo librational motion (*i.e.*, restricted rotation) in the potential field of the ion. For restricted rotation, the partition function has the form[12]

$$f_{lib} = \frac{4\pi^2(8\pi^3 I_A I_B I_C)^{1/2}(kT)^{3/2}}{2h^3} S \quad (19)$$

with

$$S = \int_0^\pi e^{-\bar{U}_n(\theta)/kT} \sin\theta \, d\theta \quad (20)$$

where $\bar{U}_n(\theta)$ includes only the θ dependent terms of U_0 in eq 13, *i.e.*

$$\bar{U}_n(\theta) = \lambda_n \left\{-\frac{Ze\mu\cos\Theta}{r^2} + \frac{Ze\Theta_z(3\cos^2\theta - 1)}{2r^3}\right\} \quad (21)$$

I_A, I_B, and I_C are the three principal moments of inertia of a water molecule and the symmetry factor of water was chosen as 2. The internal vibrational modes of a bound water molecule are assumed to be independent of the field of the ion. The partition function for the three internal vibrational degress of freedom is

$$f_{iv} = \sum_{i=1}^{3} (1 - e^{-h\nu_i/kT})^{-1}$$

where ν_i's are the fundamental vibrational frequencies of the water molecule. Utilizing eq 16, 18, and 19 the respective total partition function for a bound water molecule in the initial and activated states becomes

$$f_{bw}^0 = (1 - e^{-h\nu^0/kT})^{-1} \frac{2\pi m_w kT}{h^2} A_f \times \frac{4\pi^2(8\pi^3 I_A I_B I_C)^{1/2}(kT)^{3/2}}{2h^3} S_{bw}^0 f_{iv} \quad (22)$$

and

$$f_{bw}^* = (1 - e^{-h\nu^*/kT})^{-1} \frac{2\pi m_w kT}{h^2} A_f \times \frac{4\pi^2(8\pi^3 I_A I_B I_C)^{1/2}(kT)^{3/2}}{2h^3} S_{bw}^* f_{iv} \quad (23)$$

(12) E. A. Moelwyn-Hughes, "Physical Chemistry," 2nd ed, MacMillan, New York, N. Y., 1961, Chapter VIII.

where ν^0 and ν^* are the respective frequencies corresponding to $\bar{U}_{n_{bw}}{}^0$ and $\bar{U}_{n_{bw}}{}^*$; $S_{bw}{}^0$ and $S_{bw}{}^*$ are defined by eq 20 and 21 with $\lambda_{n_{bw}}{}^0$ and $\lambda_{n_{bw}}{}^*$, respectively. The vibrational partition function f_{iv} is assumed to be the same in both initial and activated states.

(3) Construction of Partition Function $f_{fw}{}^*$. The free, noninteracting water molecules in the activated state were assumed to move in a constant potential cage with the restricted volume V_f arising from the surrounding molecules. Consequently the three translational motions of a free water molecule in the activated state are restricted in V_f. (Here V_f should not be confused with v_f.) The free volume V_f was estimated by considering close packing of inert hard spheres as shown in Figure 1. Thus for the ion with n_w primary water molecules

$$V_f = \frac{1}{n_w}\left[{}^4/_3\pi(r_i + 3r_w)^3 - \left({}^4/_3\pi r_i{}^3 + n_w{}^4/_3\pi r_w{}^3 + \tfrac{1}{2}\, n_w'{}^4/_3\pi r_w{}^3\right)\right] \quad (24)$$

where n_w' is the number of water molecules in the secondary hydration shell which is estimated as

$$n_w' = \frac{{}^4/_3\pi(r_i + 4r_w)^3 - {}^4/_3\pi(r_i + 2r_w)^3}{{}^4/_3\pi r_w{}^3} \quad (25)$$

The partition function for restricted translation in three dimensions is

$$f_{\text{rest. tr.}} = \frac{(2\pi m_w kT)^{3/2}}{h^3} V_f \quad (26)$$

Even though the total potential energy of free water molecules in the activated state was assumed to be zero ($\epsilon_{fw}{}^* = 0$), this does not imply that each term in $\epsilon_{fw}{}^*$ is equal to zero. Thus, a free water molecule in the activated state may undergo librational motion determined by the angular dependent potential energy similar to eq 21. Hence

$$\bar{U}_{n_{fw}{}^*}(\theta) = \lambda^*\left\{-\frac{Ze\mu\cos\theta}{r^{*2}} + \frac{Ze\Theta_z(3\cos^2\theta - 1)}{2r^{*3}}\right\} \quad (27)$$

where $\lambda^* = \lambda_{n_{bw}{}^0}$ as previously discussed. r^* is the separation distance in the activated state. r^* is assumed as a first approximation to be equal to the equilibrium distance in the initial state, $r_i + r_w$. This choice of r^* follows from the constraint imposed by the fixed potential cage approximation. Thus the partition function for the restricted rotation of a free water molecule takes the same form as eq 19 and 20 when eq 27 is employed. As discussed in the previous section, the three internal vibrational modes are assumed unaltered in the activation process, so that the same partition function f_{iv} is used. The total partition function of a free water molecule takes the following form

$$f_{fw}{}^* = \frac{(2\pi m_w kT)^{3/2}}{h^3} V_f \frac{4\pi^2(8\pi^3 I_A I_B I_C)^{1/2}(kT)^{3/2}}{2h^3} S_{fw}{}^* f_{iv} \quad (28)$$

where $S_{fw}{}^*$ is defined as eq 20 with eq 27.

Calculation and Discussion

In this paper we considered the dehydration of quadrihydrated ions ($n_{bw}{}^0 = 4$) except for the iodide ion for which $n_{bw}{}^0 = 3$.

The potential energy of interaction U_0 (eq 13) of a bound water molecule with the ion at equilibrium was calculated by taking $r = r_i + r_w$ and $\theta = 0$ or π for cations or anions, respectively, $\mu = 1.87$ D, $\Theta_z = 0.4 \times 10^{-26}$ esu cm^2.[13] The other physical constants used in the calculation are listed in Table I. The calculated values of U_0 are compared with the measured values of $\Delta H_0{}^\circ{}_1$ in the gas phase in Table II, which shows good agreement. Using eq 9 the scaling factor λ_n was calculated and the values are shown in Table III. The integral S (eq 19) was calculated numerically by using Simpson's rule. From the eq 7, 15, 22, 23, and 28 we calculated the standard free energy of activation for dehydration ΔG^* at 25° and tabulated the results in Table IV.

The results exhibit a nonlinear dependence of ΔG^* with increasing $n_{fw}{}^*$ for each ion. The relative order of ΔG^* is $Li^+ > Na^+ > K^+$, and $Cl^- > Br^- > I^-$ for the same degree of dehydration, *i.e.*, when each ion has lost the same number of bound water molecules.

The relaxation lifetime τ of a bound water molecule in the primary hydration shell for the cations Li^+, Na^+, and K^+ is $\sim 10^{-9}$ sec.[14] The corresponding activation energy calculated from the relation $\tau = (h/kT)e^{\Delta G^*/RT}$ indicates that our activation energy results for these cations are in good agreement when compared for the case $n_{bw}{}^0 = 4$, $n_{bw}{}^* = 3$, and $n_{fw}{}^* = 1$.

Besides the absolute values of ΔG^*, the relative values of ΔG^* for different ions as a function of degree of dehydration yield valuable information in such processes as ionic diffusion through biological membranes and specific adsorption of ions at the electrode-solution interphase.

Applications

(1) Diffusion of Ions into Biological Membranes. One of the contributions to the overall free energy of activation for diffusion of ions into restricted openings such as membrane pores is the activation energy for dehydration of the primary hydrated ion at the membrane pore-solution interphase.[2,4] For the squid axon membrane in the resting (polarized) state, a membrane pore is assumed to form a restricted opening to the primary hydrated cations. Thus, an ion penetrates the membrane pore if it loses a portion of its hydration shell. Of particular interest is the behavior of Li^+, Na^+, and K^+ ions. Thus, from Table IV the standard free energy of activation for dehydration of quadrihydrated Li^+, Na^+, and K^+ ions are in the order $Li^+ > Na^+ > K^+$ for the same degree of dehydration. Experimental permeabilities of Li^+, Na^+, and K^+ ions for the squid axon in the resting state are in the order $P_K > P_{Na} > P_{Li}$.[15] Since the calculated free energies of activation for dehydration alone predict the same order of permeabilities, it is quite likely that the penetration of ions into membrane pores (in the resting state) is energetically dominated by the dehydration process.

(2) Specific Adsorption of Ions at the Electrode-Solution Interphase. Andersen and Bockris[6] have calculated the standard free energy of super-equivalent adsorption $\Delta G_{sea}{}^\circ$ (specific or contact adsorption) of various ions at the potential of zero charge. The results indicate that $\Delta G_{sea}{}^\circ > 0$ for Cl^-, Br^-, and I^- ions while $\Delta G_{sea}{}^\circ > 0$ for Na^+ and K^+ ions. Thus, significant adsorption occurs essentially for these halide ions in the order $I^- > Br^- >$

(13) S. G. Kulolich, *J. Chem. Phys.*, **50**, 3751 (1969).
(14) I. M. Klotz in "Membranes and Ion Transport," Vol. 1, E. E. Bittar, Ed., Wiley-Interscience, New York, N. Y., 1970, Chapter 4, p 108.
(15) J. W. Woodbury, S. H. White, M. C. Mackey, W. I. Hardy, and D. B. Chang, "Physical Chemistry an Advanced Treatise," Vol. IXB, H. Eyring, Ed., Academic Press, New York, N. Y., 1970, Chapter 11, p 959.

TABLE I: Physical Constants Used in the Calculation

	H_2O	Li^+	Na^+	K^+	Cl^-	Br^-	I^-
r, Å[a]	1.38	0.78	0.98	1.33	1.81	1.96	2.20
$\alpha \times 10^{24}$, cm^3 [b]	1.44[e]	0.03	0.15	0.8	4.41	5.84	8.91
I, eV[c]	8.65[d]	75.62	47.29	31.81	3.62	3.37	3.065

[a] V. M. Goldschmidt, Skrifter Det. Norske Videnshaps-Akad. Oslo, I. Matem.-Naturvid. Klasse, 1926, No. 2. [b] J. N. Wilson and R. M. Curtis, *J. Phys. Chem.*, **74**, 187 (1970). Model II of Table III. [c] R. C. Weast, Ed., "Handbook of Physics and Chemistry," 50th ed, The Chemical Rubber Publishing Co., Cleveland, Ohio, 1969, pp E73, E74. [d] J. L. Webb, "Enzyme and Metabolic Inhibitors," Vol. 1, Academic Press, New York, N. Y., 1963, p 225. [e] Reference 12, p 383.

TABLE II: Comparison of the Calculated Potential Energies (U_0) with the Measured Enthalpies ($\Delta H_0°_1$)[a]

Cation	$-U_0$	$-\Delta H_0°_1$	Anion	$-U_0$	$-\Delta H_0°_1$
Li^+	28.2	31.0[b]	Cl^-	12.9	13.1
Na^+	22.9	24.0	Br^-	11.7	12.6
K^+	16.5	17.9	I^-	10.0	10.2

[a] Values in kcal/mol. References 9 and 10. [b] Extrapolated value by replotting $\Delta H_{n-1}°_n$ vs. n.

TABLE III: Calculated Scaling Factor λ_n

Ions	λ_1	λ_2	λ_3	λ_4
Li^+	1.0	0.916	0.833	0.757
Na^+	1.0	0.913	0.828	0.765
K^+	1.0	0.950	0.879	0.824
Cl^-	1.0	0.985	0.954	0.927
Br^-	1.0	0.988	0.963	0.938
I^-	1.0	0.980	0.961	

Cl^- as confirmed by experiment.[5] A primary conclusion of their treatment is that specific adsorption does not involve chemical bonding with the substrate electrode (liquid mercury). The total standard free energy of activation for specific adsorption of Cl^-, Br^-, and I^- ions consists of several contributions one of which is the standard free energy of activation for dehydration ΔG^* as calculated in this paper. From Table IV the activation energy of dehydration for the halide ions is in the order $Cl^- < Br^- < I^-$. This result alone predicts that the amount of specific adsorption of the halide ions at the potential of zero charge is in the order $I^- < Br^- < Cl^-$ as is found experimentally. That the values of $\Delta G_{sea}°$ for anions follow the same order as that predicted by ΔG^* indicates that the standard free energy of activation for dehydration plays a major role in determining the overall activation energy for specific adsorption.

It is interesting to note that the experimental upper limit of the relaxation time for specific adsorption of ions on mercury is 5×10^{-6} sec.[16,17] Our results for anions are $\sim 10^{-8}$ sec, which fall well below this upper limit.

Comments

In the activated state it was assumed that the distance r^* between the free water and the ion is approximately given by the initial equilibrium distance $r_{eq} = r_i + r_w$. Although the assumption $r_{eq} \approx r^*$ certainly differs from the actual situation, it is in part justifiable by the introduction of the potential cage approximation which also accounts for the influence of the surrounding liquid on the dehydration process. When a free water molecule is produced by rotating the water dipole to its activated orientation without stretching the ion-water bond, it moves within the potential cage of volume V_f. Although the total potential energy of interaction of the free water molecule with other constituents in the cluster is zero, it still retains some angular dependence through the librational integral S_{fw}^*. Further approximations in the present formulation are (a) the total partition function for the ion-water cluster in the liquid is based upon the quasicrystalline solid approximation where each independent particle is constrained to move within their own free volumes; (b) the potential energy barrier V_0 is constructed from one ion-water pair interaction and the scaling factor λ_n based upon experimental gas-phase measurements.

TABLE IV: Standard Free Energy of Activation (ΔG^* in kcal/mol) for Dehydration of Primary Hydrated Ions in Aqueous Solution

Initial state	Activated state						
n_{bw}^0	n_{bw}^*	n_{fw}^*	Li^+	Na^+	K^+	Cl^-	Br^-	I^-
4	3	1	7.6	7.3	6.2	7.7	7.1	
4	2	2	23.4	9.2	15.9	17.6	16.3	
4	1	3	48.4	38.9	31.4	30.1	27.6	
4	0	4	83.1	66.5	50.1	43.2	38.9	
3	2	1						7.0
3	1	2						15.8
3	0	3						25.1

ΔG^* consists of two contributions, the logarithmic term involving the ratio of partition functions and the potential energy barrier V_0 as shown in eq 7. The relative contribution of V_0 to ΔG^* for a given ion becomes more significant than that of the logarithmic term as the degree of dehydration increases. The value of ΔG^* as a function of degree of dehydration for a given ion is mainly dependent on λ_n. On the other hand, the relative value of ΔG^* for different ions at the same degree of dehydration is primarily dependent on r.

The simplistic model utilized in this formulation for calculating free energies of activation serves as a first step in constructing a more fundamental treatment. A detailed approach to evaluating the potential energy function would involve a quantum mechanical treatment of the entire ion-water cluster in the liquid. Various improvements of the model would involve the addition of secondary hydration shell interactions and others. The present model may be replaced by the more correct treatment of the many body problem in the vicinity of ions in the liquid.

The present treatment can be extended to other ions in water, nonaqueous solvents, and porous networks which involve dehydration effects.

(16) V. I. Melik-Gackazyan, *Zh. Fiz. Khim.*, **26**, 560 (1952).
(17) T. N. Andersen, J. L. Anderson, D. D. Bode, Jr., and H. Eyring, *J. Res. Inst. Catal., Hokkaido Univ.*, **16**, 449 (1968).

Acknowledgment. The authors wish to express their gratitude to Professor Franklin F. Offner for his numerous suggestions, discussions, and assistance throughout the course of this work. The authors are indebted to Professor Hugh M. Hulburt for several critical discussions as well as his continuous encouragement. The authors also wish to thank the reviewers for their comments. This work has been supported by USPHS Contract No. NS08137.

Theoretical Behavior of Interacting Protein Systems in Density Gradients at Sedimentation Equilibrium

G. J. Howlett and P. D. Jeffrey*

Department of Physical Biochemistry, John Curtin School of Medical Research, Australian National University, Canberra, A.C.T., 2601, Australia *(Received October 24, 1972)*

A method is described for calculating sedimentation equilibrium concentration distributions, in density gradients, of reacting systems of macromolecules. The way in which thermodynamic nonideality may be included in the treatment is indicated. The results of computations for a number of model interacting systems are presented to illustrate the influence of the equilibrium constant and the molecular weights and partial specific volumes of the reacting species on the resulting concentration distributions. It is pointed out that the degree of resolution observed with an interacting system in a density gradient depends on the same factors as in a nonreacting mixture, but that an interaction may be detected by changing conditions which affect the equilibrium constant and thereby alter the appearance of the concentration gradient pattern. Analysis of concentration distributions in terms of true or apparent weight-average molecular weights of interacting systems involving species of different partial specific volumes reveals a characteristic concentration dependence which may be useful in the qualitative interpretation of density gradient patterns. The computational method presented permits a more detailed quantitative analysis of interacting systems by curve fitting experimental results in terms of postulated models. The comparison of a calculated concentration distribution with an experimental one for a single macromolecular solute suggests that reasonable precision may be attained by such a procedure.

Introduction

The technique of banding macromolecules at sedimentation equilibrium in the density gradient formed by the distribution of some suitable low molecular weight substance such as cesium chloride or sucrose in water is well established.[1] Detailed accounts of the factors contributing to the density gradient and to the concentration distribution of the macromolecule in such systems have been given,[2-4] and many experimental studies illustrating the application of the method to obtain information about heterogeneity, molecular weight, and solvation have been published.[1,4-7] However, previous treatments of the sedimentation equilibrium of macromolecules in density gradients have usually been restricted to discussions either of a single species or nonreacting mixtures, and little attention has been given to the behavior of interacting systems of macromolecules. Indeed the only publications pertaining to interacting systems at sedimentation equilibrium in density gradients seem to be those of Kegeles, *et al.*,[8] and Ten Eyck and Kauzmann.[9] The former authors showed that the effects of pressure on an $A + B \rightleftharpoons C$ system may give rise to two or three bands at sedimentation equilibrium depending on the equilibrium constant for the reaction, the relative densities of the species, and the proportions of reactants present in the initial mixture. In the case of dimerization, variation in the equilibrium constant could result in the appearance of one or two peaks in the concentration distribution. In the treatment given by Ten Eyck and Kauzmann,[9] in which equations were derived which allowed for the effects of varying pressure and degree of hydration on the equilibrium constant for a reaction involving a volume change, the parameters chosen for the monomer–dimer reaction considered were such as to give rise to only one peak in the sedimentation equilibrium concentration distribution. Inasmuch as details of the method of computation were not given by Ten Eyck and Kauzmann[9] while that of Kegeles, *et al.*,[8] involved a counter-current distribution analog, it seemed of general

(1) J. E. Hearst and C. W. Schmid, *Pure Appl. Chem.*, **26**, 513 (1971).
(2) J. B. Ifft, D. H. Voet, and J. Vinograd, *J. Phys. Chem.*, **65**, 1138 (1961).
(3) J. E. Hearst and J. Vinograd, *Proc. Nat. Acad. Sci. U.S.*, **47**, 999 (1961).
(4) J. Vinograd and J. E. Hearst, *Fortschr. Chem. Org. Naturst.*, **20**, 372 (1962).
(5) J. E. Hearst and J. Vinograd, *Proc. Nat. Acad. Sci. U.S.*, **47**, 1005 (1961).
(6) J. E. Hearst, J. B. Ifft, and J. Vinograd, *Proc. Nat. Acad. Sci. U.S.*, **47**, 1015 (1961).
(7) J. B. Ifft and J. Vinograd, *J. Phys. Chem.*, **66**, 1990 (1962).
(8) G. Kegeles, L. Rhodes, and J. L. Bethune, *Proc. Nat. Acad. Sci. U.S.*, **58**, 45 (1967).
(9) L. F. Ten Eyck and W. Kauzmann, *Proc. Nat. Acad. Sci. U.S.*, **58**, 888 (1967).

interest to describe a method for calculating equilibrium concentration distributions of interacting systems in density gradients which includes the calculation of the appropriate density gradient for the postulated experimental conditions, as well as the variation of the equilibrium constant with pressure.

Recent studies of the effects of pressure in conventional sedimentation equilibrium experiments with interacting systems exhibiting volume changes[10-13] have led to equations and computational methods which allow the experimental results obtained with such systems to be analyzed, and concentration distributions for model systems to be calculated. In the present work the treatment is extended to sedimentation equilibrium experiments in density gradients.

It is also of interest to examine in more detail the effect on the qualitative appearance of concentration or concentration gradient patterns of variations in such parameters of an interacting system as the molecular weights of the participating species, the equilibrium constant for the reaction, and the magnitude of the volume change accompanying it. It is not feasible to include all the possibilities but results are presented for model systems covering what is felt to be a reasonable range of these parameters.

Finally, consideration is given to the evaluation of molecular weights from the results of density gradient sedimentation equilibrium experiments, in relation to the detection of an interaction and whether it is accompanied by a volume change. In this connection the possibility of elucidating the details of an interaction by comparing experimental results with those calculated for model systems is discussed.

Theory

The system to be considered consists of the solvent (component 1), a low molecular weight solute to form the composition density gradient (component 2), and a macromolecular component (component 3). It has been shown[3] that the effective density gradient at sedimentation equilibrium in such a system at constant temperature is given by

$$\left(\frac{d\rho}{dr}\right)_{eff} = \left[\frac{1}{\beta^0} + \frac{(\kappa - \kappa_s)(\rho^0)^2}{1 - \left(\frac{\partial\rho_0{}^0}{\partial a_1{}^0}\right)_P \left(\frac{da_1}{d\rho^0}\right)}\right]\left[1 - \left(\frac{\partial\rho_0{}^0}{\partial a_1{}^0}\right)\left(\frac{da_1{}^0}{d\rho^0}\right)\right]\omega^2 r \quad (1)$$

The superscript 0 refers to quantities at atmospheric pressure and the subscript 0 to quantities at band center.

$$1/\beta^0 = (d\rho/d \ln a_2)^0 M_2(1 - \bar{v}_2{}^0/\rho^0)/RT \quad (2)$$

where ρ is the density, a_2 the solute activity on the molal scale, M the molecular weight, $\bar{v}$ the partial specific volume, R the gas constant, T the absolute temperature, ω the angular velocity, r the radial distance from the axis of rotation, κ the isothermal compressibility of the solution of component 2 in component 1, and κ_s the isothermal compressibility of the solvated macromolecule. The significance of the various terms in eq 1 when taken in conjunction with $\omega^2 r$ may be summarized as follows. β^0 describes the composition density gradient, that due to the distribution of component 2. $\kappa(\rho^0)^2$ describes the density gradient due to the compression of the solution of component 2, and $\kappa_s(\rho^0)^2$, the contribution made by the compression of the solvated polymer. The terms containing $(\partial\rho_0{}^0/\partial a_1{}^0)_P(da_1{}^0/d\rho^0)$ arise by considering the dependence of the solvated partial specific volume, $\bar{v}_s$, of the macromolecule on solute activity, and allow for the contribution macromolecules of varying extents of solvation will make to the density gradient. Hearst, *et al.*,[3,5,6] have shown that eq 1, together with information from a series of density gradient sedimentation equilibrium experiments, and isopiestic data for the dependence of solvent activity on component 2 concentration and solution density, can be used to determine the isothermal compressibility of the solvated macromolecule and its solvated partial specific volume and degree of solvation.

From the point of view of the present paper a more convenient formulation of the effective density gradient is[3]

$$(d\rho/dr)_{eff} = d\rho^0/dr + \kappa\rho_0{}^2\omega^2 r - (\partial\rho_s{}^0/dr)_P - \kappa_s\rho_0{}^2\omega^2 r \quad (3)$$

The term

$$d\rho^0/dr = \omega^2 r/\beta^0 \quad (4)$$

is usually referred to as the *composition* density gradient and the sum

$$d\rho^0/dr + \kappa\rho_0{}^2\omega^2 r = (d\rho_t/dr)_p \quad (5)$$

as the *physical* density gradient. The physical density gradient, and the corresponding density at any radial distance r, can be calculated for a given angular velocity from eq 4 and 5 provided κ, β^0, and ρ^0 are known at r.

The function β^0 is obtained from physical data for solutions of component 2 in component 1 and eq 2. Values of β^0 as a function of ρ^0 have been tabulated for a number of salts and sucrose by Ifft, *et al.*[2] All of the calculations in the present paper were made taking cesium chloride as component 2 and water as component 1 at 25°. Cesium chloride solutions were chosen because there are suitable data available and because cesium chloride is a commonly used salt, forming gradients covering a wide density range and of quite high resolving power.[2] For the purpose of their calculations Ifft, *et al.*,[2] calculated an explicit relation between β^0 and ρ^0 for solutions of cesium chloride in water at 25° in the form of a cubic polynomial. This gave a sufficiently good fit over the required density range but showed large deviations at densities higher than about 1.6 g/ml. A more satisfactory fit to the same data over the entire concentration range has been obtained for use in the present work in the form of a pentic polynomial derived by the method of orthogonal polynomials. A polynomial of the same form was derived for solutions of sucrose in water for β^0 *vs.* ρ^0 data, evaluated over the entire concentration range for which activity data were available at 25°. Although the sucrose data were not used in this study, it was thought worthwhile to include the polynomial derived, as sucrose gradients are commonly used and may be preferred to cesium chloride gradients in experiments with interacting systems which are sensitive to changes in ionic strength. The success of the pentic poly-

(10) G. J. Howlett, P. D. Jeffrey, and L. W. Nichol, *J. Phys. Chem.*, **74**, 3607 (1970).
(11) G. J. Howlett, P. D. Jeffrey, and L. W. Nichol, *J. Phys. Chem.*, **76**, 777 (1972).
(12) G. J. Howlett, P. D. Jeffrey, and L. W. Nichol, *J. Phys. Chem.*, **76**, 3429 (1972).
(13) G. Kegeles, S. Kaplan, and L. Rhodes, *Ann. N.Y. Acad. Sci.*, **164**, 183 (1969).

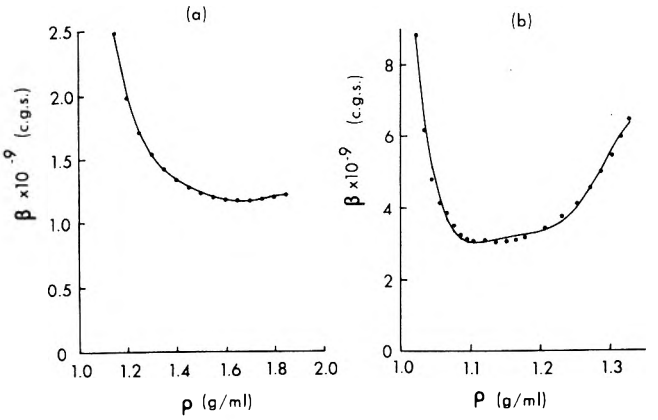

Figure 1. β *vs.* ρ for (a) aqueous cesium chloride solutions and (b) aqueous sucrose solutions at 25° and atmospheric pressure. The cesium chloride data (filled circles) were obtained from Ifft, *et al.*,[2] and the solid line calculated from the relationship $\beta = -73.7258256\rho^5 + 211.797375\rho^4 - 238.452919\rho^3 + 133.700562\rho^2 - 38.5017978\rho + 5.95147986$. The sucrose data (filled circles) were obtained from Jeffrey[14] and the solid line calculated from the relationship $\beta = -5.87005371 \times 10^4\rho^5 + 5.90942166 \times 10^4\rho^4 - 2.24341737 \times 10^4\rho^3 + 4.06403006 \times 10^3\rho^2 - 3.50144205 \times 10^2\rho + 1.44986446 \times 10$ (see text).

nomials in fitting the data for sucrose and cesium chloride solutions is illustrated in Figure 1,[14] where the coefficients of the polynomial expressions are also given.

The method of computation used in the present study may be described by outlining the calculation of the physical density gradient. A suitable density is assigned to a given radial position, say the meniscus, r_m. The relationship between β^0 and ρ^0 allows evaluation of β^0 at this density, which together with the value of the isothermal compressibility of the solution, κ, and the angular velocity, ω, is used to calculate the physical density gradient at r_m from eq 5. Application of the improved Euler method[15] then results in values of the physical density gradient and the corresponding density at a second value of r at a small increment Δr from r_m. The predictor–corrector method[15] can then be used to calculate the values of the physical density gradient and the physical density at suitable radial increments down the solution column.

The above method of computation can be applied to obtain the distribution of an interacting system in a density gradient provided the necessary equilibrium conditions are satisfied. Consider a polymerization reaction represented by $nA \rightleftharpoons C$ where $n(>1)$ is the degree of polymerization. The equilibrium constant for association is given by

$$X = c_C/c_A{}^n \tag{6}$$

For a thermodynamically ideal system the sedimentation equilibrium equations for monomer and polymer may be written[11]

$$\left(\frac{\mathrm{d}\ \ln\ c_A}{\mathrm{d}(r^2)}\right)_r = (\phi_A)_r M_A \tag{7a}$$

$$\left(\frac{\mathrm{d}\ \ln\ c_C}{\mathrm{d}(r^2)}\right)_r = (\phi_C)_r M_C \tag{7b}$$

where $(\phi_i)_r = (1 - \bar{v}_i\rho)_r\omega^2/2RT$ (i = A or C). Multiplication of eq 7a by n and subtraction of the result from (7b) with the substitution of $nM_A = M_C$ and $\Delta V = M_C\bar{v}_C - M_C\bar{v}_A$ where ΔV is the molar volume change of the reaction, gives

$$\left(\frac{\mathrm{d}\ \ln\ (c_C/c_A{}^n)}{\mathrm{d}(r^2)}\right)_r = \left(\frac{\mathrm{d}\ \ln\ X}{\mathrm{d}(r^2)}\right)_r = -\left(\frac{\Delta V\rho\omega^2}{2RT}\right)_r \tag{8}$$

It has been pointed out in previous publications[10,11] that combination of the thermodynamic expression for the pressure dependence of the equilibrium constant in a reaction involving a volume change, $\mathrm{d}\ \ln X/\mathrm{d}P = -\Delta V/RT$, with the radial dependence of pressure in a centrifugal field, $\mathrm{d}P/\mathrm{d}(r^2) = \omega^2\rho/2$, leads to exactly the same result. The significance of this in the present context is that the use of the sedimentation equilibrium eq 7a and 7b to calculate concentration gradients as a function of radial distance gives values which take into account the correct variation of equilibrium constant with pressure while ensuring that chemical equilibrium is maintained at each level in the cell.

In order to apply the predictor–corrector method, values of the composition density, ρ, the concentration of monomer c_A, the equilibrium constant X, and the partial specific volumes $\bar{v}_A$ and $\bar{v}_C$ are specified at a given radial position, say the meniscus, r_m. The physical density and density gradient at r_m are evaluated as before, and the concentration of polymer, c_C, calculated from c_A and X. The solution density including the contribution of the macromolecular component may then be calculated at r_m from the expression

$$\rho = \rho_p + \sum_i (1 - \bar{v}_i\rho_p)c_i \tag{9}$$

where i refers to A and C and $\bar{v}_i$ are the values of the solvated partial specific volumes of the macromolecular species at the solute activity corresponding to ρ_p. The improved Euler method and the predictor–corrector method can then be used, as indicated above, to calculate concurrently the values of the density gradient, the density, the concentration gradient, and the concentration of the macromolecular species at selected radial values down the solution column, by the use of the relationships between β^0 and ρ^0, and eq 3, 6, and 7.

If values of the solvated partial specific volumes of the macromolecular species as a function of solute activity and of the isothermal compressibilities of the solvated macromolecules were available, the above method of calculation would yield the *effective* density gradient (eq 1 and 3) and density, and the corresponding macromolecular concentration gradient and concentration, as a function of radial distance, for any desired set of experimental conditions. In the results presented below, the effect of varying solvation has been omitted because it will be unique to a particular macromolecule in a specific environment and would have to be determined experimentally for individual systems. Likewise, the terms involving the compressibilities have not been included because their inclusion, while affecting slightly the quantitative distributions, is not necessary to the discussion of the model systems with which this paper is concerned. Some computations were performed in which the contribution of the distribution of the macromolecular component to the effective density at each point was included, assuming a constant degree of solvation. The results showed that the effect on the final density gradient and concentration distribution was negligible. Examination of eq 9 reveals that this is expected in banding experiments because at the

(14) P. D. Jeffrey, *Biochim. Biophys. Acta*, **158**, 295 (1968).
(15) D. D. McCraken and W. S. Dorn in "Numerical Methods and Fortran Programming," Wiley, New York, N. Y., 1964, p 330.

band position the partial specific volume of the macromolecule is equal to the reciprocal of the solution density, and thus, in the neighborhood of the band, the second term in the equation is close to zero, especially at the concentrations customarily used in banding experiments with macromolecules.

For computations such as those discussed here, the assignment of values to the composition density and to the concentration of a macromolecular constituent at a given radial position is the most convenient procedure. Where it is required to compare hypothetical experiments under different conditions, but with the same solution composition, or to analyze the results of an actual experiment, a conservation of mass condition and an iterative procedure must be included in the computation.

The macromolecular component specified in the preceding discussion was a thermodynamically ideal monomer–single higher polymer system. However, the treatment may readily be extended to other kinds of systems, such as those including more than one kind of polymer and those of the type A + B $\rightleftharpoons$ C, by writing appropriate additional equations of the form given in eq 7a and 7b. Similarly, nonideality may be included, if for each constituent, eq 7a and 7b are written

$$\left(\frac{\mathrm{d}\ \ln c_i}{\mathrm{d}(r^2)}\right)_r = (\phi_i M_i)_r - \left(\frac{\mathrm{d}\ \ln y_i}{\mathrm{d}(r^2)}\right)_r \qquad (10)$$

where y_i is the activity coefficient on the weight per unit volume concentration scale and may be expressed as a power series in total concentration by

$$y_i(r) = e^{BM_i c(r)}$$

where $c(r) = \Sigma_i c_i(r)$. Equilibrium equations for thermodynamically nonideal interacting systems accompanied by volume changes have been given in previous publications.[11,16] A computed sedimentation equilibrium density gradient for a single macromolecular species in which the effect of nonideality is included is given in the Results section, together with the distributions calculated for various ideal monomer–single polymer systems and A + B $\rightleftharpoons$ C system.

Results and Discussion

Calculated Concentration Distributions. The results of computations of sedimentation equilibrium concentration and concentration gradient distributions for various model macromolecular systems are presented in the accompanying figures. All of the calculations were carried out for density gradients formed by aqueous cesium chloride solutions at 25° and an angular velocity of 60,000 rpm. The parameters which were varied were the molecular weights and partial specific volumes of the interacting species and the equilibrium constants for the reactions. These quantities were chosen to resemble those of known interacting proteins so that the resulting concentration distributions would illustrate the variability which might be observed in practice. The computations were made with the aid of a digital PDP/8I computer using programs written in Focal, and the results plotted directly with a Hewlett-Packard 7200A graphic plotter.

Figure 2 shows the density gradient, the concentration, and the concentration gradient at sedimentation equilibrium for a protein of molecular weight 450,000 and partial specific volume 0.73 ml/g. These values of molecular weight and partial specific volume are approximately

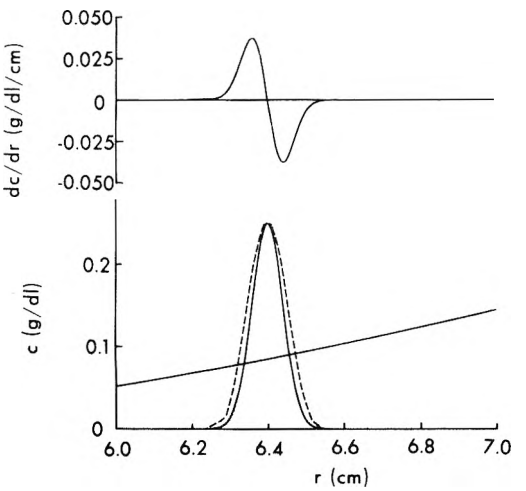

Figure 2. Sedimentation equilibrium concentration and concentration gradient distributions calculated for a single macrospecies (M = 450,000, $\bar{v}$ = 0.73 ml/g) in a cesium chloride density gradient at 60,000 rpm and 25°. The solid lines refer to a thermodynamically ideal macromolecule (B = 0), while the dashed line shows the concentration distribution calculated for $B = 1 \times 10^3$ ml/g. The calculated density, shown as a line in the lower diagram, extends from 1.3 g/ml at r = 6.0 cm to 1.48 g/ml at r = 7.0 cm.

those of the hemocyanin pentamer.[17] The influence of thermodynamic nonideality on the concentration distribution is shown by the broken line, where the value of the virial coefficient B was taken as 1×10^{-3} ml/g. This is about two orders of magnitude higher than that expected experimentally[18] and was used so that the qualitative effect of nonideality would be visible in the figure. It is seen that the computed band width is broadened in the nonideal example. This is in agreement with the equations derived by Schmid and Hearst[19] and also with their experimental observation of the effect of concentration on the width of the band formed by T7 DNA in cesium chloride density gradients. These workers concluded that accurate molecular weights could be obtained from the results of sedimentation equilibrium experiments in density gradients, provided that the apparent molecular weights, measured at a series of concentrations, were extrapolated to infinite dilution. Further comments on the determination of molecular weights in density gradient sedimentattion equilibrium experiments, utilizing the results shown in Figure 2, are given in a later section.

Concentration distributions calculated for thermodynamically ideal interacting systems, consisting of a monomer in equilibrium with a polymer, are shown in Figures 3–5.[20,21] The values used for the molecular weights in the computations represent those for the dimerization of α-chymotrypsin, the hexamerization of α-chymotrypsin, and the pentamerization of hemocyanin, respectively. The volume changes accompanying the formation of the various polymeric species are somewhat arbitrary although they are based on figures reported in the literature for the systems used here as models.

(16) G. J. Howlett and L. W. Nichol, *J. Biol. Chem.*, **247**, 5681 (1972).
(17) C. H. Moore, R. W. Henderson, and L. W. Nichol, *Biochemistry*, **7**, 4075 (1968).
(18) C. Tanford in "Physical Chemistry of Macromolecules," Wiley, New York, N. Y., 1963.
(19) C. W. Schmid and J. E. Hearst, *J. Mol. Biol.*, **44**, 143 (1969).
(20) G. Kegeles and M. Johnson, *Arch. Biochem. Biophys.*, **141**, 59 (1970).
(21) K. E. Van Holde and L. B. Cohen, *Biochemistry*, **3**, 1803 (1965).

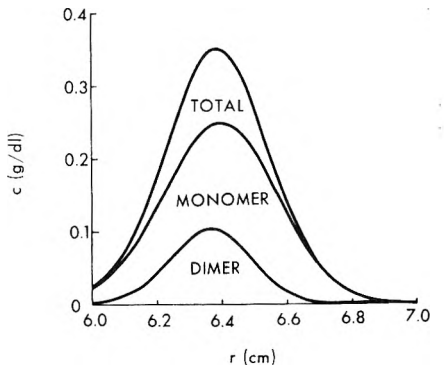

Figure 3. Sedimentation equilibrium concentration distributions calculated for a polymerizing protein in a cesium chloride density gradient at 60,000 rpm and 25°. The molecular weights and partial specific volumes were respectively 24,000 and 0.73 ml/g for the monomer, and 48,000 and 0.733 ml/g for the dimer. The volume increase on dimer formation was taken as 142 ml/mol of monomer[20] and the starting conditions were chosen to give approximately equal concentrations of the two species at sedimentation equilibrium. The calculated density extends from 1.3 g/ml at r = 6.0 cm to 1.48 g/ml at r = 7.0 cm.

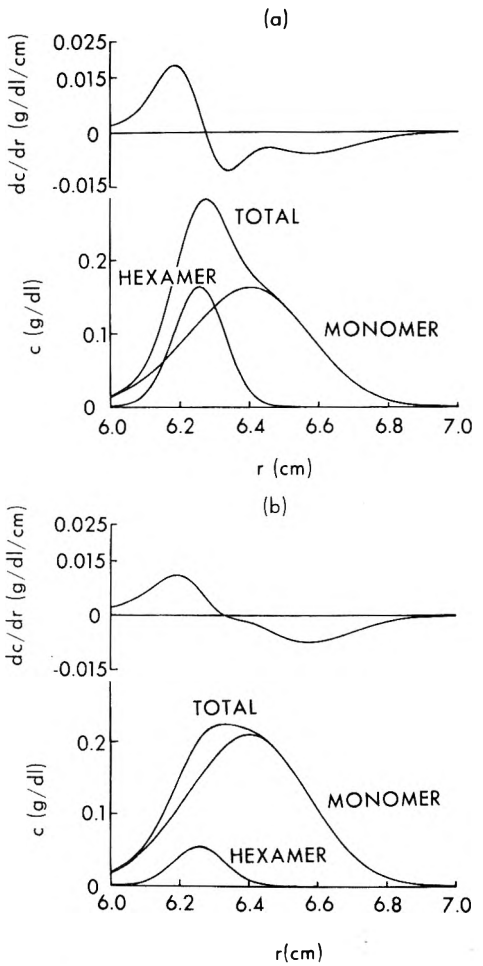

Figure 4. Sedimentation equilibrium concentration and concentration gradient distributions calculated for a polymerizing protein in a cesium chloride density gradient at 60,000 rpm and 25°. The molecular weights and partial specific volumes were respectively 24,000 and 0.73 ml/g for the monomer, and 144,000 and 0.744 ml/g for the hexamer. The volume change per mole of monomer is the same as that used in Figure 3. The calculated density extends from 1.30 g/ml at r = 6.0 cm to 1.48 g/ml at r = 7.0 cm. The equilibrium constant for hexamer formation at atmospheric pressure was (a) 0.61×10^{18} $(g/ml)^{-5}$ and (b) 0.45×10^{17} $(g/ml)^{-5}$. The initial total concentration in each case was 0.1 g/dl.

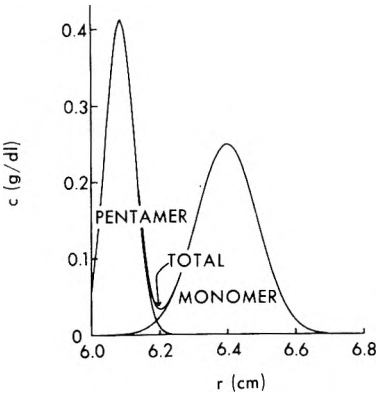

Figure 5. Sedimentation equilibrium concentration distributions calculated for a polymerizing protein in a cesium chloride density gradient at 60,000 rpm and 25°. The molecular weights and partial specific volumes were respectively 90,000 and 0.73 ml/g for the monomer, and 450,000 and 0.76 ml/g for the pentamer. The volume change is based on that reported for a hemocyanin by Van Holde and Cohen[21] and an equilibrium constant giving approximately equal concentrations of the two species at sedimentation equilibrium was used in the calculation. The calculated density extends from 1.30 g/ml at r = 6.0 cm to 1.44 g/ml at r = 6.8 cm.

Figure 3 qualitatively resembles Figure 2 of Ten Eyck and Kauzmann,[9] which was also calculated for the dimerization of α-chymotrypsin with slightly different values of the parameters, and shows that the concentration distribution in such a system would give no indication that a reaction accompanied by a volume change was occurring. This may be contrasted with the result shown in Figure 4a, which illustrates graphically the effect on the resolution in the concentration and concentration gradient patterns of increasing molecular weight and volume change. The marked alteration in the appearance of concentration and concentration gradients which can result from a change in the equilibrium constant is demonstrated in Figure 4b which was calculated for the same system as Figure 4a but with a decreased equilibrium constant for hexamer formation. The alterations are more distinctly observed in the concentration gradient patterns as Ten Eyck and Kauzmann[9] noted.

It is pointed out that changing the pressure, for example, by layering mineral oil on top of the solution column, has the effect of altering the equilibrium constant for a reaction involving a volume change. Thus Figure 4a and 4b can be regarded as showing the effect of increased pressure on the distribution of species in such a system when there is a volume increase on polymerization. A variety of factors such as pH, temperature, and ionic strength may alter the equilibrium constant of a protein interaction. Such alterations are normally detected in sedimentation equilibrium experiments in which there is no significant density gradient, by changes in the dependence of the apparent weight-average molecular weight on concentration. When there is a volume change accompanying the reaction and the macromolecular component is banded in a density gradient, changes in the equilibrium constant with changing conditions, may, in certain instances, be visible in the appearance of the concentration gradient pattern without the necessity for detailed measurements and calculations.

The degree of resolution obtainable in favorable circumstances in density gradient experiments, even in systems in which the species are in rapid chemical equilibrium, is illustrated in Figure 5. The extremely high resolution,

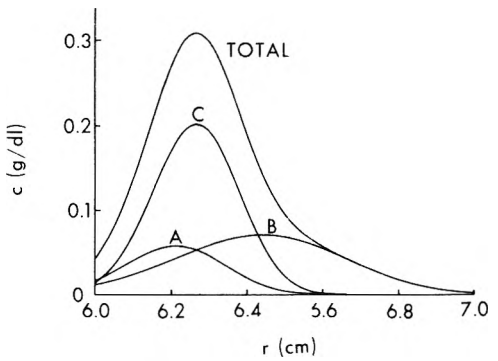

Figure 6. Sedimentation equilibrium concentration distributions calculated for an A + B ⇌ C system in cesium chloride density gradient at 60,000 rpm and 25°. The molecular weights and partial specific volumes were respectively A, 45,000 and 0.748 ml/g; B, 14,400 and 0.726 ml/g; C, 59,400 and 0.742_7 ml/g. The equilibrium constant for the reaction was 0.8×10^5 mol^{-1}.[22] The calculated density extends from 1.3 g/ml at r = 6.0 cm to 1.48 g/ml at r = 7.0 cm.

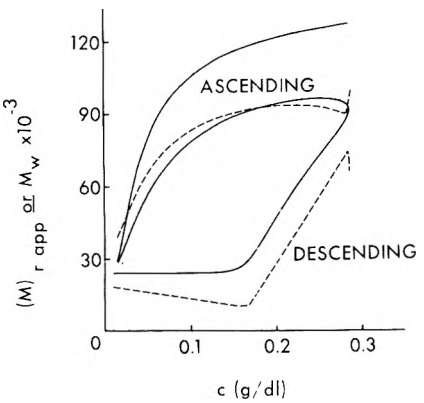

Figure 7. Apparent (broken line) and true (solid line) weight-average molecular weights for the polymerizing system illustrated in Figure 4a. Ascending and descending refer to molecular weights evaluated on the centripetal and centrifugal sides, respectively, of the band maximum as described in the text. The upper solid line shows the curve obtained when the polymerization is not accompanied by a volume change.

with the two peaks being virtually identifiable with monomer and polymer, respectively, is similar to that illustrated for a monomer–dimer system by Kegeles, *et al.*,[8] and emphasizes the fact that in an interacting system, as in a mixture, the resolution of peaks due to species which band at different densities, in a given density gradient, depends essentially on the magnitude of the difference in partial specific volumes between the species and their molecular weights. Accurate values of the solvated partial specific volumes of each of the species could be obtained from a density gradient experiment with such a system. It should be pointed out, in respect to Figures 2–5 (and Figures 5–7 of Kegeles, *et al.*[8]) that although the concentrations of some of the species appear to decrease to zero, they are in fact always finite in accordance with the sedimentation equilibrium condition.

In a polymerization, the possibility of any peak resolution necessarily relies on a volume change accompanying the reaction. In this regard, the use of equilibrium density gradients in the study of systems of the type A + B ⇌ C may have wider application, since even if there is no such volume change, there may exist in solution species of differing partial specific volumes. The computed concentration distribution for such a reaction, that between ovalbumin (A) and lysozyme (B), is given in Figure 6.[22] The partial specific volume of the complex, $\bar{v}_C = 0.742_7$ ml/g, was calculated on the basis of no volume change on reaction. Figure 6 shows that the total concentration distribution which may be observed experimentally is markedly asymmetric. Curves of similar shape might however be obtained even if there were no interaction between A and B in a mixture. The detection of the interaction would depend on either a detailed analysis of the curve, as discussed in the next section, or on further experiments in which environmental conditions expected to affect the equilibrium constant for the interaction were changed. Clearly, in an A + B ⇌ C system of the type discussed here, the absence of any effect of pressure on the distribution would not rule out the possibility of an interaction. The variation possible in concentration distributions of A + B ⇌ C systems in which there is a volume change on complex formation have been discussed by Kegeles, *et al.*,[8] and are referred to briefly in the Introduction.

Evaluation of Molecular Weights. The molecular weight of a single homogeneous macromolecular species is usually evaluated from the band it forms at sedimentation equilibrium in a density gradient by use of the expression[4]

$$\sigma^2 = \frac{RT\rho_0}{M(d\rho/dr)_0\omega^2 r_0} \qquad (11)$$

where σ is the standard deviation of the concentration distribution and the other quantities are as defined in eq 1. Equation 11 refers to a thermodynamically ideal macromolecule and gives the solvated molecular weight if the effective density gradient is used. The computed concentration distribution shown in Figure 2 was used to assess the potential accuracy obtainable from the application of eq 11 in the absence of experimental error. The variance was calculated from the expression[23]

$$\sigma^{2\prime} = \sum_{-\infty}^{\infty} cr^2\, dr \Big/ \sum_{-\infty}^{\infty} c\, dr - \left(\sum_{-\infty}^{\infty} cr\, dr \Big/ \sum_{-\infty}^{\infty} c\, dr\right)^2 \qquad (12)$$

where the denominators serve to normalize the concentrations, c. Values of concentration at radial distances, r, corresponding to increments of $r^2 \leq 0.05$ cm^2 were used to calculate σ^2, which was then substituted in eq 11 together with the calculated value of the density gradient and the initially set value of the density at the peak maximum, r_0. Comparison of the calculated molecular weight, 449,000, with the true value, 450,000, used to generate the concentration distribution shows that the application of eq 11 and 12 to the results of density gradient sedimentation equilibrium experiments is capable of yielding highly accurate molecular weights. The same calculation for the nonideal case shown in Figure 2 gave a value of 363,000 for the apparent molecular weight, while a calculation for a distribution utilizing a more realistic value of 0.5×10^{-5} ml/g for the virial coefficient[18] gave 448,000. The results for the nonideal cases emphasize the necessity for evaluating apparent molecular weights at a number of concentrations and extrapolating to infinite dilution in an experimental determination.

Of more relevance to the study of interacting molecules is the measurement of the weight-average molecular weight as a function of the total concentration. In a sedimentation equilibrium experiment with a thermodynamically ideal interacting system involving species of different

(22) G. J. Howlett and L. W. Nichol, *J. Biol. Chem.*, in press.
(23) I. Guttman and S. S. Wilks in "Introductory Engineering Statistics," Wiley, New York, N. Y., 1967, p 84.

partial specific volumes, the quantity which is determined experimentally is an apparent weight-average molecular weight defined by

$$(M)_{r,\mathrm{app}} = \left(\frac{\mathrm{d}\ \ln c}{\mathrm{d}(r^2)}\frac{1}{\phi_x}\right)_r = \left(\frac{\sum_i M_i c_i \phi_i}{\phi_x \sum_i c_i}\right)_r \qquad (13)$$

where the c_i are the individual species concentrations, $c = \Sigma c_i$ is the total concentration, and ϕ_i is as defined in eq 7. The notation $(M)_{r,\mathrm{app}}$ signifies the fact that an apparent molecular weight is obtained because in practice only a single value (indicated by the subscript x) for the partial specific volume can be substituted in the ϕ_x term. The value used depends on what is experimentally available, and may be the partial specific volume of any one of the reacting species, or some average value. Equation 13 is applicable to density gradient sedimentation equilibrium experiments, provided the appropriate value of the density at a given radial position is used in the evaluation. In a density gradient sedimentation equilibrium experiment where a band is formed, molecular weights can be evaluated as a function of increasing concentration on one side of the band maximum, and of decreasing concentration on the other side of it. In the present study the molecular weights evaluated on the centripetal side of the maximum are referred to as "ascending," and those on the centrifugal side as "descending."

Molecular weight *vs.* concentration curves calculated by eq 13 from the concentration *vs.* radial position data for the polymerizing system shown in Figure 4a are given in Figure 7. The dependence of the true weight-average molecular weight, $M_w = \Sigma M_i c / \Sigma c_i$, on concentration when there is a volume change (Figure 4a) is given by the lower solid line in Figure 7. Although not accessible experimentally, true weight-average molecular weights can be evaluated for a model system because the required values of c_i are known at each value of r. The weight-average molecular weight on the ascending side of the peak differs markedly from that at the same total concentration on the descending side because of the influence of the pressure at different radial positions on the equilibrium constant for the interaction. As the concentration approaches zero on each side the weight-average molecular weight approaches that of the monomer (24,000), producing the characteristic appearance of the molecular weight dependence shown in the figure.

In an experiment, only apparent weight-average molecular weights could be determined (eq 13) and the dashed line in Figure 7 shows the curves obtained when the partial specific volume substituted in ϕ_x was given a value equal to the reciprocal of the density at the peak maximum. This value was chosen, rather than that of one of the reacting species, because it could be evaluated in the sedimentation equilibrium experiment itself. The concentration dependence of $(M)_{r,\mathrm{app}}$ is similar to that of M_w in showing the effect of pressure on the distribution, but the form of the equation for $(M)_{r,\mathrm{app}}$ necessarily leads to a discontinuity in the curve unless it is possible to choose a value of ϕ_x which equals zero at precisely the value of r where $\mathrm{d}\ \ln c/\mathrm{d}(r)^2$ equals zero. In the figure the apparent weight-average molecular weight does not approach the molecular weight of the monomer at zero concentration because of the choice of partial specific volume mentioned above. If the partial specific volume of the monomer were known its use in the evaluation of $(M)_{r,\mathrm{app}}$ would give the correct monomer molecular weight on extrapolation of both ascending and descending curves to infinite dilution.

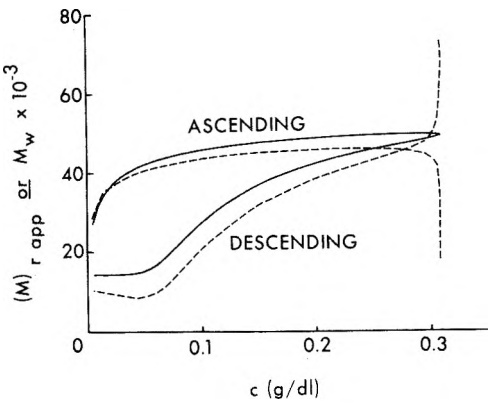

Figure 8. Apparent (broken line) and true (solid line) weight-average molecular weights for the A + B ⇌ C system illustrated in Figure 6. Ascending and descending refer to molecular weights evaluated on the centripetal and centrifugal sides, respectively, of the band maximum as described in the text.

The $(M)_{r,\mathrm{app}}$ curves in Figure 7 correspond to those which could be evaluated experimentally, and show that the application of eq 13 to the concentration distribution determined in a density gradient sedimentation equilibrium experiment would reveal the presence of species of different partial specific volumes in systems which showed little, or no evidence, of density heterogeneity in the concentration distributions themselves (*e.g.*, Figure 4b). Moreover, in an interaction the species favored by increasing pressure could be deduced from the relative magnitudes of the apparent weight-average molecular weights at the same concentration on the ascending and descending sides of the peak. It may be pointed out that the nonsuperposition of the ascending and descending $(M)_{r,\mathrm{app}}$ *vs.* concentration curves shown in Figure 7 for an interacting system accompanied by a volume change corresponds to the nonsuperposition which would be observed in two separate conventional sedimentation equilibrium experiments, in which different initial loading concentrations and/or speeds were used.[10,11] The curve obtained when the polymerization is not accompanied by a volume change is also shown in Figure 7. The dependence of weight-average molecular weight on total concentration is the same as that obtained from an interacting system in a conventional sedimentation equilibrium experiment and there is no difference in values measured on the ascending and descending side of the peak.

Figure 8 shows M_w and $(M)_{r,\mathrm{app}}$ *vs.* concentration curves calculated for the A + B ⇌ C system illustrated in Figure 6. These curves qualitatively resemble those for a polymerizing system and also those which would be obtained for a mixture of A and B in which no reaction was occurring, but in which the species had different partial specific volumes. An interaction could be detected qualitatively from the $(M)_{r,\mathrm{app}}$ curves evaluated from a single density gradient sedimentation equilibrium experiment, only if the equilibrium constant and the initial concentrations used were such as to lead to an $(M)_{r,\mathrm{app}}$ higher than that of either reactant. This is not the case for the example illustrated, where the highest well-defined $(M)_{r,\mathrm{app}}$ is close to the molecular weight of species A (45,000). In this situation the possibility of an interaction might be inves-

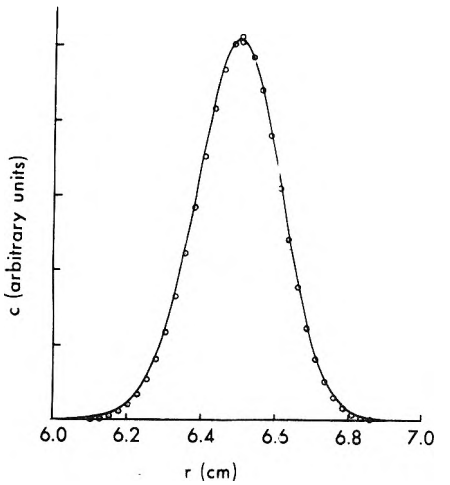

Figure 9. Comparison of experimental (circles) and calculated (line) sedimentation equilibrium concentration distributions for bovine mercaptalbumin in a 2.47 *m* cesium chloride solution at 56,100 rpm and 25°. The density at the band maximum was taken as 1.282 g/ml[7] and $\bar{v}$ for the protein as its reciprocal, 0.78 ml/g. The solid line was plotted directly from the computer output using a Hewlett-Packard 7200 A graphic plotter on a photographic enlargement of the experimental distribution originally presented by Ifft and Vinograd.[7]

tigated by another experiment under different conditions designed to affect the equilibrium constant and thus alter the dependence of $(M)_{r,\mathrm{app}}$ on concentration, or perhaps more satisfactorily, by computing theoretical $(M)_{r,\mathrm{app}}$ *vs.* *c* curves for various interacting and noninteracting models and curve fitting the experimental data.

In the latter connection an experimental distribution obtained for a single macromolecular species at sedimentation equilibrium in a density gradient was used to investigate the precision possible in curve fitting by the kind of computations described in this paper. The method described in the Theory section was used to compute the sedimentation equilibrium concentration distribution of bovine serum mercaptalbumin in a cesium chloride density gradient, given the molecular weight and final concentration of the macromolecule and the density of the cesium chloride solution at the banding position. The data used were taken from the study by Ifft and Vinograd[7] and the values of the relevant parameters are given in the legend to Figure 9 which compares the computed concentration distribution with that obtained experimentally. A possible error of 10% in the determination of the density at band maximum, noted by those authors,[7] is probably responsible for the discrepancy between the density gradient molecular weight and that evaluated by other methods.[18] The important point is that the extremely good agreement of the computed distribution with the experimental points shown in Figure 9 indicates that it should be possible to analyze experimental distributions successfully by comparing them with those calculated for various models. It is anticipated that with interacting systems such a curve-fitting procedure should yield the molecular weights and partial specific volumes of the species banded in the density gradient, and the equilibrium constant for the reaction, with about the same precision as that available from the analysis of conventional sedimentation equilibrium experiments. In discussing the interpretation of results obtained from sedimentation equilibrium experiments with interacting systems in density gradients only the variation of the equilibrium constant with pressure has been explicitly considered. The presence of steep gradients and high concentrations of a third component such as cesium chloride or sucrose may cause a significant variation in the equilibrium constant with radial position. Providing the form of such dependence was known from separate experiments for a given system it could be included in the analysis.

Summary

A method has been presented for calculating sedimentation equilibrium concentration distributions, in density gradients, of reacting systems involving macromolecules of different partial specific volumes. The procedure described ensures that the appropriate density variation is included in the sedimentation equilibrium equations, that chemical equilibrium is maintained at all levels in the density gradient, and that the variation of the equilibrium constant with pressure is correctly described. The way in which thermodynamic nonideality may be included in the treatment is indicated.

Distributions computed for a number of model interacting systems demonstrate that experimental patterns may range in appearance from apparently symmetrical to apparently almost completely resolved peaks. The factors affecting the degree of resolution in a given density gradient are the same as those in a mixture, namely, the difference in the partial specific volumes and the magnitudes of the molecular weights of the macrospecies. The existence of a reaction may be detected experimentally by alterations in the appearance of concentration gradient patterns brought about by changing conditions which affect the equilibrium constant.

A thorough analysis of the complete equilibrium concentration distribution, either for a single polymerizing solute or an A + B $\rightleftharpoons$ C system, in terms of apparent weight-average molecular weights, provides a more sensitive indication of the presence of an interaction and whether it is accompanied by a positive, negative, or zero volume change. The computational procedures outlined should allow the parameters characterizing macromolecular interactions to be evaluated with acceptable precision from the results of density gradient sedimentation equilibrium experiments by curve fitting of the kind commonly used in conjunction with conventional sedimentation equilibrium experiments. The treatment is applicable to experiments in which there are appreciable density gradients but where the macromolecular component does not form a band.

Conductometric Behavior of Electrolytes in Hexamethylphosphotriamide at 25°[1]

Paolo Bruno, Mario Della Monica,* and Ettore Righetti

Istituto di Chimica Analitica dell'Università di Bari, Bari, Italy *(Received November 22, 1972)*

Publication costs assisted by the Centro di Chimica Analitica Strumentale

Conductance measurements at 25° are reported for $NaClO_4$, $KClO_4$, $LiNO_3$, $NaNO_3$, KNO_3, NaSCN, KSCN, NaBr, KPi, and n-Pr_4NBr in hexamethylphosphotriamide (HMPT) and the data are analyzed with the Fuoss–Onsager equation. Potassium salts are more conducting than the corresponding sodium salts and the difference in equivalent conductivity of 0.21 ± 0.03 unit substantiates the Kohlrausch law of independent ion migration in HMPT. The Stokes radius of the ions has been corrected following a suggestion by Robinson and Stokes. The correct ionic radius in HMPT solution shows that while alkaline metal cations are solvated by approximately two HMPT molecules, the anions can be considered as naked. All of the studied salts, except KNO_3 and n-Pr_4NBr, were found to be completely disassociated in that solvent.

Introduction

The hexamethylphosphotriamide is a polar aprotic solvent particularly used in organic chemical reactions. Its molecular shape is that of a pyramid[2] with a positive charge density symmetrically distributed over the three nitrogen and the phosphorus atoms and a high electron density located on the oxygen atom.

This solvent shows a high dipolar moment, an intermediate value of the dielectric constant, and a large value for the viscosity. In spite of these interesting physical properties little work has been done on the properties of the electrolyte solutions and on the ion–solvent interaction in this medium. Brusset and coworkers[3] report a qualitative conductometric study of KI in HMPT; from the curve of the equivalent conductivity *vs.* concentration they deduce that KI is not completely dissociated in this solvent. The conductivity of some tetraalkylammonium salts and $KClO_4$ in HMPT appeared in a recent paper,[4] and it shows indeed no association of the studied salts in this medium.

In this paper the conductance measurements in HMPT have been extended to several 1-1 valent electrolytes in order to provide information concerning the interaction between solvent molecules and all of the considered ions.

Experimental Section

Materials. Hexamethylphosphotriamide (Fluka A.G. pract.) dried with molecular sieves 3A (Union Carbide) in the form of $\frac{1}{16}$-in. pellets was allowed to stand in contact with barium oxide for 2 days. The liquid was decanted and then fractionated at 20 mm pressure. The middle fraction with a specific conductance 1–1.2 × 10^{-7} ohm^{-1} cm^{-1} was used.

Sodium perchlorate (Fisher Certified Reagent) was recrystallized from conductivity water and dried in a vacuum oven at 130° for 24 hr. The potassium perchlorate used was purified in two different ways. A sample (Fisher Certified) was recrystallized three times from conductivity water and dried *in vacuo* over phosphoric oxide for 10 hr at 100°; before use the temperature was raised at 130° for 10 hr. Another sample (Carlo Erba Reagent Grade) was recrystallized from conductivity water and dried for 12 hr in a vacuum oven at 100°.

Potassium picrate was prepared following a method previously described.[5] Reagent grade lithium, potassium, and sodium nitrates and sodium bromide were recrystallized three times from conductivity water and dried for 24 hr *in vacuo* at 90°. Fisher Certified ACS potassium and sodium thiocyanates were recrystallized from conductivity water and dried for 48 hr *in vacuo* at 60°. Tetrapropylammonium bromide was recrystallized from a methanol–ether mixture and then dried for 12 hr in a vacuum oven at 90°.

The thermostat was an oil-filled bath kept at 25 ± 0.005°. The apparatus used for the conductivity measurements, the procedure employed to realize the various solutions, and the standardization of the cells are reported in a previous note.[5] The conductance of pure solvent was subtracted from the conductance of each solution.

Results and Discussion

The equivalent conductance and concentration of each solution have been reported in Tables I and II.[6] Equivalent conductance data were analyzed using Kay's least-squares program[7] and an IBM 360/65 computer. The Fuoss–Onsager equations[8] were used in the form

$$\Lambda = \Lambda_0 - Sc^{1/2} + Ec \log c + (J - F\Lambda_0)c \quad (1)$$

for unassociated electrolytes and in the form

$$\Lambda = \Lambda_0 - S(c\gamma)^{1/2} + Ec\gamma \log (c\gamma) + (J - F\Lambda_0)c\gamma - K_A f^2 c\gamma \quad (2)$$

for associated electrolytes.

(1) This work was taken from the doctoral thesis of E. Righetti.
(2) H. Normant, *Angew. Chem. Int. Ed. Engl.*, **6**, 1046 (1967).
(3) H. Brusset, P. Delvalle, J. Garcin, and P. Rajaonera, *Bull. Soc. Chim. Fr.*, 3800 (1969).
(4) C. Atlani, J. C. Justice, M. Quintin, and J. E. Dubois, *J. Chim. Phys.*, **66**, 180 (1969).
(5) P. Bruno and M. Della Monica, *J. Phys. Chem.*, **76**, 1049 (1972).
(6) Equivalent conductance data will appear following these pages in the microfilm edition of this volume of the journal. Single copies may be obtained from the Business Operations Office, Books and Journals Division, American Chemical Society, 1155 Sixteenth St., N.W., Washington, D. C. 20036. Remit check or money order for $3.00 for photocopy or $2.00 for microfiche, referring to code number JPC-73-1258.
(7) R. L. Kay, *J. Amer. Chem. Soc.*, **82**, 2099 (1960).
(8) R. M. Fuoss and F. Accascina, "Electrolytic Conductance," Interscience New York, N. Y., 1959.

TABLE III: Conductance Parameters for Hexamethylphosphotriamide Solutions

Salt	Λ_0	a	K_A	$\sigma\Lambda$
$NaClO_4$	21.14 ± 0.05	4.9 ± 0.3		0.03
$KClO_4$	21.35 ± 0.05	4.6 ± 0.2		0.02
$LiNO_3$	24.95 ± 0.05	4.9 ± 0.1		0.01
$NaNO_3$	24.06 ± 0.05	4.1 ± 0.1		0.02
KNO_3	24.33 ± 0.06	2.4 ± 0.6	59 ± 8	0.05
NaSCN	25.99 ± 0.04	4.6 ± 0.1		0.05
KSCN	26.17 ± 0.05	4.3 ± 0.1		0.02
NaBr	23.88 ± 0.05	4.5 ± 0.1		0.02
KPi	17.36 ± 0.05	5.2 ± 0.2		0.02
n-Pr_4NBr	25.10 ± 0.05	3.2 ± 0.8	71 ± 8	0.05

In the above two equations, $E = E_1\Lambda_0 - E_2$, $S = \alpha\Lambda_0 + \beta$; $J = \sigma_1\Lambda_0 + \sigma_2$, γ is the degree of disassociation, f is the mean activity coefficient of the electrolyte, and K_A is the association constant.

In HMPT at 25°, E_1, E_2, α, and β have constant values of 9.815, 38.244, 0.9875, and 26.275, respectively, while σ_1 and σ_2 depend on the chosen value of the minimum approach distance. The following physicochemical constants of pure solvent were taken: d = 1.019 g/cm^3;[9] ϵ_0 = 29.64;[2] and η = 0.0334 P.[10]

Table III gives the conductance parameters obtained from eq 1 and 2. The standard deviations in each parameter are also included together with the standard deviations of the individual points. A number of duplicate conductance determinations have been made and the parameters reported in Table III are their mean values.

Equation 2 gives the best fit in all cases but, apart from KNO_3 and n-Pr_4NBr, it also gives negative association constants; since this is without physical meaning the parameters reported in Table III were then calculated for all the salts, except for KNO_3 and n-Pr_4NBr, from eq 1. In the calculations with both eq 1 and 2 the term F was not taken into account.

A survey of the data reported in Table III shows constant differences of 0.21 ± 0.03 Λ unit for the Λ_0 of $KClO_4$-$NaClO_4$, KSCN-NaSCN, and KNO_3-$NaNO_3$ couples. This fact seems to prove the reliability of the Kohlrausch law of independent ion migration in HMPT.

The Λ_0 value of $KClO_4$ salt, obtained by averaging the Λ_0 values of two series, differs from the value reported in the literature by 0.17 Λ unit.[4] This small difference is possibly due to different purification methods of the solvent used (in ref 4 the purification of the solvent was not discussed).

Ion-Size Parameter. The minimum approach distances of ions a, as given by the above two equations deserve some considerations. At the present time it is not fully understood whether the minimum approach distance of ions is to be attributed to the true dimension of the ions in solution. Fuoss and Accascina[11] postulated that the ion-ion contacts occur between bare ions and not between their cospheres; this assumption was deduced by the results of KBr and KI in water where the a distances were found practically coincident with the sum of the crystallographic radii of the ions; the small difference between the a value and the sum of the radii of the bare ions relative to KCl salt (0.07 Å) was explained assuming a small association degree for this salt in water. $KClO_4$ in dimethyl sulfoxide is also a case for which a minimum approach distance very close to the sum of the radii of naked K^+ and ClO_4^- ions is reported in the literature.[5]

Apart from these few examples the results for a large number of systems, both in water and in nonaqueous solvents, seem however to indicate that the values of the a distances of the involved ions are either greater or smaller than the sum of the radii of the naked ions. This is also what happens in HMPT where the a distances of $LiNO_3$, $NaNO_3$, $NaClO_4$, and $KClO_4$ salts are greater than the sums of the radii of their bare ions while the a distances of KPi, KNO_3, and n-Pr_4NBr salts are unrealistically small.

In the conductance equation (1) the coefficient of the concentration c includes two factors: the term J from which the minimum approach distances a are derived and the $F\Lambda_0$ term which takes into account the viscosity change in the solution as the concentration increases. In some nonaqueous solvents the F term can be considered negligible,[12] especially when we are dealing with small ions, but it becomes important when ions of large hydrodynamic radius in viscous media are concerned. The results of a recent work regarding a couple of electrolytes in some nonaqueous solvents is significant in this respect.[5] In addition, the term including the association constant in eq 2 is linear with concentration and can hardly be separated from the $(J - F\Lambda_0)$ term as the association constant gets smaller. As a consequence of the above considerations, when viscosity data in dilute solutions are not available or in presence of very small association constants the minimum approach distances of ions given by eq 1 and 2 have little significance.

A different way of obtaining the solvated radius of the ions in HMPT solution has been attempted through the individual ionic mobilities. Transference numbers in this solvent are not available. In this instance the same contribution to the conductivity (equal to 6.1 Λ units in HMPT) for the cation and for the anion in tetra-n-butylammonium tetraphenylboride salt solution can be assumed to approximate limiting ionic equivalent conductances.[13] Starting from the λ_0 value of Na ion, reported in the literature,[4] the limiting equivalent conductance in HMPT of a series of ions has been calculated and the results are reported in Table IV, where the r_s values obtained from the Stokes law

$$r_\epsilon = \frac{0.82|z|}{\lambda_0\eta} \qquad (3)$$

are also reported.

Following a suggestion due to Robinson and Stokes,[14] the radii of the cations in solution have been corrected and the results obtained (r_{cor}) are reported in the same Table IV. In the Robinson and Stokes method the tetraalkylammonium ions are assumed unsolvated because of their low charge density and the crystallographic radii of these ions are taken to be the correct hydrodynamic values r_{cor}. It follows that a plot of r_{cor}/r_s (the correction factor) against the Stokes law radius can be constructed; hence the correct radii of other cations with r_s values known from conductivity data and lying in the range covered by the plot are deduced.

Figure 1 shows instead the plot of the $\lambda_0\eta$ values against the reciprocal crystallographic radii of the ions. The cor-

(9) J. E. Dubois and A. Bienvenue, *Tetrahedron Lett.*, 1809 (1966).
(10) J. E. Dubois and H. Viellard, *J. Chim. Phys.*, **62**, 699 (1965).
(11) See ref 8, pp 203–205.
(12) D. F. Evans, C. Zawoyski, and R. L. Kay, *J. Phys. Chem.*, **69**, 3878 (1965).
(13) R. M. Fuoss and E. Hirsch, *J. Amer. Chem. Soc.*, **82**, 1013 (1960).
(14) R. H. Robinson and R. H. Stokes, "Electrolyte Solutions," Butterworths, London, 1959.

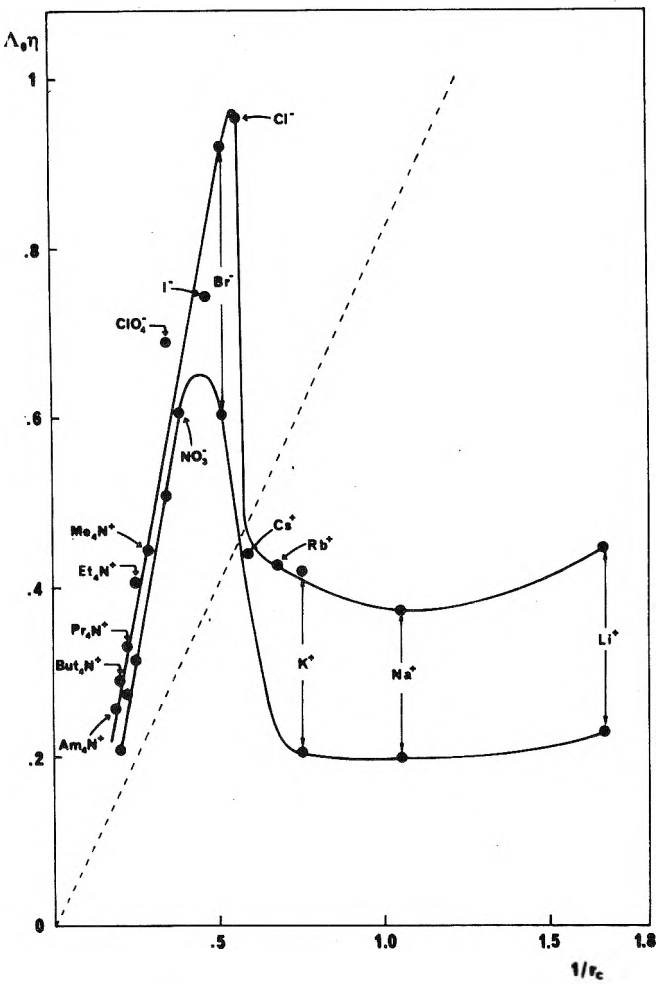

Figure 1. The Walden product for some ions as a function of reciprocal crystallographic radius in hexamethylphosphotriamide (lower curve) and sulfolane (upper curve). Theoretical Stokes law is shown by the dotted line.

TABLE IV: Equivalent Limiting Conductances, Stokes Radii, Solvated Radii, and Walden Products of Ions in Hexamethylphosphotriamide Solutions

Ion	λ_0	r_c[a]	r_s	r_{cor}	$\lambda_0\eta$
Li^+	6.8	0.60	3.61	4.8	0.227
Na^+	5.9	0.95	4.16	5.0	0.197
K^+	6.1	1.33	4.04	4.9	0.203
Et_4N^+	9.4	4.00	2.61	—	0.314
n-Pr_4N^+	7.1	4.52	3.50	—	0.234
n-Bu_4N^+	6.1	4.94	4.02	—	0.204
Br^-	18.0	1.95	1.36		0.601
ClO_4^-	15.2	2.92	1.61		0.508
SCN^-	20.1	—	1.22		0.671
NO_3^-	18.1	2.64	1.36		0.605
Pi^-	11.3	5.0[b]	2.18		0.377

[a] E. R. Nightingale, Jr., *J. Phys. Chem.*, **63**, 1381 (1959). [b] Reference 5.

rect radii of the solvated alkaline metal cations can be read on the abscissa within the range spanned by the $\lambda_0\eta$ values of the tetraalkylammonium ions. The $\lambda_0\eta$ values of Et_4N^+ and Bu_4N^+ are taken from the literature.[4] For comparison the Walden product for some other ions in sulfolane[15] are reported in Figure 1. One can see there that the curves in the two solvents show the same trend.

A suggestive improvement of the Stokes continuum theory which considers the retardation due to the relaxation of the solvent dipoles around a moving ion has been made by Zwanzig.[16] The proposed equation is

$$\lambda_0\eta = F^2/N(6\pi r + B/r^3) \quad (4)$$

where B is a function of the dielectric relaxation time of the solvent, τ and of the dielectric constant of the solvent at low and infinite frequency, ϵ_0 and ϵ, respectively.

The Zwanzig theoretical curve has not been reported in Figure 1 because of the lack of the τ and the ϵ terms. Nevertheless in solvents where eq 4 has been tested there is no agreement between theoretical predictions and the experimental data since the r values required by eq 4 are unrealistically small.

A comparison between the correct radius of Na^+ and K^+ ions in this solvent, and in a series of protic and aprotic nonaqueous solvents,[15] shows that these ions have in HMPT the highest solvated radius. This fact can be attributed to both the very high value of the dipole moment and the large volume of the HMPT molecule. Ascribing a volume of 290 Å^3 to the HMPT molecule, a rough estimate of the average number of solvent molecules firmly bonded in the first hydration shell can be evaluated through the relationship

$$h = \frac{4/3\pi(r_{cor}^3 - r_c^3)}{290} \quad (5)$$

where r_c is the crystallographic radius of the involved ion. For sodium and potassium ions the hydration number thus calculated is approximately 2. Steric considerations are in agreement with the idea that the first hydration shell of monovalent cations in HMPT cannot be formed by more than two solvent molecules. However, under the strong field generated by cations with a high charge density, more than two HMPT molecules can be coordinated, a fact shown by some complexes of the transition metals in this solvent.[17]

It should also be noted that according to the charge density of the monovalant cation the interaction between the central ion and the solvent molecules can be high enough to break the solvent structure beyond the first hydration shell. Therefore, the higher mobility of lithium ion in HMPT when compared with that of sodium and potassium ions does not indicate that the solvated radius of the lithium ion is smaller than the one for sodium and potassium ions. In other words, the anomalous mobility of lithium ion in HMPT can be due to a loosening of the dipole-dipole interactions caused by lithium ion in the surrounding solvent. The effect of the structure-breaking of the solvent molecules lowers the medium viscosity and as a consequence the ions experience in solution a resistance to motion smaller than predicted from the Stokes law. If the above assumption is correct, one should expect that the structure-breaking effect will be enhanced in solvents with high viscosity. This is what happens in dimethylformamide, dimethyl sulfoxide, hexamethylphosphotriamide, and sulfolane (with viscosities of 0.00796, 0.01992, 0.0334, and 0.1029 P, respectively) where the Walden products of lithium ion increase when going from dimethylformamide to sulfolane.

The anion Stokes radii are outside the range covered by the tetraalkylammonium ions; thus it is not possible to

(15) M. Della Monica and L. Senatore, *J. Phys. Chem.*, **74**, 205 (1970).
(16) R. Zwanzig, *J. Chem. Phys.*, **38**, 1603 (1963).
(17) J. T. Donoghue and R. S. Drago, *Inorg. Chem.*, **1**, 866 (1962).

calculate their correct values *vic* Figure 1. Nevertheless, rough values can be estimated as follows: the Stokes law (dotted straight line in Figure 1) gives a linear dependence of the Walden products on the reciprocal effective radii of the ions in solution and the slope of the straight line should be 0.82 $|z|$. The Walden products of the anions and of the tetraalkylammonium ions are indeed on a straight line even if the slope of this line is different from the predicted one, 0.82 $|z|$. Thus, assuming the Stokes law to be correct in principle the anions should be considered unsolvated in HMPT as the tetraalkylammonium ions. This fact is not surprising when one considers that the positive charge of the HMPT dipole extends on the phosphorus atom and on the three nitrogen atoms, hence giving a rather small charge density; since the interactions between anions and the solvent molecules in aprotic media are essentially of the ion–dipole type the anions can be assumed to travel through the solution without any solvent molecule attached to them. Kinetic studies also support this point; in fact, the anion reactivity in reactions such as the alkylation with C_2H_5Br and C_4H_9Br of sodiomalonic acid derivatives in benzene is increased by the addition of a certain amount of HMPT.[2]

Ionic Association. Perchlorates and thiocyanates as well as NaBr and KPi are completely dissociated in HMPT. With regard to the nitrates of alkaline metals, while lithium and sodium salts are dissociated some association is found for KNO_3. *n*-Pr_4NBr salt also shows an appreciable amount of association in HMPT.

At the present time the pattern of ionic association in nonaqueous solvents is still a point to be cleared. In protic solvents where a systematic study has been made, the results show that the association constants depend on the characteristic of the solvent. Thus, while in ethanol the cation dependence of the association constants of lithium, sodium, potassium, cesium, tetramethylammonium, and tetrabutyl ammonium chlorides increase in going from lithium to cesium and then decrease in going from cesium to tetrabutylammonium ion,[18] in trifluoroethanol the same salts show association constants continuously decreasing as the cation size increases.[19]

The association in the aprotic solvents, as a rule, decreases as the ion-size of the electrolyte increases, but large differences in the amount of association are found when going from one solvent to another. In fact, while in acetonitrile,[12] acetone,[12] and nitromethane[20] the association constants of salts with a common ion are slightly decreasing, the association constants for lithium chloride, bromide, and iodide in sulfolane[21] and for lithium, sodium, and potassium picrate in nitrobenzene[21] drastically decrease as the ion size increases.

The behavior of alkaline metal nitrates in HMPT follows the same association pattern of the salts in acetonitrile and acetone; namely, association slowly increases in going from lithium and sodium nitrates to potassium nitrate. This behavior can be explained considering that lithium and sodium ions, because of their large charge density, are firmly bonded to the solvent molecules while potassium ion is less bonded to the dipole of the solvent. This fact is also in agreement with the above suggestion that lithium ion, in spite of its high mobility, is to be considered as a strongly solvated ion in HMPT.

When discussing corrections to solvated radii, ions like *n*-Pr_4N^+ and Br^- have been assumed as completely naked in HMPT. This assumption, if correct, accounts for the association of *n*-Pr_4NBr salt in this solvent. More information about the association in HMPT can also be drawn from a systematic study on other alkaline metal and tetraalkylammonium electrolytes like chlorides, bromides, iodides, and nitrates. We are currently engaged in this problem and will give the results in a further communication.

(18) D. F. Evans and P. Gardam, *J. Phys. Chem.*, **72**, 3281 (1968).
(19) D. F. Evans, J. A. Nadas, and M. A. Matesich, *J. Phys. Chem.*, **75**, 1708 (1971).
(20) R. L. Kay, S. C. Blum and H. I. Schiff, *J. Phys. Chem.*, **67**, 1223 (1963).
(21) R. Fernandez-Prini and J. E. Prue, *Trans. Faraday Soc.*, **62**, 1257 (1966).

Reduction of Mercuric Chloride to Mercurous Chloride Induced by the Oxidation of Oxalic Acid[1a]

M. Kimura,[1b] I. M. Kolthoff,* and E. J. Meehan

Department of Chemistry, University of Minnesota, Minneapolis, Minnesota 55455 *(Received December 5, 1972)*

The oxidation of oxalic acid by cerium(IV) or manganese(VII) in the presence of mercuric chloride induces the reduction of the latter to mercurous chloride (calomel). The amount of calomel formed is about the same in absence or presence of manganese(II). The results are accounted for by a sequence of free-radical reactions which is initiated by the reaction $C_2O_4^{2-}$ + Ce(IV) → CO_2 + $CO_2\cdot^-$ + Ce(III) leading to the overall induced reaction $2HgCl_2 + C_2O_4^{2-} \rightarrow Hg_2Cl_2 + 2Cl^- + 2CO_2$. The amount of calomel formed increases with increasing temperature and with decreasing rate of addition of the oxidant. The induced reaction was also studied with cobalt(III) oxalate, with iron(III) oxalate, in the dark and light, and with the Fenton reaction mixture (iron(II)-hydrogen peroxide). When chromium(VI) is the oxidant, no calomel is formed in its presence. Oxygen and chloride ions are powerful inhibitors; no calomel is formed in solutions saturated with oxygen, or in solutions more than 1 *M* in potassium chloride.

Introduction

The slow addition of a trace of a strong oxidizing agent (Ce(IV), Mn(VII), or Cr(VI)) to dilute oxalic acid in dilute sulfuric acid in the presence of Mn(II) causes the formation of free radicals which can bring about the reduction of oxygen to hydrogen peroxide.[2-4] This reduction corresponds to the induced (thermodynamically favorable, but normally very slow) reaction

$$O_2 + H_2C_2O_4 \rightarrow H_2O_2 + 2CO_2$$

and the amount of peroxide formed is much larger than the amount of oxidant added. The induced reduction of mercury(II) chloride to mercury(I) chloride (calomel) initiated by the above free radicals is the subject of the present paper. It is shown that (in the absence of oxygen) the slow addition of a trace of the strong oxidants to oxalic acid containing Mn(II) and sulfuric acid can bring about the induced reaction

$$2HgCl_2 + C_2O_4^{2-} \rightarrow Hg_2Cl_2 + 2CO_2 + 2Cl^-$$

As in the previously cited work,[2-4] it is found that the amount of mercury(II) chloride reduced is much larger than the amount of oxidant added. The light-initiated reduction of mercury(II) chloride by oxalate in neutral medium has long been known as Eder's reaction, and a mechanism accounting for the photochemical reaction was proposed first by Cartledge. In the present study the kinetics and mechanisms of the chain reactions involved in the induced reduction of mercury(II) chloride have been studied with various oxidizing agents as initiators, in the dark and light, and in the presence of oxygen and of chloride ions. Both of the latter are retarders of the induced reduction.

Experimental Section

All chemicals were reagent grade. In all cases manganese(II) was added as the sulfate. Experimental details and conditions and analytical methods were the same as described previously.[2-4] Unless stated otherwise, oxygen-free nitrogen was bubbled through the reaction mixtures. Experiments in light were carried out by exposing the reaction mixture to a tungsten lamp (110 V). The amount of calomel formed was determined by weighing after filtering through a glass-sintered crucible, washing, and drying at 80°. In order to compare conveniently the amount of calomel with the initial concentration of oxalic acid, the amount of calomel formed is expressed as molarity, which refers to the volume of the final reaction mixture.

Results

Cerium(IV) or Manganese(VII) as Oxidants. The effect of the amount of Ce(IV), expressed in equivalent percentage of the initial amount of oxalic acid, and added over a period of 2 or 4 hr, is presented in Table I. Unless stated otherwise the number of moles of calomel formed was almost equal to the number of moles of oxalic acid reacted minus twice the number of equivalents of oxidant added. Since the amount of calomel formed was much larger than corresponds to the amount of oxidant added, a chain reaction must occur which corresponds to the overall reaction

$$C_2O_4^{2-} + 2HgCl_2 \rightarrow 2CO_2 + Hg_2Cl_2 + 2Cl^- \quad (1)$$

(In this and subsequent equations, oxalate is written as $C_2O_4^{2-}$ rather than as $H_2C_2O_4$.) The relative efficiency of oxidant in initiating the reaction increases markedly with decreasing amount of oxidant added and also with increasing temperature. Table II illustrates this effect over the range 0–75° at varying rates of addition of oxidant. Variation of concentration of sulfuric acid from 0.1 to 0.5 *M* caused a small decrease in extent of reaction (from 2.3×10^{-3} to 1.7×10^{-3} *M* calomel formed, at 1 equiv % addition in 2 hr at 25°) and further increase to 1 *M* caused a small further decrease (1×10^{-3} *M*). The amount of calomel formed increased greatly with increasing concentration of oxalic acid. For example, the addition of 1 equiv % of cerium(IV) in 2 hr at 50° to 0.001, 0.005, or 0.01 *M* oxalic acid caused formation of 0.001, 0.0041, and 0.0082 *M*

(1) (a) This investigation was carried out under a grant from the National Science Foundation. (b) Present address: Department of Applied Chemistry, Yamagata University, Yonezawa-shi, Japan.
(2) I. M. Kolthoff, E. J. Meehan, and M. Kimura, *J. Phys. Chem.*, **75**, 3343 (1971).
(3) I. M. Kolthoff, E. J. Meehan, and M. Kimura, *Talanta*, **19**, 1179 (1972).
(4) I. M. Kolthoff, E. J. Meehan, and M. Kimura, *Talanta*, **20**, 81 (1973).

TABLE I: Reduction of Mercury(II) Chloride Induced by Addition of Cerium(IV)[a]

Ce(IV) added as equiv % of oxalic acid	Hg_2Cl_2 formed, $M \times 10^3$		
	Addition in 2 hr		Addition in 4 hr
	25°	75°[b]	25°
20	3.6		3.6
4.5	2.2		2.9
1.0[c]	1.7	9.3[d]	2.0
0.4		5.2	
0.1		2.5	
0		0.0	

[a] Reaction mixture 0.01 M in oxalic acid, 0.1 M in mercury(II) chloride, and 0.5 M in sulfuric acid; dark; N_2 saturated. [b] 0.1 M H_2SO_4. [c] Corresponds to 2×10^{-4} M Ce(IV). [d] Corresponds to 93% of oxalic acid used in reaction 1.

TABLE II: Effect of Temperature and Time of Addition of 1 Equiv % of Cerium(IV)[a]

Temp, °C	Hg_2Cl_2 formed, $M \times 10^3$, in addition time, hr				
	0.1	0.5	1	2	4
0				0.1	
25	0.4	1.0	1.5	2.3	3.4
50	3.1[b]		7.3	8.2	
75	6.0			9.3	

[a] Reaction mixture as Table I except 0.1 M sulfuric acid; same results in dark and light. [b] 3.2 was found 2 hr after the addition.

calomel, respectively. Increase of the concentration of mercury(II) also increases the extent of reaction 1. With conditions as in Table I, addition of 1 equiv % of cerium(IV) in 2 hr at 50° to solutions 0.01, 0.04, or 0.1 M in mercury(II) chloride caused 32, 52, and 83% of the oxalic acid to react according to reaction 1. Presence of Mn(II) up to 0.1 M in mixtures as in Table I increased the extent of reaction only to slight extent. Only a few experiments were carried out with manganese(VII) as oxidant. Using the same reaction mixture and conditions as in Table II and adding 1 equiv % of manganese(VII) in 2 hr at 50°, the amount of calomel corresponded to 78% of the initial concentration of oxalic acid as compared to 82% with cerium(IV).

Chromium(VI) as Oxidant. The essential difference from results described above is that no detectable reaction occurred in the absence of Mn(II). At 50° and upon adding 1 equiv % of Cr(VI) in 2 hr to a mixture 0.01 M in oxalic acid, 0.1 M in sulfuric acid, and 0.1 M in mercury(II) chloride, the concentrations of mercury(I) chloride formed were 0.001, 0.004, 0.005, and 0.005 M in the presence of 0.001, 0.01, 0.05, and 0.1 M Mn(II), respectively.

Cobalt(III) as Oxidant. This was used as the trioxalate complex, prepared as previously described.[2] A 0.01 M solution which was 0.1 M in sulfuric acid and 0.1 M in mercury(II) chloride, but with no added oxalic acid, was kept oxygen free for 2 hr at 50° after which time considerable amounts of Co(III) still remained. The amount of calomel formed was 0.0144 M, corresponding to 48% of the 0.03 M oxalate originally present in the complex. At 25° the decomposition of the complex is much slower than at 50°, but the induced reduction of mercury(II) chloride is still considerable. A mixture initially 1.2×10^{-3} M in the Co(III) complex, 0.04 M in oxalic acid, and 0.1 M in mercury(II) chloride and sulfuric acid after 3 hr (oxygen free) at 25° yielded 2.3×10^{-3} M calomel. 90% of the original Co(III) remained.

TABLE III: Manganese(II)–Hydrogen Peroxide as Oxidant[a]

[Mn(II)], M	Temp, °C	$M \times 10^3$					
		Hg_2Cl_2 formed		$H_2C_2O_4$ reacted		H_2O_2 reacted	
		dark	light	dark	light	dark	light
0.01	25	0	6		6		0.2
0.01	75		12				1.5[b]
0.1	25	1.5	8		9	0.1	0.3
0.1	75	20	26	19	27	1.1	1.6

[a] Reaction mixture 0.1 M in oxalic acid and sulfuric acid, 0.1 M in mercury(II) chloride, and 2.1×10^{-3} M in hydrogen peroxide; 3 hr in a closed vessel in a nitrogen atmosphere. [b] Added 1×10^{-4} M iron(III).

Manganese(II)–Hydrogen Peroxide Couple as Oxidant. No calomel was formed in the absence of Mn(II). In its presence calomel formation occurred (Table III); as was the case with Ce(IV), the amount formed was greater at 75° than at 25°, and increased with increasing concentration of Mn(II). At 75° the same results were found in dark and in light, but at 25° there was much more extensive light than dark reaction. Since oxygen is a pronounced inhibitor of the chain reaction (*vide infra*) it is evident that no oxygen can be formed in the decomposition of the peroxide.

Iron(III) as Oxidant in Light. Fenton Reaction. In a reaction mixture 0.1 M in oxalic acid, mercuric chloride, and sulfuric acid and 10^{-4} M in iron(III) sulfate no calomel was formed in the dark in 3 hr at 25 or 75°. However, when exposed to tungsten light the induced reaction occurred. At 25° the amount of calomel formed corresponded to 2.5×10^{-3} M, and to 3.3×10^{-3} M in the additional presence of 0.1 M manganese(II). It is well known that oxalatoferrate slowly decomposes in light with formation of iron(II). It was therefore expected that the calomel formation would be increased in the presence of hydrogen peroxide which not only oxidizes the iron(II), but also yields the OH· free radical. Indeed, when the above reaction mixture was made 2×10^{-3} M in hydrogen peroxide, a trace of calomel was formed in the dark after 3 hr at 25°, corresponding to 0.7×10^{-3} M, but to 14×10^{-3} M in light, the same amount being formed at 75° in light. In the latter experiments in light all hydrogen peroxide had disappeared after 3 hr, while practically none had reacted in the dark. Even as little as 10^{-5} M iron(III) in the presence of the peroxide greatly enhances induced reaction 1, the amount of calomel formed after 3 hr at 25° corresponding to 9×10^{-3} M. It is well known that the combination of hydrogen peroxide with a little iron(II) induces the oxidation of many reducing agents (so-called Fenton reaction) whereas no reaction occurs in the absence of iron(II). Experiments were carried out with the above reaction mixture which was made 2.1×10^{-3} in hydrogen peroxide and 1×10^{-4} M in iron(II) instead of iron(III). After 3 hr in the dark both at 25 and 75° the amounts of calomel formed corresponded to 6×10^{-3} M, while the amounts of peroxide which disappeared corresponded to $0.5_5 \times 10^{-3}$ M. In light the corresponding values at 25 and 75° were 13×10^{-3} (calomel) and 2.1×10^{-3} M (peroxide), respectively. Note that again at both temperatures all peroxide had reacted. Even with 10^{-5} M iron(II) in the initial reaction mixture 11×10^{-3} M calomel was formed in light after 3 hr at 25°, while the amount of peroxide de-

composed corresponded to only 0.5×10^{-3} *M*. In all these experiments the number of moles of oxalic acid disappeared was almost equal to the number of moles of calomel formed.

Effect of Retarders. Oxygen. As in the Eder reaction oxygen is a powerful retarder of the induced reduction of mercury(II) chloride by oxalic acid. For example, in a reaction mixture the same as in Table I, to which 1 equiv % of Ce(IV) was added in 4 hr and through which oxygen was passed, no calomel was formed either at 25 or 75°; the hydrogen peroxide concentration formed was 0.12×10^{-3} *M* after 4 hr. In the presence of 0.1 *M* Mn(II) and at 25° a trace of calomel (corresponding to 0.1×10^{-3} *M*) was formed, but peroxide concentration was 2.8×10^{-3} *M* (formed).

Chloride (in nitrogen atmosphere). In a reaction mixture as in Table I to which 1 equiv % of Ce(IV) was added in 2 hr the amounts of calomel formed at 25° corresponded to 2.3, 0.4_4, 0.1_5, 0.06, and 0×10^{-3} *M* and at 50° to 8.2, 4.2, 1.2, 0.8, and 0×10^{-3} *M* in the presence of 0, 0.05, 0.1, 0.2, and 1 *M* potassium chloride, respectively. In all experiments the number of moles of oxalic acid which disappeared in the reaction period was almost equal to the number of moles of calomel formed.

Discussion

As stated previously, the induced reduction of mercury(II) chloride by oxalic acid, eq 1, is a chain reaction. With Ce(IV) the initiating reaction is

$$C_2O_4^{2-} + \text{Ce(IV)} \rightarrow CO_2 + CO_2\cdot^- + \text{Ce(III)} \quad (2)$$

The sequence which follows is analogous to that proposed by Cartledge[5] for the Eder reaction

$$CO_2\cdot^- + HgCl_2 \rightarrow \text{Hg(I)} + 2Cl^- + CO_2 \quad (3)$$

$$\text{Hg(I)} + C_2O_4^{2-} \rightarrow Hg + CO_2 + CO_2\cdot^- \quad (4)$$

$$HgCl_2 + Hg \rightarrow Hg_2Cl_2 \quad (5)$$

The sequence of eq 3–5 corresponds to chain reaction 1. Termination presumably occurs mainly *via*

$$CO_2\cdot^- + \text{Ce(IV)} \rightarrow CO_2 + \text{Ce(III)} \quad (6)$$

with some termination *via*

$$\text{Hg(I)} + CO_2\cdot^- \rightarrow Hg + CO_2 \quad (7)$$

The assumption of steady-state concentrations for $CO_2\cdot^-$, Hg(I), and Hg, together with the assumptions that the rate constant of eq 2 is smaller than the rate constant of the subsequent reactions involving free radicals, and that the consumption of Ce(IV) occurs mainly in eq 2, leads to the result

$$[Hg_2Cl_2]_{formed} = \sqrt{\frac{k_b}{k_a + [HgCl_2][C_2O_4^{2-}]\tau/c_0}}[C_2O_4^{2-}][HgCl_2]\tau \quad (8)$$

where $k_a = k_6/2k_2k_3$, $k_b = k_3k_4/2k_7$, and c_0 indicates the total concentration of oxidant added over the time interval τ. When the initial concentrations of oxalic acid and mercury(II) chloride are much larger than the concentration of calomel formed, the former concentrations will remain almost constant during the reaction period. Under these circumstances eq 8 predicts a linear relation between $\{\tau/[Hg_2Cl_2]_{formed}\}^2$ and τ/c_0. This is found experimentally as shown in Figure 1. It is no longer true at large extents of reaction 1.

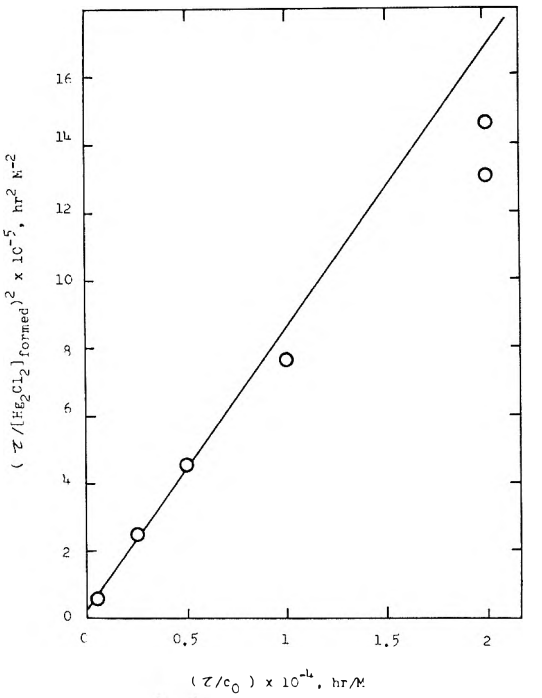

Figure 1. Plot of $\tau^2/[Hg_2Cl_2]^2_{formed}$ *vs.* τ/c_0 (*cf.* eq 8 and Table II): $c_0 = 2 \times 10^{-4}$ *M*, 25°.

It is interesting that Cr(VI) in 0.1–0.5 *M* sulfuric acid does not initiate the reaction unless Mn(II) is present. Presumably the chromium(VI) oxalate complex, written as Cr(VI)Ox, reacts as follows

$$\text{Cr(VI)Ox} \rightarrow \text{Cr(IV)} + 2CO_2 \quad (9)$$

$$\text{Cr(VI)} + \text{Cr(IV)} \rightarrow 2\text{Cr(V)} \quad (10)$$

$$\text{Cr(V)} + C_2O_4^{2-} \rightarrow \text{Cr(III)} + 2CO_2 \quad (11)$$

Since there is no formation of calomel, this must mean that Cr(VI) does not react with $C_2O_4^{2-}$ to yield Cr(V), CO_2, and $CO_2\cdot^-$, in analogy to initiating reaction 2 with Ce(IV). Alternatively, the absence of induced reaction might mean a very rapid reaction of $CO_2\cdot^-$ with Cr(VI). However, since induced reaction is observed in the presence of Mn(II), this possibility is ruled out.

The effect of Mn(II) can be accounted for by the reactions

$$\text{Cr(VI)Ox} + \text{Mn(II)} \rightarrow \text{Mn(III)Ox} + \text{Cr(V)} \quad (12)$$

$$\text{Mn(III)Ox} \rightarrow \text{Mn(II)} + CO_2 + CO_2\cdot^- \quad (13)$$

followed by reaction 11. The initiating reaction with the Co(III) complex is analogous to eq 13.

The reaction in light and dark between hydrogen peroxide and oxalic acid in the presence of Mn(II) and oxygen has been discussed previously.[3] In the presence of mercury(II) chloride and absence of oxygen, the reaction sequence appears to be (where Ox denotes oxalate in any form)

$$H_2O_2 + \text{Mn(II)} + \text{Ox} \rightarrow \text{Mn(III)Ox} + OH^- + OH\cdot \quad (14)$$

$$OH\cdot + \text{Mn(II)} + \text{Ox} \rightarrow \text{Mn(III)Ox} + OH^- \quad (15)$$

followed by eq 13. From the effects of light at 25 and 75° (Table III) it seems that dark reaction 13 is much faster at 75° than at 25°, whereas the rate of the analogous photoreaction is little affected by temperature. The effect of

(5) G. H. Cartledge, *J. Amer. Chem. Soc.*, **63**, 906 (1941).

iron(III) on the calomel formation in the light is accounted for by the photodecomposition of oxalatoferrates which has been studied in detail by Cooper and DeGraff[6]

$$Fe(III)Ox + h\nu \rightarrow Fe(II) + CO_2 + CO_2\cdot^- \quad (16)$$

the $CO_2\cdot^-$ free radical initiating the chain reaction. In the additional presence of hydrogen peroxide the iron(II) formed reacts as

$$Fe(II) + H_2O_2 + Ox \rightarrow Fe(III)Ox + OH^- + OH\cdot \text{ (measurable rate)}$$

the OH· reacting with $C_2O_4^{-2}$

$$OH\cdot + C_2O_4^{2-} \rightarrow OH^- + CO_2 + CO_2\cdot^- \text{ (fast)} \quad (17)$$

followed by reactions 3–5. Under our experimental conditions all hydrogen peroxide had disappeared at the end of the reaction period and the number of moles disappeared was considerably smaller than the number of moles of calomel formed, which is accounted for by reactions 16, 3, 4, and 5. From the experimental results it is clear that the rate of the photodecomposition of oxalatoferrate in the presence of peroxide determines to a great extent the amount of calomel formed. The reactions involving peroxide, iron(II) and (III), oxalate, and oxygen in the dark and light have been discussed in a previous paper.[4]

The retarding effect of oxygen is easily accounted for by the reaction

$$CO_2\cdot^- + O_2 \rightarrow O_2CO_2^- \quad (18)$$

The $O_2CO_2^-$ reacts further by a chain mechanism which yields hydrogen peroxide.[2] Apparently the reaction of $CO_2\cdot^-$ with O_2 is much faster than that with mercuric chloride (eq 3). Actually hydrogen peroxide formation in an oxygen atmosphere under conditions described previously[2,3] is not affected by the presence of mercuric chloride.

The retarding effect by the chloride ion is accounted for by several reactions. Mercuric chloride with chloride ion forms complexes $HgCl_3^-$ and $HgCl_4^{2-}$ which may react with $CO_2\cdot^-$ with a slower rate than $HgCl_2$ (eq 3). Also the rate of reaction 5 may be decreased by the complex formation. Furthermore chloride promotes the reaction

$$Hg_2Cl_{2(solid)} + Cl^- \rightarrow Hg(I) + HgCl_3^-$$

which has been studied by Sillen, *et al.*[7] The solubility of calomel is increased by chloride. In a reaction mixture such as in Table I, but which was 2 *M* in potassium chloride the solubility at 50° was 1×10^{-5} *M*. Probably the main cause of the retarding effect of chloride is that the stability of Hg(I) formed in reaction 3 greatly decreases

$$2Hg^+ \rightleftharpoons Hg_2^{2+}$$

since $[Hg_2^{2+}]$ becomes extremely small in the presence of excess chloride ion.[8]

(6) G. D. Cooper and B. A. DeGraff, *J. Phys. Chem.*, **75**, 2897 (1971).
(7) B. Lindgren, A. Jenssen, and L. G. Sillén, *Acta Chem. Scand.*, **1**, 479 (1947).
(8) I. M. Kolthoff and C. P. Barnum, *J. Amer. Chem. Soc.*, **62**, 3061 (1940).

Catalyzed Reaction between Oxalate Ion and Peroxodisulfate. I. Copper(II) as Catalyst

Masaru Kimura

Department of Applied Chemistry, Yamagata University, Yonezawa 992 Japan *(Received October 27, 1972)*

According to the composition of the reaction mixture, two separate mechanisms of the reaction are presented to account for the copper-catalyzed reaction between oxalate and peroxodisulfate. (1) In an excess of oxalate the catalyzed reaction kinetics are half order in catalyst, first order in peroxodisulfate, and zero order in the oxalate concentration. The reaction is completely inhibited by the presence of 1% acrylonitrile, and remarkably inhibited by the molecular oxygen. (2) In a low concentration of oxalic acid, in the relatively high concentrations of catalyst, and in 0.1 *M* sulfuric acid, the catalyzed reaction is almost zero order in the catalyst, first order in peroxodisulfate, and half order in the oxalic acid concentration. The reaction is not subject to the inhibition by the molecular oxygen but is completely inhibited by 1% acrylonitrile. Iron(III) and manganese(II) are considerably strong inhibitors of the reaction, and the former is much more effective inhibitor than the latter. The effects of the various factors on the copper-catalyzed reaction between oxalate and peroxodisulfate are reported. Mechanisms and kinetic treatments are presented to account for these facts.

Introduction

Recently, cobalt(II) catalysis on the reaction between oxalic acid and peroxodisulfate was investigated[1]. The cobalt-catalyzed reaction was not subject to inhibition by molecular oxygen, but was completely inhibited by 1% acrylonitrile or 1% allyl acetate. Ben-Zvi and Allen[2] have studied the copper-catalyzed reaction of oxalate with peroxodisulfate and found that molecular oxygen is a strong inhibitor of the catalyzed reaction. However, only one de-

(1) M. Kimura, *J. Phys. Chem.*, submitted for publication.
(2) (a) T. L. Allen, *J. Amer. Chem. Soc.*, **73**, 3589 (1951); (b) E. Ben-Zvi and T. L. Allen, *ibid.*, **83**, 4352 (1961).

termination in the oxygen-saturated and in the nitrogen-saturated solution has been compared. No quantitative investigation of the oxygen inhibiting effect has been made. The effect of oxygen on the free radical reactions is quite general and is an important aspect. An intensive investigation of the kinetics of the reaction between oxalate and peroxodisulfate is made in the present paper.

Experimental Section

Chemicals. Reagent grade potassium peroxodisulfate of Kanto Kagaku Co., Inc. was recrystallized twice from the redistilled water and dried at 40° in a vacuum desiccator. The redistilled water was prepared from the anion-cation exchange resin water first by successive distillation from the dilute alkaline permanganate solution and finally without adding any reagent in a glass still. The redistilled water was used for all the experiments and also to wash the glassware. The reaction vessel was always filled with the redistilled water for at least one day before use. All other chemicals used were of the guaranteed reagents and were used without further purification.

Technique. The reaction vessel was placed in a thermostat and oxygen and/or nitrogen gas was bubbled through the contents (90 ml) before the reaction was started. A reaction was started by adding peroxodisulfate (10 ml) which was also in a thermostat and had oxygen and/or nitrogen gas bubbled through it. The concentration of the dissolved oxygen gas was continually checked and controlled to fairly good constancy by bubbling nitrogen and/or oxygen gas. The whole vessel was covered with black adhesive plastic tape to ensure darkness. The aliquot samples were withdrawn at appropriate times and mixed with a cold solution of 0.5% acrylonitrile to stop the reaction. Then the concentration of peroxodisulfate was measured. A total time of about 5 min was needed from the withdrawal of the solution until completion of the analysis of peroxodisulfate.

Analysis. The concentration of peroxodisulfate was determined by using polarograms at 0.2 V *vs.* sce at 25° in a solution of 0.5% acrylonitrile, 0.01% polyacrylamide, and 0.05 *M* sulfuric acid. Polyacrylamide was used as a maximum suppressor. Concentration of oxygen in the reaction mixture was determined by using a Dissolved Oxygen Meter, Model DO-IA of Toa Electronics Co., Ltd.

Results. Experiments in Excess of Oxalate

Decomposition of Peroxodisulfate without Catalyst or Oxalate. In the same conditions as in the experiments of the copper-catalyzed reaction, the rate of the decomposition of peroxodisulfate was checked. In the initial solution of 0.004 *M* potassium peroxodisulfate and 0.1 *M* potassium oxalate, the decomposition of peroxodisulfate was only 2% in 10 hr at 40° in the dark, in either oxygen or nitrogen saturated solution. In the same condition as in the above except 0.004 *M* cupric sulfate instead of 0.1 *M* potassium oxalate, the decomposition was also 2% in 10 hr. The 2% was practically equal to the decomposition of peroxodisulfate without any other chemical reagents. Kolthoff and Miller[3] have determined the rate constants of the decomposition of peroxodisulfate. The calculated value from their data is $k_1 = 1.2 \times 10^{-5}$ min^{-1} at 40°, and the decomposition of about 1% in 10 hr is calculated.

Catalyzed Reaction by Copper(II). The reaction between oxalate ion and peroxodisulfate is greatly enhanced by the presence of copper(II). A few examples are shown in Figure 1. As can be seen in Figure 1, the catalyzed

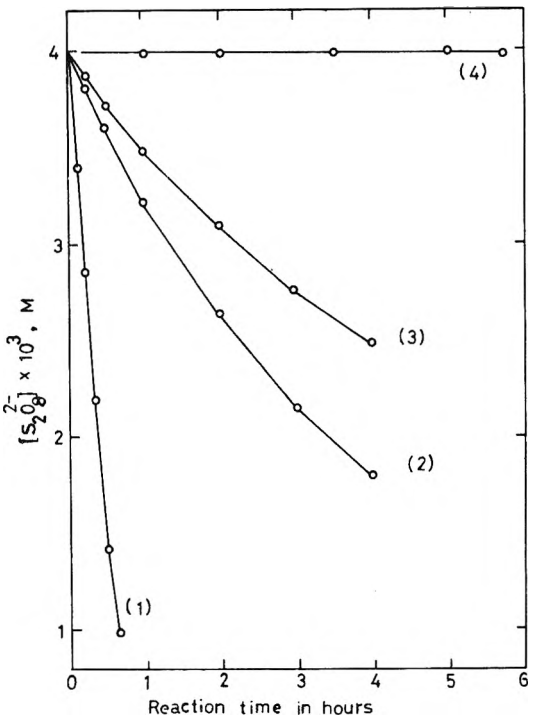

Figure 1. Examples of kinetics run at 40°. Initial solution: 4 × 10^{-3} *M* in potassium peroxodisulfate; 0.1 *M* in potassium oxalate; 4 × 10^{-4} *M* in cupric sulfate; pH 6.5; dark; (1), N_2 saturated; (2), air saturated; (3), O_2 saturated; (4). as in (1) but in 1% acrylonitrile.

reaction is completely inhibited by 1% acrylonitrile, and the about 1% decomposition in 6 hr is actually equal to the uncatalyzed decomposition of peroxodisulfate. The reaction is considerably inhibited by the molecular oxygen; however, even in the oxygen saturated solution the reaction proceeds to a large extent.

Dependence of Peroxodisulfate. During an experiment the logarithm of the persulfate concentration decreased linearly with time. This indicates that the kinetics of the reaction are first order in persulfate and are described by the equation

$$-d[S_2O_8^{2-}]/dt = k_{app}[S_2O_8^{2-}]$$

where k_{app} indicates an apparent rate constant to be a function of the copper concentration and the oxygen concentration. The above rate law was fulfilled in both the presence and absence of oxygen.

Dependence of Copper(II). To determine the order of reaction with respect to catalyst, total concentration of copper(II) was varied from 1 × 10^{-6} to 4 × 10^{-3} *M*. The values of k_{app} were plotted against the square root of the copper concentrations. As can be seen in Figure 2 the plot is on a straight line and the intercept is practically zero. This indicates that the reaction rate is proportional to the square root of the catalyst concentrations. [Cu(II)] in Figure 2 indicates the total concentration of various forms of copper(II) with oxalate. In excess of oxalate they would be mostly the dioxalatocuprate(II) complex.

Dependence of the Oxygen Concentration. The catalyzed reaction rate was determined in a reaction mixture

(3) I. M. Kolthoff and I. K. Miller, *J. Amer. Chem. Soc.*, **73**, 3055 (1951); the kinetics are described by the equation $-d[S_2O_8^{2-}]/dt = k_1[S_2O_8^{2-}] + k_2[H^+][S_2O_8^{2-}]$. The values of k_1 and k_2, respectively, are 6.0 × 10^{-5} min^{-1} and 3.5 × 10^{-3} M^{-1} min^{-1} at 50° at an ionic strength of 0.4. The activation energy for the k_1 path is 33.5 kcal and for the k_2 path 26.0 kcal.

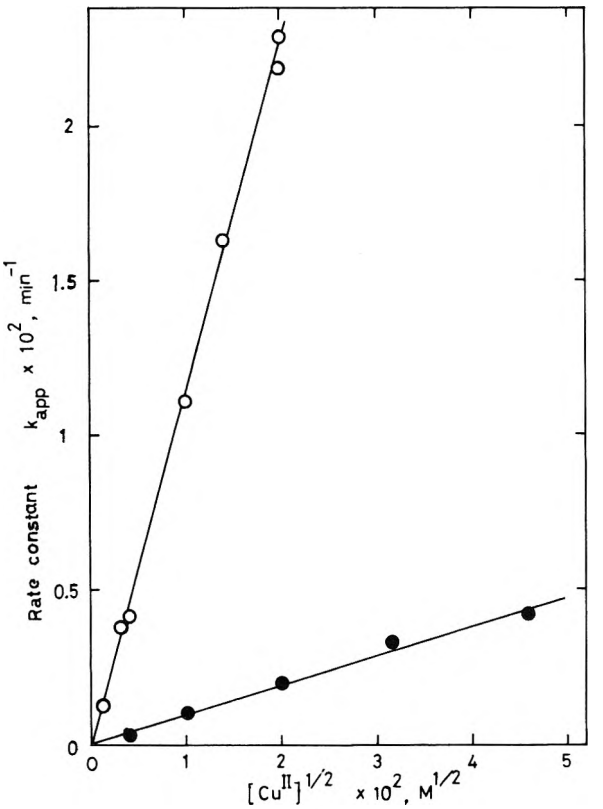

Figure 2. Plot of k_{app} *vs.* $[Cu^{II}]^{1/2}$. Conditions as in Figure 1, except varied concentrations of copper(II): ●, O_2 saturated; ○, N_2 saturated.

TABLE I: Effect of Oxygen on the Reaction Rate[a]

Concn of oxygen, *M*	Rate constant, $k_{app} \times 10^3$, min^{-1} Obsd	Calcd
0 (N_2 sat.)	23.0, 23.7	22.2
3×10^{-6}	13.3	14.8
6×10^{-6}	12.3	11.9
9×10^{-6}	8.8	10.3
1.9×10^{-5}	6.8	7.6
3.7×10^{-5}	5.8	5.8
5.3×10^{-5}	5.3	5.0
6.2×10^{-5}	5.0	4.7
9.3×10^{-5}	5.0	4.0
1.0×10^{-4}	4.3	3.9
1.2×10^{-4}	4.0	3.7
2.8×10^{-4}	3.3	2.9
9.6×10^{-4} (O_2 sat.)	2.0	2.3

[a] Solution 0.004 *M* in potassium peroxodisulfate, 0.1 *M* in potassium oxalate, and 4×10^{-4} *M* in cupric sulfate; 40°; dark.

of the varied concentrations of the dissolved oxygen. The values of k_{app} obtained are listed in Table I together with the calculated values which are discussed later.

Under conditions similar to those in Table I, Ben-Zvi and Allen[2b] have reported k_{app} to be 22.4×10^{-3} min^{-1} in the nitrogen- and 3.9×10^{-3} min^{-1} in the oxygen-saturated solution at 40.5°. These values are in good agreement with the corresponding data in Table I. Ben-Zvi and Allen have taken special efforts to clean the reaction vessel and also have taken special precautions for surface effects.

Effect of the Oxalate Concentration. The effect of the oxalate concentration on the rate was checked over a wide range of concentrations. (See Table II.) The rate appears to be independent of the oxalate concentration in the range 0.05 to 0.1 *M*. However, the rate decreases markedly at concentrations lower than 0.05 *M*. It is interesting to note that the inhibiting effect of oxygen becomes extremely small when the oxalate concentrations are lower than 0.01 *M*.

TABLE II: Effect of Oxalate Concentration on the Catalyzed Reaction[a]

Concn of oxalate, *M*	$k_{app} \times 10^3$, min^{-1} N_2 sat.	O_2 sat.
0.001	4.0	3.5
0.002	6.3	5.0
0.01	11	8.3
0.05	23	3.3
0.1	23, 24	2.0

[a] Conditions as in Table I except for the varied concentrations of potassium oxalate.

TABLE III: Effect of Sulfuric Acid Concentration[a]

Concentration of sulfuric acid added, *M*	$k_{app} \times 10^3$, min^{-1} N_2 sat.	O_2 sat.
0 (pH 6.5)	23, 24	2
0.01 (pH 4.2)	21	
0.02 (pH 3.7)	22	1.3
0.05 (pH 2.2)	20	3
0.1	23	7
0.2	23	12

[a] Condition as in Table I except for the varied concentrations of sulfuric acid.

Effect of the Concentration of Sulfuric Acid. The effect of the sulfuric acid concentration was not large in the nitrogen saturated solution but it was rather large in the oxygen-saturated solutions. (See Table III.)

Experiments in Low Concentration of Oxalic Acid and Relatively High Concentration of Catalyst in 0.1 *M* Sulfuric Acid Solution

In this section the experiments are mostly carried out in the solutions of 0.002 or 0.02 *M* copper(II), 0.002 or 0.005 *M* oxalic acid, and 0.1 *M* sulfuric acid. The major reason for this composition is for purpose of solving the fact that the inhibiting effect of oxygen on the copper catalyzed reaction almost disappears at very low concentrations of oxalate.

Kinetics. The dependence of the peroxodisulfate concentration on the rate was essentially the same as in the preceding section. However, the plot of logarithms of the persulfate concentration with time deviates from a straight line after about $t_{1/2}$. This is why the reaction rate depends on the oxalic acid concentration. Accordingly, the rate constant (k_{app}) was determined from the rate of the initial stage of reaction.

Stoichiometry. To verify the stoichiometry of the reaction a kinetic run was followed up to the final stage of the reaction. Some examples are given in Figure 3. As can be seen in Figure 3, the molar concentration of oxalic acid reacted is equal to that of peroxodisulfate, so the overall reaction must be

$$S_2O_8^{2-} + C_2O_4^{2-} \longrightarrow 2SO_4^{2-} + 2CO_2$$

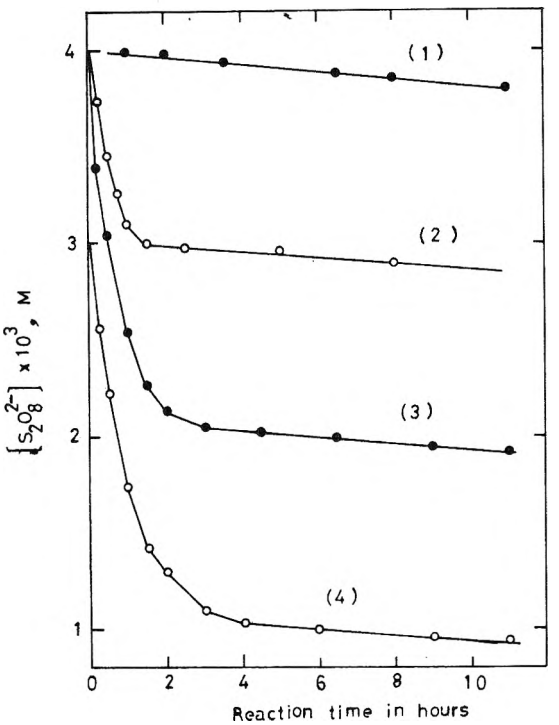

Figure 3. Examples of kinetics run in low concentrations of oxalic acid at 40°. Initial solution: (1), 4×10^{-3} *M* in potassium peroxodisulfate, 0.02 *M* in cupric sulfate, and 0.1 *M* in sulfuric acid; N_2 saturated, and in the dark; (2), conditions as in (1) except to contain 1×10^{-3} *M* in oxalic acid; (3), conditions as in (1) except to contain 2×10^{-3} *M* in oxalic acid; (4), conditions as in (3) except 3×10^{-3} *M* in peroxodisulfate instead of 4×10^{-3} *M*.

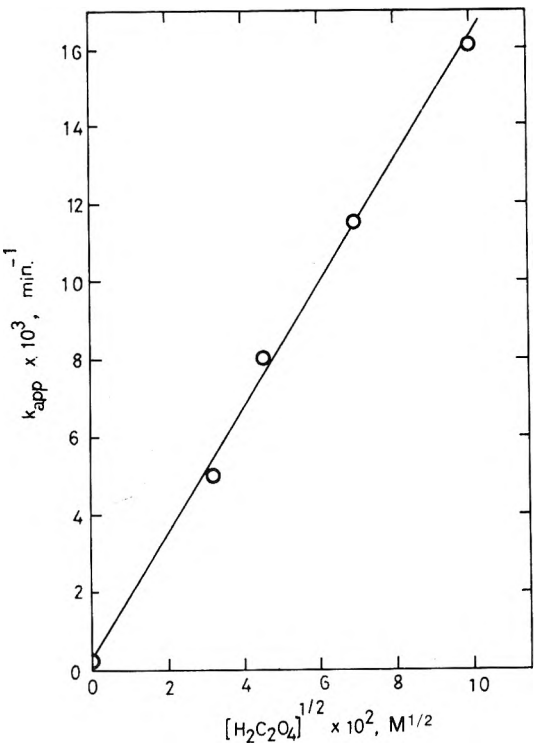

Figure 4. Plot of k_{app} *vs.* square root of oxalic acid concentration. Solution 0.004 *M* in potassium peroxodisulfate, 0.02 *M* in cupric sulfate, 0.1 *M* in sulfuric acid, and varied concentrations of oxalic acid; 40°; dark; nitrogen atmosphere.

Dependence of the Oxalic Acid Concentration. In order to know the reaction order with respect to the oxalic acid concentration, the reaction rate was measured at varied concentrations of oxalic acid from 1×10^{-3} to 1×10^{-2} *M*. The values obtained are plotted *vs.* the square root of the oxalic acid concentration in Figure 4. The plot of k_{app} *vs.* $[H_2C_2O_4]^{1/2}$ showed a straight line, and the intercept was not zero. The value of intercept corresponds to the rate constant of decomposition of peroxodisulfate.

Dependence of Copper(II). The dependence of the catalyst concentration was examined in the wide range of the copper(II) concentration, from 2×10^{-4} to 2×10^{-2} *M*. It appears that the reaction rate is essentially independent of the copper concentration (Table IV).

Effect of Oxygen. The catalyzed reaction rate was measured in the nitrogen-saturated and the oxygen-saturated solution. As can be seen in Table V, the rate was practically identical in both reaction atmospheres.

Effect of Other Substances. The effects of a few substances on the catalyzed reaction were checked and listed in Table V together with the oxygen effect. The reaction was completely inhibited by the presence of 0.5% acrylonitrile and considerably inhibited by iron(III) and manganese(II). The inhibiting effect of iron(III) was over 10 times that of manganese(II).

Copper-Catalyzed Reaction between Hydrogen Peroxide and Peroxodisulfate. In the same composition of solution except that hydrogen peroxide is placed instead of oxalic acid, the copper-catalyzed reaction was measured. The results are given in Table V together with those in the oxalic acid reaction scheme. As can be seen in the table, there is essentially no difference in the reaction rate between the hydrogen peroxide and the oxalic acid reaction scheme catalyzed by copper(II).

Discussion

In the excess amount of oxalate almost all of the copper(II) should be dioxalatocuprate(II) in the solution, calculated from the equilibrium constants.[4] However, the symbol $Cu^{II}Ox$ is used for all the forms of the oxalato complexes in this paper. Copper(III) also would form one or more complexes with oxalate, and the symbol $Cu^{III}Ox$ is used for all the forms of the oxalato complexes. The following reaction mechanism is postulated to account for the facts under the conditions of Table I or Figure 1.

$$S_2O_8^{2-} \longrightarrow 2SO_4^- \quad \text{[very slow]} \qquad (1)$$

$$Cu^{II}Ox + SO_4^- \longrightarrow Cu^{III}Ox + SO_4^{2-} \qquad (2)$$

$$Cu^{III}Ox \longrightarrow Cu^{II}Ox + CO_2 + CO_2^- \qquad (3)$$

$$CO_2^- + O_2 \rightleftharpoons O_2CO_2^- \quad \text{[rapid]} \qquad (4)$$

$$S_2O_8^{2-} + CO_2^- \longrightarrow SO_4^{2-} + SO_4^- + CO_2 \qquad (5)$$

$$S_2O_8^{2-} + O_2CO_2^- \longrightarrow SO_4^{2-} + SO_4^- + CO_2 + O_2 \qquad (6)$$

Reaction 1 is the initial reaction, and reactions 2 to 6 constitute a chain reaction. The most probable terminating reactions are

$$CO_2^- + SO_4^- \longrightarrow SO_4^{2-} + CO_2 \quad \text{[fast]} \qquad (7)$$

$$O_2CO_2^- + SO_4^- \longrightarrow SO_4^{2-} + CO_2 + O_2 \quad \text{[fast]} \qquad (8)$$

The radical which is formed in reaction 3 may be either

(4) "Stability Constants of Metal-Ion Complexes," compiled by L. G. Sillen and A. E. Martel, The Chemical Society, Burlington House, London, W. 1, 1964, p 361.

TABLE IV: Dependence of the Copper Concentration[a]

Concn of copper(II), M	$k_{app} \times 10^3$, min^{-1}
2×10^{-4}	4.8
5×10^{-4}	5.0
1×10^{-3}	5.3
2×10^{-3}	5.3
5×10^{-3}	5.5
1×10^{-2}	6.7
2×10^{-2}	8.0

[a] Solution 0.004 M in potassium peroxodisulfate, 2×10^{-3} M in oxalic acid, 0.1 M in sulfuric acid, and the varied concentrations of cupric sulfate; 40°; nitrogen atmosphere; dark.

TABLE V: Effect of Oxygen and Other Substances[a]

Substances added	$k_{app} \times 10^3$, min^{-1}	
	N_2 sat.	O_2 sat.
None[b]	12.7[b]	14.0[b]
None	10.8	11.0
2×10^{-4} M Fe(III)	6.7	
2×10^{-3} M Fe(III)	1.7	
5×10^{-3} M Mn(II)	4.2	
2×10^{-2} M Mn(II)	3.1	
0.5 % acrylonitrile	*ca.* 0.2	*ca.* 0.2
0.5 % acrylonitrile[b]	*ca.* 0.2[b]	*ca.* 0.2[b]

[a] Solution 0.004 M in potassium peroxodisulfate, 0.005 M in oxalic acid, 0.002 M in cupric sulfate, 0.1 M in sulfuric acid, and substances added; 40°; dark. [b] Condition as in *a*, except 0.005 M H_2O_2 instead of $H_2C_2O_4$.

CO_2^- or $C_2O_4^-$; however, the two forms do not appear to be distinguishable on the basis of kinetic or spectroscopic evidence.[5] Following the consensus of the previous workers, CO_2^- is written in the present paper. The assumption of steady states for SO_4^-, CO_2^-, $O_2CO_2^-$, and $Cu^{III}Ox$ leads to

$$[CO_2^-]^2 + \frac{k_1}{k_5 + k_6K[O_2]}[CO_2^-] = \frac{k_1k_2[Cu^{II}Ox]}{(k_5 + k_6K[O_2])(k_7 + k_8K[O_2])} \quad (I)$$

where k_n indicates the rate constant of reaction (n), and K is the equilibrium constant of reaction 4. If the chains are long, the second term on the left can be neglected. This leads to

$$-d[S_2O_8^{2-}]/dt = \left(k_1 + \sqrt{\frac{(k_5 + k_6K[O_2])k_1k_2[Cu^{II}Ox]}{k_7 + k_8K[O_2]}}\right)[S_2O_8^{2-}] \quad (II)$$

It is obvious from Figure 2 that the term of $k_1[S_2O_8^{2-}]$ is very small to be negligible, and that the chain must be long. Consequently, eq III is derived.

$$-d[S_2O_8^{2-}]/dt = \sqrt{\frac{(1 + a[O_2])[Cu^{II}Ox]}{b + c[O_2]}}\,[S_2O_8^{2-}] = k_{app}[S_2O_8^{2-}] \quad (III)$$

where, $a = k_6K/k_5$, $b = k_7/(k_1k_2k_5)$, $c = k_8K/(k_1k_2k_5)$. Plots of k_{app} *vs.* $[Cu(II)]^{1/2}$ should be on a straight line in which the slope corresponds to the values of $[(1 + a[O_2])/(b + c[O_2])]^{1/2}$. Using the data of Table I, eq III was treated to minimize the sum of squares of the per cent deviations between the observed and calculated values.[6] This leads to the following values and standard deviations for the parameters: $a = (3.53 \pm 1.18) \times 10^3$, $b = (8.13 \pm 1.39) \times 10^{-1}$, and $c = (3.32 \pm 0.42) \times 10^5$. These parameters yield the calculated values which are listed in Table I. The root means square deviation between observed and calculated values was 11%. If it may be assumed that the value of k_7 is almost equal to that of k_8, $K = 4 \times 10^5$ M^{-1} and $k_6/k_5 = 9 \times 10^{-3}$ are obtained. This may be the reason why oxygen retards greatly the reaction rate in which CO_2^- free radical is involved. In the above reaction mechanism, it is postulated that SO_4^- oxidizes $Cu^{II}Ox$ to $Cu^{III}Ox$ but does not oxidize $C_2O_4^{2-}$. The oxidation of Cu(II) and oxalate by SO_4^- is a competing reaction, and the former appears to be much faster than the latter. It is quite general that the complex formation leads to favorable conditions for the oxidation of metal ions. This may be presumably why the oxidation of Cu(II) to Cu(III) is favored over the reduction when the complex forming-oxalate exists in excess.

At a low concentration of oxalate the reaction rate becomes considerably slow, and the inhibiting effect by oxygen becomes extremely small. This may indicate that the oxidation of copper to trivalent state becomes difficult, and that on the contrary the reduction to the univalent by CO_2^- or $O_2CO_2^-$ occurs. There are several evidences that copper(II) is reduced by CO_2^- and $O_2CO_2^-$ radicals. For example, in an investigation of the oxidation of formic acid by X-rays in aqueous solutions including copper(II), the reaction A_1 has been shown[7].

$$Cu^{2+} + CO_2^- \longrightarrow Cu^+ + CO_2 \quad (A_1)$$

Kolthoff, *et al.*,[8] have recently studied on the effect of copper on the formation of hydrogen peroxide upon the oxidation of oxalic acid, and presumed the reactions A_2 and A_3.

$$Cu(II) + O_2CO_2^- \longrightarrow Cu(I) + CO_2 + O_2 \quad (A_2)$$

$$Cu(II) + HO_2 \longrightarrow Cu(I) + H^+ + O_2 \quad (A_3)$$

According to Andersen and Hart,[9] and many subsequent workers, HCO_2 (*i.e.*, the protonated CO_2^-) reacts with molecular oxygen

$$HCO_2 + O_2 \longrightarrow HO_2 + CO_2 \quad (4a)$$

In order to examine the existence of the reactions A_3 and 4a, hydrogen peroxide instead of oxalic acid was used in a copper-catalyzed reaction and compared with the reaction between oxalic acid and peroxodisulfate (see Table V). The reaction between hydrogen peroxide and peroxodisulfate was also enhanced by the presence of copper(II) ion, and the reaction rate was comparable with that of oxalic acid with peroxodisulfate. Therefore reactions A_3 and 4a would be expected. The copper-catalyzed reaction between hydrogen peroxide and peroxodisulfate may be accounted for by the following mechanism.

$$S_2O_8^{2-} \longrightarrow 2SO_4^- \quad (1)$$

$$S_2O_8^{2-} + H^+ \longrightarrow SO_4 + HSO_4^- \quad (1a)$$

(5) G. D. Cooper and B. A. deGraff, *J. Phys. Chem.*, **75**, 2897 (1971).
(6) The least-squares method is that described by R. H. Moore and R. K. Zeiger in Los Alamos Scientific Laboratory Report No. LA-2367 (1958) with addenda.
(7) J. H. Baxendale and D. Smithies, *Z. Phys. Chem.*, **7**, 242 (1956).
(8) I. M. Kolthoff, E. J. Meehan, and M. Kimura, *Talanta*, **20**, 81 (1973).
(9) A. R. Andersen and E. J. Hart, *Radiation Res.*, **14**, 689 (1961).

$$H_2O_2 + SO_4^- \longrightarrow HO_2 + SO_4^{2-} + H^+ \quad (9)$$

$$H_2O_2 + SO_4 \longrightarrow HO_2 + SO_4^- + H^+ \quad (9a)$$

$$Cu(II) + HO_2 \longrightarrow Cu(I) + O_2 + H^+ \quad (A_3)$$

$$S_2O_8^{2-} + Cu(I) \longrightarrow Cu(II) + SO_4^- + SO_4^{2-} \quad (10)$$

When the composition of reaction mixture was the low concentration of oxalic acid and the relatively high concentrations of copper, the catalyzed reaction did not appear to be inhibited by molecular oxygen, and the reaction rate was comparable with that between hydrogen peroxide and peroxodisulfate. These two facts would indicate that the reaction mechanism must be analogous to the mechanism of the reaction between hydrogen peroxide and peroxodisulfate. Consequently the following mechanism was presumed to account for the reaction under the conditions of low concentrations of oxalic acid, the relatively high concentrations of copper, and of an acidic medium.

$$S_2O_8^{2-} \longrightarrow 2SO_4^- \quad (1)$$

$$S_2O_8^{2-} + H^+ \longrightarrow SO_4 + HSO_4^- \quad (1a)$$

$$C_2O_4^{2-} + SO_4 \longrightarrow SO_4^- + CO_2^- + CO_2 \quad (11)$$

$$C_2O_4^{2-} + SO_4^- \longrightarrow SO_4^{2-} + CO_2^- + CO_2 \quad (12)$$

$$CO_2^- + O_2 \rightleftharpoons O_2CO_2^- \quad (4)$$

$$O_2CO_2^- + H^+ \longrightarrow HO_2 + CO_2$$
$$CO_2^- + O_2 + H^+ \longrightarrow HO_2 + CO_2 \quad (4a)$$

$$Cu(II) + CO_2^- \longrightarrow Cu(I) + CO_2 \quad (A_1)$$

$$Cu(II) + O_2CO_2^- \longrightarrow Cu(I) + CO_2 + O_2 \quad (A_2)$$

$$Cu(II) + HO_2 \longrightarrow Cu(I) + O_2 + H^+ \quad (A_3)$$

$$S_2O_8^{2-} + Cu(I) \longrightarrow Cu(II) + SO_4^- + SO_4^{2-} \quad (10)$$

The most probable termination reaction will be

$$Cu(I) + SO_4^- \longrightarrow Cu(II) + SO_4^{2-} \quad (13)$$

The assumption of steady states for SO_4, SO_4^-, CO_2^-, $O_2CO_2^-$, HO_2, and Cu(I) leads to

$$[Cu(I)]^2 + k_1[Cu(I)]/k_{10} = \frac{(k_1 + k_{1a}[H^+])k_{12}}{k_{10}k_{13}}[C_2O_4^{2-}] \quad (IV)$$

The second term on the left will be negligible because the chain is long, so the overall rate is described as

$$-d[S_2O_8^{2-}]/dt = \left(k_0 + \sqrt{\frac{k_0k_{10}k_{12}[C_2O_4^{2-}]}{k_{13}}}\right)[S_2O_8^{2-}] \quad (V)$$

where $k_0 = k_1 + k_{1a}[H^+]$.

Since the concentration of oxygen does not appear in eq V, the reaction rate should be independent of oxygen. Equation V is consistent with the experimental results. A plot of k_{app} *vs.* $[H_2C_2O_4]^{1/2}$ was a straight line as shown in Figure 4. The intercept should correspond with the rate of the uncatalyzed decomposition of peroxodisulfate. From the intercept, the value of $k_0 = 2 \times 10^{-4}$ min^{-1} was obtained. This is in good agreement with the value of 3.3×10^{-4} min^{-1} which is calculated using the literature data[3] for the conditions of $[H^+] = 0.2$ *M* and at 40°. As can be seen in Table V, iron(III) is a strong inhibitor. This may be accounted for by the following reactions.

$$CO_2^- + Fe^{3+} \longrightarrow CO_2 + Fe^{2+} \quad [fast] \quad (14)$$

$$SO_4^- + Fe^{2+} \longrightarrow SO_4^{2-} + Fe^{3+} \quad [fast] \quad (15)$$

Two radicals of CO_2^- and SO_4^- are removed from the reaction scheme by a chain reaction of eq 14 and 15. Therefore the catalyzed reaction would be greatly inhibited by even a small amount of iron(III). Baxendale and Smithies[7] have reported the reaction of (A_1) and (14). Generally with CO_2^- and the other organic radicals Baxendale and coworkers have pointed out that Cu^{2+} is more reactive than Fe^{3+}, and especially with CO_2^- in 0.1 *N* H_2SO_4, the rate constant for Cu^{2+} is about 6 times as large as that for Fe^{3+}. This is consistent with the fact that iron(III) is a strong inhibitor and that, however, it can inhibit incompletely even when the amount of iron(III) existed equally to that of copper(II). It is well known that Fe^{2+} reacts with peroxodisulfate.

$$S_2O_8^{2-} + 2Fe^{2+} \longrightarrow 2Fe^{3+} + 2SO_4^{2-} \quad (16)$$

However, reaction 16 will hardly occur under the situation because reaction 15 will be much faster than reaction 16.

The inhibiting effect of manganese(II) was much weaker than that of iron(III). In the case of manganese(II), the following reactions may be presumed.

$$Mn(II) + SO_4^- \longrightarrow Mn(III)Ox + SO_4^{2-} \quad (17)$$

$$Mn(III)Ox \longrightarrow Mn(II) + CO_2^- + CO_2 \quad (18)$$

$$Mn(III)Ox + CO_2^- \longrightarrow Mn(II)Ox + CO_2 \quad (19)$$

If reaction 18 were as fast as reaction 17 and only reactions 17 and 18 occurred, manganese(II) could not inhibit the catalyzed reactions. So reaction 18 must be relatively slow and reaction 19 would occur to some extent. Reactions 17 and 19 will be the cause of the inhibiting effect. In case of iron(III), the internal redox reaction of oxalatoferrate(III) as in reaction 18 does not occur in the dark but occurs in the light.[5] Hydrogen ion accelerated the copper-catalyzed reaction. This may be mainly due to the promotion of initiation reaction 1a by hydrogen ion. Protonations of CO_2^- and $O_2CO_2^-$ also probably have an effect on the radical reaction rate. Oxalatocuprate(II) will be $Cu(C_2O_4)_n^{(2-2n)}$ in which n should be changed by the hydrogen ion concentrations in solution, and the oxidation potential of copper will change accordingly. Thus a few effects of hydrogen ion on the reaction probably will occur simultaneously.

Acknowledgment. The author wishes to thank the Japanese Ministry of Education for the financial support granted for this research.

Solvent Effects on the Solvolysis of Covalent Sulfonylmethyl Perchlorates in Aqueous Media. The Effect of Water Structure on Proton Transfer Reactions

L. Menninga and Jan B. F. N. Engberts*

Department of Organic Chemistry, The University, Zernikelaan, Groningen, The Netherlands *(Received January 22, 1973)*

A detailed kinetic study has been made of the general base-catalyzed solvolysis of two arylsulfonylmethyl perchlorates in water and in water perturbed by the presence of organic cosolvents or salts. In the absence of added base, reaction rates may be interpreted as a measure of the dynamic basicity of the solvent since water or alcohols are the only active Brønsted bases under these conditions. The peculiar kinetic behavior in the mixed solvents may be explained as an immediate consequence of the increase in the dynamic basicity of water when the hydrogen-bond network in water ("water structure") is strengthened. In accordance with this interpretation, reaction rates (relative to those in pure water) are increased in the presence of "structure-making" salts (R_4NCl) while "structure-breaking" salts (NaCl, LiCl, NaBr, $NaClO_4$) reduce the reaction rates. A possible interpretation of the effect of water structure is given.

Introduction

The structure of liquid water[1] has intrigued chemists for a long time. During the last decade a number of theories have been advanced to account for the unique properties of this solvent.[2,3] Among these, Frank and Wen's "flickering cluster model" has been one of the most successful attempts to describe the cooperativity of hydrogen-bonding interactions in water.[4] More recently, however, new detailed molecular theories have been evolved, especially by Stillinger[5] and Scheraga[6] and their coworkers, which imply the absence of large clusters of anomalous density. These results revealed a clear tendency for the formation of tetrahedral hydrogen bonds between neighboring water molecules but often with a considerable degree of bending away from hydrogen bond linearity and ideal approach directions.

An even more controversial area is how far reaction rates in aqueous media respond to changes in the structuredness ("ice-likeness") of water. Although the effect of structure-making and structure-breaking additives on rates of enzymatic processes and on the conformation and physiological function of proteins may be of considerable importance,[7,8] pertinent studies on simpler organic systems are few and largely restricted to nucleophilic substitution reactions.[9-14]

In the present investigation we have employed the rates of slow proton transfer from a covalent arylsulfonylmethyl perchlorate (a carbon acid) to water as a probe to study effects of water structure on this type of proton transfer reactions. We believe that the rate variations, induced by additives which from other studies are known either to promote or to break water structure, can be largely accounted for by considering the dynamic basicity of water as a function of the degree of structuredness of the solution.[15]

Results

Solvolyses in Hydroxylic Solvents. Previous work has shown that the hydrolysis of alkyl- and arylsulfonylmethyl perchlorates (1) is subject to general base catalysis involving rate-determining deprotonation followed by rapid product determining steps.[16]

$$\underset{1}{RSO_2CH_2OClO_3} + B \xrightarrow[\text{slow}]{-BH^+} RSO_2\bar{C}HOClO_3 \xrightarrow[\text{fast}]{H_2O} RSO_2H + HCOOH + ClO_3^-$$

The easily measured rates of solvolysis of **1a** (R = *p*-$CH_3C_6H_4$) and **1b** (R = *p*-$NO_2C_6H_4$) in water and several alcohols (Table I) indicate that solvent molecules of sufficient basicity can function as the Brønsted base B. Since nearly equal rates of solvolysis are observed in the pure solvent and in the presence of dilute perchloric acid (Table I), the contribution of OH^- or RO^- to the rate of solvolysis is negligible in these systems. Therefore, the rates of solvolysis in the absence of added base provide a quantitative measure for the propensity of solvent molecules to induce irreversible deprotonation from the substrate. Consequently the reaction can be used as a kinetic probe for the dynamic basicity of solvent molecules in aqueous solutions and in mixed aqueous solvent systems.

Hydrolysis in Dioxane–Water Mixtures. In Figure 1 relative rates of solvolysis of **1a** (at 25°) are plotted *vs.* mole fraction (n) of hydroxylic solvent in mixtures of dioxane

(1) Throughout this paper, by "water structure" the diffusionally averaged structure ("D-structure") is meant, while "more structured" and "less structured" are defined relative to pure water at 25°.
(2) D. Eisenberg and W. Kauzmann, "The Structure and Properties of Water," Oxford University Press, London, 1969.
(3) H. J. C. Berendsen in "Theoretical and Experimental Biophysics," A. Cole, Ed., Marcel Dekker, New York, N. Y., 1967, p 1.
(4) H. S. Frank and W. Y. Wen, *Discuss. Faraday Soc.*, **24**, 133 (1957).
(5) (a) A. Rahman and F. H. Stillinger, *J. Chem. Phys.*, **55**, 3336 (1971); (b) *ibid.*, **57**, 128 (1972).
(6) A. T. Hogler, H. A. Scheraga, and G. Némethy, *J. Phys. Chem.*, **76**, 3229 (1972).
(7) R. Lumry and S. Rajender, *Biopolymers*, **9**, 1125 (1970).
(8) W. P. Jencks, "Catalysis in Chemistry and Enzymology," McGraw-Hill, New York, N. Y., 1969.
(9) E. M. Arnett, W. G. Bentrude, J. J. Burke, and P. M. Duggleby, *J. Amer. Chem. Soc.*, **87**, 1541 (1965).
(10) J. A. Fee and T. H. Fife, *J. Phys. Chem.*, **70**, 3268 (1966).
(11) R. E. Robertson, *Progr. Phys. Org. Chem.*, **5**, 213 (1967).
(12) R. E. Robertson and S. E. Sugamori, *Can. J. Chem.*, **50**, 1353 (1972).
(13) H. S. Golinkin and J. B. Hyne, *Can. J. Chem.*, **46**, 125 (1968).
(14) F. Hibbert and F. A. Long, *J. Amer. Chem. Soc.*, **94**, 7637 (1972).
(15) Preliminary communication: L. Menninga and J. B. F. N. Engberts, *Tetrahedron Lett.*, 617 (1972).
(16) A. Bruggink, B. Zwanenburg, and J. B. F. N. Engberts, *Tetrahedron*, **25**, 5655 (1969).

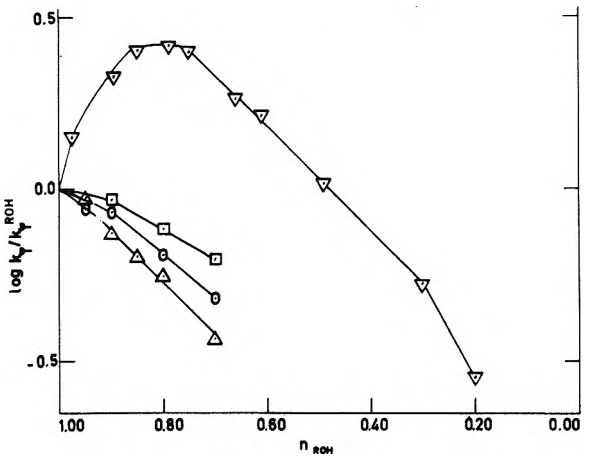

Figure 1. Relative rates of solvolysis *vs.* mole fraction of hydroxylic solvent: △, **1a** in dioxane–glycol; ⊙, **1a** in dioxane–EtOH; ⊡, **1b** in dioxane–EtOH; ▽, **1a** in dioxane–H_2O.

TABLE I: Pseudo-First-Order Rate Constants for the Solvolysis of 1a and 1b in H_2O, D_2O, and Alcohols (25°)

Compd	Medium	Dielectric constant	$k_\psi 10^5$, sec^{-1}
1a	H_2O	78.4	60.5
1a	H_2O (10^{-3} *M* HCl)		56.8
1a	D_2O	77.9	36.0
1a	EtOH	24.3	63.3
1a	EtOH (10^{-2} *M* HCl)		60.3
1a	*n*-BuOH	17.1	54.6
1a	*sec*-BuOH	15.8	54.6
1a	*i*-BuOH	17.7	46.2
1a	*t*-BuOH	9.9	56.7
1a	Glycol	37.7	59.4
1b	H_2O	78.4	325
1b	EtOH	24.3	578
1b	*t*-BuOH	9.9	676

with water, ethanol, and ethylene glycol and, in addition, of **1b** in dioxane–ethanol. As expected, the addition of dioxane, a solvent of low basicity[17] and dielectric constant (ϵ = 2.2 at 25°) causes a gradual decrease of the reaction rate in the dioxane–alcohol mixtures. In aqueous dioxane, this behavior is also observed at lower mole fractions of water. Unexpectedly, however, the initial addition of dioxane to water leads to an *increase* in rate and upon further addition the rate passes through a maximum at about n_{H_2O} = 0.79. The data in Table II show that the addition of dioxane to water causes large, mutually compensatory changes in ΔH^* and ΔS^*. A similar effect, although less pronounced, is observed when water is replaced by deuterium oxide as the solvent.

In dioxane–water at mole fractions of water between about 0.15 and 0.60 a fairly linear relationship between log k_ψ and the water concentration is observed with a slope of 1.9 ± 0.1. This suggests the participation of two strongly bound water molecules in the transition state for deprotonation. Since in a separate study[18] it was shown that the sulfonyl moiety is a much stronger hydrogen bond acceptor than the covalent perchlorate function while the methylene group is a hydrogen bonding donor site,[16] a possible pathway for deprotonation may be depicted as shown in Figure 2.

Solvolysis in Alcohol–Water Mixtures. Relative reaction rates (at 25°) for the solvolysis of **1a** and **1b** in several

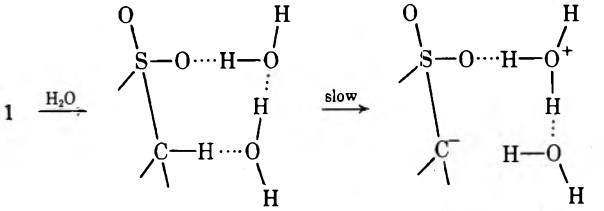

Figure 2. Possible mode of deprotonation from **1**.

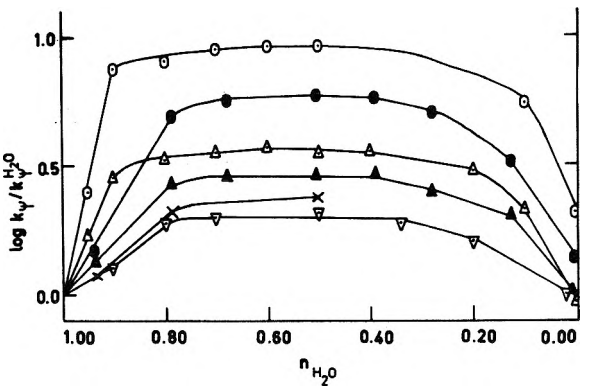

Figure 3. Relative rates of solvolysis *vs.* mole fraction of water: ▽, **1a** in glycol–H_2O; ×, **1a** in EtOH–H_2O at 39.80°; ▲, **1a** in EtOH–H_2O; △, **1a** in *t*-BuOH–H_2O, ●, **1b** in EtOH–H_2O; ⊙, **1b** in *t*-BuOH–H_2O.

TABLE II: Activation Parameters for the Solvolysis of 1a and 1b in Different Solvents

Substrate	Solvent	ΔH^*, kcal mol^{-1}	ΔS^*, eu
1a	H_2O	22.3 ± 0.4	−7 ± 1
1a	D_2O	19.4 ± 0.3	−17 ± 1
1a	Dioxane–H_2O (n_{H_2O} = 0.79)	13.5 ± 0.5	−32 ± 2
1a	EtOH–H_2O (n_{H_2O} = 0.94)	18.3 ± 0.3	−19 ± 1
1a	EtOH–H_2O (n_{H_2O} = 0.78)	16.2 ± 0.3	−24 ± 1
1a	EtOH–H_2O (n_{H_2O} = 0.50)	16.6 ± 0.4	−20 ± 1
1a	EtOH–H_2O (n_{H_2O} = 0.28)	15.5 ± 0.3	−25 ± 1
1a	EtOH–H_2O (n_{H_2O} = 0.13)	15.5 ± 0.3	−26 ± 1
1a	EtOH	16.9 ± 0.4	−22 ± 1
1a	*t*-BuOH–H_2O (n_{H_2O} = 0.90)	16.1 ± 0.4	−24 ± 2
1a	*t*-BuOH–H_2O (n_{H_2O} = 0.50)	14.0 ± 0.4	−29 ± 1
1a	*t*-BuOH–H_2O (n_{H_2O} = 0.10)	15.0 ± 0.5	−26 ± 2
1a	*t*-BuOH	15.1 ± 0.5	−27 ± 2
1b	H_2O	18.6 ± 0.4	−15 ± 2
1b	EtOH–H_2O (n_{H_2O} = 0.50)	13.8 ± 0.5	−25 ± 2
1b	EtOH	15.4 ± 0.4	−23 ± 1
1b	*t*-BuOH–H_2O (n_{H_2O} = 0.90)	15.0 ± 0.8	−23 ± 2
1b	*t*-BuOH–H_2O (n_{H_2O} = 0.50)	13.1 ± 0.7	−28 ± 2
1b	*t*-BuOH–H_2O (n_{H_2O} = 0.10)	14.5 ± 0.6	−23 ± 2
1b	*t*-BuOH	13.7 ± 0.5	−27 ± 2

alcohol–water mixtures of varying composition are shown in Figure 3. The rates in the pure alcohols (Table I) reveal that the dynamic basicity of these solvents is approximately equal to that of water.[19] Several recent studies[20,21]

(17) The perchlorates **1a** and **1b** are stable in pure dioxane at 25° for extended periods of time.
(18) J. Dallinga and J. B. F. N. Engberts, to be published.
(19) As judged from the second-order rate constants, $k_2 = k_\psi/c_{ROH}$, the dynamic basicity of the alcohols is slightly higher than that of water.
(20) E. M. Arnett, J. J. Burke, J. V. Carter, and C. F. Douty, *J. Amer. Chem. Soc.*, **94**, 7837 (1972).
(21) F. Franks and D. J. G. Ives, *Quart. Rev., Chem. Soc.*, **20**, 1 (1966).

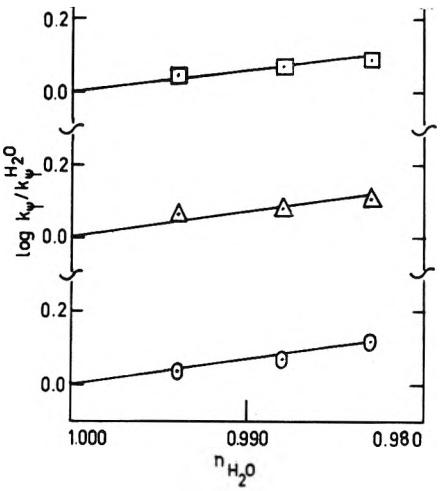

Figure 4. Relative rates of solvolysis of **1a** *vs.* mole fraction of water: ⊙, *n*-BuOH–H_2O; ◬, sec-BuOH–H_2O; ⊡, *i*-BuOH–H_2O.

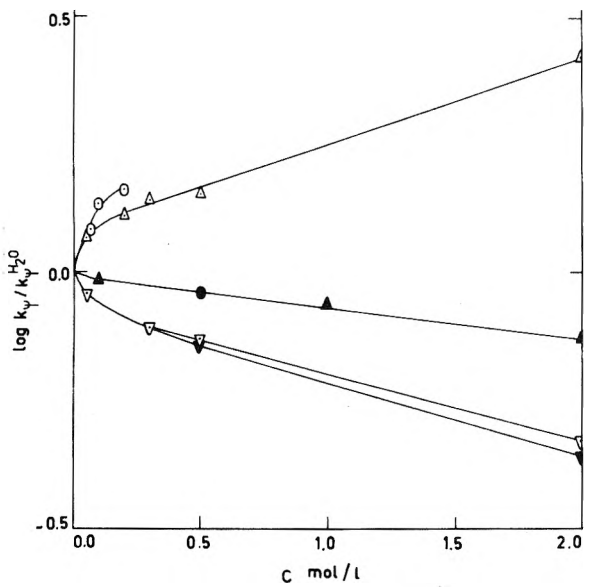

Figure 5. Relative rates of solvolysis of **1a** *vs.* salt concentration: ▼, NaBr; ▽, $NaClO_4$, ▲, NaCl; ●, LiCl; △, Me_4NCl; ⊙, $(n\text{-Bu})_4NCl$.

point to the same conclusion, but the relative dynamic basicities will certainly be dependent on the type of reaction under study since other factors than basicity (including the dielectric constant) will also determine the observed rates (see Discussion). As shown in Figure 3 the first addition of alcohol to water again causes significant rate accelerations. These effects are too large to be ascribed to the increase in basicity of the medium due to the presence of alcohol molecules of slightly enhanced basicity as compared with water (EtOH for **1a**, EtOH and *t*-BuOH for **1b**). In addition, the results given in Figure 3 permit the following conclusions: (i) rate maxima are reached at lower mole fractions of water in the series *t*-BuOH > EtOH > glycol; (ii) the log k/k_w values at the kinetic maxima decrease in the same series; (iii) the rate maximum for **1a** in EtOH–H_2O is decreased at 39.80°. The results given in Figure 3 show that the rate maxima are much broader than the one in dioxane–water as is understandable in view of the approximately equal dynamic basicities of both components of the solvent mixture.

In Figure 4 some relative rates are given for the solvolysis of **1a** in mixtures of water with three isomeric butanols. Again, rate enhancements are found upon addition of these alcohols to water despite their lower dynamic basicity as compared with water (Table I). Unfortunately, only a very limited range in n_{H_2O} could be studied due to the limited solubility of these butanols.

Hydrolysis in Aqueous Salt Solutions. Relative rates of hydrolysis of **1a** (at 25°) in the presence of neutral, inert salts are given in Figure 5. Two types of salt effects are observed. One group of salts, including LiCl, NaCl, NaBr, and $NaClO_4$, induces a decrease in the rates of hydrolysis. In contrast, rate enhancements are observed in the presence of tetraalkylammonium chlorides. Comparison with the rates found in the mixed aqueous solutions shows that the rate in 1 *M* $(CH_3)_4NCl$ is approximately equal to that in H_2O containing 2.8 *M* dioxane, 6.2 *M* EtOH, or 2.5 *M* *t*-BuOH.

Discussion

The significant rate enhancements observed upon the first addition of an organic solvent of low basicity (dioxane) or of comparable basicity (alcohols) to water illustrate the unique properties of water. No straightforward explanation of the rate variations in these media seems possible in terms of the effect of either the dynamic basicity of the additive or the solvent polarity as given by various empirical measures.[22] The kinetic data given thus far suggest that in highly aqueous mixed solvents, effects on the structure of water should be invoked to explain the kinetic behavior although these effects are difficult to separate from other influences. A number of studies, including measurements of excess heats of mixing, partial molal volumes, and ultrasound absorption and velocity, indicate that the first increments of a cosolvent containing apolar groups increase the structure of water until a maximum of structure is reached at a mole fraction of water characteristic for the additive.[21,23] Interpretations of this effect have mostly been given using the flickering cluster model of water.[4] From our results we conclude that in the media of high water content (*i.e.*, $n_{H_2O} > 0.6$) the dynamic basicity of the solvent is closely controlled by the degree of water structure. Further support for the theory that strengthening of the water association is accompanied by an increase in dynamic basicity is provided by the following observations: (i) the differences in kinetic effects and size of the rate maxima found upon addition of *t*-BuOH, EtOH, and glycol to water correspond to the differences in structure-making effects of these alcohols;[9,21,24] (ii) rate enhancements are observed in aqueous solutions containing salts that are known to promote water–water interactions (tetraalkylammonium chlorides), while the presence of structure-breaking salts (LiCl, NaCl, NaBr, $NaClO_4$) decreases the rates of deprotonation;[25] (iii) the size of the kinetic maximum is reduced at higher temperature (**1a** in EtOH–H_2O at 25.00 and 39.80°) because the structure-making effect is opposed by the increased thermal energy of the water molecules; (iv) no increase in rate is found upon addition of dioxane to ethanol (Figure 1). In ethanol no large three-dimensional hydrogen bond networks exist that are characteristic for water.[21]

Our interpretation is also supported by the independent study of Hibbert and Long[14] in which it was shown that

(22) E. M. Kosower, "An Introduction to Physical Organic Chemistry," Wiley, New York, N. Y., 968, p 293.
(23) B. Z. Gorbunov and Y. J. Naberukhim, *J. Mol. Structure*, **14**, 113 (1972).
(24) C. H. Spink and J. C. Wyckoff, *J. Phys. Chem.*, **76**, 1660 (1972).
(25) M. J. Blandamer, *Quart. Rev., Chem. Soc.*, **24**, 169 (1970).

the rates of detritiation of malononitriles in mixed aqueous solvents and in salt solutions correlate with effects on the structure of water.[26]

Now the question should be posed whether the kinetic maxima in the mixed aqueous solutions and the rate enhancement in the presence of structure-making salts are due to a destabilization of the substrate, a stabilization of the transition state, or both effects simultaneously. Arnett and his coworkers[9] have amply demonstrated that the partial molal heats of solution of several alkyl halides and sulfonates in mixtures of water with ethanol show endothermic maxima at mole fractions of water where the rates of solvolysis exhibit maxima. This indicates that the effect of water structure on rates of nucleophilic substitution reactions should at least partially be interpreted in terms of substrate stability. Unfortunately, the solubility and reactivity of the arylsulfonylmethyl perchlorates do not permit calorimetric studies in more highly aqueous solutions. However, it seems most likely that transition state effects will be chiefly responsible for the rate variations. Recent nmr studies[28] have provided evidence that increased water structure is accompanied by an enhanced hydrogen-bonding acceptor ability of water.[29] Although in the transition state for the deprotonation from the perchlorates the proton transfer is rather incomplete (Brønsted $\beta \approx 0.5$), stabilization by hydrogen bonding to the solvent will be strongly increased relative to the initial state and will be more efficient when more structured water is involved. This means that, if the process of deprotonation may be visualized as tentatively depicted in Figure 2, further hydrogen bonding of the two water molecules will be enhanced in the cybotactic region.[22] The importance of the proposed effects may be judged in terms of the activation parameters obtained for the various solvents (Table II). Addition of relatively small amounts of dioxane or alcohols to water causes large, mutually compensatory changes[30] in ΔH^* and ΔS^*. The decrease in ΔH^* and the more negative ΔS^* in the kinetic maxima may mainly be attributed to the participation of water molecules of enhanced structuredness (entropically unfavorable) and basicity (energetically favorable) in the transition state solvation. Analogous changes in ΔH^* and ΔS^* occur on changing the solvent from water to the more structured deuterium oxide. The salt effects may also be explained mainly in terms of transition state solvation. Substantial salting-in of the polar transition state by tetraalkylammonium ions is an expected process[14,31] and will find its origin in the presence of the large, cationic species containing the structure-making alkyl groups.[25] An opposite explanation may be given for the structure-breaking halide and perchlorate anions.

The reaction rates in the mixed solvents at lower mole fractions of water ($n_{H_2O} \leq 0.6$) will also be influenced by several factors but are perhaps more straightforward to interpret. After the kinetic maximum is reached when dioxane is gradually added to water, reaction rates are decreased because water is replaced by the much less basic dioxane and, in addition, water structure is now being destroyed. The effect of decreasing solvent polarity is difficult to estimate at the moment but is expected to slow down the rates since the transition state is more polar than the initial state.[32] The rates in the pure alcohols (Table I) suggest, however, that the influence of dielectric constant is not very large unless it is entirely compensated for by large differences in basicity of these alcohols. The rate-retarding effect of decreasing dielectric constant will certainly be more pronounced when proton transfer in the transition state is more complete. This is illustrated in the detritiation of malononitriles[14] where the large Brønsted coefficient (0.98 ± 0.2) points to an ion pairlike transition state. As a consequence, the rates of deprotonation are now appreciably lower in EtOH than in water.

In conclusion we note that, despite the obvious complexity of (mixed) aqueous solutions, our results appear to establish that water structure is one of the factors determining the dynamic basicity of these solvents. In addition, the variation of the dynamic basicity on changing solvent composition will be substrate dependent and subject to characteristic enthalpy–entropy compensation phenomena.

Experimental Section

Analytically pure **1a** and **1b** were synthesized as reported previously.[16] The recommended safety precautions were taken in handling these compounds. The water used in the kinetic measurements was demineralized and distilled twice in an all-quartz distillation unit. Deuterium oxide was obtained from Reactor Centrum Nederland (99.94% D_2O) and was used as such. The organic solvents and the salts were of the best grade available, usually from Merck. Dioxane (p.a.) was filtered through active, neutral alumina in a nitrogen atmosphere and stored under nitrogen at 0°. The alcohols were dried and distilled before use. Karl Fischer titrations were used to determine the water content (in vol %) of the organic solvents, which are given between parentheses: dioxane (0.019), EtOH (<0.2), *n*-BuOH (0.17), *sec*-BuOH (0.20), *i*-BuOH (0.24), *t*-BuOH (0.01), and ethylene glycol (0.65). $(n\text{-Bu})_4NCl$ was crystallized twice from chloroform and dried over P_2O_5 *in vacuo* for 24 hr.

Solvent mixtures were usually made up by weight. The pH of the aqueous salt solutions and of the highly aqueous mixed solvents was checked in all cases.

The kinetic technique (uv spectroscopy) has been described.[16] Pseudo-first-order kinetics were observed for at least three half-lives. Rate constants were reproducible to within 2%. After completion of all kinetic runs the uv spectrum of the reaction products was taken in order to ensure that no side reactions had occurred. The thermodynamic quantities of activation were calculated from rate constants at several temperatures usually between 25 and 45° (**1a**) or 16 and 30° (**1b**). Errors in ΔH^* and ΔS^* were calculated according to Schalenger and Long.[33]

(26) The author's previous view[27] that water structure is decreased by small amounts of EtOH, dioxane, or DMSO was corrected in the full paper.[14]
(27) F. Hibbert, E. A. Waters, and F. A. Long, *J. Amer. Chem. Soc.*, **93**, 2829 (1971).
(28) J. E. Gordon, *J. Amer. Chem. Soc.*, **94**, 650 (1972).
(29) *Ab initio* MO–SCF calculations on the linear water trimer (D. Hankins, J. W. Moskowitz, and F. H. Stillinger, *J. Chem. Phys.*, **53**, 4544 (1970)) revealed an increase in the net negative charge on each open acceptor site as compared to the water monomer.
(30) The enthalpy–entropy compensation phenomena have been the subject of a lengthy discussion (see ref 7).
(31) F. A. Long and W. F. McDevit, *Chem. Rev.*, **51**, 119 (1952).
(32) The solubility of the perchlorates **1** in apolar solvents suggests that the dipole moment of these compounds cannot be large.
(33) L. L. Schalenger and F. A. Long, *Advan. Phys. Org. Chem.*, **1**, 1 (1963).

Deuterium Isotope Effects in Complexation Kinetics. II. Lanthanide(III) Sulfate Systems[1]

Jeffry Reidler and Herbert B. Silber*

Department of Chemistry, University of Maryland Baltimore County, Baltimore, Maryland 21228 *(Received July 27, 1972)*

The complexation reaction between La(III), Nd(III), Gd(III), and Dy(III) with SO_4^{2-} was investigated in H_2O and D_2O at 25°. In all cases the complexation rate constant, k_{34}, and the dissociation rate constant, k_{43}, for each cation were different in the two solvents. The values of $10^{-8}k_{34}$ in H_2O and D_2O are La 0.84 and 0.24 sec^{-1}, Nd 1.9 and 0.80 sec^{-1}, Gd 8.2 and 6.9 sec^{-1}, and Dy 0.91 and 1.1 sec^{-1}; and $10^{-7}k_{43}$ equals La 3.8 and 7.0 sec^{-1}, Nd 4.8 and 7.1 sec^{-1}, Gd 3.8 and 0.74 sec^{-1}, and Dy 4.5 and 2.1 sec^{-1}. These data were compared to other lanthanide deuterium isotope studies to establish that the isotope effect is not a function of the solvated cation alone, but rather of the cation–ligand complex.

Introduction

Systematic kinetic studies of lanthanide complexation reactions have attempted to probe the nature of the solvated lanthanide ion in terms of the Eigen–Diebler multistep complexation reaction[2,3]

$$M^{m+}(aq) + L^{n-}(aq) \underset{k_{21}}{\overset{k_{12}}{\rightleftharpoons}} M^{m+}(H_2O)_xL^{n-} \underset{k_{43}}{\overset{k_{34}}{\rightleftharpoons}} ML^{m-n}(aq) \quad (1)$$

step 12 step III

Although for many cations the slow process is step III involving slow cation–solvent exchange, the analysis of neodymium(III) sulfate complexation in H_2O and D_2O indicated that the cation–ligand bond formation step was in fact the rate-determining step.[1] This study was undertaken for two reasons. First, to extend the results to other lanthanide(III) sulfate systems to determine if a turnover point exists in the lanthanide series where cation solvent exchange becomes rate determining. Second, to compare an additional ligand series of deuterium isotope effects with the previously determined ones using anthranilate ion and murexide as ligands[4] to discover if the deuterium effects for each cation are independent of the ligand.

Although the lanthanide(III)–sulfate systems have been independently investigated by Purdie and coworkers[5-7] and by Atkinson and Grecsek,[8] the calculated rate constants were significantly different. It was therefore necessary to repeat their measurements in H_2O to minimize errors in comparisons with the D_2O results. The lanthanides investigated include La, Gd, and Dy, as well as the previously determined Nd.

Experimental Section

The lanthanide sulfate solutions were made by the addition of sulfuric acid to the oxides (Research Inorganics), which were at least 99.9% pure. Standardized H_2SO_4 (Baker analyzed reagent grade) or D_2SO_4 (Diaprep, 99.5% isotopic purity) was added and heat was applied to form the aqueous solutions. The D_2O was at least 99.8% isotopically pure (Biorad and Diaprep). The residual H_2O in the D_2O lanthanide solutions was less than 0.5%, as determined by nmr analysis.

The ultrasonic absorption measurements were carried out at selected frequencies between 10 and 270 MHz, using standard techniques.[9] The apparatus consisted of Matec Models 666 pulse comparator, 120 master synchronizer, 600 RF pulse generator and receiver, and 960 RF source. X-Cut quartz crystals with fundamental frequencies of 4, 5, and 10 MHz were obtained from Valpey-Fisher. The experimental vibration frequencies were measured using a Gertsch FM3 frequency meter in conjunction with a Heath RF signal generator. A double-wall type interferometer cell was thermostated at 25° by a Forma circulating temperature bath. Sound velocities were not directly measured and were assumed to be that of the pure water value.

The pH values of the solutions were approximately 2 or above, because solutions of high acidity reacted with the stainless steel cell, and to prevent hydrolysis of the lanthanides. The pH was measured with a Corning Digital 112 pH meter in conjunction with a semimicro Corning combination electrode and standard buffers. All calculations were carried out on a Wang 700 programmable calculator.

Results

An excess ultrasonic absorption was measured over the whole frequency range for all four lanthanide systems. For chemical relaxation, the ultrasonic absorption, α/f^2, is given by

$$\alpha/f^2 = \sum_i \frac{A_i}{1 + (f/f_{R_i})^2} + B \quad (2)$$

where A_i = relaxation amplitude, f = frequency, f_{Ri} = relaxation frequency, and B = background. Although at high frequencies the absorption did not come down to the

(1) Part I: H. B. Silber, *Chem Commun.*, 731 (1971).
(2) H. Diebler and M. Eigen, *Z. Phys. Chem. (Frankfurt am Main)*, **20**, 200 (1959).
(3) M. Eigen and K. Tamm, *Z. Electrochem.*, **66**, 93, 107 (1969).
(4) H. B. Silber, R. D. Farina, and J. H. Swinehart, *Inorg. Chem.*, **8**, 819 (1969).
(5) N. Purdie and C. A. Vincent, *Trans. Faraday Soc.*, **63**, 2745 (1967).
(6) D. P. Fay, D. Litchinsky, and N. Purdie, *J. Phys. Chem.*, **73**, 544 (1969).
(7) D. P. Fay and N. Purdie, *J. Phys. Chem.*, **74**, 1160 (1970).
(8) J. J. Grecsek, Ph.D. Thesis, University of Maryland, College Park, 1970.
(9) H. B. Silber, N. Scheinin, G. Atkinson, and J. J. Grecsek, *J. Chem. Soc., Faraday Trans. 1*, **68** 1200 (1972).

TABLE I: Lanthanum Sulfate Data

10^2c, M	10^4d, M	pH/pD	$10^3\theta(c)$, M	$\phi(c)$	$10^{17}A_{III}$[a]	$f_{R_{III}}$, MHz	$10^{17}B$[a]
			A. H_2O (K_c = 4200, K_{12} = 1300)				
0.700	0.654	2.990	1.07	0.502	178 ± 5	13.4 ± 0.4	23.5 ± 0.4
1.40	1.31	2.746	1.16	0.522	315 ± 5	14.2 ± 0.2	23.7 ± 0.4
1.98	3.03	2.302	1.21	0.533	423 ± 10	14.3 ± 0.1	26.6 ± 0.3
2.97	4.55	2.165	1.32	0.554	543 ± 10	14.6 ± 0.3	28.0 ± 2.1
3.96	6.06	2.078	1.46	0.579	706 ± 10	14.9 ± 0.3	31.3 ± 3.0
4.95	7.58	2.007	1.63	0.606	833 ± 10	15.0 ± 0.3	36.7 ± 3.7
7.00	6.54	2.034	1.96	0.649	1214 ± 12	15.5 ± 0.3	45.2 ± 6.5
			B. D_2O				
1.02	1.69	3.29	1.05	0.586	283 ± 7	13.2 ± 0.3	31.4 ± 0.5
2.56	4.22	3.04	1.31	0.639	637 ± 6	14.1 ± 0.2	36.3 ± 1.1
3.20	5.27	2.96	1.47	0.665	865 ± 7	13.1 ± 0.5	41.7 ± 1.7
4.00	6.59	2.89	1.70	0.696	1025 ± 2	13.7 ± 0.1	40.4 ± 0.9
4.01	6.80	2.75	1.69	0.695	958 ± 13	14.3 ± 0.3	37.5 ± 2.6
5.02	1.93	2.62	1.99	0.729	1180 ± 17	14.1 ± 0.2	37.4 ± 1.5
5.01	8.50	2.65	2.01	0.730	1227 ± 13	13.6 ± 0.2	43.3 ± 1.7

[a] Units = nepers cm^{-1} sec^2.

TABLE II: Gadolinium Sulfate Data

10^2c, M	10^4d, M	pH/pD	$10^3\theta(c)$, M	$\phi(c)$	$10^{17}A_{III}$[a]	$f_{R_{III}}$, MHz	$10^{17}B$[a]
			A. H_2O (K_c = 4500, K_{12} = 200)				
0.361	3.88	3.456	0.977	0.164	55.3 ± 2.0	27.0 ± 1.5	21.9 ± 0.6
0.722	7.76	3.266	1.12	0.183	91.3 ± 0.9	30.1 ± 0.5	22.6 ± 0.3
1.08	11.6	3.123	1.18	0.191	129 ± 1	31.1 ± 0.6	23.9 ± 0.6
1.49	42.9	2.215	1.18	0.191	158 ± 2	32.0 ± 0.7	25.7 ± 0.7
1.19	69.0	2.407	1.24	0.200	131 ± 2	31.8 ± 0.7	24.7 ± 0.6
1.80	19.4	2.914	1.25	0.201	190 ± 2	33.8 ± 0.6	24.8 ± 0.7
2.24	64.3	2.318	1.30	0.207	232 ± 5	32.0 ± 1.0	29.6 ± 1.5
1.79	104	2.307	1.32	0.209	176 ± 1	35.0 ± 0.4	24.4 ± 0.5
2.99	173	1.930	1.41	0.221	236 ± 2	35.3 ± 0.7	29.4 ± 2.6
3.73	107	1.902	1.42	0.222	333 ± 3	33.9 ± 0.6	30.7 ± 1.7
			B. D_2O				
0.129	16.6	4.84	0.906	0.154	48.4 ± 23	16.2 ± 0.9	29.5 ± 0.3
0.360	4.68	3.83	1.02	0.170	760 ± 2.4	20.7 ± 1.1	31.5 ± 1.1
0.721	9.36	3.30	1.24	0.199	133 ± 2	22.6 ± 0.7	34.2 ± 1.2
0.901	11.7	3.16	1.29	0.206	147 ± 3	22.1 ± 0.9	42.6 ± 3.0
0.388	49.8	4.38	1.33	0.210	91.0 ± 1.6	24.0 ± 0.6	29.8 ± 0.4
1.80	23.4	2.95	1.43	0.224	245 ± 2	28.0 ± 0.5	37.4 ± 1.8
1.29	166	3.69	1.61	0.244	237 ± 2	27.9 ± 0.5	34.3 ± 1.5

[a] Units = nepers cm^{-1} sec^2.

value expected if only a single relaxation was present, the amplitude of this high-frequency relaxation was usually too low to obtain useful relaxation information, consistent with the results of other workers. The H_2O background value used was $B = 23.0 \times 10^{-17}$ nepers cm^{-1} sec^2 and deviations from this are attributed to the faster relaxation. The relaxation parameters obtained as described previously[9] are summarized in Tables I-III.

The identification of the low-frequency peak with step III of reaction 1 has previously been made with sulfate,[5-8] nitrate,[9] and acetate ligands.[10] The excess absorbance deviation from the background at high frequency indicates the existence of a more rapid step which is identified with step 12, especially since 0.05 M $Nd_2(SO_4)_3$ is known to have a measured B of $(22.4 \pm 1.1) \times 10^{-17}$ nepers cm^{-1} sec^2 from high-frequency measurements.[11] For reaction 1 under these experimental conditions, Tamm has shown that the relaxation time expressions for steps 12 and III are[12]

$$\tau_{12}^{-1} = 2\pi f_{R_{12}} = k_{21} + k_{12}\theta(c) \quad (3)$$

$$\tau_{III}^{-1} = 2\pi f_{R_{III}} = k_{43} + k_{34}\phi(c) \quad (4)$$

A scheme similar to that of the nitrate system,[9] modified to include the presence of HSO_4^-, was used to evaluate $\theta(c)$ and $\phi(c)$.

(10) V. L. Garza and N. Purdie, *J. Phys. Chem.*, **74**, 275 (1970).
(11) K. Fritsch, C. J. Montrose, J. L. Hunter, and J. F. Dill, *J. Chem. Phys.*, **52**, 2242 (1970).
(12) K. Tamm, "Dispersion and Absorption of Sound by Molecular Processes," D. Sette, Ed., Academic Press, New York, N. Y., 1963, pp 175-222. Tamm uses dissociation constants in his expression, thus the equilibrium constants used in this paper are reciprocals of Tamm's.

TABLE III: Dysprosium Sulfate Data

10^2c, M	10^4d, M	pH/pD	$10^3\theta(c)$, M	$\phi(c)$	$10^{17}A_{III}$[a]	$f_{R_{III}}$, MHZ	$10^{17}B$[a]
			A. H_2O (K_c = 4100, K_{12} = 1350)				
0.250	0.287	3.593	0.867	0.541	72 ± 4	15.2 ± 0.9	22.0 ± 0.4
1.00	1.15	3.159	1.13	0.605	227 ± 5	16.0 ± 0.4	25.1 ± 0.6
2.50	2.87	3.033	1.29	0.637	513 ± 9	16.1 ± 0.3	28.8 ± 1.1
3.50	4.65	2.840	1.43	0.660	650 ± 8	16.8 ± 0.2	29.0 ± 1.0
5.01	6.64	2.771	1.70	0.698	832 ± 8	17.6 ± 0.2	32.2 ± 0.9
			B. D_2O				
0.465	0.452	4.39	1.01	0.577	90 ± 9	13.4 ± 1.4	29.0 ± 0.7
1.12	1.09	3.83	1.41	0.655	177 ± 6	14.3 ± 0.5	30.1 ± 0.4
1.86	1.81	3.53	1.53	0.674	287 ± 7	14.0 ± 0.4	33.9 ± 0.6
4.65	4.52	3.29	1.76	0.703	561 ± 7	16.0 ± 0.2	34.3 ± 0.8

[a] Units = nepers cm^{-1} sec^2.

The initial concentration of $Ln_2(SO_4)_3$ is c and the excess sulfate (H_2SO_4 + Na_2SO_4) is d, and the association constant for $LnSO_4^+$ complexation, K_c, is

$$K_c\pi_\gamma = \frac{1-\alpha}{\alpha\left(\frac{c(1+2\alpha)+d}{1+[H]/K_a}\right)} \quad (5)$$

where π_γ is the activity coefficient ratio, α is the degree of dissociation of $LnSO_4^+$, and K_a is the bisulfate dissociation constant. The Davies equation was used to determine π_γ.[13] For this system $\theta(c)$ is given by

$$\theta(c) = \pi_\gamma\left\{[Ln^{3+}] + [SO_4^{2-}]\left(1+\left(\frac{\partial \ln \pi_\gamma}{\partial \ln [Ln^{3+}(aq)]}\right)_{[SO_4^{2-}]}\right)\right\} \quad (6)$$

By substitution, eq 6 becomes

$$\theta(c) = \pi_\gamma\left\{2\alpha c + \frac{c(1+2\alpha)+d}{1+\frac{[H^+]}{K_a}}\left(1+\frac{\partial \ln \pi\gamma}{\partial \ln [Ln^{3+}]}\right)_{[SO_4^{2-}]}\right\} \quad (7)$$

and

$$\frac{\partial \ln \pi_\gamma}{\partial \ln [Ln^{3+}]} = \frac{2.303(6c\alpha A)}{(1+\sqrt{I})^2}\left(8+\frac{\left(4+\frac{[H^+]}{K_a}\right)}{\left(1+\frac{[H^+]}{K_a}\right)}\right)(0.6(1+\sqrt{I})^2 - 1/\sqrt{I}) \quad (8)$$

A small computer program was written to calculate π_γ, α, I, and $\theta(c)$ for each solution. In H_2O, the bisulfate pK_a was assumed to be 1.99[14] while in D_2O pK_a equals 2.34.[15] The pD was obtained relative to H_2O buffers by[16]

$$pD = pH + 0.40 \quad (9)$$

The quantity $\phi(c)$ is given by[12]

$$\phi(c) = \frac{\theta(c)}{K_{12}^{-1} + \theta(c)} \quad (10)$$

Equation 10 shows that $\phi(c)$, and hence k_{34} and k_{43}, are sensitive to the choice of K_{12}. In terms of an Eigen-type mechanism, step 12 involves the diffusion together of a solvated cation with a solvated anion, followed by water loss from the anion solvation shell. In terms of the three-step sequence one has

$$Ln^{3+}(aq) + SO_4^{2-}(aq) \underset{I}{\rightleftharpoons} Ln^{3+}(H_2O)_xSO_4^{2-} \underset{II}{\rightleftharpoons} Ln^{3+}(H_2O)_ySO_4^{2-} \underset{III}{\rightleftharpoons} LnSO_4^+(aq) \quad (11)$$

where

$$K_{12} = K_I(1 + K_{II}) \quad (12)$$

Step I is diffusion controlled and K_I can be calculated from the Bjerrum equation. However, K_{II} is not diffusion controlled and the magnitude is a function of the relative stabilities of two different outer-sphere complexes. Hence, in this paper K_{12} was not assumed but was calculated from K_c and the rate data. To calculate the best K_{12} consistent with the relaxation data, eq 4 and 12 were combined and rearranged to obtain

$$\tau_{III}^{-1} = k_{34}\left\{\frac{(1+K_c\theta(c))}{(1+K_c\theta(c)+K_{III})}\frac{(1+K_{III})}{K_{III}}\right\} = k_{34}X \quad (13)$$

τ_{III}^{-1} was plotted as a function of X with different values of K_{III} assumed. The K_{III} value which gives a zero intercept results in an internally consistent K_{12} and K_{III}. This technique was utilized to obtain the step III rate constants in H_2O.

In D_2O, the $NdSO_4^+$ high-frequency absorption data were essentially the same as in H_2O and thus K_{12} was assumed to be the same in both solvents.[1] With the other lanthanides the high-frequency absorption data were slightly higher in D_2O than H_2O, which was attributed to the higher background found in D_2O in the absence of salts. Hence K_{12} was also assumed to be the same in both solvents. A cyclic calculation was used to obtain the rate constants in which K_c was assumed, $\theta(c)$ and $\phi(c)$ calculated, least-squares analysis to obtain the step III rate constants, and K_{III} was carried out and a new K_c was calculated *via* $K_c = K_{12}(1 + K_{III})$. This process was continued until K_c assumed and calculated agreed to with 0.1%. The final results for the four lanthanides are shown in Table IV, and Figure 1 represents the kinetic data for Gd.

(13) C. W. Davies, "Ion Association," Butterworth, Washington, D. C., 1962, p 46.
(14) A. A. Noyes and M. A. Stewart, *J. Amer. Chem. Soc.*, **32**, 1133 (1910); M. S. Sherrill and A. A. Noyes, *ibid.*, **48**, 1861 (1926); M. H. Lietzke and R. W. Stoughton, *J. Phys. Chem.*, **65**, 2247 (1961).
(15) M. H. Lietzke and R. W. Stoughton, *J. Phys. Chem.*, **67**, 652 (1963).
(16) R. G. Bates, "Determination of pH Theory and Practice," Wiley, New York, N. Y., 1964, pp 219–220.

TABLE IV: Lanthanide Sulfate Kinetic Results at 25°[a]

	H_2O				D_2O	
Cation	K_c	K_{12}	$10^{-8}k_{34}$, sec^{-1}	$10^{-7}k_{43}$, sec^{-1}	$10^{-8}k_{34}$, sec^{-1}	$10^{-7}k_{43}$, sec^{-1}
La	4200	1300	0.84 ± 0.01	3.8 ± 0.69	0.24 ± 0.01	7.0 ± 1.5
Nd	4370	900	1.9 ± 0.2	4.8 ± 1.0	0.80 ± 0.56	7.1 ± 3.3
Gd	4500	200	8.2 ± 1.2	3.8 ± 2.4	6.9 ± 1.7	0.74 ± 3.6
Dy	4100	1350	0.91 ± 0.10	4.5 ± 0.91	1.1 ± 0.5	2.1 ± 3.5

[a] The same value of K_{12} was used in both solvent systems. K_c in D_2O can be calculated from K_{12} and the reported k_{34} and k_{43} results.

TABLE V: Effect of Alternate Calculation Procedures upon the Experimental Results

					Ratio of H_2O to D_2O rate constants			
Lanthanide	K_c	K_{12}	$10^{-8}k_{34}$, sec^{-1} (D_2O)	$10^{-7}k_{43}$, sec^{-1} (D_2O)	k_{34}[a]	k_{34}[b]	k_{43}[a]	k_{43}[b]
			A. K_c and K_{12} Remain Unchanged as D_2O is Substituted for H_2O					
La	4200	1300	0.35	3.8	2.4	3.5	0.57	0.54
Gd	4500	200	7.8	0.089	1.1	1.2	8	5
Dy	4100	1350	1.4	0.16	0.65	0.83	28	2

K_c[c]	$10^{-8}k_{34}$, sec^{-1}	$10^{-7}k_{43}$, sec^{-1}	K_c[a]
	B. Effect of K_c on the Gd(III) Rate Constants in D_2O		
4,500	7.80	0.089	177,000
20,000	6.91	0.762	18,400
19,000	6.93	0.745	18,900
18,900	6.93	0.743	18,900

K_c	K_{12}	$10^{-8}k_{34}$, sec^{-1} (H_2O)	$10^{-7}k_{43}$, sec^{-1} (H_2O)	$10^{-8}k_{34}$, sec^{-1} (D_2O)	$10^{-7}k_{43}$, sec^{-1} (D_2O)	$k_{34}(H_2O)/k_{34}(D_2O)$
		C. Effect of the Choice of K_{12} on the Gd(III) Rate Constants				
4500	200	8.2 ± 1.2	3.8 ± 2.4	7.8 ± 2.3	0.089 ± 4.5	1.1
4500	1180	5.4 ± 0.8	−1.2 ± 0.4	4.3 ± 0.4	−1.0 ± 0.4	1.3

[a] Calculated. [b] From Table IV. [c] Assumed.

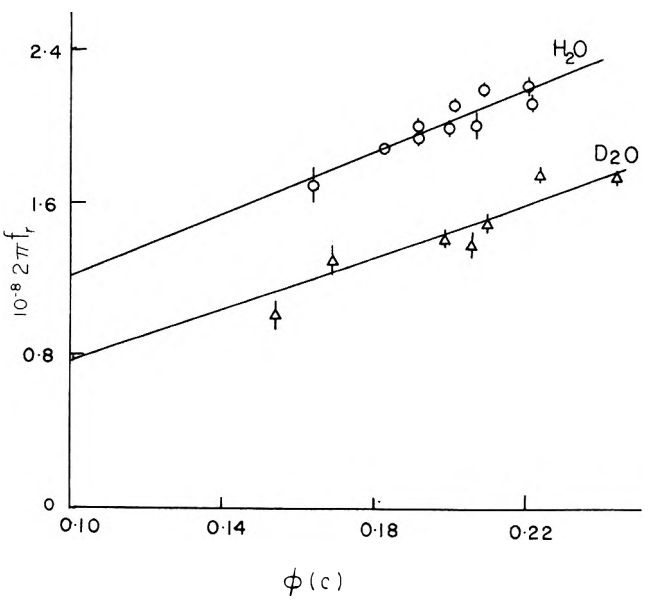

Figure 1. Relaxation data for $Gd_2(SO_4)_3$ in H_2O and D_2O.

The final K_c only represents the internally consistent value. The experimental error in K_c is determined by the reported errors in k_{34} and k_{43}. Thus, for Gd(III) the K_c is 18,900 but the range due mainly to errors in k_{43} is from 2600 to infinity. The question must be asked if the kinetic differences in the two solvents are artifacts caused by the choice of K_c in the calculations. An alternate set of calculations carried out for La, Gd, and Dy, based on the assumption that both K_c and K_{12} remain invariant in the H_2O and D_2O solutions, is summarized in Table V. Using this procedure differences in k_{34} and k_{43} are obtained from those where K_c was permitted to vary from the H_2O value in the heavy water solutions. However, the ratios of the respective rate constants do not significantly deviate from those calculated in this paper (except for the k_{43} ratio for Dy which reflects the large experimental errors). Thus, the reported trends cannot be explained in terms of differences in K_c between the two solvents.

The lack of influence upon the choice of K_c in the D_2O solutions is illustrated in Table V for Gd, where K_c was varied from 4500 to 20,000. If K_c is much lower than the H_2O constant, negative numbers are calculated for k_{43}. For any K_c between 4000 and 20,000, all of the calculated k_{34} rate constants agree within experimental error. Thus, differences in the k_{34} rate data cannot be caused by the choice of K_c in D_2O.

Another parameter which may be responsible for the observed differences in the Gd case is that K_{12} = 200 is much lower than for the other rare earths. The results

were recalculated assuming K_{12} is the mean result for the other lanthanides, and this is also shown in Table V. Although k_{34} decreased as K_{12} increased, k_{43} became negative and this is not a realistic result. Furthermore, the ratio of the k_{34} rate constants in the two solvents remains essentially the same, and this is the quantity which is useful in establishing the trends reported in this study.

Thus, even though alternate calculation techniques can be employed to obtain rate constants from the relaxation data, resulting in some modifications in the magnitudes of the rate constants, neither the relative values for each cation nor the trends within the series can be attributed to these effects.

Graphical analysis of the other three lanthanide systems shows similar results to those shown for Gd in Figure 1. In all cases the ionic concentrations within the D_2O and H_2O solutions are similar for each cation system and hence the rate differences cannot be attributed to concentration effects.

Discussion

The ultrasonic data in H_2O were extended over a much larger frequency range and consisted of many more experimental frequencies than in the previous studies.[5-8] This should yield more accurate relaxation data. A comparison of the calculated k_{34} and k_{43} for the sulfate systems is shown in Figure 2.

The values of k_{43} are similar to those obtained by Grecsek[8] if one assumes a similar experimental error. Grecsek's values of k_{34}, except for $GdSO_4^+$, are consistently higher. These differences arise in that Grecsek used graphical data analysis over a more restricted frequency range.

Greater differences result when one compares the results of Purdie and coworkers.[6] They assume K_{12} to be constant for all of the lanthanides. As in this paper, eq 4 was used to calculate the rate constants. Only in the case of $SmSO_4^+$ is sufficient data present to check the results.[6] Substitution of the calculated rate constants k_{34} and k_{43}, along with the given $\phi(c)$ into eq 4 yields calculated relaxation times ($2\pi f$) of 438–517 MHz. However, the experimental results range from 158 to 229 MHz. Purdie made the assumption that a certain limiting concentration of complexes must be present before the excess absorption occurred. The value of $\phi(c)$ for this point was used to determine k_{43}. However, if one assumes $\phi(c)$ to be correct as given in the paper, and obtains K_{12} using eq 13, a much improved data fit is obtained. The recalculation of Purdie's data yields the following results: $K_{12} = 365$; $k_{34} = 4.1 \times 10^8$ sec^{-1}; $k_{43} = 3.4 \times 10^{-7}$ sec^{-1}; and the calculated relaxation times range between 159 and 229 MHz, in agreement with the experimental results. When these recalculated Sm(III) results are replotted in Figure 2, the data follow the trend established in this study.

It is noteworthy that the trends within all three studies are identical. The complexation rate constants increase toward the middle of the series, reach a maximum, and then decrease again. The interpretation of this trend in terms of a change in coordination number has been made.[6,8] One of the rationales for this study was to discover if a change in the rate-determining step occurred within the series. Such a change could produce the same type of rate-determination variation.

In an earlier temperature jump study involving lanthanide–anthranilate complexation in H_2O and D_2O, a modification of reaction 1 was observed[4]

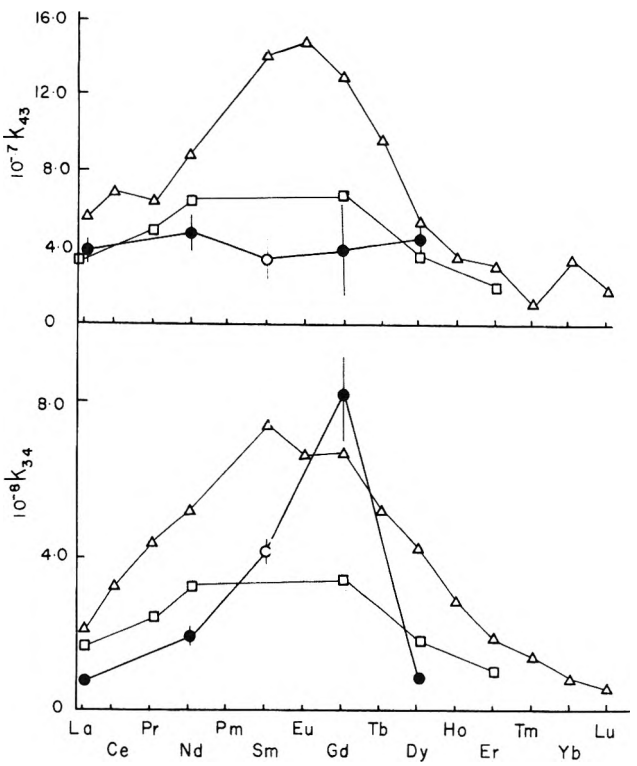

Figure 2. Summary of lanthanide sulfate kinetic results: △, ref 6; □, ref 8; ○, this study; ●, recalculated from ref 6.

$$Ln^{3+} + An^- \underset{k_b}{\overset{k_f}{\rightleftharpoons}} LnAn^{2+} \qquad (14)$$

where An^- represents anthranilate. For the anthranilate system at 12.5°, the value of k_b was essentially the same in H_2O and D_2O, but significant differences occurred in k_f, between solvents. The deuterium isotope effect will be represented by the ratio of a given rate constant in H_2O to that in D_2O. The magnitude of the deuterium isotope effect increased from 1 to about 6 from La through Gd. The two rare earths after Gd, Tb, and Dy had the same rate constants in H_2O and D_2O. After Dy the deuterium isotope effect increased to a value approximately 5 at Lu. With murexide as the ligand, the D_2O effect was approximately 3 for Gd and slightly over 1 for Dy.[4] That paper had preliminary D_2O results for acetate systems,[4] but recent work confirms that the process observed in the acetate system involved the formation of the bisacetato complex[17] and will not be considered further.

The Nd system was similar to the anthranilate system in which the dissociation isotope effect was significantly different from the complexation one.[1] From the data the conclusion was reached that the deuterium isotope effect occurred in the rapid portion of step III, including cation–solvent exchange, followed by the slow step of cation–ligand bond formation. This hypothesis would also apply to the anthranilate system. The ratios of the H_2O to D_2O rate constants obtained here are for La, k_{34} ratio = 3.5 and $k_{43} = 0.5$; Nd, $k_{34} = 2.3$ and $k_{43} = 0.7$; Gd, $k_{34} = 1.2$ and $k_{43} = 5$; and Dy, $k_{34} = 0.8$ and $k_{43} = 2$. One pattern of results occurs for the two light rare earths in which there is a large complexation isotope effect and a smaller, but opposite effect in the dissociation step. For Gd and

(17) M. Doyle and H. B. Silber *J. Chem. Soc., Chem. Commun.*, 1067 (1972).

Dy, the complexation isotope ratio is close to 1, but there is a large decrease in the dissociation rate constant upon switching to D_2O. Thus, one pattern of results occurs for the light rare earths, a second for the heavy rare earths, and the changeover occurs near Gd. This trend is typical in systematic studies of lanthanides and has often been interpreted in terms of different coordination number species existing for the light and heavy lanthanides.[18,19] A detailed interpretation of the significance of the isotope ratio for each individual lanthanide is not possible. However, the data cannot be explained by a single process occurring in step III, but must be interpreted in terms of at least two steps. This is the case with an Eigen-type mechanism where this step consists of cation–solvent exchange followed by cation–ligand bond formation. The large isotope differences observed for the association and dissociation steps is not consistent with the rate-determining cation–solvent, as explained previously.[1]

The kinetic isotope data for each lanthanide in this study is considerably different than that found with anthranilate. The big difference occurs with Gd where a large complexation isotope effect occurs with anthranilate but not with sulfate. A possible explanation arises in that both sets of studies were carried out at different temperatures, and that each of the systems in each solvent has considerably different activation parameters. This explanation cannot be resolved in this study.

One of the questions which this study set out to answer was whether or not similar deuterium isotope effects occur for a given lanthanide cation with different ligands. The experimental answer is that the deuterium isotope effects are not a function of solvated cation alone, but instead are a function of the solvated cation–ligand complex.

Acknowledgments. The authors thank Drs. Vitullo and Pollack for several helpful discussions. Partial support for this research came from the Frederick Gardner Cottrell Program of the Research Corporation.

(18) J. H. Spedding, *et al.*, *J. Phys. Chem.*, **70**, 2423, 2430, 2440, 2450 (1966).
(19) T. Moeller, D. F. Martin, L. C. Thompson, R. Ferris, G. R. Feistel, and W. J. Randall, *Chem. Rev.*, **65**, 1 (1965).

Catalysis of *p*-Nitrophenol Laurate Hydrolysis in Solution Showing Transition from Reversed to Normal Micelles

S. Friberg,* L. Rydhag,

The Swedish Institute for Surface Chemistry, Stockholm, Sweden

and G. Lindblom

University of Lund, Chemical Center, Lund, Sweden *(Received December 12, 1972)*

Publication costs assisted by the Swedish Board for Technical Development

Catalysis of the hydrolysis of *p*-nitrophenol laurate by normal and reversed micelles was investigated in their common solution area in the system water–cetyltrimethyltetraammonium bromide–water. Maximal reaction rates were found at the critical micellization concentrations for both kinds of micelles. In the range where transformation of one kind of micelle into the other could be expected, the reaction rates were minimal. The enhancement factor in the aqueous part was 1500, which is higher than has been reported earlier for such systems.

Catalysis by surfactant micelles has been investigated for more than a decade following the pioneering work by Duynstee and Grunwald in 1959.[1] Extensive reviews[2-4] of progress in the field have recently been published. The investigations prior to 1970 were, however, concerned exclusively with the effect of micelles in aqueous solutions which show the well-known association structure with the hydrophobic part of the surfactant forming the central part of the micelle and the polar parts oriented toward the surrounding aqueous solution.

In amphiphilic liquids such as hexanol *reversed* micelles may also be formed when water and an ionic surfactant are added in sufficient quantities.[5] The first report on the catalytic influence of such reversed micelles on the hydrolysis of a phenol ester was published in 1971[6] with reference to reversed micelles of water and cetyltrimethylammonium bromide (CTAB) in hexanol. Corresponding

(1) E. F. J. Duynstee and E. Grunwald, *J. Amer. Chem. Soc.*, **81**, 4540 (1959).
(2) E. H. Cordes and R. B. Dunlop, *Accounts Chem. Res.*, **2**, 329 (1969).
(3) H. Morawetz, *Advan. Catal.*, **20**, 341 (1969).
(4) E. J. Fendler and J. H. Fendler, *Advan. Phys. Org. Chem.*, **8**, 271 (1969).
(5) P. Ekwall, L. Mandell, and P. Solyom, *J. Colloid Interface Sci.*, **35**, 266 (1971).
(6) S. Friberg and S. I. Ahmad, *J. Phys. Chem.*, **75**, 2001 (1971).

investigations of other reactions in nonaqueous systems[7,8] showed a more pronounced catalytic effect. Later the system water–hexanol–CTAB was also used to demonstrate hydrolysis catalysis in lyotropic liquid crystals[9] for the first time. Earlier results[10] of ester hydrolysis in a liquid crystalline phase showed reduced reaction rates when the surfactant was nonionic.

Thus, considering that catalysis by both normal[1] and reversed[6] micelles as well as by liquid crystalline phases[9] had been displayed, we found it worthwhile to investigate the rate of hydrolysis in a solution exhibiting a transition from normal to reversed micelles, such as, the isotropic liquid solution region in the system water–CTAB–butanol.[11]

Materials and Methods

Materials. Analytical reagents, *p*-nitrophenyl laurate (Schuchardt, München), 1-butanol (Fluka), and cetyltrimethylammonium bromide (CTAB) (Merck), were used. The water was distilled twice and buffered to pH 11.5 by means of a 0.01 *M* sodium phosphate buffer.

Phase Region. The region of the isotropic solution in the system was determined by the addition of water and CTAB to homogeneous samples untill turbidity was observable. The temperature was kept constant at 30 ± 0.1° during the determination.

Light Scattering. The intensity of scattered light at an angle of 90° was determined by means of a Sophica photodiffusogoniometer 42000. The cells were cleaned with chromosulfuric acid and rinsed several times by distilled water. Final rinsing was effected by condensation of water vapor in the inverted cell. The cells were filled and rotated in an ultracentrifuge at 30,000 rpm for 4 hr to sediment dust particles.

Reaction Rates. Kinetic measurements were performed by determining, at various times, the amount of *p*-nitrophenolate ion from the extinction at 400 mμ by means of a Zeiss PMQII spectrophotometer. The initial concentration of *p*-nitrophenyl laurate ester was 2.4×10^{-5} *M* in all determinations.

Nmr Measurements. The ^{79}Br and ^{81}Br nmr measurements were performed with a Varian V-4200 nmr spectrometer equipped with a 12-in. V-3603 magnet and a Varian Mark II Fieldial as described previously.[12] The sample temperature was 30 ± 2° measured with a thermocouple before and after recording a series of spectra. The reported line widths are the arithmetical means of two–four spectra, and the individual measurements are usually within 5% of the mean.

Results

Properties of the Solution. The solution region of the system formed a broad continuous area extending from the bulfer corner to the butanol corner (Figure 1). The limit against the butanol–CTAB axis was a straight line with an approximate CTAB–water molar ratio of 1:6. The width of the region toward the water corner was about 20% (w/w). The compositions of the samples for the kinetic determinations are indicated in the figure.

The intensity of the scattered light at a right angle and the Br line width for series 3 are indicated as a function of the water content in Figure 2. At a water concentration below 40% (w/w) the intensity of the scattered light was low (Figure 2) and the ΔB values were too high to be conveniently determined. In the 40–60% (w/w) water range a sharp reduction in the line width took place and was accompanied by a pronounced rise in the intensity of the scattered light. Between 60 and 70% (w/w) water both factors were fairly constant. A sharp reduction between 70 and 80% (w/w) was followed by a less sharp decrease up to about 95% (w/w). Solutions with water content in excess of 95% were not investigated owing to numerous determinations of the properties of solutions in this range.[13]

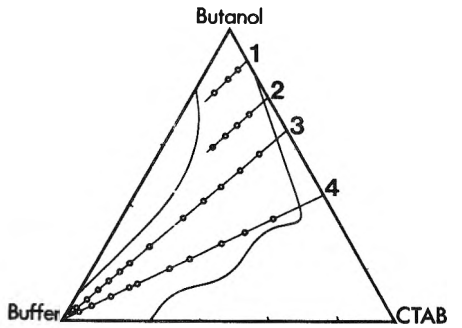

Figure 1. The solution region in the system cetyltrimethyltetraammonium bromide–butanol–water buffered at pH 11.5 with phosphate buffer. The composition of samples for which reaction rates were determined is indicated in the figure.

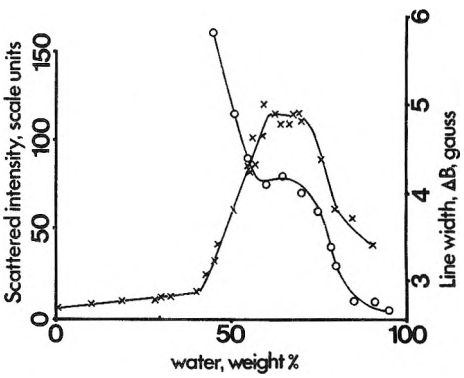

Figure 2. Light scattering and ^{81}Br line width as a function of water content for series 3 according to Figure 1.

Reaction Rates. The reaction rate for a first-order reaction is given for a different series in Figure 3. At low water contents the reaction rate was enhanced by an increasing water content. For series 3 and 4 the rates passed a low maximum at 40 and 60% water. A shallow minimum was observed for these series in the 70–75% water range followed by a pronounced maximum at about 90% water.

The position of the low maximum was increased to higher percentages of water when the hexanol/CTAB ratio was decreased. The position of the pronounced maximum in the 90–95% water range was not determined with corresponding accuracy.

Discussion

The interpretation of the results from light scattering and nmr determinations both indicated that association into micellar aggregates took place in a concentration range of a few per cent around 40% water (w/w) for the

(7) E. J. Fendjler, J. H. Fendler, R. T. Medacy, and W. A. Woods, *Chem. Commun.*, 1497 (1971).
(8) J. H. Fendler, *Chem. Commun.*, 642 (1972).
(9) S. I. Ahmad and S. Friberg, *J. Amer. Chem. Soc.*, **94**, 5196 (1972).
(10) K. S. Murthy and E. G. Rippie, *J. Pharm. Sci.*, **59**, 459 (1970).
(11) G. Gillberg, H. Lehtinen, and S. Friberg, *J. Colloid Interface Sci.*, **33**, 40 (1970).
(12) G. Lindblom, H. Wennerstrom, and B. Lindman, *Chem. Phys. Lett.*, **8**, 489 (1971).
(13) P. Ekwall, L. Mandell, and K. Fontell, *J. Colloid Interface Sci.*, **29**, 9 (1969).

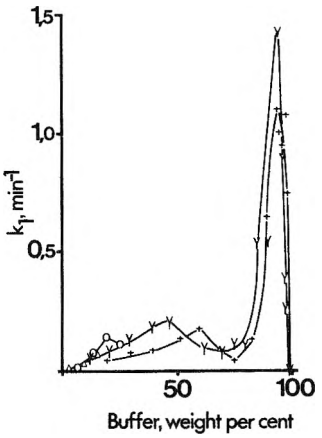

Figure 3. Reaction rates *vs.* water content for different series according to Figure 1: series 1, Δ; series 2, O; series 3, Y; series 4, +.

series with a butanol/CTAB ratio of 2. The drop of line width to a level of 4 G at the association concentration was in accordance with the results from investigations of the hexanol solution in the system water–CTAB–hexanol.[14] A comparison with these results indicated that addition of the water gave rise to micelles of a reversed structure in a continuous medium of butanol with dissolved water and CTAB. The premise about a formation of reversed micelles was supported by a calculation of the amounts of the totally included water (40% w/w) which were solubilized and molecularly dispersed. Pure butanol dissolved 20% (w/w) water in a molecularly dispersed form. The added CTAB 20% (w/w) required some further water in order to form ion pairs. Maximum 15% (w/w) CTAB was dissolved in pure butanol (Figure 1, right part). The necessary water to bring the remaining 5% (w/w) of CTAB into solution could be estimated from the slope of the right-hand limit of the solution area in Figure 1. A reasonable estimation was 5% (w/w) of the water being needed in order to dissolve the remaining CTAB.

The content of butanol and of CTAB could safely be estimated to account for 20% (w/w) of the water as molecularly dispersed. The remaining 20% (w/w) can not reasonably be sufficient to form a continuous aqueous phase containing normal micelles.

Since the micelles in the aqueous corner are normal micelles and since no phase transition could be observed the conclusion of the results must be an evidence of a transformation from reverse to normal micelles in a one-phase region of an isotropic liquid. This conclusion draws attention to the structure of reversed micelles and their transition into normal micelles. Reversed micelles have been postulated to be spherical[15] but other forms are also probable. It has recently been shown[16] by low-angle X-ray diffraction investigations that reversed micelles of monoglycerides in triglyceride solution actually possessed a lamellar structure containing several layers. In the present case a preliminary determination of the low-angle X-ray diffraction pattern showed no signs of multilayer structures in any water range. This result gave evidence that the structures did not contain a sufficient number of ordered, sequential layers for the X-rays to give the multireflection patterns which are characteristic of a liquid crystalline phase. A liquid crystalline phase should furthermore have given rise to a pronounced widening of the nmr lines. This was not found and the formation of a multilayer structure similar to a liquid crystalline phase in the transition region between reversed and normal micelles must be ruled out for the present solution.

In need of more precise experimental investigations of the structure in the transformation region, the present results give sufficient basis for the following interpretation. The formation of reversed micelles was initiated when about 40% (w/w) of the water was added in series 3 (Figure 1). A transition region to normal micelles was then observed between 60 and 70% (w/w) water. Normal micelles of various structures account for water percentages in excess of the last value. The variations in reaction rates *vs.* the water content with two rate maxima at 45 and 95% (w/w) of water corresponding to two kinds of micelles were in accordance with this interpretation.

The rise in the reaction rate was less sudden and the maximum rate for the reversed micelles showed slightly lower values compared with the results in hexanol.[6] The less sudden increase could be ascribed to the formation of premicellar aggregates, which would also have some catalytic effect on the hydrolysis. The formation of premicellar aggregates has been observed in aqueous solutions of sodium carboxylates with a chain length of four.[17] The reduction of the maximum reaction rate when the cmc is reduced in aqueous systems due to shorter chain lengths has been observed recently[18] in the catalytic effect of alkyl sulfates on the Hg^{2+} induced aquation of $CO(NH_3)_5Cl^{2+}$. The influence of the substrate on the micellization was not observable; the concentration of the ester was only 2.4×10^{-5} *M*. The localization of the substrate was not determined; it is obvious that at least part of the differences between the rates in the aqueous and nonaqueous part of the solution might occur due to differences in localization of the substrate.

For both the series which contained normal and reversed micelles a minimum was observed between the two maxima at critical concentrations for reversed and normal micelles. These results gave evidence that no structural conditions with specific catalytic effects existed in the concentration range when a transformation from reversed to normal micelles took place. A simple consideration of reaction rates suggests an inverse relation between water content in excess of cmc and reaction rate. Such an assumption is in accordance with a minimum between the two maxima. An inverse relation is not followed exactly, but this is no surprise since deviations appear to be the rule.[18] It has been demonstrated earlier that changes in reaction rates are sensitive to changes in micellar structure.[9]

The pronounced maximum at high water content displayed an enhancement factor of about 1500 for normal micelles, which is considerably higher than the values of 200–500 which have earlier been reported in aqueous systems.[2-4] The specific cause for this increase in reaction rates was not investigated, as it was beyond the original scope of the study. The influence of nonionic[19] as well as ionic[20] substances has been determined and a reasonable pattern of the combined effects on charge density and

(14) G. Lindblom, B. Lindman, and L. Mandell, *J. Colloid Interface Sci.*, **34**, 262 (1970).
(15) P. Ekwall, *J. Colloid Interface Sci.*, **29**, 16 (1969).
(16) K. Larsson, *Chem. Phys. Lipids*, **9**, 181 (1972).
(17) I. Danielsson and P. Stenius, *J. Colloid Interface Sci.*, **37**, 264 (1971).
(18) J.-R. Cho and H. Morawetz, *J. Amer. Chem. Soc.*, **94**, 375 (1972).
(19) D. S. Kemp and K. Paul, *J. Amer. Chem. Soc.*, **92**, 2553 (1970).
(20) C. A. Bunton, M. Minch, and L. Sepulvede, *J. Phys. Chem.*, **75**, 2707 (1972).

electric double layer now appears to have been determined.[21] With regard to these factors we would only want to point out that the enhancement factor in the present case is higher than those found earlier in aqueous systems; in completely nonaqueous systems considerably larger factors have been found.[7,8]

Acknowledgment. The experimental assistance of Mrs. B. M. Hultin is gratefully acknowledged. The investigations were financed by Swedish Board for Technical Development.

(21) C. A. Bunton, *Proc. Amer. Chem. Soc., Conf. React. Kinet. Mic. Membr.*, 73 (1972).

Equilibrium and Kinetics of the Acid Dissociation of Several Hydroxyalkyl Radicals[1,2]

Gary P. Laroff and Richard W. Fessenden*

Radiation Research Laboratories, Center for Special Studies and Department of Chemistry, Mellon Institute of Science, Carnegie-Mellon University, Pittsburgh, Pennsylvania 15213 *(Received December 22, 1972)*

Publication costs assisted by Carnegie-Mellon University and the U. S. Atomic Energy Commission

The equilibrium constants for the dissociation of the hydroxyl proton of several hydroxyalkyl radicals in aqueous solutions at about 20° have been determined by esr. The values expressed as pK_a are for $\dot{C}H_2OH$, 10.7; for $CH_3\dot{C}HOH$, 11.5; and for $(CH_3)_2\dot{C}OH$, 12.0. These values are in good agreement with those determined previously in pulse radiolysis experiments. The radical $(CF_3)_2\dot{C}OH$ is found to be a strong acid with pK_a = 1.7. In all cases the pK is 4–8 units lower than for the corresponding alcohol. The dynamics of the equilibrium $\dot{R}OH + OH^- \rightleftarrows \dot{R}O^- + HOH$ has been investigated for the radicals $CH_3\dot{C}HOH$ and $(CH_3)\dot{C}OH$ by means of the esr line broadening associated with the dissociation. Values for the forward and reverse rate constants are, for $CH_3\dot{C}HOH$, 7×10^9 and 4×10^5, and, for $(CH_3)_2\dot{C}OH$, 9×10^9 and 1.8×10^6 (M^{-1} sec^{-1}). The values for the forward reactions are clearly diffusion controlled. The rates for the reverse reactions (protonation by water) are seen to be so fast as to be accessible to direct pulse experiments only in the nsec region. Depending upon the pK and the forward rate constant a number of patterns of esr line broadening as a function of pH are possible. The various behaviors are discussed and examples given of most of them. Of particular importance is the conclusion that exchange of protons with high pK values (>16) will be readily observable in basic solution.

Introduction

The esr spectra of hydroxyalkyl radicals derived from alcohols show changes as the solution pH is varied in the approximate range 10–13.[3] These changes can be illustrated by the behavior of the radical $(CH_3)_2\dot{C}OH$. In neutral water the spectrum is the well-known septet split by the OH hyperfine splitting of ~0.5 G. As the pH is raised the lines broaden and then ultimately narrow to give a new septet with a somewhat smaller hyperfine constant for the CH_3 protons and no splitting by an OH proton. This latter spectrum is attributed to the dissociated or ketyl form of the radical, $(CH_3)_2\dot{C}O^-$. In the intermediate region the central line of the septet is narrow but the lines with nonzero magnitudes of I_z for the six CH_3 protons are progressively wider away from the center of the spectrum and the line separation is intermediate between that of the two limiting forms. The line broadening effects must be caused by the dynamics of the dissociation equilibrium

$$\dot{R}OH \rightleftarrows \dot{R}O^- + H^+ \qquad (1)$$

and the fact that the esr parameters are different for the two forms of the radical. Because the time scale involved with esr line broadening is $\sim 10^{-8}$–10^{-7} sec it is immediately evident that the reverse of reaction 1 cannot be important because of the low H^+ concentration and that the actual process is most likely

$$\dot{R}OH + OH^- \underset{k_r}{\overset{k_f}{\rightleftarrows}} \dot{R}O^- + HOH \qquad (2)$$

Two types of information are likely to come from a detailed study of this phenomenon, namely, the equilibrium constant for the dissociation and the kinetics of the protonation–deprotonation. The equilibrium constants for a number of the simpler aliphatic alcohols have already been determined by pulse radiolysis[4] but a determination by a totally different method is desirable because the optical method has, in at least one case, led to an incorrect conclusion.[5] The esr method, in cases where rapid ex-

(1) Supported in part by the U. S. Atomic Energy Commission.
(2) Based on portions of a dissertation submitted by G. P. Laroff in partial fulfillment of the requirements for the degree of Doctor of Philosophy at Carnegie-Mellon University.
(3) K. Eiben and R. W. Fessenden, *J. Phys. Chem.*, **75**, 1186 (1971).
(4) K.-D. Asmus, A. Henglein, A. Wigger, and G. Beck, *Ber. Bunsenges. Phys. Chem.*, **70**, 756 (1966).

change can be achieved, directly links the two limiting spectra to forms of the same chemical intermediate differing by only a simple acid–base equilibrium.[6] Esr measurement of the equilibrium is also necessary as background information for the interpretation of the line broadening experiments. Measurement of the dynamics of equilibrium 2 is important for esr studies because of the insight it gives into the problem of line broadening often encountered with aqueous solutions of radicals with dissociable protons. In addition, because radicals such as $(CH_3)_2\dot{C}OH$ can be produced by both abstraction from the alcohol and attachment of e_{aq}^- to the ketone, a knowledge of the kinetics of the protonation of the ketyl radical is fundamental to the complete understanding of pulse radiolysis experiments.

Experimental Section

The apparatus and general procedural details were as previously described.[3] Radicals were produced by irradiation of N_2O saturated aqueous solutions of 0.1 *M* methanol, ethanol, or 2-propanol or 0.01 *M* hexafluoro-2-propanol (from Hynes Chemical Research Corp.). The sample solution was cooled prior to entry into the sample cell. Measurement of the solution temperature under typical electron beam current and flow conditions showed that the experiments pertain to 20° within about ±2° under all conditions used. The pH was adjusted with KOH or $HClO_4$ and measured with a Corning Model 112 digital readout meter with a Sargent-Welch Model S-30070-10 combination pH electrode. Readings for buffered solutions were reproducible to ±0.01 pH unit. Solutions of pH >12 (and no buffer) were titrated against standard acid to the phenolphthalein end point.

Second-derivative presentation was used for the measurement of line positions and first derivatives were recorded for most line width measurements. In a few cases line widths were measured from second-derivative spectra where this approach was necessary to reduce interference from the background signal of the silica cell. Because the field modulation amplitudes used to give reasonable signal-to-noise ratios cause significant line broadening it was necessary to correct for this effect. The field modulation amplitudes at the various instrument settings were calibrated by fitting the observed line amplitudes and widths of $(CH_3)_2\dot{C}OH$ to curves of apparent peak-to-peak amplitude and line width as calculated for modulation broadened Lorentzian lines by Wahlquist.[7] The curve given by him for the reduced apparent width (apparent width divided by true line width) as a function of the reduced modulation amplitude is not in the proper form for making corrections but must be replotted to give reduced apparent width as a function of modulation amplitude divided by apparent width. With this curve the true line width can readily be found given the apparent width and modulation amplitude. A similar curve was constructed for over-modulated second derivatives by considering that the second (or low-frequency) field modulation sweeps the observation point over the already broadened first-derivative function (as from Wahlquist) and evaluating the required integral numerically. Only the case where the two modulation amplitudes were equal was considered. For all but the narrowest lines the corrections for modulation broadening were small. Corrections must also be made for the overlapping lines of the complex patterns caused by the second-order structure and hydroxyl proton splittings. In this case it is appropriate to synthesize the known pattern of lines with a sequence of component line widths and to use visual criteria to select the best fit to the experimental curves. Spectrum synthesis was carried out with a Hewlett-Packard 9100-A calculator equipped with a 9125-A plotter and 9101-A extended memory.

Measurement of Equilibrium Constants

Measurement of the equilibrium constant for the dissociation of the radicals is necessary before the kinetic problem can be treated so this aspect will be discussed first. The qualitative observation that a single spectrum is observed with a pH-dependent splitting suggests that the exchange is rapid at most values of pH. At the fast exchange limit where the lines are narrow, the spectrum represents a weighted average of the spectra of the dissociated and undissociated forms. A plot of the hyperfine constant (or *g* factor) should show a sigmoid transition between the values for the two forms with an inflection at the p*K* for the dissociation. To facilitate accurate measurement of the line positions it was convenient to increase the forward and reverse rates by adding a buffer[8] so that the main reaction becomes

$$\dot{R}OH + B^- \rightleftharpoons \dot{R}O^- + BH \qquad (3)$$

The most rapid reaction occurs when the p*K* of the buffer matches that of the radical. For the present purposes phosphate with a third p*K* of 12.32 was convenient. All measurements concerned with the p*K* of the three aliphatic alcohols were made in the presence of 1 *M* phosphate. Although the ionic strength of these solutions is very high the fact that only one charged species appears on each side of eq 2 suggests that the equilibrium will not be greatly shifted by the ionic solute. In agreement with this idea is the fact that no significant shift of line positions was found upon adding phosphate. In the case of hexafluoro-2-propanol the dissociation occurred in strongly acid solutions which provided a rapid exchange directly.[9]

The results for the four radicals $\dot{C}H_2OH$, $CH_3\dot{C}HOH$, $(CH_3)\dot{C}OH$, and $(CF_3)_2\dot{C}OH$ are shown in Figure 1 together with the expected sigmoid curves calculated on the basis of a simple dissociation equilibrium and the concept of a weighted average. The limiting values of the esr parameters used in this calculation are given in Table I and the p*K* values (expressed in terms of the acid dissociation, reaction 1) in Table II. The results obtained for the three aliphatic alcohols are in excellent agreement with the values determined previously by pulse radiolysis.[4] In each of these cases the p*K* of the radical is 4–5 units lower than for the parent alcohol. For the hexafluoro-2-propanol the decrease in p*K* of the radical by 8 units is even greater. The radical $(CF_3)_2\dot{C}OH$ is seen to be a strong acid as a result of the electron-withdrawing effect of the six fluorine atoms.

Dynamics of the Equilibrium

The kinetics of the dissociation were studied only for $(CH_3)_2\dot{C}OH$ and $CH_3\dot{C}HOH$. The mechanism of base-cat-

(5) See the discussion regarding glycine in acid solution given by P. Neta, M. Simic, and E. Hayon, *J. Phys. Chem.*, **76**, 3507 (1972).
(6) See the results for glycine given by H. Paul and H. Fischer, *Helv. Chim. Acta*, **54**, 485 (1971).
(7) H. Wahlquist, *J. Chem. Phys.*, **35**, 1708 (1961).
(8) This technique was used by H. Paul and H. Fischer in their study of the radical derived from glycine.[6]
(9) In this instance an acid-catalyzed exchange, $ROH + H^+ \rightleftharpoons ROH_2^+$, occurs, see, e.g., H. Fischer, *Mol. Phys.*, **9**, 149 (1965).

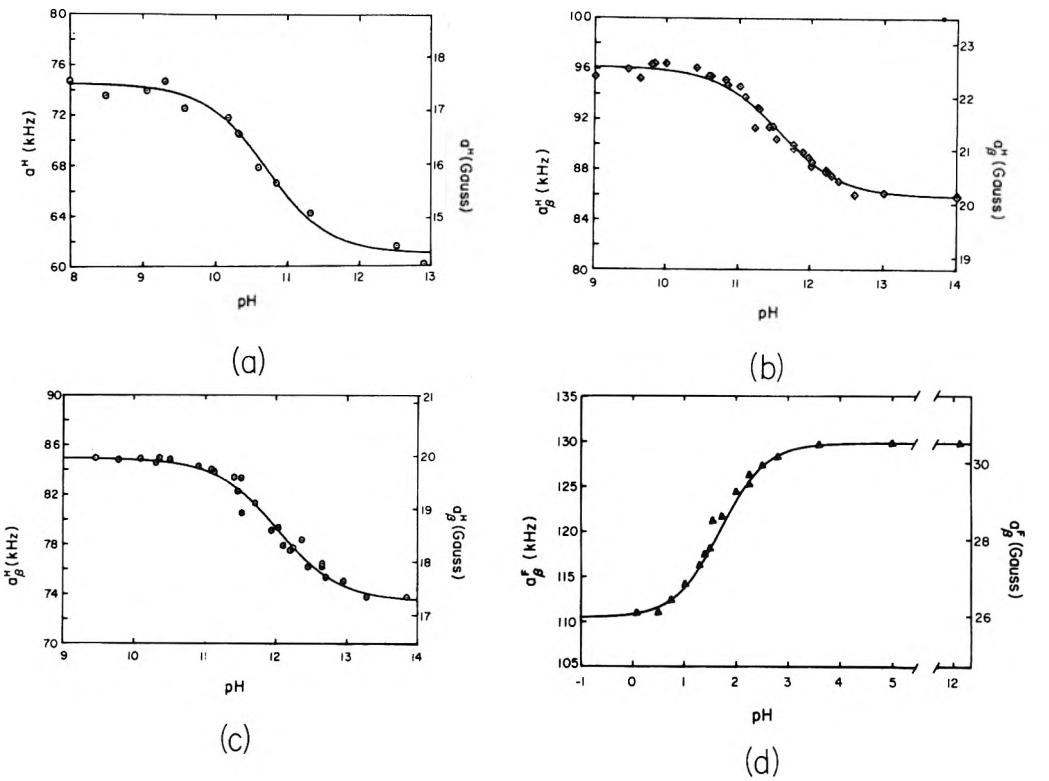

Figure 1. Hyperfine constants as a function of pH for the radicals (a) CH_2OH, (b) $CH_3\dot{C}HOH$ (a_β shown), (c) $(CH_3)_2\dot{C}OH$, and (d) $(CF_3)_2\dot{C}OH$. The solutions for the three studies at high pH contained 1 *M* phosphate to increase the rate of proton exchange and narrow the esr lines. The solid curves are calculated from the data in Tables I and II under the assumption that the spectrum represents the weighted average of the concentrations of the dissociated and undissociated forms of the radicals.

TABLE I: Hyperfine Constants for Hydroxyalkyl Radicals[a]

Radical	a_α^H	a_β^H	a_{OH}^H	g
$\dot{C}H_2OH$	17.50		1.00	2.00317
$\dot{C}H_2O^-$	14.33			2.00367
$CH_3\dot{C}HOH$	14.90	22.71	0.10	2.00321
$CH_3\dot{C}HO^-$	11.11	20.16		2.00359
$(CH_3)_2\dot{C}OH$		19.94	0.47	2.00315
$(CH_3)_2\dot{C}O^-$		17.26		2.00335
$(CF_3)_2\dot{C}OH$		25.95[b]	*c*	2.00311
$(CF_3)_2\dot{C}O^-$		30.50[b]		2.00356

[a] Values in Gauss. Where a comparison is possible the values are essentially the same as those given in ref 3. [b] Value of a_β^F. [c] a_{OH}^H could not be observed because of rapid exchange.

TABLE II: p*K* Values of Alcohols and Their Associated Radicals

Alcohol	p*K* of alcohol	Radical	p*K* of radical: This work[a]	p*K* of radical: Ref 4	Δp*K*
CH_3OH	15.09[b]	$\dot{C}H_2OH$	10.71	10.7	−4.38
CH_3CH_2OH	15.93[b]	$CH_3\dot{C}HOH$	11.51	11.6	−4.42
$(CH_3)_2CHOH$	17.1[b]	$(CH_3)_2\dot{C}OH$	12.03	12.2	−5.07
$(CF_3)_2CHOH$	9.8[c]	$(CF_3)_2\dot{C}OH$	1.70		−8.1

[a] Value accurate to ±0.1. [b] J. Murto, *Acta. Chem. Scan.*, **18**, 2 (1964), quoting his results reported in *Ann. Acad. Sci. Fenn., Sec. A.* No. 117 (1962); *Suom. Kemistilehti B*, **35**, 157 (1962). [c] Measured by titration.

alyzed exchange can be represented by

$$\underline{\dot{R}OH^*} + OH^- \rightleftharpoons \underline{\dot{R}O^-} + H^*OH \qquad (4)$$
$$\underline{\dot{R}OH} + OH^{*-}$$

where the asterisk denotes a particular spin state of the OH proton in the radical. If the equilibrium is to the left then any line broadening encountered must be the result of only the exchange of the OH proton and the presence of small concentrations of the form $\dot{R}O^-$ is of no direct consequence except as an intermediate in the exchange. Treatment of this part of the problem can be carried out using well-known theories of dynamic effects in magnetic resonance.[10] For a given spin state of the aliphatic protons in the radical (*i.e.*, for a given doublet in the spectrum) the two spin states of the OH proton allow the line to be at two "sites" with equal probability. As the exchange rate increases the lines of such a doublet will broaden and eventually collapse to a single narrow line at the center of the former doublet. The maximum line width possible corresponds to the original OH splitting. If the equilibrium is such that a significant fraction of the radicals exist in the dissociated form then a further line broadening is possible as a result of the change in *g* factor and the hyperfine constants for the aliphatic protons upon dissociation and the transformations of the radical back and forth between the two forms. Because of the variable proportions of these forms the situation is less readily visualized than for the simple exchange alone.

A complete analysis requires that the three underlined forms in eq 4 be considered in one model. However, such a treatment is rather complex and an initial attempt was made to treat the exchange and dissociation separately. The observations on the radical $(CH_3)_2\dot{C}OH$ show that an exchange of the OH proton can occur without a significant shift of the equilibrium to the right. It is possible, there-

fore, to consider the dissociation as affecting the g factor and hyperfine constant without taking the OH proton splitting into account. The two forms of the spectra which must be considered are that of the neutral form of the radical with the OH doublets replaced by single lines at their centers and that of the dissociated form. A "two-site" theory with variable proportions of the two forms is used. The shift upon dissociation is different for different lines, being greater for those furthest from the center. For the situations encountered here the dissociation broadens a given line by the greatest amount near the pK of the radical with lesser effects predicted away from this point. Note that the greatest broadening is not necessarily exactly at the pK. The maximum broadening of a line in the spectrum depends directly on the size of the shift in position of the line upon dissociation. Depending upon the actual kinetics of the processes and the equilibrium constant the overall behavior can vary considerably. The separation of the effects of exchange and dissociation will be justified below by the detailed results for $(CH_3)_2\dot{C}OH$. For $CH_3\dot{C}HOH$ the small size of the OH splitting limits the broadening caused by exchange so that in this case only the dissociation is of direct importance.

The full equation for intermediate rates of exchange derived by use of the modified Bloch equations (eq 10-23 to 10-25 of Pople, *et al.*[10]) were used in treating both contributions. Because this equation cannot readily be expressed as a Lorentzian of a certain width, the derivative was calculated and plotted with the Hewlett-Packard 9100A calculator for various exchange rates and the widths measured. The observed line width should then be the sum of the contributions from the natural line width and the contributions from the exchange and dissociation processes

$$(T_2)_{obsd}^{-1} = (T_2)_0^{-1} + (T_2)_{ex}^{-1} + (T_2)_{dis}^{-1}$$

The calculated equilibrium curves of Figure 1 were used to evaluate the relative fractions of the two forms of the radicals in the calculation of $(T_2)_{dis}$.

The first step in the analysis is the measurement of observed line width either directly or, where complex second-order structure occurs, by reference to synthesized patterns. The width so determined was then corrected by the procedure described in the Experimental Section. This method ignores the fact that a line broadened by overmodulation is no longer of Lorentzian shape. However, because only small corrections were involved in most cases no serious error is likely.

The corrected line widths are shown in Figure 2 for $(CH_3)_2\dot{C}OH$ and Figure 3 for $CH_3\dot{C}HOH$. (The widths are expressed in magnetic field units as measured, *i.e.*, in kHz for proton nmr.) The data in the first case correspond to the line immediately below the center of the spectrum ($I_z = +1$ for the CH_3 protons). This line has a shift (or site separation) of 14.03 kHz upon dissociation of the OH proton. All other lines in this spectrum move further upon dissociation and hence are considerably wider under most conditions, precluding accurate measurement. With $CH_3\dot{C}HOH$ two lines could conveniently be studied to give a cross check. These lines correspond to the values of $(\frac{1}{2},\frac{1}{2})$ and $(-\frac{1}{2},\frac{1}{2})$ for the z components of angular momenta for the CH_3 and CH protons, respectively (a_α is taken to be negative), and have shifts of 5.52 and 14.91 kHz, respectively. In Figure 2 are shown calculated curves of line width *vs.* pH for several values of the rate constant k_f for $(CH_3)_2\dot{C}OH$. The double peak which shows the contributions from the two parts of the process is very evident. It is clear that the effect of the exchange dominates in the region pH 10–11 while at pH >11 the dissociation is most important. The contribution to the line width of one of these effects in the region dominated by the other is small, thus justifying the separation into two contributions. The height of the curve in the region pH 11–12 fixes the rate constant quite accurately. The solid curve is for $k_1 = 9 \times 10^9\ M^{-1}\ sec^{-1}$ and is chosen as the best fit. Although the observed broadening seems to start at too low a pH for this value (*i.e.*, the experimental points are considerably above the curve) a small error in pH for these unbuffered solutions could account for the difference and the agreement is regarded as satisfactory.

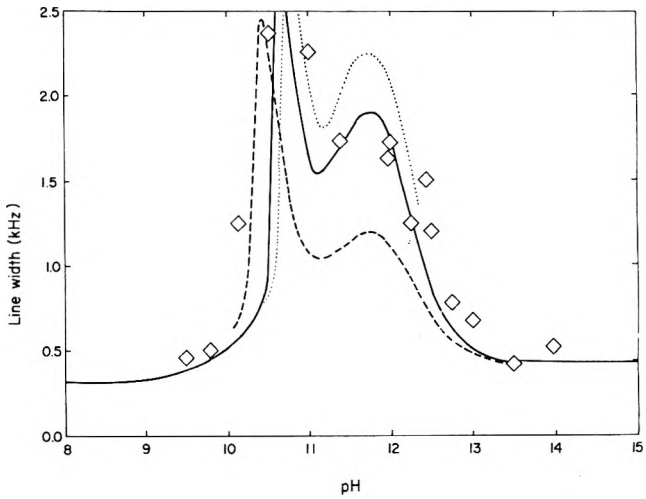

Figure 2. Line width (in units of proton nmr frequency) corrected for modulation broadening and overlap of the second-order components for the first line below the center of the spectrum of $(CH_3)_2\dot{C}OH$. Curves are calculated for forward rate constants of 9×10^9 (solid), 7×10^9 (dotted), and $1.4 \times 10^{10}\ M^{-1}\ sec^{-1}$ (dashed). The peak at pH ~10.5 results from line broadening by exchange and that at pH ~12 from line broadening by dissociation.

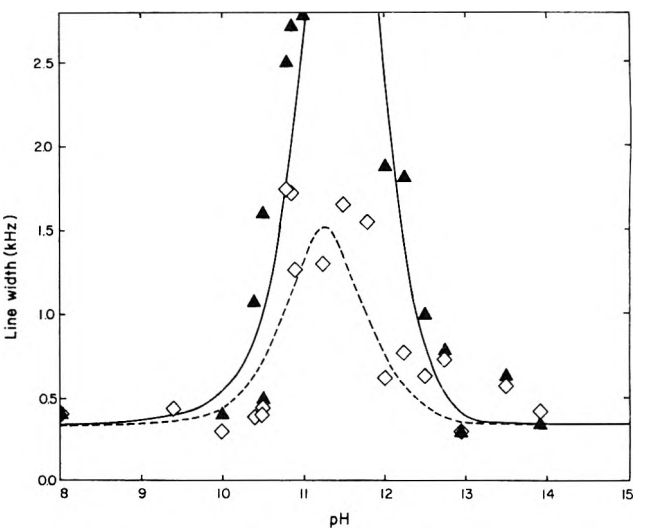

Figure 3. Corrected line widths for the lines $(\frac{1}{2},\frac{1}{2})$ (◇) and $(-\frac{1}{2},\frac{1}{2})$ (▲) (see text) of the radical $CH_3\dot{C}HOH$. Calculated curves are for a forward rate constant of $7 \times 10^9\ M^{-1}\ sec^{-1}$. The calculated maximum width for the latter line is about 6 kHz.

(10) J. A. Pople, W. G. Schneider, and H. J. Bernstein, "High Resolution Nuclear Magnetic Resonance," McGraw-Hill, New York, N.Y., 1959, Chapter 10.

With $CH_3\dot{C}HOH$ only one maximum is seen in Figure 3. The rate constant is fixed closely as 7×10^9 M^{-1} sec^{-1} by the height of the peak for the smaller site separation and calculation. Use of this value for the data from the other line (site separation 14.91 kHz) gives a very good fit also. The rates for the forward and reverse rates are given in Table III. (The reverse rate is determined from the forward rate and the pK value.)

The values of the rate constants can be discussed by reference to the theory outlined by Eigen.[11] For a reaction with no charge neutralization

$$XH + Y^- \rightleftarrows X^- + YH \qquad (5)$$

and $pK_{YH} > pK_{XH}$ the forward rate should be diffusion controlled and the reverse rate will depend on the difference in pK of the two acids.

In the case of $(CH_3)_2\dot{C}OH$, $pK_{H_2O} - pK_{ROH} = 15.75 - 12.03 = 3.72$ so that the forward rate should be $\sim 10^{10}$ while the reverse rate should be $10^{(10-3.72)} = 1.9 \times 10^6$ M^{-1} sec^{-1} as required by the pK. The values found, 9×10^9 and 1.8×10^6 M^{-1} sec^{-1}, are remarkably close to the predictions. For $CH_3\dot{C}HOH$ the forward rate is comparable (7×10^9) and the reverse rate is 4.1×10^5 to be compared with the calculated value of 5.8×10^5. The observed values for the forward rates are close to those for the weak acid phenol ($k_f = 1.4 \times 10^{10}$).[11]

Types of Line Broadening Behavior

The fact that the forward rates for these radicals are the same as those for diamagnetic molecules is not surprising although dissociation of the OH group has a significant effect on the radical site as measured by the change in magnetic parameters. Having found "normal" behavior for these radicals it is reasonable to suppose that dissociation of other similar types of proton will occur with comparable rate constants. It is possible, therefore, to predict the pH values at which line broadening will occur as a result of exchange and/or dissociation. A detailed discussion seems in order because of the frequency with which this type of behavior has been encountered in recent work in these laboratories (some examples will be given below). Several types of behavior are possible.

(a) For radicals with no special features which would decrease the forward rate of reaction with OH^-, the controlling factor is the pK of the dissociation. With $pK < 10$ ($k_f[OH^-] < 10^6$ sec^{-1}) the dynamics of the dissociation will be slow and discreet spectra for the dissociated and undissociated forms of the radicals should be observed.[12]

(b) For any radical with a pK in the range from 10 to about 12.5, behavior like that found for the hydroxyalkyl radicals studied here should exist. The lines will broaden starting at pH 10 ($k_f[OH^-] = 10^6$ sec^{-1}), will remain broad depending upon the change in magnetic parameters upon dissociation, and will finally narrow at some higher pH to the appropriate average spectrum.

(c) If the pK is >12.5 but less than that of water (15.75), the forward rate will remain at $\sim 10^{10}$ M^{-1} sec^{-1} and broadening will still occur starting at pH 10 as a result of the exchange alone. In this case collapse of the doublets caused by the dissociable proton should be complete (unless this splitting is unusually large) before an appreciable concentration of the radical is in the dissociated form. No changes in the other hyperfine parameters should be found.

(d) If the pK of the radical is comparable to or greater than that of water the forward rate constant will be less than 10^{10} M^{-1} sec^{-1} and the line broadening caused by exchange will begin at a higher pH.

(e) It is also possible, because of some special feature of the radical, for the forward rate constant to be less than the normal value. In this case the types of behavior discussed above will also be shifted toward higher pH as in (d).

TABLE III: Rate Constants for Dissociation of Hydroxyalkyl Radicals (Eq 2)[a]

Radical	k_f, M^{-1} sec^{-1}	k_r, M^{-1} sec^{-1}	pK
$(CH_3)_2\dot{C}OH$	9×10^9	1.8×10^6	12.0
$CH_3\dot{C}HOH$	7×10^9	4.1×10^5	11.5

[a] Estimated accuracy based on sensitivity of the calculated curve to the values is about $\pm 1 \times 10^9$ for k_f.

Examples of most of these types of esr behavior are available and will be discussed. In addition, one kinetic measurement should be mentioned. Buxton,[13] by a competitive technique, has found that the reaction

$$\dot{O}H + OH^- \rightleftarrows \dot{O}^- + HOH$$

has a forward rate constant of 1.2×10^{10} M^{-1} sec^{-1}. The equilibrium constant for $\dot{O}H$ (11.9)[14] is very similar to that of $(CH_3)_2\dot{C}OH$ and invites a comparison. The similar values of the forward rate constants (1.2 and 0.9×10^{10} M^{-1} sec^{-1}) help to further define normal behavior.

The radical $\dot{C}H_2OH$ (pK = 10.7) provides an example of a pK in the lowest range discussed (case a) but because of the large intrinsic line width and relatively low signal intensities no detailed study was made. The radical $[\overline{O_2C}\text{-}\overline{CHCHCO_2}H]^{2-}$ (pK = 10.7)[15] formed by addition of e_{aq}^- to fumarate provides another example although here the forward rate may be retarded as the result of the charge of the radical. In this case superimposed esr spectra of the di- and trianions are seen near pH 10 but some line broadening is observed.[16] The radical $(CH_3)_2\dot{C}OH$ discussed above provides an example where exchange and dissociation occur in the same pH region (case b). Several radicals have been observed in these laboratories which appear to have high pK values but which show line broadening associated with exchange of a dissociable proton (case c). These radicals are hydroxycyclohexadienyl[17] from the reaction of OH and benzene, $H_2NCOCH_2\text{-}NO_2^-$,[18] from the trapping of H_2NCO with $CH_2{=}NO_2^-$, and $\underline{\dot{O}C(CO_2^-){=}CHCH(OH)\dot{C}CO_2^-}$.[19] In each case the spectrum at pH <10 shows an OH splitting (NH in the

(11) M. Eigen, *Angew. Chem.*, **75**, 489 (1963); *Angew. Chem., Int. Ed. Engl.*, **3**, 1 (1964).
(12) On the low pH side of the pK the forward reaction is rate determining and will define the line broadening. A first-order rate of 10^6 sec^{-1} will produce an excess line width of 32.8 mG. This value is useful for comparison because it is comparable to natural line widths observed for many radicals. (In this calculation line width is defined as peak-to-peak on the first derivative and a factor of 0.5 has been included to take account of the fact that only one-half the exchanges will invert the OH proton spin.)
(13) G. V. Buxton, *Trans. Faraday Soc.*, **66**, 1656 (1970).
(14) J. Rabani and M. S. Matheson, *J. Phys. Chem.*, **70**, 761 (1966); J. L. Weeks and J. Rabani, *ibid.*, **70**, 2100 (1966).
(15) J. Lilie and R. W. Fessenden, *J. Phys. Chem.*, **77**, 674 (1973).
(16) O. P. Chawla and R. W. Fessenden, unpublished results.
(17) R. W. Fessenden, *J. Chem. Phys.*, **58**, 2489 (1973). With the radical C_6H_6OH the 0.42-G splitting by the OH proton is almost completely averaged out at pH 12.0 with an *excess* width remaining of about 50 mG.
(18) D. Behar and R. W. Fessenden, *J. Phys. Chem.*, **76**, 3945 (1972). The proton (NH) of concern in $H_2NCOCH_2NO_2^-$ has a hyperfine constant of 0.35 G. The splitting is observed at pH 10.4 but complete averaging has occurred by pH 12.7.

second case) which is averaged out by exchange at pH >12. Under the latter conditions all of the other hyperfine constants and the g factor are identical within experimental error to those observed at pH <10. In the last example[19] the line broadening began at pH 11 so that the forward rate constant in that case must be closer to 10^9 than to 10^{10} M^{-1} sec^{-1}. Detailed studies of the line broadening in these cases have not as yet been carried out.

A number of reasons for lower than normal forward rates are given by Eigen.[11] Among these are hydrogen bridge structures which prevent an easy transfer of the proton to OH^- and interference by other nearby negatively charged groups as in nitrilotriacetate (NH^+ dissociation). Excellent examples of both of these effects for radicals have been observed (case e). The great stability of the electron adducts to o-nitrophenol,[3] maleate,[20] and phthalate[21] toward dissociation has been noted. Each of these radicals has a hydrogen bridge structure, such as I for the

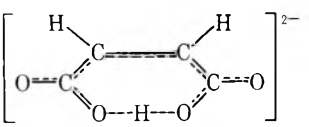

I

case of maleate, and because no change in the spectrum was observed to pH 14 the forward rate constant must be $<10^6$ M^{-1} sec^{-1}. The radical $^-O_2CC(OH)CO_2^-$ derived from tartronic (hydroxymalonic) acid provides an example where the forward rate is influenced by the charge on the radical. Here dissociation is observed above pH 12 with no line broadening. The pK is estimated to be 12.7 from the relative signals of the two species. (Assignment of the two spectra to the dissociated and undissociated radicals is confirmed by observation of the ^{13}C-containing radicals of both species.[22]) From the lack of line broadening of the undissociated form at pH 14 the rate constant must also be $<10^6$ M^{-1} sec^{-1}.

Conclusion

The results given here confirm the pK values of several hydroxyalkyl radicals and show the strongly acidic nature of the radical $(CF_3)_2COH$. The kinetics of the protonation-deprotonation of the two radicals studied in detail are found to be quite normal and to conform to expectations regarding the rate constants. The values for the reaction of the acid forms with OH^- are about 10^{10} M^{-1} sec^{-1} with values for the reverse reaction, protonation by reaction with water, as determined by the pK. The rates for this latter reaction are such that, in the cases studied, nsec resolution would be necessary for a direct determination in a pulse experiment.

A number of types of esr line broadening behavior are distinguishable depending upon the pK of the radical and the rate for its reaction with OH^-. Examples of a number of these have been discussed including cases where the reaction with OH^- is slowed markedly by hydrogen bridge structures or high negative charge density. The arguments presented show clearly that effects of proton exchange should be observable in basic solution even for radicals with a high pK (>16) for which no significant fraction is dissociated.

(19) R. H. Schuler, G. P. Laroff, and R. W. Fessenden, *J. Phys. Chem.*, **77**, 456 (1973). The OH proton splitting for 3-hydroxy-2,5-dicarboxyfuranyl radical is 0.53 G and at pH 12.6 almost complete averaging was found with an observed line width of 0.08 G.
(20) P. Neta and R. W. Fessenden, *J. Phys. Chem.*, **76**, 1957 (1972).
(21) P. Neta and R. W. Fessenden, *J. Phys. Chem.*, **77**, 620 (1973).
(22) G. P. Laroff, Ph.D. Dissertation, Carnegie-Mellon University, 1972.

Binary and Ternary Ion-Exchange Equilibria. Sodium–Cesium–Manganese–Dowex 50W-X8 and Cesium–Manganese–Strontium–Dowex 50W-X8 Systems

R. K. Bajpai, A. K. Gupta, and M. Gopala Rao*

Department of Chemical Engineering, Indian Institute of Technology, Kanpur-16, India *(Received September 11, 1972)*

A single-particle radioactive-tracer technique has been employed for equilibrium measurements of two ternary systems, *viz.*, Sr^{2+}–Mn^{2+}–Cs^+ and Mn^{2+}–Cs^+–Na^+, and the five-component binary systems with Dowex 50W-X8 resin. All the measurements were made at a temperature of 23°. Experimental binary equilibrium data have been analyzed using a generalized phase equilibria theory. A simple correlation has been proposed to predict resin phase activity coefficients of ions in a ternary system. Using these activity coefficients and equilibrium constants of the two binary pairs containing the most selective ion, resin-phase selectivities for ternary systems have been successfully predicted.

Introduction

Ion-exchange equilibria has been a subject of investigation for over 50 years. Most of the earlier work was generally confined to binary ionic systems. Frequent occurrence of multicomponent systems in industrial practice makes the understanding of such systems very much desirable. As the introduction of each additional component in the system increases the experimentation many times, the need for predicting such data from somewhat more easily accessible binary data has long been felt. Creditable work

in this direction has been carried out by Dranoff and Lapidus,[1] Pieroni and Dranoff,[2] Smith,[3] Soldatov and Kharevich,[4] Meyer,[5] and Jasz and Lengyel.[6]

However, their work suffers from two main limitations: empirical methods were used in some of their correlations, and comparisons were made between experimentally observed binary equilibrium data and those deduced from the ternary experimental equilibrium data. Little attempt has been made to predict ternary equilibria from the binary data. Lack of information regarding resin-phase activity coefficients of ions in ternary systems, and an inadequate treatment of binary data, have often hampered further progress in this area.

David and coworkers[7,8] have used a single-particle radioactive-tracer technique (SPRT) in their experimental work on binary ion-exchange equilibria. This technique offers some unique advantages in the accurate analysis of ionic compositions in the resin phase, and also leads to a reduction of the number of experimental measurements.

The object of the present study was (i) to establish the use of SPRT technique for the measurement of ternary equilibrium relationship, and (ii) to examine the feasibility of predicting the ternary ion-exchange equilibria from binary data.

Five binary systems, *viz.*, Sr^{2+}–Mn^{2+}, Sr^{2+}–Cs^{+}, Mn^{2+}–Cs^{+}, Mn^{2+}–Na^{+}, Cs^{+}–Na^{+}, and two ternary systems, Sr^{2+}–Mn^{2+}–Cs^{+} and Mn^{2+}–Cs^{+}–Na^{+}, have been investigated. Dowex 50W-X8 resin was employed in the study which was conducted at 23°.

Theory

When ion-exchange resin is in equilibrium with an external solution, the electrochemical potential of any counterion in the two phases must be the same.

$$\bar{\eta}_i = \eta_i \tag{1}$$

where $\bar{\eta}_i$ is the electrochemical potential of the ith species in the resin phase. $\bar{\eta}_i$ is defined as

$$\bar{\eta}_i = \bar{\mu}_i + Z_i F \bar{\phi}$$

where $\bar{\mu}_i$ is the chemical potential of the ith species, $\bar{\phi}$ is the electric potential, Z_i is the valency of the ith counterion, and F is Faraday's constant.

From the above, it can be shown that

$$E_{\text{Don}} \equiv \bar{\phi} - \phi = \frac{1}{Z_i F}\left[RT \ln \frac{a_i}{\bar{a}_i} - \pi \bar{v}_i\right] \tag{2}$$

where E_{Don} is termed Donnan potential; a_i and $\bar{a}_i$ are the activities of the ith species in the solution and resin phase, respectively; $\bar{v}_i$ is the partial molal volume of the ith counterion; and π is the swelling pressure.

Donnan potential acts equally on all ions present in the system. Application of the above principle to counterions i and j leads to

$$\ln \left(\frac{\bar{a}_i}{a_i}\right)^{Z_j}\left(\frac{a_j}{\bar{a}_j}\right)^{Z_i} = \frac{\pi}{RT}(Z_i \bar{v}_j - Z_j \bar{v}_i)$$

However, the contribution of the right-hand side term is generally small and one may write

$$\left(\frac{\bar{a}_i}{a_i}\right)^{Z_j}\left(\frac{a_j}{\bar{a}_j}\right)^{Z_i} = 1 \tag{3}$$

Standard state for the solution phase is defined as hypothetical 1 m solution of solute, in which activity coefficient of the solute is unity. For all practical purposes, extremely dilute solutions approach the ideal case. Though the resin-phase standard state may also be defined in a similar manner, it is general practice to define it as the corresponding monoionic form of the resin in equilibrium with pure solvent outside. Mears and Thain[9] have observed that the deviation from ideality is not significant even when the resin is in equilibrium with dilute external solution. In the present study, solutions of 0.1 N anion concentrations were used.

For the above standard states, eq 3 can be written as

$$\left(\frac{\bar{a}_i}{a_i}\right)^{Z_j}\left(\frac{a_j}{\bar{a}_j}\right)^{Z_i} = K_j^{\,i} \tag{4}$$

$K_j^{\,i}$ is termed the equilibrium constant for the pair (i,j).

Introducing activity coefficient, γ, and mole fraction, X, in eq 4, one gets

$$K_j^{\,i} = \left(\frac{\bar{X}_i}{X_i}\right)^{Z_j}\left(\frac{X_j}{\bar{X}_j}\right)^{Z_i}\left(\frac{\bar{\gamma}_i}{\gamma_i}\right)^{Z_j}\left(\frac{\gamma_j}{\bar{\gamma}_j}\right)^{Z_i} \tag{5}$$

For a system having ions A and B, simplified forms of eq 5 can be obtained by dropping either the resin-phase activity coefficients or activity coefficients in both the phases

$$K_{C_B}^{\,A} = \left(\frac{\bar{X}_A}{X_A}\right)^{Z_B}\left(\frac{X_B}{\bar{X}_B}\right)^{Z_A} \tag{6}$$

$$K_{C_B'}^{\,A} = K_{C_B}^{\,A}\left(\frac{\gamma_B^{Z_A}}{\gamma_A^{Z_B}}\right) \tag{7}$$

where $K_{C_B}^{A}$ and $K_{C'_B}^{A}$ are termed selectivity coefficient and modified selectivity coefficient, respectively.

Ternary Ionic Equilibrium

For a system containing three counter ions A, B, and C, it can be shown that

$$(K_B^{\,A})^{Z_C}(K_C^{\,B})^{Z_A}(K_A^{\,C})^{Z_B} = 1 \tag{8}$$

The above relationship is called the triangle rule.[10]

Equation 4 is applicable to any ionic pair (i,j) in a multicomponent system. Since binary equilibrium constants are characteristic of the pairs, they may be used to predict ternary ion-exchange equilibria provided the resin-phase activity coefficients of ions in such a system are known. Activity coefficients of binary systems cannot be used as such because activity coefficient of an ion (say A) in one binary pair (A,B) and in another binary pair (A,C) having the same mole fraction of A, need not be the same, particularly due to the strong influence of the other ion. Assuming that every ion present in a system makes only its own contribution of the binary pair toward the activity coefficient, one can define a weighted average activity coefficient of ions in the resin phase as

(1) J. S. Dranoff and L. Lapidus, *Ind. Eng. Chem.*, **49**, 1297 (1957); **50**, 1648 (1958); **53**, 71 (1961).
(2) L. J. Pieroni and J. S. Dranoff, *AIChE J.*, **9**(1), 42 (1963).
(3) S. E. Smith, *Eng. Bull. Purdue Univ., Eng. Ext. Ser.*, **132** pt 2, 932 (1968).
(4) V. S. Soldatov and O. F. Kharevich, *Dokl. Akad. Nauk. Beloruss. SSR*, **12**(2), 140 (1968).
(5) W. Meyer, *Nucl. Sci. Abstr.* **21**(1), 20 (1967); Ph.D. Thesis, Oregon State University, 1964.
(6) A. Jasz and T. Lengyel, *Acta Chim. Acad. Sci. Hung.*, **33**, 395 (1962).
(7) J. C. Kuo and M. M. David, *AIChE J.*, **9**(3), 365 (1963).
(8) M. G. Rao and M. M. David, *AIChE J.*, **10**, 213 (1964).
(9) P. Mears and J. F. Thain, *J. Phys. Chem.*, **72**, 2789 (1968).
(10) R. M. Barrer and J. D. Falconer, *Proc. Roy. Soc., Ser. A*, **236**, 227 (1956).

$$\bar{\gamma}_i = \sum_{\substack{k=1 \\ k\neq i}}^{n} \frac{\bar{\beta}_k}{\sum_{\substack{j=1 \\ j\neq i}}^{n} \bar{\beta}_j} \bar{\gamma}_i \Bigg|_{ik} \qquad (9)$$

where $\bar{\beta}_i$ is the equivalent ionic fraction in the resin phase of ion i and n is the number of components (three) in the system.

Experimental Procedure

In the SPRT technique, a single resin bead is employed for the equilibrium measurements. After a careful examination under a microscope, resin beads, without any cleavages or blemishes and in the size range of 0.80–1.20 mm in diameter, were selected from a batch of Dowex 50W-X8 resin. Experimental details regarding the handling of a single resin bead, tagging it with a radioactive tracer, and the procedure for the measurement of capacity of a single resin bead are given elsewhere.[8]

A single resin bead in a particular cationic form is tagged with the corresponding radioactive isotope and is equilibrated with accurately measured quantity (0.5–1.0 ml) of 0.1 N solution of a known composition, in a 1.7-cm diameter polyethene vial with a snap-in cap. The total count rate, in counts per minute (CPM), of the resin bead and solution is measured by means of a scalar, scintillation detector, and a well-shield assembly. After equilibration for approximately 24 hr, the resin bead is removed from the solution, thoroughly washed with double-distilled water, and transferred to another vial having a geometry similar to the one previously used. The count rate of the bead is again measured. From a reduction in its count rate, one can calculate the fraction of the tagged ion in the resin phase at equilibrium as follows

$$\text{fraction} = \frac{\text{CPM of bead}}{\text{CPM of (bead + solution) − CPM of bead}} \times \frac{\text{capacity of bead}}{\text{equivalents of the ion in the feed solution}}$$

Correction for the background activity will have to be applied to the count rates. Experimentation may either be performed with one bead at a time or a number of beads at the same time. In case only one bead is used, one ionic fraction can be determined at a time. Fractions of other counterions in the resin phase can be obtained by tagging the bead in different ionic forms and equilibrating with 1 ml of solution of the same composition as used earlier. However, when a number of beads at a time are used, beads in different ionic forms can be equilibrated separately and individually, with the same external solution in different vials. Each bead gives one ionic fraction. Both the methods, when used on a test run, produced identical results.

In the present study, a number of beads were used to obtain the equilibrium data. The data were reproducible within ±2%. Data for the Sr^{2+}–Cs^{+} binary equilibrium in the present study were compared with these obtained by Meyer[5] who employed a liquid-scintillation technique. The agreement was excellent. Similarly, data for the Na^{+}–C^{+} binary equilibria in the present study compared very well with the data of Jasz and Lengyel.[6] Though only one ionic fraction in a binary and two ionic fractions in a ternary system completely define the resin-phase composition, in the present study all the fractions were experimentally determined individually and the sum total was found to be close to unity.

Results and Discussion

Ion-exchange isotherms for various binary systems under investigation are presented in Figures 1–5. Ternary ion-exchange equilibrium data are shown as per the representation of Streat and coworkers[11] in Figures 6 and 7. In ternary diagrams, loci of resin-phase compositions corresponding to a constant solution phase fraction of one of the species have been plotted. Intersection of two lines in the ternary plots, corresponding to two constant ionic fractions in the solution phase, fixes the ternary resin-phase composition. All data were obtained at a solution phase anionic concentration of 0.1 N.

Selectivity sequence of ions under investigation was found to be $Sr^{2+} > Mn^{2+} > Cs^{+} > Na^{+}$. This is in full accord with results obtained by the earlier research workers[12] and supports the effects of valency and ionic solvation on selectivity.

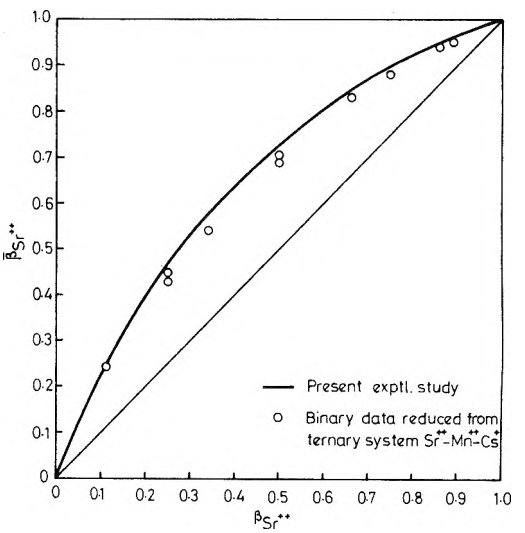

Figure 1. Binary equilibrium isotherm for the system Sr^{2+}–Mn^{2+}–Dowex 50W-X8.

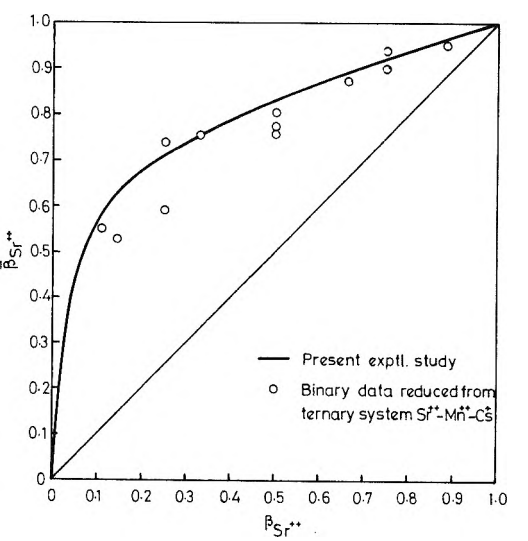

Figure 2. Binary equilibrium isotherm for the system Sr^{2+}–Cs^{+}–Dowex 50W-X8.

(11) B. A. Bennet, F. L. D. Cloete, and M. Streat, "Ion Exchange in Process Industries," Society of Chemical Industry, London, 1970, p 182.
(12) F. Helfferich, "Ion Exchange," McGraw-Hill, New York, N.Y., 1962, Chapter 5.

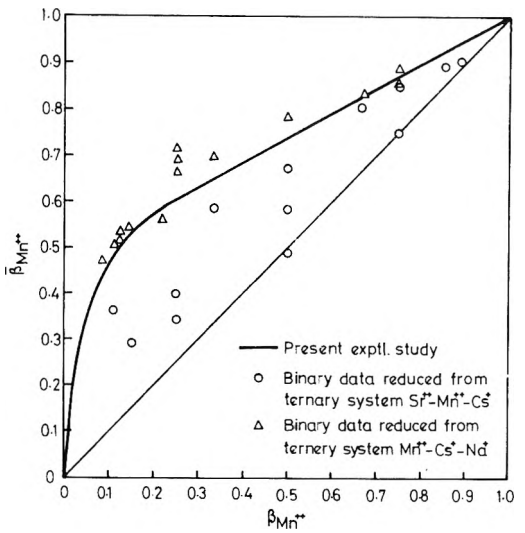

Figure 3. Binary equilibrium isotherm for the system Mn^{2+}–Cs^{+}–Dowex 50W-X8.

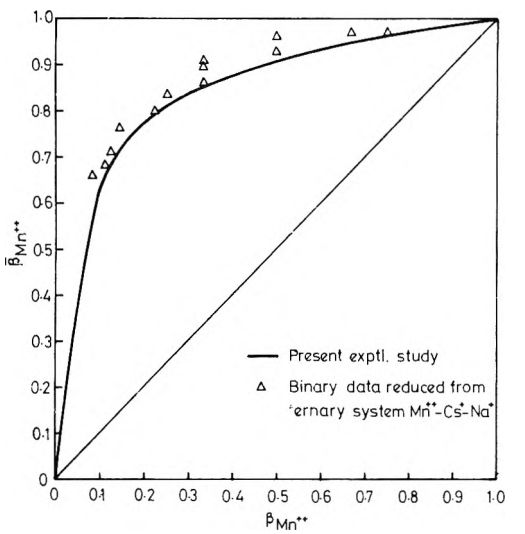

Figure 4. Binary equilibrium isotherm for the system Mn^{2+}–Na^{+}–Dowex 50W-X8.

Selectivity coefficients, as defined by eq 6 for binary equilibria, varied widely with solution phase composition. The variation with external solution composition was less in case of homovalent and more for heterovalent systems. Incorporation of solution phase activity coefficients, as indicated by eq 7, did not show much improvement. This indicates a strong dependence of resin-phase activity coefficients on ionic composition and that the ratio $(\bar{\gamma}_A{}^{Z_B}/\bar{\gamma}_B{}^{Z_A})$ does not remain constant over the entire composition range.

In the light of the above observation, and since data reported in literature on resin-phase activity coefficients are very scarce, an attempt was made to predict them from our experimental binary data. Hogfeldt, *et al.*,[13] and Argersinger, *et al.*,[14] derived thermodynamically rigorous expressions for resin-phase activity coefficients. They assumed the ion exchanger as a solid solution of resinates. The expressions are

$$Z_B \ln \bar{\gamma}_A = -\bar{\beta}_B \ln K_{C'_B}{}^{A} + \int_{\bar{\beta}_A}^{1} \ln K_{C'_B}{}^{A} \, d\bar{\beta}_A \quad (10)$$

$$Z_A \ln \bar{\gamma}_B = +\bar{\beta}_A \ln K_{C'_B}{}^{A} - \int_{0}^{\bar{\beta}_A} \ln K_{C'_B}{}^{A} \, d\bar{\beta}_A \quad (11)$$

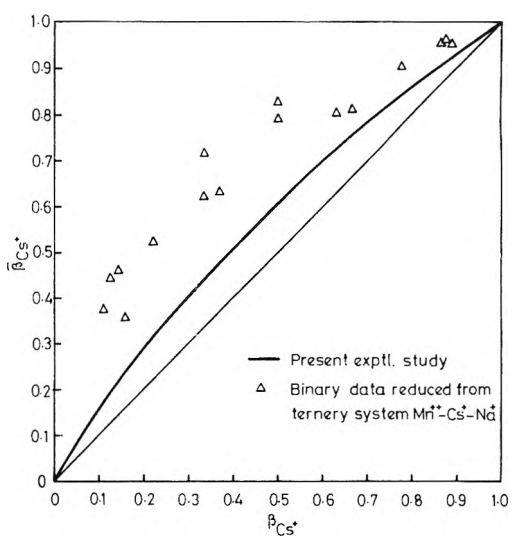

Figure 5. Binary equilibrium isotherm for the system Cs^{+}–Na^{+}–Dowex 50W-X8.

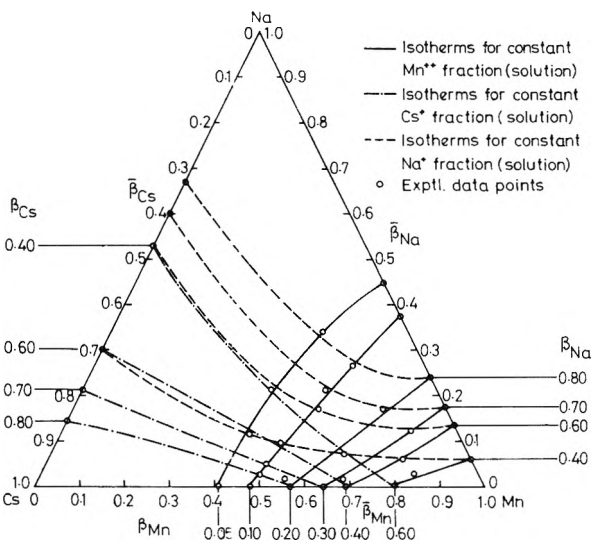

Figure 6. Ternary equilibrium diagram for the system Na^{+}–Cs^{+}–Mn^{2+}–Dowex 50W-X3.

The corresponding expression for thermodynamic equilibrium constant is

$$\ln K_B{}^{A} = \int_0^1 \ln K_{C'_B}{}^{A} \, d\bar{\beta}_A \quad (12)$$

where $\bar{\beta}_A$ and $\bar{\beta}_B$ are the equivalent fractions of ions A and B, respectively, in the resin phase.

Binary equilibrium constants and the resin-phase activity coefficients of ions in binary pairs were calculated using the above expressions. Plots of activity coefficients *vs.* equivalent ionic fractions in the exchanger are shown in Figures 8–12. It is clear that activity coefficients of an ion vary strongly from pair to pair depending upon the nature of the other ion present. Binary equilibrium constants are presented in Table I.

The triangle rule defined by eq 8 was not found to be applicable for the component binaries. In fact, it failed by a factor of 2.

(13) E. Hogfeldt, E. Ekedhal, and L. G. Sillen, *Acta Chem. Scand.*, **4**, 1471 (1950).
(14) W. J. Argersinger, A. W. Davidson, and O. D. Bonner, *Trans. Kansas Acad. Sci.*, **53**, 404 (1950); *J. Amer. Chem. Soc.*, **74**, 1044 (1952).

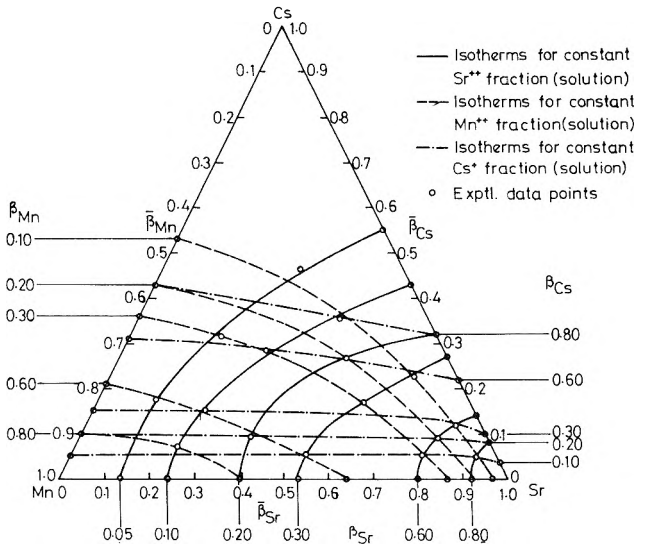

Figure 7. Ternary equilibrium diagram for the system Cs^+–Mn^{2+}–Sr^{2+}–Dowex 50W-X8.

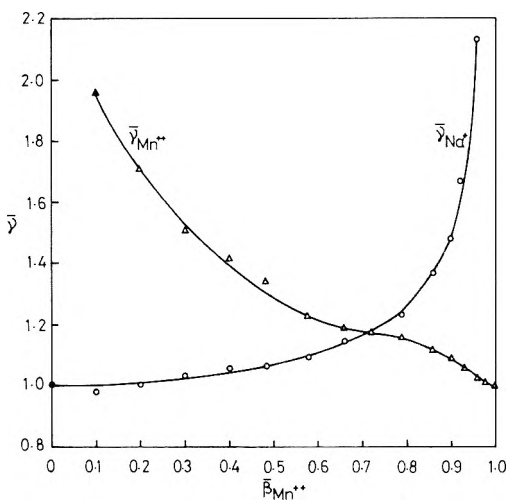

Figure 8. Activity coefficients of the ions in the system Mn^{2+}–Na^+–Dowex 50W-X8.

TABLE I: Thermodynamic Equilibrium Coefficients of Binary Systems

System A	B	K_B^A	System A	B	K_B^A
Mn^{2+}	Na^+	37.02	Mn^{2+}	Cs^+	8.53
Sr^{2+}	Cs^+	20.84	Cs^+	Na^+	1.69
Sr^{2+}	Mn^{2+}	12.20			

Binary equilibrium data were also calculated from experimental ternary data neglecting the presence of the third ion. The data thus reduced are also shown in Figures 1–5. While Sr^{2+}–Cs^+ and Sr^{2+}–Mn^{2+} binaries reduced from Sr^{2+}–Mn^{2+}–Cs^+ ternary were fairly close to those experimentally observed, reduced Mn^{2+}–Cs^+ binary did not agree with the actual data (Sr^{2+} is the most selective ion in this ternary). A similar behavior was also observed with Mn^{2+}–Cs^+–Na^+ ternary system; reduced Cs^+–Na^+ binary data did not compare well with the experimental observations while those for the other two component binaries are in fair agreement with the experimental ones (Mn^{2+} is the most selective ion in this case). This observation is in variance with the hypothesis of some of the earlier research workers (ref 1–3, 5, 6) that binary equilibrium data can be predicted from ternary equilibrium obser-

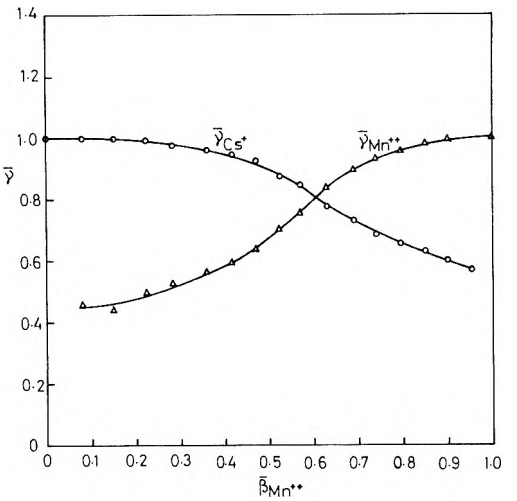

Figure 9. Activity coefficients of the ions in the system Mn^{2+}–Cs^+–Dowex 50W-X8.

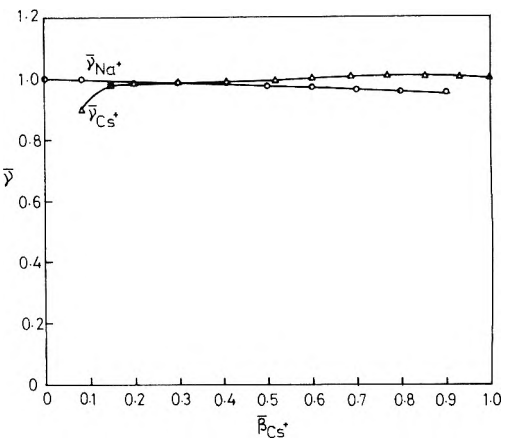

Figure 10. Activity coefficients of the ions in the system Cs^+–Na^+–Dowex 50W-X8.

TABLE II: Comparison of Experimental and Calculated Ternary Equilibrium Data for the Sr^{2+}–Mn^{2+}–Cs^+ System

Solution-phase composition (% equiv)			Resin-phase composition (% equiv) Exptl			Calcd		
Sr^{2+}	Mn^{2+}	Cs^+	Sr^{2+}	Mn^{2+}	Cs^+	Sr^+	Mn^{2+}	Cs^+
10.0	10.0	80.0	45.6	20.4	34.0	43.9	21.5	34.6
10.0	80.0	10.0	24.2	74.1	1.7	23.7	73.6	2.7
80.0	10.0	10.0	92.2	4.9	2.9	93.3	4.2	2.5
20.0	20.0	60.0	50.3	22.7	27.0	52.9	23.7	23.4
20.0	60.0	20.0	40.6	55.1	4.3	42.3	51.3	6.4
60.0	20.0	20.0	79.1	18.2	2.7	82.8	11.0	6.2
30.0	60.0	10.0	54.0	44.6	1.4	53.8	43.5	2.7
60.0	30.0	10.0	80.8	16.6	2.6	81.2	16.2	2.6
10.0	60.0	30.0	26.1	62.5	11.4	26.7	62.4	10.9
60.0	10.0	30.0	82.8	5.9	11.3	84.3	5.8	9.9
10.0	30.0	60.0	33.0	40.6	26.4	34.1	41.0	24.9
30.0	10.0	60.0	71.8	9.9	18.3	65.6	10.9	23.5
33.3	33.3	33.3	58.7	23.3	18.0	62.1	26.0	11.9
5.0	60.0	35.0	14.1	38.5	17.4	15.8	70.5	13.7
5.0	30.0	65.0	20.3	48.5	31.2	21.6	49.5	28.9
5.0	10.0	85.0	30.5	23.0	46.5	30.8	29.1	40.1

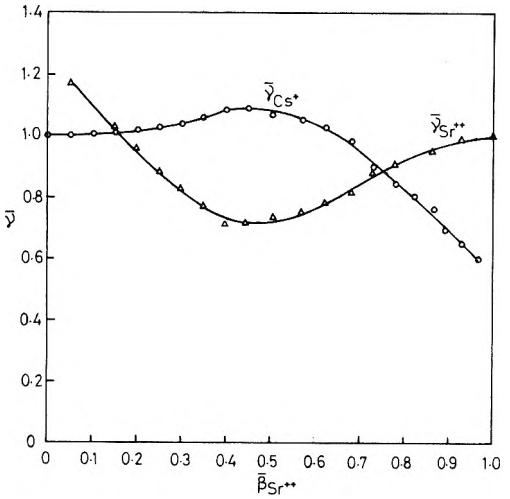

Figure 11. Activity coefficients of the ions in the system Sr^{2+}–Cs^+–Dowex 50W-X8.

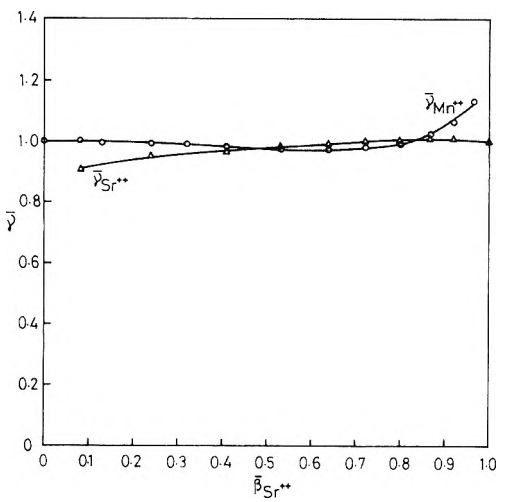

Figure 12. Activity coefficients of the ions in the system Sr^{2+}–Mn^{2+}–Dowex 50W-X8.

TABLE III: Comparison of Experimental and Calculated Ternary Equilibrium Data for the Mn^{2+}–Cs^+–Na^+ System

Solution-phase composition (% equiv)			Resin-phase composition (% equiv)					
			Exptl			Calcd		
Mn^{2+}	Cs^+	Na^+	Mn^{2+}	Cs^+	Na^+	Mn^{2+}	Cs^+	Na^+
10.0	10.0	80.0	57.7	15.9	26.4	57.8	11.1	31.1
10.0	20.0	70.0	54.1	24.0	21.9	53.3	18.1	28.6
10.0	30.0	60.0	54.8	28.3	16.9	50.2	24.1	25.7
30.0	10.0	60.0	77.0	5.5	17.5	83.1	5.6	11.3
10.0	60.0	30.0	49.3	41.2	9.5	45.1	40.7	14.2
30.0	60.0	10.0	67.9	30.6	1.5	72.8	25.4	1.8
10.0	70.0	20.0	49.5	45.5	5.0	44.1	46.2	9.7
20.0	70.0	10.0	55.0	43.3	1.7	60.8	36.3	2.9
10.0	80.0	10.0	49.3	48.3	2.4	43.1	52.0	4.9
60.0	20.0	20.0	83.0	14.1	2.9	95.4	3.7	0.9
40.0	20.0	40.0	78.6	15.4	6.0	86.4	7.9	5.7
20.0	40.0	40.0	65.7	28.7	5.6	65.7	22.2	12.1
5.0	15.0	80.0	47.1	18.9	34.0	35.5	20.2	44.3
5.0	35.0	60.0	42.1	36.3	21.6	30.6	34.7	34.7
5.0	60.0	35.0	41.9	46.7	11.4	29.4	49.5	21.1

TABLE IV: Comparison of Experimental and Calculated Ternary Equilibrium Data for the Ba^{2+}–Cu^{2+}–Na^+ System

Solution-phase composition (% equiv)			Resin-phase composition (% equiv)					
			Exptl[a]			Calcd		
Ba^{2+}	Cu^{2+}	Na^+	Ba^{2+}	Cu^{2+}	Na^+	Ba^{2+}	Cu^{2+}	Na^+
15.0	5.0	80.0	94.0	3.4	2.6	95.3	2.2	2.5
15.0	15.0	70.0	89.3	8.0	2.7	89.4	7.7	2.9
5.0	5.0	90.0	81.7	11.8	6.5	82.3	6.9	9.9
5.0	15.0	80.0	66.4	33.6	0.0	72.1	18.8	9.1
30.0	10.0	60.0	92.7	7.3	0.0	94.4	3.7	1.9
20.0	20.0	60.0	89.7	10.3	0.0	88.3	9.1	2.6
10.0	30.0	60.0	70.9	28.0	1.1	80.0	15.9	4.1
25.0	5.0	70.0	89.9	10.1	0.0	95.8	2.1	2.1
10.0	20.0	70.0	82.8	17.2	0.0	84.3	11.5	4.2
20.0	10.0	70.0	92.7	7.3	0.0	92.8	4.8	2.4
25.0	15.0	60.0	93.8	6.2	0.0	91.6	6.2	2.2
5.0	10.0	85.0	73.8	19.7	6.5	76.6	13.8	9.6
10.0	5.0	85.0	93.0	0.4	6.6	93.7	2.7	3.6
2.5	2.5	95.0	75.6	8.4	16.0	68.1	7.5	24.4
2.5	30.0	67.5	36.6	63.4	0.0	39.9	47.4	12.7

[a] Reference 3.

vations by neglecting the presence of the third ion. According to the present study, the prediction of binary data for the pair not containing the most selective ion will not be satisfactory.

In the present investigation, attempts were made to predict ternary ion-exchange equilibria from the component binaries. Binary equilibrium constants, calculated earlier, were utilized for this purpose. Solution-phase activity coefficients were calculated using the law of constant ionic strength. Resin-phase activity coefficients of ions in a ternary system were calculated from their corresponding values in the component binary pairs, using eq 9. Note that an iterative procedure will be required to calculate the resin-phase activity coefficients as the resin-phase composition is not initially known. As an approximation for the first trial, one can ignore the effect of activity coefficients in the resin phase. A knowledge of equilibrium distribution of ions in any two binary pairs of a ternary system should normally be sufficient. But, as the triangle rule failed, predictions from all three combinations did not give the same result. However, if the two binary pairs were so chosen to contain the most selective ion in each of them, the computed ternary data agreed very well with the experimental data. This is an important finding of the present study. The computations for the systems Sr^{2+}–Mn^{2+}–Cs^+ and Mn^{2+}–Cs^+–Na^+ are shown in Tables II and III, respectively.

The above procedure was used to predict the ternary data for the Ba^{2+}–Cu^{2+}–Na^+ system, studied by Smith.[3] The equilibrium data of Ba^{2+}–Cu^{2+}, Cu^{2+}–Na^+, and Ba^{2+}–Na^+ binaries used in the computations were obtained by Rai,[15] Subba Rao and David,[16] and Kuo and David,[7] respectively. Results of the computations are presented in Table IV. Again, there is a good agreement between the experimental and predicted equilibrium values.

Acknowledgments. The authors gratefully acknowledge the financial support rendered by the Council of Scientific and Industrial Research, India.

(15) J. H. Rai, Thesis University of Washington, Seattle, 1964.
(16) H. C. Subba Rao and M. M. David, *AIChE J.*, 3, 187 (1957).

Competitive Solvation of Magnesium Ion in Water–Acetone Solutions. A Proton Magnetic Resonance Study of the Hybrid Solvation Shells of Magnesium(II)

Flavio Toma,* Marc Villemin, and Jean Marie Thiéry

Département de Biologie, Centre d'Etudes Nucléaires de Saclay, 91190 Gif-sur-Yvette, France *(Received September 18, 1972)*

Publication costs assisted by the Commissariat à l'Energie Atomique

Magnesium ion solvation is studied in aqueous acetone solutions with a water-to-Mg(II) molar ratio ranging from 0 to 6. Complex spectra are observed for the proton magnetic resonance of water and acetone at low temperature (down to −95°). These spectra are interpreted in terms of a competitive solvation mechanism corresponding to the simultaneous equilibria between *hexacoordinated* Mg(II) solvation shells containing only water, only acetone, or both solvents (hybrid solvation shells). A simple ionic model of these different solvation shells accounts reasonably well for the observed chemical shifts of water and acetone protons.

Introduction

The knowledge of the interactions occuring in electrolyte solutions is outstandingly important for the comprehension of many biological processes.[1] Among the properties of ions in solution, the solvation shells of cations are of primary interest since they are involved in the interaction mechanism of metal ions with biological ligands.[2-4] The use of aqueous and nonaqueous organic solvents is now extensive in the physicochemical approach to conformations and interactions of different biological molecules as, *e.g.*, polypeptides,[5-7] nucleotides,[8] and biological dyes.[9-11] Since most of these systems require metal ions for their biological action, the knowledge of cation solvation in water and in pure or aqueous organic solution is often necessary. Ion solvation studies in binary or ternary mixtures containing water as one component at low concentration are particularly important since water is almost always present in the organic solutions of biological compounds even under the best experimental conditions. In such cases selective[12] or preferential solvation[13-15] or else competitive solvation[16,17] may occur which superimposes on other phenomena as, *e.g.*, ion pairing. The situation is further complicated because most biologically interesting cations as the alkaline and alkaline earth metals form labile solvation shells, so that a physical distinction between molecules in the first solvation shell and in the bulk solution becomes rather difficult.

A "magnetic distinction" among solvent molecules in the two environments may be provided in some cases by nuclear magnetic resonance which has been widely applied to the study of electrolyte solutions[18-21] and allows the investigation of chemical exchange phenomena which are fast at room temperature.[22] Under proper conditions two separate ^1H[19-21] or ^{17}O[23] resonance signals can be observed corresponding to solvent molecules bound to the metal ion and to free solvent molecules, respectively. This line separation technique provides a direct and almost unambiguous method for the measurement of the primary solvation numbers (n) of cations.[19,20,24] It allows, at the same time, a more detailed and quantitative description of solute–solvent and solute–solute interactions by the complete line shape analysis carried out with appropriate computer programs.[25-27]

Magnesium ion solvation has been studied in different systems by ^1H[24-31] and ^{17}O[32-33] nmr. Some data are also available on ^{25}Mg nmr.[34-36] In contrast to the different n

(1) L. P. Kayushin, Ed., "Water in Biological Systems," Consultants Bureau, New York, N.Y., 1969.
(2) A. S. Mildvan in "Enzymes: Kinetics and Mechanism," Vol. 2, P. D. Boyer, Ed., Academic Press, New York, N.Y., 1970, pp 446–536.
(3) P. George, R. J. Witonsky, M. Trachtman, C. Wu, W. Dorwart, L. Richman, W. Richman, F. Shurayh, and B. Lentz, *Biochim. Biophys. Acta*, **223**, 1 (1970).
(4) R. C. Phillips, P. George, and R. J. Rutman, *J. Amer. Chem. Soc.*, **88**, 2631 (1966).
(5) F. P. Pitner and D. W. Urry, *J. Amer. Chem. Soc.*, **94**, 1399 (1972).
(6) S. Fermandjian, J. L. Morgat, and P. Fromageot, *Eur. J. Biochem.*, **24**, 252 (1971).
(7) S. Fermandjian, D. Greff, and P. Fromageot, 3rd American Peptide Symposium, Boston, Mass., June 19–23, 1972.
(8) C. D. Barry, J. A. Glasel, A. C. T. North, R. J. P. Williams, and A. V. Xavier, *Biochem. Biophys. Res. Commun.*, **47**, 166 (1972).
(9) S. Shibata, Y. Ogihara, N. Kobayashi, S. Seo, and I. Kitagawa, *Tetrahedron Lett.*, **27**, 3179 (1968).
(10) P. C. Pham Van, J. C. Bouhet, J. M. Thiéry, and P. Fromageot, to be submitted for publication.
(11) R. E. Moore and P. J. Scheuer, *J. Org. Chem.*, **31**, 3272 (1966).
(12) H. Schneider in "Solute–Solvent Interactions" J. F. Coetzee and C. D. Ritchie, Ed., Marcel Dekker, New York, N.Y., 1969, pp 301–342.
(13) L. S. Frankel, C. H. Langford, and T. R. Stengle, *J. Phys. Chem.*, **74**, 1376 (1970).
(14) L. S. Frankel, T. R. Stengle, and C. H. Langford, *Chem. Commun.*, **17**, 393 (1965).
(15) J. Padova, *J. Phys. Chem.*, **72**, 796 (1968).
(16) A. Fratiello, R. E. Lee, V. M. Nishida, and R. E. Schuster, *Inorg. Chem.*, **8**, 69 (1969).
(17) A. Fratiello, V. Kubo, and R. E. Schuster, *Inorg. Chem.*, **10**, 744 (1971).
(18) C. Deverell, *Progr. Nucl. Magn. Resonance Spectrosc.*, **4**, 235 (1969).
(19) H. G. Hertz, G. Stalidis, and H. Versmold, *J. Chim. Phys.*, 177 (1969).
(20) H. G. Hertz, *Angew. Chem., Int. Edit. Engl.*, **9**, 124 (1970).
(21) J. F. Hinton and E. S. Amis, *Chem. Rev.*, **67**, 367 (1967).
(22) C. S. Johnson, Jr., *Advan. Magn. Resonance*, **1**, 33 (1965).
(23) See references cited in ref 19 and 20.
(24) A. Fratiello, R. E. Lee, V. M. Nishida, and R. E. Schuster, *J. Chem. Phys.*, **48**, 3705 (1968).
(25) S. Nakamura and S. Meiboom, *J. Amer. Chem. Soc.*, **89**, 1765 (1967).
(26) R. G. Wawro and T. J. Swift, *J. Amer. Chem. Soc.*, **90**, 2792 (1968).
(27) T. D. Alger, *J. Amer. Chem. Soc.*, **91**, 2220 (1969).
(28) J. H. Swinehart and H. Taube, *J. Chem. Phys.*, **37**, 1579 (1962).
(29) N. A. Matwijoff and H. Taube, *J. Amer. Chem. Soc.*, **90**, 2796 (1968).
(30) L. W. Harrison and T. J. Swift, *J. Amer. Chem. Soc.*, **92**, 1963 (1970).
(31) F. J. Vogrin, P. S. Knapp, W. L. Flint, A. Anton, G. Highberger, and E. R. Malinowski, *J. Chem. Phys.*, **54**, 178 (1971).

values observed for Mg(II) solvation either from measurements of the temperature dependence of water proton chemical shift in aqueous solutions[31] (which give the overall solvation numbers, *i.e.*, the primary and secondary solvation shell of cations and the anion solvation[37]) or from line width measurements,[38] the ^1H line separation technique shows that $n = 6$ for Mg(II) in all studied systems.[24-30] The results indicate that over a large temperature range stable hexasolvated shells are formed by Mg(II) with water,[29] methanol,[25] ethanol,[27] or ammonia,[30] respectively, in the corresponding pure solvents, and with water[24,26,29] or methanol[29] in aqueous or methanolic acetone solutions. Selective (or preferential) solvation of Mg(II) by water and methanol, respectively, is observed in the latter solutions since acetone does not compete either with water (as shown for other cations (ref 16, 17, 24, 39, and 40)) or with methanol and probably because the ligand/Mg(II) ratio has a much larger value than that required for complete solvation. When the ratio $[H_2O]/[Mg(II)]$ in organic solutions has a value close to six or smaller, the question arises whether Mg(II) holds the coordination number six and if so by which mechanism. We have shown[35] that in a water–acetone solution of magnesium perchlorate such as $[H_2O]:[Mg(II)] = 1:2$ the three peaks observed for the proton spectrum of water at low temperatures can be accounted for by an equilibrium involving at least three solvates: $[Mg(H_2O)_i(acetone)_{6-i}]^{2+}$ ($i = 1$ and 2) and $[Mg(acetone)_6]^{2+}$. We called the former hybrid solvation shells (HSS). According to the proposed mechanism all possible HSS ($i = 1$ to 5) must be present in the relative concentration range $0 < [H_2O]/[Mg(II)] < 6$.[35] A mean solvation number close to six was found for Mg(II) is this solution. Unambiguous assignment of water peaks was not possible at that stage. The possibility of observing separate HSS for Mg(II) in organic solution when $[H_2O]/[Mg(II)] < 6$ seemed important to us since in this laboratory work is in progress on the interactions of Mg(II) with different biological compounds as studied in aqueous organic systems. In order to confirm definitely our interpretation we extended our investigation to water–acetone solutions of magnesium perchlorate in the relative concentration range $0 < [H_2O]/[Mg(II)] \leq 6$. We were stimulated to carry on our work in this direction since a mechanism similar to that observed in aqueous acetone seems to be involved in Mg(II) solvation in aqueous methanol[25] as well as in Co(II)[41] and Ni(II) solvation[42] in the same system. Also recent epr investigations indicate the existence of Mn(II) HSS in different solvent mixtures.[43]

In the present article we are concerned with the results obtained for $0 < [H_2O]/[Mg(II)] \leq 6$ and with a semiempirical interpretation of the pmr spectra of these solutions in terms of the individual HSS of Mg(II) existing therein.

Experimental Section

(1) Chemical Preparation. Magnesium perchlorate hexahydrate (reagent grade) was recrystallized several times from doubly distilled water and was thereafter dehydrated by the previously described procedure.[35] The final water content was determined by the Karl Fischer reaction and was found to be 2.03%, *i.e.*, $[Mg(II)]:[H_2O] = 1:0.24$. Magnesium content was determined by titration with EDTA solutions using Black Eriochrome T as endpoint indicator of the reaction. Saturated solutions of the salt thus obtained were prepared in previously purified anhydrous acetone[35] (Merck reagent grade) and were filtered in order to eliminate the small amounts of MgO formed during thermal dehydration. After lyophilization of these solutions the salt contained 1.5% water ($[Mg(II)]:[H_2O] = 1:0.19$) and the amount of Mg(II) corresponded to $[Mg]:[ClO_4] = 1:2$. A stock 0.18 *m* solution of the salt thus obtained was prepared in dry acetone. Weighed amounts of water were added to different aliquots of this solution to obtain the required Mg(II)-to-water concentration ratios. Three solutions were prepared: $[Mg(II)]:[H_2O]:[Me_2CO] = 1:0.81:87.09$, $1:2.76:87.09$, and $1:4.58:87.09$. In the following text we will refer to these solutions as respectively 1:1, 1:3, and 1:5 solutions. A 0.28 *m* acetone solution of $Mg(ClO_4)_2 \cdot 6H_2O$ was also prepared and is referred to as the 1:6 solution. All solutions were prepared and handled in a glove box under a continuous flow of dry nitrogen. The nmr tubes were sealed and stored at low temperature when not used.

(2) Nmr Measurements. The 90-MHz pmr spectra were recorded on a Spectrospin KIS-2 spectrometer working under the same conditions as described in ref 35. The 100-MHz spectra were obtained with a Jeol JNM-PS 100 spectrometer and the 250-MHz spectrum was obtained with a Thomson-CSF TSN-250 spectrometer. Chemical shifts were measured with respect to TMS used as internal standard and are given within ±0.2 Hz. Each spectrum was recorded three to five times to ascertain that line shapes were reproducible and that thermal equilibrium was reached. Temperature values were determined each time before and after recording the spectrum by measurement of the chemical shift difference between OH and CH_3 protons of pure anhydrous methanol. Although the absolute temperature values thus obtained are not very accurate (*ca.* ±1°) the temperature stability of our samples during the measurements was better than 0.5°.

(3) Computer Analysis of Experimental Spectra. All spectra were digitalized by means of a Benson S.A. LNC 610 digital reader connected to a PDP-8 computer. In order to ensure a good line shape reproduction by digitalization, 700 to 800 points (1 point/0.1 Hz) were taken for each spectrum. Spectra were then studied on a PDP-12 computer connected to a 556 Tektronix dual-beam CR oscilloscope. The curve-fitting program allowed mixing of Lorentzian absorption and dispersion curves or alternatively of Gaussians and their first derivatives. Adjustment was checked either by visual comparison of the experimental and the calculated spectra or by inspection of their difference curve. The maximum deviation of the difference curve was within 1–2% of the maximum peak height. This gives an estimate of ±5% on the calculated areas of the spectra. The analysis of the 1:3 spectra of

(32) J. Neely and R. E. Connick, *J. Amer. Chem. Soc.*, **92**, 3476 (1970).
(33) R. E. Connick and K. Wuthrich, *J. Chem. Phys.*, **51**, 4506 (1969).
(34) M. Ellenberger and M. Villemin, *C. R. Acad. Sci., Ser. B*, **266**, 1430 (1968).
(35) F. Toma, M. Villemin, M. Ellenberger, and L. Brehamet, *Magn. Resonance Relat. Phenomena, Proc. Congr. AMPERE, 16th, 1970*, 317 (1971).
(36) R. G. Bryant, *J. Magn. Resonance*, **6**, 159 (1972).
(37) R. W. Creekmore and C. N. Reilley, *J. Phys. Chem.*, **73**, 1563 (1969).
(38) T. J. Swift and W. G. Sayre, *J. Chem. Phys.*, **44**, 3567 (1966).
(39) A. Fratiello, R. E. Lee, and R. E. Schuster, *Chem. Commun.*, **2**, 37 (1969).
(40) A. Fratiello, V. M. Nishida, R. E. Lee, and R. E. Schuster, *J. Chem. Phys.*, **50**, 3624 (1969).
(41) Z. Luz and S. Meiboom, *J. Chem. Phys.*, **40**, 1058 (1964).
(42) Z. Luz and S. Meiboom, *J. Chem. Phys.*, **40**, 1066 (1964).
(43) L. Burlamacchi, G. Martini, and M. Romanelli, *J. Chem. Phys.*, to be submitted for publication.

water was carried out taking into account only the clearly distinguishable bands in the temperature range in which five signals are observed. The best fits were obtained with Lorentzian line shapes but in several cases better fits were obtained with a 10–20% dispersion mode. The origin of this can be ascribed to (i) the bad phase correction on the spectrometer; (ii) the inhomogeneity of the magnetic field, namely, bad corrections of the y and r^2 field gradients; (iii) the strong overlap of two (or more) bands having half-line widths comparable to their chemical shift difference and an intensity ratio smaller than 0.5 (see Discussion). In the conditions of our work we estimate the contribution of i and ii to be 5% maximum. When a dispersion contribution to the normal Lorentzian lineshape was necessary, the areas of the single experimental bands could not be obtained by the calculated values $I\Delta$ (where I is the intensity of the peak and Δ its half-line width at half-intensity). The "true" areas were then determined by taking into account in the computer calculations the normal Lorentzian line shape with the corresponding proper parameters plus the small band resulting from the difference curve. For this reason errors in peak areas do not exceed ±5%. No such problem was encountered in the analysis of the acetone signals of the 1:3 solution.

Results

The 90-MHz water spectrum of the 1:1 solution shows three resonance lines below −55° which coalesce beginning with the upfield peak as temperature rises (Figure 1). At −22° only one peak is observed which shifts to higher fields and becomes sharper at higher temperatures. The 100-MHz acetone spectrum of the same solution is composed of two signals below −70° (Figure 2). As demonstrated in our previous work[35] the low-field signal corresponds to acetone molecules bound to Mg(II) (its intensity is dependent on the salt concentration), the deshielding of acetone protons being consistent with Mg(II) solvation by acetone. At −75° the bound acetone peak is not shifted further downfield; for lower temperature solvation acetone gives the two resonance lines 2b and 2c. This suggests that acetone in the 1:1 solution participates in at least two different types of solvation shells of Mg(II). The solvated species represented by line 2c are clearly more abundant in this solution than the species corresponding to line 2b. The analogy between the water and acetone low-temperature spectra in the 1:1 solution is meaningful.

Five signals are observed in the 90-MHz spectrum of water in the 1:3 solution from −65° to the freezing point of the solution (Figure 3). Coalescence of the resonance signals occurs as usual regularly as the temperature rises, beginning with the upfield peak. At about −41° only one coalesced signal is observed which shifts to higher fields and sharpens as the temperature is increased. Two separate resonance lines are observed in the 100-MHz acetone spectrum of this solution from −75 to −80°. At this temperature the downfield peak (corresponding to acetone molecules in the solvation shell of Mg(II)) does not shift to lower fields. At −84° two resonance lines are found for bound acetone molecules (Figure 4). From the curve-fitting data of this spectrum (Table I) and the composition of the solution (1.54 mol of Mg, 4.27 mol of water, and 134.18 mol of acetone) it is calculated that 5.06 mol of acetone are bound to Mg(II). This gives the following ratios $[Mg(II)]:[H_2O]:[Me_2CO]$ = 1:2.77:3.28 from which a

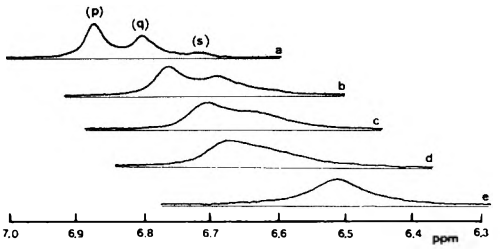

Figure 1. 90-MHz proton spectra of water in the 1:1 solution at −57 (a), −42 (b), −35.5 (c), −31.5 (d), and −18° (e). In Figures 1, 3, 5, 7, and 8, water peaks are labeled with the letters p, q, . . ., w. The same code is adopted throughout this article: *e.g.*, peak 3t refers to peak t of Figure 3; r stands for rotation side bands and w for free water.

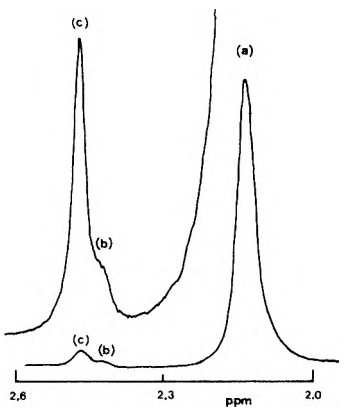

Figure 2. 100-MHz spectrum of acetone in the 1:1 solution at −90° (the upper spectrum was recorded at higher amplitude): (a) free acetone resonance signal; (b and c) bound acetone signals. In the Discussion, peak 2b refers to peak b of this figure.

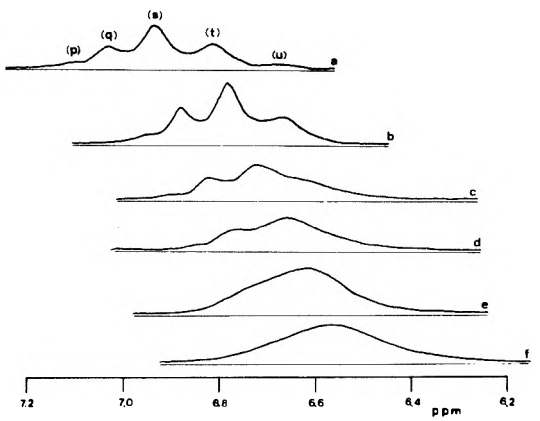

Figure 3. 90-MHz spectra of water in the 1:3 solution at −79.5 (a), −62 (b), −57 (c), −52.5 (d), −42.5 (e), and −40.5° (f). (See Figure 1 for peak notation.)

mean solvation number $\bar{n}$ = 6.05 is obtained for Mg(II). Furthermore 2.66 mol of acetone are found for peak 4b and 2.39 mol for peak 4c; these peaks are nearly equally populated in contrast to the corresponding peaks 2b and 2c for the 1:1 solution.

Below *ca.* −70° the pmr spectrum of water in the 1:5 solution shows four signals which coalesce regularly from the upfield to the lowfield peak as temperature increases (Figure 5). The spectrum of acetone in the same solution is composed of two peaks (Figure 6) from −82° to the freezing point of the solution (*ca.* −100°). The downfield peak 6b is assigned to acetone molecules in the solvation shells of Mg(II).

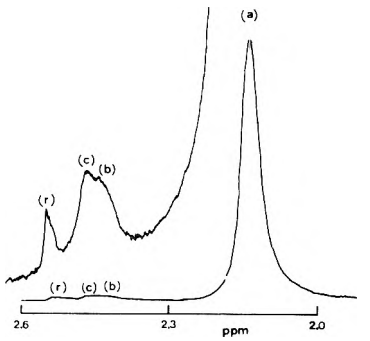

Figure 4. 100-MHz spectrum of acetone in the 1:3 solution at −84° (the upper spectrum was recorded at higher amplitude): (a) free acetone signal, (b and c) bound acetone signals, (r) rotation side band. (See Figures 1 and 2 for peak notation.)

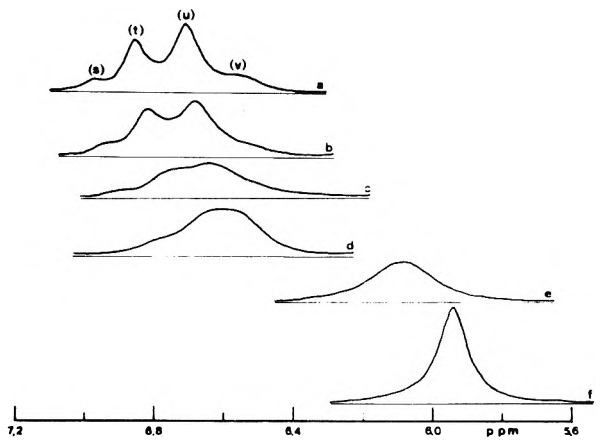

Figure 5. 90-MHz spectra of water in the 1:5 solution at −74.5 (a), −70.5 (b), −68 (c), −65 (d), −35.5 (e), and −23.5° (f). (See Figure 1 for peak notation.)

TABLE I: Curve-Fitting Data of the 100-MHz Spectrum of Acetone in the 1:3 Solution at −84° [a]

Peak	δ	Δ	I
4a	2.14	2.1	29 000
4b	2.43	2.7	466
4c	2.47	2.2	514

[a] Peaks 4a, 4b, and 4c are labeled in Figure 4. The δ values are given in ppm; Δ are the half-line widths at half-maximum height measured in Hz. The intensities (I) are given in arbitrary units.

In the 1:6 solution water gives a unique pmr signal from room temperature to *ca.* −70°. This signal is shifted to low fields and broadens considerably as the temperature decreases. Below −75° four resonance lines appear (Figure 7); the separation of 7w from 7t, 7u, and 7v resonances occurs in the temperature range from −75 to −77°. At lower temperatures the whole spectrum shifts to lower fields while the chemical shift difference between 7w and 7v remains approximately constant (Table II). Correspondingly, the pmr spectrum of acetone in the 1:6 solution below −90° is characterized by a shoulder on the low-field side of the acetone peak (not reported here). The shoulder coalesces at higher temperatures and cannot be better resolved down to −95° (freezing point of the solution). The δ value of peak 7w corresponds with a good approximation to the water chemical shift in aqueous acetone at the same water concentration and temperature. We assign peak 7w to "free" water in the 1:6 solution,

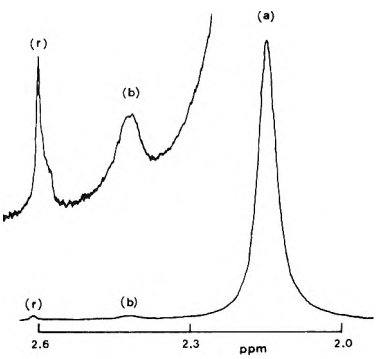

Figure 6. 100-MHz spectrum of acetone in the 1:5 solution at −91° (the upper spectrum was recorded at higher amplitude): (a) free acetone signal, (b) bound acetone signal, and (r) rotation side band. (See Figures 1 and 2 for peak notation.)

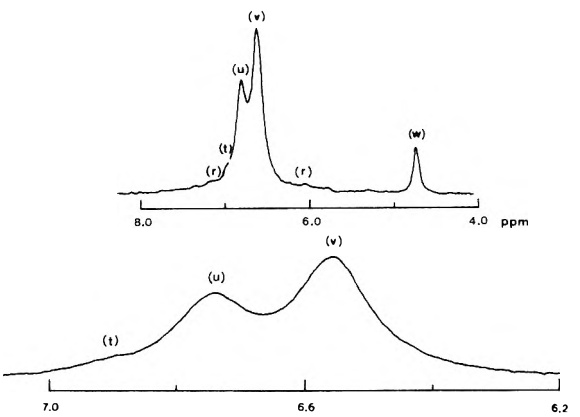

Figure 7. 90-MHz spectrum of water in the 1:6 solution at −88.5°; the lower spectrum (recorded on an expanded scale) clearly shows three resonance lines for the bound water. (See Figure 1 for peak notation.)

i.e., to water molecules which do not participate directly in Mg(II) solvation.

The above results on proton resonance of water in the 1:1, 1:3, 1:5, and 1:6 solutions and the previous results on the 1:0.5 solution[35] are summarized in Table II. It is clear that by "summing up" the water signals (corresponding to molecules bound to Mg(II)) of the different spectra at the same temperature a six peak spectrum is obtained. This is the minimum number of peaks expected for all the hydrated solvation shells $[Mg(H_2O)_i(Me_2C{-}O)_{6-i}]^{2+}$ (i = 1 to 6) simultaneously present in these water acetone solutions, six more lines being theoretically possible if one takes into account the different stereoisomers for i = 2, 3, or 4 and the chemical nonequivalence of water molecules in two of these isomers and for i = 5.[35] As shown previously, the temperature dependence of water chemical shifts in the above solutions is accounted for by hydrogen bond interactions between molecules in the first and second solvation shells.[35]

Discussion

The features of water and acetone spectra in 1:1, 1:3, 1:5, and 1:6 solutions strongly support our previous assumption of the existence of Mg(II) hybrid solvation shells in these solutions.[35] The multiple spectral pattern observed for water must arise from the simultaneous presence of different solvation shells since it is likely that, except in the 1:6 solution, no free water can exist in these

TABLE II: Nmr Parameters of Water Peaks in Different Solutions[a]

Peak symbols / Peak assignments		p WA_5	q W_2A_4	s W_3A_3	t W_4A_2	u W_5A	v W_6	w Free water
Solutions	Data							
1:0.5[b]	δ	7.17	7.09	6.97				
	$d\delta/dT$	−0.0093	−0.0090	−0.0087				
1:1	δ	7.20	7.12	7.01				
(Figure 1)	$d\delta/dT$	−0.0090	−0.0088	−0.0093				
1:3	δ	7.14	7.12	7.01	6.89	6.73		
(Figure 3)	$d\delta/dT$	−0.0083	−0.0096	−0.0097	−0.0085	−0.0086		
1:5	δ			7.01	6.89	6.74	6.57	
(Figure 5)	$d\delta/dT$			−0.0094	−0.0101	−0.0087	−0.0074	
1:6	δ				6.88	6.73	6.55	4.74
(Figure 7)	P_r				4.7	24.8	60.5	10.0
1:6	δ				6.76	6.61	6.45	4.59
(−77.0°)	P_r				4.0	35.6	48.6	11.8

[a] In stoichiometric formulas, Mg(II) has been omitted for simplicity: *e.g.*, W_4A_2 represents $[Mg(H_2O)_4(Me_2CO)_2]^{2+}$. The δ (ppm) values are relative to −88.5° for the first four solutions and to −88.5 and −77.0° for the 1:6 solution. The slopes $d\delta/dT$ (ppm/degree) were obtained either by linear least-squares fittings of the δ values directly read on the experimental spectra (1:1 and 1:5 solutions) or by complete curve fittings in the case of the 1:0.5[35] and 1:3 solutions. The relative populations (P_r) for the 1:6 solutions (at −88.5 and −77.0°) were obtained from the curve-fitting data by calculating the ratio of the area of each peak to the overall area of the spectrum. [b] Reference 35.

solutions (the relative chemical shifts between free and bound water range from 2 to 3 ppm (ref 24, 26, 29, and 35)). The chemical inequivalence of bound water molecules cannot be ascribed to ion pairing. Penetration of perchlorate ions in the first solvation shell of Mg(II) is in fact excluded since the mean solvation number is very close to six in all these solutions even at low water concentration where the ion pairing is expected to be the most effective: $\bar{n} = 6.0$ in the 1:3 solution and $\bar{n} = 5.9$ in the 1:0.5 solution (bound acetone in this solution was redetermined by the more accurate computer method described in this paper).

The dependence of water spectra on water concentration is that expected in presence of HSS formed by a solvent competition mechanism between water and acetone giving rise to a stepwise complex formation

$$[Mg(H_2O)_{i-1}(Me_2CO)_{6-(i-1)}]^{2+} + H_2O \rightleftarrows [Mg(H_2O)_i(Me_2CO)_{6-i}]^{2+} + Me_2CO \quad (1)$$

where the hydration number i ranges from 1 to 6. When the ratio $[H_2O]/[Mg(II)]$ is very small (and tends to zero in the limiting case) the monohydrated shell $[Mg(H_2O)(Me_2CO)_5]^{2+}$ is expected to predominate in solution in equilibrium with small amounts of the dihydrated shell $[Mg(H_2O)_2(Me_2CO)_4]^{2+}$ and eventually of $[Mg(H_2O)_3(Me_2CO)_3]^{2+}$. This situation would give a proton spectrum for water (apart from chemical exchange effects) with at least three resonance lines one of which is much more populated than the others. Analogous considerations hold for bound acetone molecules which should give a similar spectrum. As the water to magnesium ratio is increased, the maximum distribution must occur for more highly hydrated shells. Consequently a predominant peak should appear together with a greater number of less populated peaks up to six signals at least. For water concentration such that complete solvation by water occurs to give $[Mg(H_2O)_6]^{2+}$, only two resonance lines (corresponding to bound and free water) should be observed with a relative chemical shift of *ca.* 2 ppm. An analogous mechanism has been observed for Co(II) solvation in aqueous methanol solutions[41] and seems to be effective for Mg(II) in the same system.[25] Moreover water protons in the different solvation shells have individual chemical shift values which should not differ considerably at the same temperature from one solution to another. As shown by the data of Table II this is verified for all solutions studied in this article. On the basis of the above considerations and from the observed populations of the water peaks the assignment of these peaks to individual HSS as given in Table II is quite probable.

TABLE III: Assignments of Water Peaks to Individual HSS in the 1:6 Solution[a]

Trial peak assignments	Experimental peaks			% deviation	
	7t	7u	7v	−88.5°	−77.0°
I	W_4A_2	W_5A	W_6	0.94	0.94
II	W_6	W_5A	W_4A_2	29.6	23.9
III	W_5A	W_5A	W_6	−0.45	−0.45
IV	W_6	W_5A	W_5A	5.63	8.92
V	W_3A_3	W_4A_2	W_5A	23.5	23.9
VI	W_5A	W_4A_2	W_3A_3	70.0	61.0

[a] Six trial peak assignments (I to VI) are tested with the population data at −88.5 and −77.0°, W_nA_m represents $[Mg(H_2O)_n(Me_2CO)_m]^{2+}$; peaks 7t, 7u, and 7v are those labeled in Figure 7; see Discussion for the definition and the interpretation of the per cent deviations.

TABLE IV: Assignments of Water Peaks 3p to 3u to Individual HSS in the 1:3 Solution (Figure 3)[a]

Trial peak assignments	Experimental peaks					R_{calcd}	R_{cor}
	3p	3q	3s	3t	3u		
I	WA_5	W_2A_4	W_3A_3	W_4A_2	W_5A	10.5	0.77
II	W_2A_4	W_3A_3	W_4A_2	W_5A	W_6	0.78	0.71
III	W_2A_4	W_3A_3	W_4A_2	W_5A	W_5A	0.79	0.73
IV	W_3A_3	W_4A_2	W_5A	W_5A	W_6	0.28	0.27
V	W_2A_4	W_3A_3	W_4A_2	W_4A_2	W_5A	1.06	0.97

[a] Five trial peak assignments (I to V) are tested with the population data of water and acetone peaks in the Mg(II) HSS at −88.5°; W_nA_m represents $[Mg(H_2O)_n(Me_2CO)_m]^{2+}$; R_{calcd} and R_{cor} are defined in the Discussion; their values should be compared with the experimental $R_{expt} = 0.89$.

The partial stability constants K_i of equilibria 1 could be determined from the populations of the water peaks as a function of water concentration. The results will be published further as well as the thermodynamic parameters of these chemical equilibria.

TABLE V: Calculated Electric Fields and Chemical Shifts of Water Protons in the HSS of Mg(II)[a]

	1	2		3		4		5		6
		α	β	α	β	α	β	α	β	
E_T, MV cm^{-1}	0.7233	0.7184	0.7162	0.7115	0.7090	0.7046	0.7024	0.6976	0.6954	0.6907
E_{OH}, MV cm^{-1}	0.6729	0.6696	0.6680	0.6646	0.6630	0.6597	0.6581	0.6547	0.6532	0.6498
δ_{calcd}, ppm	7.08	6.98	6.93	6.84	6.79	6.71	6.67	6.58	6.54	6.45
δ_{expt}, ppm	7.08	7.00		6.89		6.76		6.61		6.45

[a] Water chemical shifts (in ppm *vs.* TMS) at −77.0° have been calculated with the following equation: $\delta = \delta' - 11.29 \times 10^{-6} E_{OH} + 19.28 \times 10^{-12} E_T^2$ where $\delta' = 4.587$ ppm (*vs.* TMS) for free water at the same temperature in acetone solution. Symbols 1 to 6 indicate the number of water molecules in the solvation shells while α and β differentiate chemically nonequivalent water molecules; symmetry considerations lead to nine sterically different hydrate configurations corresponding to twelve chemically nonequivalent water molecules;[35] detailed computations reduce the number of nonequivalent water molecules to ten.[45]

These assignments are supported by calculations carried out with the relative populations (P_r) obtained by curve fitting. This is easily shown in the case of the 1:6 solution. The overall number of Mg(II) moles m^T_{calcd} present in this solution can be calculated with the analytical water concentration and with the P_r values of Table II (under the assumption that peak 7w corresponds to free water and peaks 7t, 7u, and 7v to individual solvation shells); in Table III, the per cent deviations $[(m^T_{calcd} - m^T_{expt})/m^T_{expt}]100$ show that water protons resonate at higher fields in more hydrated HSS, and that the assignment of peaks 7t, 7u, and 7v respectively to the tetra-, penta-, and hexahydrated solvation shells of Mg(II) is probably correct. Analogous calculations can be carried out for the 1:3 solution. In this case when peaks 3p to 3u are assigned to separate HSS one can calculate the ratio R_{calcd} between the mole number of acetone in the HSS and the mole number of acetone in $[Mg(Me_2CO)_6]^{2+}$ with the P_r data obtained by curve fitting and the analytical concentration of water and Mg(II) in the same solution. With the assumption that peak 4b corresponds to acetone molecules in $[Mg(Me_2CO)_6]^{2+}$ and peak 4c to acetone molecules in the HSS, the calculated values R_{calcd} displayed on Table IV can be compared with the experimental value $R_{expt} = 0.89$ obtained from Table I.

Under this assumption assignments II, III, and V of Table IV are the most probable. A refinement is obtained by considering that signal 4b represents the resonance of acetone molecules in {Mg(II)-(A)$_6$; Mg(II)-(W)-(A)$_5$; Mg(II)-(W)$_2$-(A)$_4$} while peak 4c corresponds to acetone in the remaining solvation shells. With these assumptions, the corrected values, R_{cor}, displayed on Table IV, show that assignment I is very probable and that the assignment of acetone peaks 4b and 4c is correct. The fact that assignments II, III, and V of Table IV seem to fit as well (analogously to assignments I and III of Table III) is not surprising. This must arise from the partial overlap of water signals which themselves result (except in the case of solvation shells with respectively one and six water molecules) from the composition of two (or three) strongly overlapping resonance lines. Very likely the latter have chemical shift differences of the same order of magnitude as their line widths and very different intensities (*i.e.*, one of the two stereoisomers present in solution predominates). This is consistent with the observed partial "dispersion character" of some of the resonance signals and is clearly demonstrated by the 250-MHz spectrum of the 1:1 solution at −65° (Figure 8). Peaks 8p, 8q, and 8s of this spectrum correspond to the three signals observed at 90 MHz for the same solution ($\delta_p - \delta_q = 0.08$ ppm; $\delta_q - \delta_s = 0.1$ ppm *vs.* 0.08 and 0.11 ppm extracted from the values of Table II). Peak 8q′ arises from the better line separation obtained at 250 MHz and represents the theoretically predicted second isomer of the dihydrated Mg(II) HSS ($\delta_q - \delta_{q'} = 0.03$ ppm) probably corresponding to the cis isomer (see further in the Discussion). Peak 8t corresponds to the tetrahydrated HSS ($\delta_s - \delta_t = 0.13$ ppm *vs.* 0.12 ppm resulting from values in Table II).

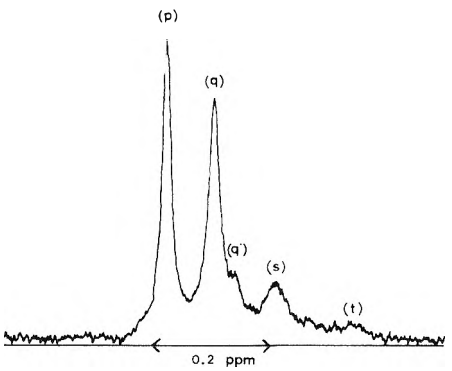

Figure 8. 250-MHz spectrum of water in the 1:1 solution at −65°: (p), (q), and (s) correspond to the water peaks observed at 90 MHz (Figure 1) and are assigned to the mono-, di-, and trihydrated shells respectively; (t) corresponds to the tetrahydrated shell while (q′) represents the second isomer of the dihydrated shell.

The above considerations are also consistent with the observed temperature dependence of the half-line widths at half-maximum height (Δ) of water peaks in the 1:3 solution as determined by computer curve fitting (Figure 9). Water molecules in the monohydrated HSS are not expected to exchange in the temperature range in which five separate signals are observed. In fact $\Delta_p \cong 1.5$ Hz from −88.5 to −52.5°. Water in the pentahydrated HSS undergoes very rapid chemical exchange as the temperature is increased; actually Δ_u increases with temperature (Figure 9). The temperature dependence of Δ_q, Δ_s, and Δ_t can be explained by assuming the following. At very low temperature (from −88 to −70°) "intermolecular exchange" represented by eq 1 is negligible while "intramolecular exchange" (*i.e.*, exchange between the two stereoisomers of the HSS with the same number of water molecules) is effective for the di-, tri-, and tetrahydrated HSS. The minima of the Δ *vs.* T curves for peaks q, s, and t would then correspond to very rapid intramolecular exchange. For higher temperatures intermolecular exchange occurs and coalescence of water peaks takes place regularly beginning from the upfield signal.

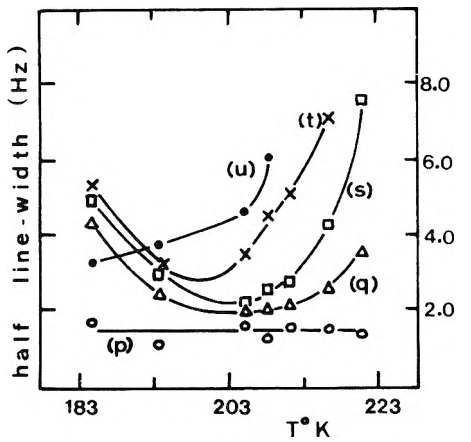

Figure 9. Temperature dependence of the half-line width at half-maximum height of water peaks in the 1:3 solution as obtained by computer curve fitting of the spectra. Symbols p, q, . . . , and u indicate the peaks labeled in Figure 3.

The deshielding of solvent protons in cation solvation shells can be explained theoretically by the interaction of the electric field E due to the ion with the proton nuclear moment[44] ($\delta = kE^2$ for an isolated proton). It seemed interesting to us to prove if a simple ionic model of the solvation shell could account qualitatively for the observed shifts and could substantiate to a certain extent the above phenomenological interpretation of water and acetone spectra in terms of hybrid solvation shells.

The electric field experienced by bound water molecules was calculated for the nine sterically different hydrated solvation shells by taking Mg(II) (assumed as a point charge) at the center of a regular octahedron (*cf.* Appendix[45] for the detailed discussion of the calculations). The results of Table V clearly show that the electric field acting on the protons is significantly different from one solvation shell to another and decreases from the mono- to the hexahydrated shell, thus indicating that the deshielding of water protons with respect to pure water is smaller for $[Mg(H_2O)_6]^{2+}$ and increases regularly up to $[Mg(H_2O)(A)_5]^{2+}$, which is in agreement with the previous peak assignment.

The chemical shift values of water in the different solvation shells were then calculated with the equation

$$\delta = aE_{OH} + bE_T^2 \qquad (2)$$

where E_T represents the strength of the electric field created on each proton by Mg(II) and the electric dipoles of the surrounding solvent molecules, and where E_{OH} is the component of E_T along the OH bonds. The second term of the right-hand side of eq 2 represents the Marshall-Pople's deshielding factor while the first term takes into account the contribution of OH bonds to the effective electric field acting on water protons.[46] The parameters a and b of eq 2 were determined by choosing as reference the δ values of the mono- and hexahydrated solvation shells with respect to free water in acetone solution at the same temperature and by putting in eq 2 the previously calculated proper values of E_{OH} and E_T (*cf.* Appendix[45] for the calibration of δ). The calculated δ values are *ca.* 0.05 ppm smaller than the experimental chemical shifts at the same temperature.

Nevertheless the differences $\delta_i - \delta_{i+1}$ (where i is the hydration number) agree fairly well with the experimental values (Table II). The calculated differences $\delta_{i\alpha} - \delta_{i\beta}$ (where α and β are defined in Table V) are of the same order of magnitude as the half-line widths observed for the corresponding resonance signals; which confirms the above conclusions.

Analogous calculations were carried out for acetone molecules bound to Mg(II) in the different solvation shells, except that the equation $\delta = kE_T^2$ was used, where E_T is the strength of the resultant electric field on the methyl protons. E_T is significantly smaller for $Mg(II)-(A)_6$ (0.2563 MV cm^{-1}) than for $Mg(II)(A)-(W)_5$ (0.2802 MV cm^{-1}), which is consistent with the above interpretation of the acetone spectra. The calculated δ values are less accurate in this case than calculated δ for water.

While this article was in preparation, Akitt has shown[47] that the experimental water chemical shifts in the solvation shells of Mg(II), Be(II), In(III), Al(III), and Sn(IV) in pure aqueous solution fit extremely well to shifts calculated on the basis of cationic electric fields. The author suggests that cationic hydration shifts are made up of a downfield contribution due to cationic electric fields and of a smaller upfield contribution due to hindered motion and orientation of water molecules in the complex. He also points out that nmr results seem to indicate, in general, no hydration for the anions. These conclusions support the assumptions made in this article.

Acknowledgments. We thank Mr. N. Esumi (Jeol France) for running the 100-MHz spectra published in this article and Mr. S. Clique for making it possible. Mr. J. J. Dunand (Thomson-CSF) kindly provided us with the 250-MHz spectrum.

(44) T. W. Marshall and J. A. Pople, *Mol. Phys.*, **1**, 199 (1958).
(45) The Appendix will appear following these pages in the microfilm edition of this volume of the journal. Single copies may be obtained from the Business Operations Office, Books and Journals Division, American Chemical Society, 1155 Sixteenth St., N.W., Washington, D. C. 20036. Remit check or money order for $3.00 for photocopy or $2.00 for microfiche, referring to code number JPC-73-1294.
(46) L. M. Jackmann and S. Sternhell, "Application of NMR Spectroscopy in Organic Chemistry," Pergamon Press, New York, N.Y., 1969, pp 67-69.
(47) J. W. Akitt, *Int. Symp. Nucl. Magn. Resonance Spectrosc., 2nd, 1972*, 1 (1972).

Hydrogen-Treated Graphitized Carbon Blacks. Limiting Isosteric Heats and Entropy Changes upon Adsorption of Hydrocarbons

Antonio Di Corcia* and Roberto Samperi

Istituto di Chimica, Università di Roma, 00185 Roma, Italy *(Received July 25, 1972)*

Publication costs assisted by Instituto di Chimica Analitica, Università di Roma

The study of the effects of hydrogen treatment at 1000° on graphitized carbon blacks was extended to the adsorption of nonpolar molecules. Before and after the hydrogen treatment on the Graphon and graphitized Sterling FT (Sterling FT-G) surfaces, the isosteric heats and entropies of adsorption at extremely low surface coverages of ethane, propane, isobutane, butane, pentane, and hexane were determined by chromatography using the eluted pulse technique. Our results were compared with some earlier determinations obtained by chromatography or by static methods. The abnormally high limiting heats and entropy changes of adsorption on untreated Graphon indicated the presence of a small fraction of surface geometric irregularities, where the interaction of an individual adsorbed molecule occurs with more than one plane of the adsorbing surface. Some experimental data suggest that surface heterogeneities can be identified as cavities with specific dimensions. These irregularities are not found on the Sterling FT-G surface, which we observed as almost completely free of strong adsorption sites. After the hydrogen treatment, the heats and entropy changes of adsorption on Graphon sharply decreased and their values are almost equal to those measured upon adsorption on Sterling FT-G. This agreement shows that the hydrogen treatment is effective in removing not only traces of surface oxides but also topographical irregularities on the carbon surface. The standard integral adsorption entropy values were calculated from retention volume measurements and by using a relation we derived. The close agreement between our values and those derived by a static method makes it evident that the gas chromatography technique can definitely also be of great use in the determination of adsorption entropies at very low surface coverages.

The preparation and the investigation of adsorbents with a highly homogeneous surface is of great interest in studying the nature of the forces that cause adsorption. Graphitized carbon blacks possess sufficiently homogeneous surfaces and they are widely used in obtaining adsorption data that are then compared with those theoretically predicted.

However, the nature of the adsorption may be significantly modified by the presence of small amounts of heterogeneous sites on the surface of these adsorbing materials. These heterogeneities are of two kinds. One is from chemical impurity made up of oxygen surface complex, presumably a burnt off residue left over from the heating of carbon blacks in order to produce graphitic carbons.[1] The other consists of geometric irregularities described in the studies by Graham[2] as being steps and recesses left in graphitized blacks. The same author calculated that on Graphon and P-33 (2700°), which are two well-known examples of graphitized blacks differing in their surface development, heterogeneous sites represent 1.24 and 0.10% of the total adsorption sites, respectively.

The influence of the chemical impurity on the adsorption of polar compounds has been extensively studied. In a previous paper,[3] we have shown that heating at 1000° in a stream of hydrogen is very effective in removing traces of oxides from the surfaces of some graphitized carbon blacks.

Geometric irregularities on a carbon surface might not be expected to produce very relevant effects. On the contrary, as Graham[2] reported that the adsorption of nitrogen on these sites gave an adsorption heat nearly twice that for the adsorption on the predominant, weaker sites. Kiselev[4] showed that hexane adsorbed on Graphon exhibited, at low surface coverages, an abnormally high initial adsorption heat of about 14 kcal/mol. Besides, the heat-coverage curves make it clear that surface inhomogeneities hamper a clear-cut manifestation of adsorbate–adsorbate interactions. Moreover, it was shown[5] that carbon tetrafluoride displays two-dimensional condensation on P-33 (2700°), but not on the less uniform Graphon.

In the last few years, gas–solid chromatography has received increasing attention especially in order to determine adsorption heats at very low surface coverages. By the introduction of high sensitivity detectors, heat determinations can be carried out at extremely small surface coverage. As a consequence, the presence on the surface of even a small number of sites with much greater adsorptive potentials can produce effects that tend to outweigh those of the rest of the surface. Therefore, to determine correctly thermodynamic data at zero coverage, the need for highly homogeneous adsorbing materials is particularly felt especially when using the chromatographic technique.

The purpose of this paper is to show that hydrogen treatment at 1000° is very effective in removing not only chemical heterogeneities but also geometric ones from the carbon surface. In order to obtain a full understanding of the nature of "active" sites and the effects of the hydrogen treatment on them, limiting heats and entropies of adsorption were measured on both treated and untreated Graphon and Sterling FT-G, for ethane, propane, isobutane, butane, pentane, and hexane. The determination of the thermodynamic data at extremely low surface coverages ($\theta \sim 1 \times 10^{-5}$) was made possible by gas chromatog-

(1) A. C. Zettlemoyer, *J. Colloid Interface Sci.*, **28**, 343 (1968).
(2) D. Graham, *J. Phys. Chem.*, **61**, 1310 (1957).
(3) A. Di Corcia and R. Samperi, *J. Chromatogr.*, **77**, 277 (1973).
(4) A. A. Isirikyan and A. V. Kiselev, *J. Phys. Chem.*, **66**, 205 (1962).
(5) D. Graham, *J. Phys. Chem.*, **62**, 1211 (1958).

raphy using the eluted pulse technique. Our results are compared here with some earlier determinations obtained either by gas chromatography or static methods. Finally, a simple relation correlating retention volume measurements with standard entropy changes upon adsorption is also given.

Experimental Section

The graphitized carbon blacks used in the present work, designated as Graphon and graphitized Sterling FT (Sterling FT-G), were provided by the Cabot Corp., Billerica, Mass. The two carbons listed above gave values for specific surface areas of 138 and 14.4 m^2/g based on nitrogen adsorption (BET) and by assigning for the cross-sectional area of N_2 a value of about 20 Å.[6] The hydrogen treatment was carried out as previously described.[3] After the treatment, surface areas of the two blacks were measured again. The surface area value for the Sterling FT-G did not show any appreciable change, while the specific surface of Graphon decreased giving a new values of 128 m^2/g. Before their use as packing materials, the original blacks were heated to 1000° and a stream of helium was passed through them in order to eliminate the possible presence of strongly adsorbed materials. After helium treatment, the blacks did not show appreciable changes in their surface developments.

A Carlo Erba gas chromatograph, Model GI (Milan, Italy), equipped with a flame ionization detector, was used. The instrument is designed to allow the injected samples to flow directly into the column. The adsorbing materials, first sieved through 60–80 mesh sieves, were packed in columns made from 2-mm i.d. glass tubings, from 1.5 to 2.0 m in length. As long as hydrogen treated materials were used, hydrogen, with a purity stated as 99.99%, was used as carrier gas. This technique was employed in order to hinder a possible slight reoxidation of the carbon surface by the oxygen[7] always present in gases of normal purity. On the other hand, when the untreated specimen was under observation the hydrogen had to be substituted by helium gas. This procedure was used because of a certain nonrepeatibility of the retention volume measurements, especially at relatively high temperatures, most likely due to a slight initial reaction between the hydrogen and the carbon surface. It was possible to keep the carrier gas flow rate to within ±0.5% during the course of a day. The temperature throughout any one set of chromatographic measurements was maintained to within ±0.1°. Repeated measurement of the retention volumes were in agreement to within 0.2–0.3%. The volumes of the hydrocarbon samples injected into the chromatographic columns were on the order of 10^{-4} cc. Where larger sized samples were injected into the column packed with untreated Graphon, a more or less pronounced asymmetry was noted in the peaks for well-retained hydrocarbons, thus indicating a departure of the adsorption isotherm from linearity. An approximate calculation of the surface coverage upon adsorption of hydrocarbons under our chromatographic conditions was made by means of a relation given by Beebe[8] which relates the surface coverage to chromatographic parameters. As an example, by using the value of 1.38 cc (stp)/g[9] for the volume of butane required to produce a monolayer coverage, we obtained a value of about 3×10^{-5}, corresponding to the final surface coverage which the pulse attained just before it was eluted from the end of the column, packed with treated Graphon at 326 K.

Discussion

Adsorption Heats from Chromatographic Data. The pressure p of gas in equilibrium with a given concentration of adsorbate is related to the isosteric heat of adsorption (q_{st}) by

$$\left(\frac{\partial \ln p}{\partial T}\right)_{n_a} = \frac{q_{st}}{RT^2} \tag{1}$$

where n_a is the number of adsorbed moles.

If the adsorption isotherm is linear (Henry's region) and the adsorbate behaves as an ideal gas both in the gas and the adsorbed phase, then the following known relations can be written

$$\pi = Kp$$

$$\pi S = n_a RT$$

and

$$pV = n_g RT$$

where π is the two-dimensional pressure (spreading pressure), K is the Henry's law constant, and S is the total surface area of the adsorbing material.

Then eq 1 can be rewritten as

$$\frac{d \ln K/T}{dT} = \frac{q_{st}}{RT^2}$$

and the K constant can be expressed as

$$K = \frac{n_a}{n_g}\frac{V}{S}$$

In a gas chromatographic column $V = V_c$, where V_c is the void space (dead volume) among the particles of the packing material. From the mass balance gsc theory we obtain $n_a/n_g = V_R'/V_0$, where V_R' is the volume of the carrier gas (passing through the column during elution of the sample) minus V_0, which is the volume needed to elute a nonadsorbable gas. If the volumes are expressed at zero pressure drop and column temperature (T_c), then, we have $V_0 \equiv V_c$.

Consequently

$$K = V_R'/S = V_s$$

and

$$\frac{d \ln V_s/T}{dT} = \frac{q_{st}}{RT^2} \tag{2}$$

where V_s is a term introduced by Kiselev to indicate the retention volume per unit of surface area of the adsorbent.

It follows from eq 2 that the isosteric heat of adsorption is given by plotting $\ln V_s/T_c$ or $\ln V_R'/T_c$ *vs.* T^{-1}. The correct calculation of V_R' has already been reported.[10]

Some authors derived the isosteric heat of adsorption by plotting, in place of $\ln (V_R'/T_c)$, $\ln t_R'$,[8,11,12] $\ln V_s$,[13] or $\ln (t_R'T_c/T_0)$,[14,15] where t_R' is the corrected retention time and T_0 is the room temperature.

The strict condition for using $\ln t_R'$ is that u_0, which is the volume flow rate measured in a device placed at the end of the column, remains constant as the temperature is altered.

(6) C. Pierce and B. Ewing, *J. Phys. Chem.*, **68**, 2562 (1964).
(7) R. Nelson Smith, J. Duffield, R. Pierotti, and J. Mooi, *J. Phys. Chem.*, **60**, 495 (1956).
(8) R. L. Gale and R. A. Beebe, *J. Phys. Chem.*, **68**, 555 (1964).
(9) S. E. Hoory and J. Prausnitz, *Trans. Faraday Soc.*, **63**, 455 (1967).
(10) E. A. Boucher and D. H. Everett, *Trans. Faraday Soc.*, **67**, 2720 (1971).
(11) G. Curthoys and P. A. Elkington, *J. Phys. Chem.*, **71**, 1477 (1967).
(12) P. A. Elkington and G. Curthoys, *J. Phys. Chem.*, **73**, 2321 (1969).
(13) H. Amariglio, *Surface Sci.*, **12**, 62 (1968).
(14) S. A. Greene and H. Pust, *J. Phys. Chem.*, **62**, 55 (1958).
(15) P. E. Eberly, Jr., *J. Phys. Chem.*, **65**, 68 (1961).

TABLE I: Limiting Isosteric Heats of Adsorption in kcal/mol

Adsorbing material	C_2H_6	C_3H_8	i-C_4H_{10}	C_4H_{10}	C_5H_{12}	C_6H_{14}
Graphon	5.62	8.4	10.80	12.20	11.02	15.08
	(326–346)[a]	(326–346)	(331–351)	(331–351)	(483–503)	(483–503)
Hydrogen-treated	4.70	5.90	6.80	7.35	8.41	9.87
Graphon	(326–346)	(326–346)	(326–346)	(326–346)	(410–430)	(410–430)
Sterling FT-G		6.10	6.95	7.54	8.43	10.15
		(330–350)	(330–350)	(330–350)	(387–407)	(387–407)
					8.82	10.50
					(329–349)	(345–365)
Hydrogen-treated		6.15	7.02	7.45	8.55	10.25
Sterling FT-G		(330–350)	(330–350)	(330–350)	(383–403)	(383–403)
Sterling MT-G[b]					8.9	10.10
Sterling MT-G[c]					8.9	10.40
Sterling FT-G[d]	4.60	5.87	6.91	7.45		
Sterling MT-G[e]	3.78	6.26		8.10	8.61	9.83
Graphon[f]					10.0	11.8
Graphon[g]				8.6		
Graphon[h]				8.2		
Graphon[i]				7.88	9.27	11.17

[a] Temperature (°K) range of retention volume measurements. [b] Reference 12. [c] Reference 16. [d] Reference 9. [e] Reference 17. [f] Reference 18. [g] Reference 19. [h] Reference 20. [i] Reference 21.

The precision in calculating the V_R' term strictly depends upon the correct measurement of the V_0 term. When a flame ionization detector is used, the dead volume measurement of the column is usually carried out by injecting into the column the adsorbate sample mixed with methane. The latter is assumed to be a nonadsorbable gas. At the lowest temperature used to eluate ethane and propane, however, methane was found to be noticeably adsorbed even on the low surface area adsorbent. In particular, it was calculated that the use of methane as the marker gas introduced an error of about 10% in the determination of the adsorption heat of ethane on Graphon. To overcome this obstacle, the determination of the dead volume of each chromatographic column under experiment was made by injecting methane at relatively high temperatures, where methane may definitely be considered to behave as a nonadsorbable gas. At varying temperatures, several determinations of the V_0 value were made and the precision of these measurements was calculated to be good to within ±0.3%. Experimental values of retention volumes for the hydrocarbons in question were determined at five temperatures and then plotted against T^{-1}, as described above. Very straight lines were always obtained. It was calculated that the adsorption heats so derived were affected by no more than a 1.5% error.

Table I[9,12,16-21] presents a list of the heats of adsorption on both hydrogen treated and untreated Graphon and Sterling FT-G derived from the retention volumes for some hydrocarbons. The temperature ranges of the retention volume measurements are also indicated. For comparison, some earlier determinations of limiting adsorption heats of the same adsorbates obtained, either by the gas chromatographic technique or static methods, together with references to the sources of these data are given in the lower portion of Table I. It was not possible to determine the isosteric heat of adsorption of ethane on Sterling FT-G, with a satisfactory accuracy. This is due to the fact that ethane on this adsorbent is adsorbed too little even at the lowest temperatures we were able to reach.

First of all, it is interesting to note that the hydrogen treatment carried out on the Graphon surface causes the adsorption heats for hydrocarbons to decrease greatly, whereas this decrease is not observed when performed on the Sterling FT-G surface. Some considerations, then, arise quite naturally from this finding. First, the surface of Graphon is contaminated by the presence of a certain kind of strong adsorption site while Sterling FT-G is not. Also, the hydrogen treatment can remove these heterogeneities.

It was demonstrated[7] that the hydrogen treatment eliminates traces of oxygen chemisorbed on the carbon surface. This removal provokes a sharp decrease in the adsorption heats at low coverages of polar substances on both Graphon[22] and Sterling FT-G.[3]

But, as can be seen, only after hydrogen treatment on Graphon is a sharp decrease observed in the limiting heats upon adsorption of nonpolar molecules. In addition, it can be expected that polar impurities should be no stronger than the rest of the carbon surface with reference to the adsorption of nonpolar molecules. These considerations make unacceptable the hypothesis that the chemisorbed oxygen is also to some extent responsible for the initial strong adsorption of nonpolar molecules on the carbon surface. Moreover, one can deduce that the Graphon surface is contaminated by a particular kind of geometric heterogeneity which the hydrogen at high temperatures is able to eradicate.

Graham[2] made the suggestion that strong sites in the graphitized carbon blacks are composed of intersections of graphitic planes or by an area of close approach between particles where the interaction of one molecule with two planes can occur. Also, the same author reported that

(16) A. V. Kiselev and Y. I. Yashin in "Gas Adsorption Chromatography," Plenum Press, New York, N. Y., 1969, p 23.
(17) S. Ross, J. K. Saelens, and J. P. Olivier, *J. Phys. Chem.*, **66**, 696 (1962).
(18) N. N. Avgul, A. A. Isirikyan, A. V. Kiselev, L. A. Lygina, and D. P. Poshkus, *Izv. Nauk SSSR, Otd. Khim. Nauk*, 1314 (1957).
(19) R. A. Beebe, M. H. Polley, W. R. Smith, and C. B. Wendell, *J. Amer. Chem. Soc.*, **69**, 2294 (1947).
(20) J. W. Ross and R. J. Good, *J. Phys. Chem.*, **60**, 1167 (1956).
(21) G. C. Chirnside and C. G. Pope, *J. Phys. Chem.*, **68**, 2377 (1964).
(22) B. Millard, E. G. Caswell, E. E. Leger, and D. R. Mills, *J. Phys. Chem.*, **59**, 976 (1955).

there was no indication of these sites being more than one type of strong site. However, as previously mentioned by Zettlemoyer,[1] the fraction of strong sites is actually far too low to be explained by the intersection of the planes in the surface. Besides, it can be safely supposed that the hydrogen treatment would not be effective in removing such a type of irregularity.

The data at our disposal indicate that the strong adsorptive sites in the Graphon surface can be better described by topographical irregularities, such as cracks, crevices, or graphite crystal defects of molecular dimensions, within which the interaction of an individual molecule can occur with more than one adsorbing plane. At the boundaries of these surface irregularities, it can be safely supposed that the carbon atoms are not arrayed in any sort of graphitic structure, as is predominant in the rest of the surface. If this is the case, then these carbon atoms are definitely more reactive than the graphitic ones. In support of this picture there is the slight decrease of the Graphon surface area, decreasing from 138 to 128 m^2/g, after the hydrogen treatment. This reduction may be due to a reaction occurring between the hydrogen and the active carbon atoms around the cavities with formation of slight hydrocarbons. As a consequence, this reaction provokes a progressive widening of the cavities to the point where the leveling process creates a surface we can consider flat. That the limiting adsorption heats of hydrocarbons on treated Graphon have values just about equal to those on Sterling FT-G, which is almost completely free of strong adsorption sites, makes it evident that the geometric irregularities have disappeared and interaction of an individual molecule occurs no longer with more than one adsorbing plane of the Graphon surface. The adsorption heat of hexane on untreated Graphon is abnormally high. The one of butane is too; so much so that it is even higher than that of pentane. This result suggests that there is more than one kind of strong site, as far as dimensions are concerned.

Upon adsorption on Sterling FT-G, by decreasing the temperature ranges of retention volume measurements, it was possible to observe a slight but noticeable increase in the adsorption heats of pentane and hexane. This increase makes it evident that, also on the Sterling FT-G surface, there is a very small fraction of geometric irregularities. However, these have adsorption energies far lower than those possessed by the active sites on Graphon.

It is noteworthy that adsorption heat values on treated Graphon are systematically slightly lower than those on Sterling FT-G, presumably due to the latter having a higher degree of graphitization.

A comparison of our experimental data with earlier determinations of limiting adsorption heats is made by first considering Sterling FT-G and Sterling MT-G and then Graphon. Sterling MT-G is another well-known example of graphitized carbon black with a surface area of about 8 m^2/g.

As far as Sterling FT-G and Sterling MT-G are concerned, it may be observed that the agreement between our tabulated adsorption heats and the others is good if the values of 3.78 and 8.10 kcal/mol respectively for ethane and butane of ref 17 are ignored. This agreement becomes very good if the comparison is restricted to our adsorption heat data and those of ref 9, which were derived from adsorption isotherms. This comparison is interesting for two reasons. First of all, it demonstrates once again that by the use of gas chromatography the determination of thermodynamic data can be made with a high accuracy. This, in addition to the advantage of simplicity and speed which gas chromatography offers over the other techniques. Second, these types of graphitized carbon blacks can be prepared reproducing their surface properties very well.

On the other hand, in the case of Graphon, as can be seen, adsorption heat data cannot be considered in satisfactory agreement. This disagreement may be due to the fact that the determinations of limiting isosteric heats were carried out at various degrees of surface coverage. Besides that, the various Graphon specimens under observation have a different degree of surface inhomogeneity. Under these conditions, the limiting isosteric heat becomes nothing more than the result of a chance surface condition of no particular significance aside from the specimen under observation. This consideration is particularly true in the case where the adsorption heat determinations are carried out by chromatography using the eluted pulse technique, which yields a single adsorption heat value at low surface coverage.

In order to obtain some information as to the modifications in the freedom of movement of an individual molecule adsorbed on Graphon and Sterling FT-G before and after the hydrogen treatment, the determination of the entropy changes upon adsorption of hydrocarbons from chromatographic data was made.

Unfortunately, only very few papers have dealt with the possibility of deriving the entropy changes upon adsorption from retention volume measurements. When this determination is reported, no mention is explicitly made to the choice of standard states in calculating the entropy loss upon adsorption.[23] Besides, to the best of our knowledge, except for Amariglio,[13] no author has attempted to compare the adsorption entropy values determined by chromatography with those obtained by static methods. For these reasons, we have felt the need to derive once more an equation relating the retention volume to the standard entropy loss upon adsorption, paying particular attention to the choice of units which indirectly determine the standard reference values.

To correlate the specific retention volume, V_s, with the integral change of entropy upon adsorption from a reference standard gas pressure, p_s, to a reference spreading pressure, π_s, let us consider the following well-known relation

$$\Delta G_{T_1}^{\circ} = -RT_1 \ln p_s/p_1$$

where ΔG_{T1}° is the standard change in free energy corresponding to a change in the pressure of the adsorbate from the standard value, p_s, to the particular value, p_1, which is in equilibrium with the standard adsorption state chosen, π_s, keeping the temperature constant at T_1.[24]

If the adsorption process occurs in the Henry's law region then $p_1 = K\pi_s$, and bearing in mind that $K = V_s = V_R'/S$, then

$$\Delta G_{T_1}^{\circ} = -RT_1 \ln \left(\frac{p_s}{\pi_s}\frac{V_R'}{S}\right) \qquad (3)$$

If the pressure, p_s, is expressed in dyne/cm^2 and the two-dimensional pressure, π_s, in dyne/cm, the Henry's

(23) L. D. Belyakova, A. V. Kiselev, and N. V. Kovaleva, Russ. *J. Phys. Chem.*, **69**, 802 (1965).
(24) J. H. De Boer, "The Dynamical Character of Adsorption," Clarendon Press, Oxford, 1953, p 113.

TABLE II: Standard Integral Entropies of Adsorption in cal/mol deg

Adsorbing material	C_2H_6	C_3H_8	i-C_4H_{10}	C_4H_{10}	C_5H_{12}	C_6H_{14}
Graphon	−10.9	−15.1	−18.2	−21.4	−14.5	−20.6
	(326)[a]	(326)	(331)	(331)	(483)	(483)
Hydrogen-treated	−9.0	−9.5	−10.0	−10.8	−10.5	−11.6
Graphon	(326)	(326)	(326)	(326)	(410)	(410)
Sterling FT-G		−9.6	−9.9	−10.6	−9.9	−11.9
		(330)	(330)	(330)	(387)	(387)
					−11.4	−14.0
					(329)	(345)
Hydrogen-treated		−9.7	−10.0	−10.5	−10.4	−12.2
Sterling FT-G		(330)	(330)	(330)	(383)	(383)
Sterling FT-G[b]	−8.57	−9.62	−10.37	−11.12		

[a] Temperature (°K) of retention volume measurement. [b] Reference 9.

law constant has the dimension of a length. Therefore, V_R' has to be expressed in cm^3 and the surface area of the adsorbent in cm^2. Besides, following de Boer, the standard references are taken as p_s = 760 Torr = 1.01 × 10^6 dyn/cm^2 and π_s = 0.338 dyn/cm. Equation 3 can then be rewritten as

$$\Delta G_{T_1}^{\circ} = -RT_1 \ln \left(3 \times 10^6 \frac{V_R'}{S}\right)$$

The standard integral change in entropy, ΔS°, may be derived from ΔG° by means of the relation $\Delta S^\circ = \Delta H^\circ/T_1 - \Delta G^\circ/T_1$, where ΔH° is the standard integral change of enthalpy. Taking into account that at surface coverage approaching zero, $\Delta H^\circ = -q_{diff} = -q_{st} + RT$, we may write

$$\Delta S^\circ = -\frac{q_{st}}{T_1} + R + R \ln 3 \times 10^6 + R \ln V_R' - R \ln S \quad (4)$$

By following eq 4, on both treated and untreated Graphon and Sterling FT-G, standard integral entropy losses upon adsorption of some hydrocarbons were derived from retention volume measurements at a certain temperature and from the limiting isosteric heat values previously discussed, and listed in Table II. The temperatures for retention volume measurements are also indicated. For comparison, standard integral entropy changes upon adsorption on Sterling FT-G of some of the hydrocarbons listed, determined by a static method and reported by Hoory and Prausnitz,[9] are also given in Table II.

As can be seen, adsorption entropy changes listed for ethane, propane, isobutane, and butane on the Sterling FT-G surface and calculated by us are in good agreement with those determined by a static method, taking into account that in determining ΔS° there is a degree of uncertainty higher than that in determining q_{st}. It was calculated that our ΔS° values have an uncertainty of ±4%. From this comparison, it turns out, then, that the gas chromatographic method, besides its usefulness in determining adsorption heats, is also useful in determining entropy changes for an individual molecule upon adsorption.

Passing from butane to pentane, there is an interruption in the normal increase in the entropy loss with increasing molecular size. This interruption may be due to the different temperatures used when measuring the retention volumes for pentane and hexane.

The examination of entropy changes upon adsorption on Sterling FT-G before and after the hydrogen treatment reconfirms that this adsorbing material is almost completely free of active sites for nonpolar substances which would limit the various motions of adsorbed molecules.

On the other hand, the presence on the Graphon surface of a small fraction of cavities with molecular dimensions, where the freedom of movement of the adsorbate is restricted, is made evident by the high entropy loss values, as compared with those on Sterling FT-G.

After the hydrogen treatment, as would be expected, the standard entropy loss upon adsorption on Graphon of hydrocarbons are greatly decreased. In addition, the new values are in good agreement with those calculated for adsorption on Sterling FT-G. This result demonstrates once again that the surface of Graphon is smoothed by the hydrogen treatment and that Graphon and Sterling FT-G have the same unit surface area properties.

Comparisons between experimental entropies of adsorption and theoretical entropy changes based on different models for the adsorbed phase are usually made to establish the degree of mobility of adsorbed molecules.

Steele[25] has shown that the kinetic state of hydrocarbons adsorbed at normal temperatures on the graphitic carbon surface corresponds to a "mobile," two-dimensional film. On the basis of the observed differences in entropy changes upon adsorption on treated and untreated Graphon, we have attempted to establish, approximately, if the kinetic state of hydrocarbons intruded in cavities of the untreated Graphon surface corresponds to that for "localized" adsorption. Computations of the adsorption entropy relative to this model have been based on the assumptions that molecules behave as harmonic, three-dimensional oscillators and that frequencies of "external vibrations" in all three directions have the same values. Also, we have assumed that both the extruding part of the surface and the cavities hinder, to the same extent, rotations of adsorbed molecules. Our attention has been limited to the adsorption of C_2H_6, C_3H_8, i-C_4H_{10}, and C_4H_{10}. Passing from adsorption on the plain carbon surface to adsorption in cavities with molecular dimensions should result in loss of two degrees of translational freedom parallel to the surface, which are replaced by two external vibrations acquired by the adsorbed molecules. As a consequence, the entropy of the adsorbed phase decreases. This theoretical decrease was calculated by making use of data reported by Hoory and Prausnitz[9] and pertaining to translational and vibrational entropies, and frequencies of

(25) W. A. Steele, *Advan. Chem., Ser.*, **No. 33**, 269 (1961).

external vibration for adsorption of hydrocarbons under consideration on a homogeneous graphitic substrate. Vibrational entropy values have been suitably modified for adsorption in cavities of the Graphon surface, as external vibrations of adsorbed molecules slightly increase with the increase of the adsorption potential. The new values of external vibrations were obtained by means of the approximate relation

$$\nu'/\nu = \sqrt{\frac{P_{ads}'}{P_{ads}}} \cong \sqrt{\frac{q_{st}'}{q_{st}}}$$

The use of the ratio between adsorption heats on untreated and treated Graphon in place of the ratio between adsorption potentials to derive vibrational frequencies was evaluated to introduce an error not higher than 6%. Theoretical decreases of entropy due transition from mobile adsorption to localized adsorption were then found to be about 15 cal/mol deg for C_4H_{10} and i-C_4H_{10}, 14.5 cal/mol deg for C_3H_8, and 14 cal/mol deg for C_2H_6.

Bearing in mind that the theoretical model adopted for localized adsorption is rather approximate, the comparison between these values and experimental differences in adsorption entropy changes on treated and untreated Graphon indicates that the kinetic state of butane intruded in cavities can be roughly fitted to the picture of localized adsorption with a residual possibility of sliding motions along the cavity walls. Also, the decrease of molecular size of hydrocarbons adsorbed in cavities results in progressive transition from localized to mobile adsorption. An analogous trend seems to be repeated passing from hexane to pentane.

The object of the above qualitative considerations is not to determine a model suitable to describe the kinetic state of adsorbates. The purpose is to point out that cavities in the Graphon surface have defined, molecular dimensions. As a consequence, the freedom of movement of the adsorbate intruded in these cracks will be strictly dependent upon its molecular size.

Conclusion

The experimental results reported here give evidence as to the presence on the Graphon surface of active sites upon adsorption of nonpolar molecules. These surface heterogeneities can be identified as cavities with a peculiar distribution as far as their dimensions are concerned. A very interesting result is that hydrogen treatment at high temperature is effective in removing not only traces of surface oxides but also the slight geometric irregularities contaminating the Graphon surface. This treatment makes possible the extensive utilization of Graphon in experimental work, whose high surface development, as compared with the other examples of graphitized Carbon Blacks, greatly simplifies measurements. Finally, it should be pointed out that gas chromatography is useful in providing a technique for following the effect of hydrogen treatment on the degree of uniformity of a graphitic substrate.

Acknowledgment. The authors are indebted to G. Devitofrancesco for measurements of the surface areas.

The Role of the Excited States in the Photoreaction of the Hexacyanochromate(III) Ion. A Sensitization Study

N. Sabbatini,* M. A. Scandola, and V. Carassiti

Istituto Chimico dell'Università, Centro per lo Studio della Fotochimica e Reattività degli Stati Eccitati dei Composti di Coordinazione del C.N.R., Ferrara, Italy *(Received December 18, 1972)*

Publication costs assisted by Consiglio Nazionale delle Ricerche, Italy

A systematic investigation on the sensitization of the $Cr(CN)_6^{3-}$ photoreaction and emission have been performed in order to identify the photoreactive state of this complex. Naphthalene, pyrazine, xanthone, and acridine sensitize the $Cr(CN)_6^{3-}$ photoaquation, while Michler's ketone, 2′-acetonaphthone, $Ru(bipy)_3^{2+}$, and erythrosin do not. Sensitization of $Cr(CN)_6^{3-}$ phosphorescence by $Ru(bipy)_3^{2+}$ and erythrosin proved that an energy transfer process involving the population of the lowest doublet state of $Cr(CN)_6^{3-}$ occurred, without causing any sensitized photoreaction. These results indicate that none of the doublet states is involved in $Cr(CN)_6^{3-}$ photochemistry. The photoreactive state is identified with the lowest quartet excited state.

Introduction

Although the photochemical behavior of Cr(III) complexes has been extensively investigated,[1] studies of the direct photoreaction alone do not suffice to obtain a definitive indication as to the role played by the doublet and quartet excited states in the photochemical reaction. In fact, it is very difficult to populate the doublet state directly by light absorption, since the doublet absorption band is very weak and is partially covered by the more intense quartet band.[1]

Sensitization studies[2-4] have been reported for several Cr(III) complexes. However, these investigations did not give definitive indication as to the excited state involved in the photoreaction. For Cr(III) complexes, in fact, there is a loss of selectivity of the spin-selection rules for intermolecular energy transfer[5] since transfer from a triplet donor to both doublet and quartet states is spin-allowed. Therefore, in order to obtain a selective population of the doublet state, one must be able to discriminate between the two states simply on energetic grounds. This is very difficult for most Cr(III) complexes, since the energy of the zero-vibrational level of the quartet state is unknown because of the distortion of this state, and besides, it is presumably very close to the energy of the doublet state.[6]

Some quenching experiments performed on $Cr(NH_3)_2(NCS)_4^-$,[7] $Cr(NH_3)_6^{3+}$,[8] and $Cr(phen)_3^{3+}$,[8] have clearly shown that for these complexes the photoreaction originates, at least in part, from the lowest quartet excited state. In fact, while the phosphorescence quenching follows a Stern–Volmer mechanism, part of the total photoaquation cannot be quenched. These studies, however, also suggest that the part of the photoaquation that can be quenched does not necessarily originate from the doublet state, since the doublet and the quartet states may be in thermal equilibrium.[7,9]

Therefore, in order to obtain more definitive information about the role played by each state, one should perform experiments on complexes in which the energy separation between the quartet and the doublet states is large enough to allow a selective population of the doublet state and to avoid complications due to the occurrence of reversible intersystem crossing. A complex which meets such a requirement is $Cr(CN)_6^{3-}$.[9]

In fact, definitive identification of the reactive excited state in $Cr(CN)_6^{3-}$ has been recently obtained by means of quenching[10] and sensitization[11] techniques. Wasgestian[10] studied the emission and the photosolvation of $Cr(CN)_6^{3-}$ in DMF. On the basis of the different dependences of phosphorescence and photoreaction on temperature and oxygen and water concentration, he showed that the chemical reaction and the phosphorescent emission cannot originate from the same excited state.

In a preliminary communication[11] we reported evidence in favor of quartet reactivity in $Cr(CN)_6^{3-}$, based on some sensitization results. This work will present in detail the results concerning a systematic investigation on the sensitization of the $Cr(CN)_6^{3-}$ photoreaction and emission.

Experimental Section

Materials. Potassium hexacyanochromate(III) (Alfa Chemicals, Beverly, Mass.) was recrystallized from water.[12] The purity of the compound used was determined by comparison of its absorption spectrum with published data.[13,14] Tetrabutylammonium hexacyanochromate(III) was prepared from $K_3[Cr(CN)_6]$ and tetra-*n*-butylammonium bromide.[10] Xanthone, Michler's ketone, and 2′-aceto-

(1) V. Balzani and V. Carassiti, "Photochemistry of Coordination Compounds," Academic Press, London, 1970.
(2) A. W. Adamson, J. E. Martin, and F. D. Camassei, *J. Amer. Chem. Soc.*, **91**, 7530 (1969); J. E. Martin and A. W. Adamson, *Theoret. Chim. Acta*, **20**, 119 (1971).
(3) V. Balzani, R. Ballardini, M. T. Gandolfi, and L. Moggi, *J. Amer. Chem. Soc.*, **93**, 339 (1971).
(4) E. Zinato, P. Tulli, and P. Riccieri, *J. Phys. Chem.*, **75**, 3504 (1971).
(5) F. Wilkinson, *Advan. Photochem.*, **3**, 241 (1964).
(6) G. B. Porter, S. N. Chen, H. L. Schläfer, and H. Gausmann, *Theoret. Chim. Acta*, **20**, 81 (1971).
(7) S. N. Chen and G. B. Porter, *Chem. Phys. Lett.*, **6**, 41 (1970).
(8) C. H. Langford and L. Tipping, *Can. J. Chem.*, **50**, 887 (1972); N. A. P. Kane-Maguire and C. H. Langford, *J. Amer. Chem. Soc.*, **94**, 2125 (1972).
(9) F. D. Camassei and L. S. Forster, *J. Chem. Phys.*, **50**, 2603 (1969).
(10) H. F. Wasgestian, *J. Phys. Chem.*, **76**, 1947 (1972).
(11) N. Sabbatini and V. Balzani, *J. Amer. Chem. Soc.*, **94**, 7587 (1972).
(12) J. H. Bigelow, *Inorg. Syn.*, **2**, 203 (1964).
(13) A. Chiang and A. W. Adamson, *J. Phys. Chem.*, **72**, 3827 (1968).
(14) H. F. Wasgestian, *Z. Phys. Chem. (Frankfurt am Main)*, **67**, 39 (1969).

TABLE I: Experimental Conditions Used in the Sensitization and Quenching Experiments

Donor	Wavelength of excitation, nm	Solvent	$Cr(CN)_6^{3-}$ concn, mol $l.^{-1}$	% of incident light absorbed by the donor	Type of experiment[a]
Naphthalene	280	H_2O–EtOH 70%	5×10^{-3}	99	r,q
Pyrazine	313	H_2O	5×10^{-3} to 2×10^{-2}	≥92	r,q
Xanthone	334	H_2O–EtOH 50%	5×10^{-3} to 2×10^{-2}	≥90	r
Acridine	334	H_2O–EtOH 50%	3×10^{-3} to 2×10^{-2}	≥99	r,q
Michler's ketone	365	H_2O–EtOH 50%	2×10^{-2}	97	r
2′-Acetonaphthone	334	H_2O–EtOH 50%	1×10^{-2}	99.9	r
$Ru(bipy)_3^{2+}$	433	H_2O	5×10^{-4} to 2×10^{-3}	≥93	r,q
	433	DMF	1×10^{-3}	96	r,e,q
Erythrosin	530	H_2O	2×10^{-2}	100	r,q
	530	DMF	2×10^{-2}	100	r,e,q

[a] r, sensitized photoreaction of $Cr(CN)_6^{3-}$; e, sensitized emission of $Cr(CN)_6^{3-}$; q, quenching of the donor emission.

naphthone "suitable for sensitizer use" (Baker Chemicals, Deventer, Holland) were used without further purification. Pyrazine (Schuchardt, Munich, Germany) was purified by vacuum sublimation. Naphthalene (Carlo Erba, Milan, Italy) and acridine (Baker Chemicals) were recrystallized from ethanol. Erythrosin (Carlo Erba) was recrystallized from water. Tris(2,2′-bipyridine)ruthenium(II) chloride was prepared and purified according to Burstall.[15] Dimethylformamide (DMF) "Baker Instra-Analyzed" was used. The other chemicals were of reagent grade.

Apparatus. Radiations of 280, 313, 334, and 365 nm were isolated from a Hanau Q 400 mercury vapor lamp by means of Ealing-TFP interference filters. Radiations of 433 and 530 nm were obtained from a Philips Attralux Spot 150-W incandescent lamp by means of Schott & Gen. interference filters (half-width 20 nm). The basic irradiation equipment was that previously described.[16] The incident light at 280, 313, 334, 365, and 433 nm was measured by means of the ferric oxalate actinometer,[17] and at 530 nm by means of the reineckate actinometer.[18] The intensity of the incident light was of the order of 10^{-7} to 10^{-6} $Nh\nu$/min. Spectrophotometric measurements were carried out with an Optica CF4 NI spectrophotometer. Luminescence measurements were performed with a Perkin-Elmer MPF-2A spectrophotofluorimeter. Potentiometric measurements were accomplished with a Knick KpH 350 potentiometer.

Procedures. The experimental conditions used in the sensitization and quenching experiments are summarized in Table I. For all of the donors, preliminary controls were carried out to verify their thermal and photochemical stability in the presence of $Cr(CN)_6^{3-}$. Trivial emission-reabsorption processes were completely negligible in the experimental conditions used. Sensitization experiments were carried out at 7° in order to minimize secondary thermal reactions.[13] When necessary, appropriate corrections were made for light absorbed by the complex. Deaerated solutions were obtained by successive freeze-thaw-pumping cycles.

Photoaquation of $Cr(CN)_6^{3-}$ in aqueous and hydroalcoholic solutions was followed potentiometrically by means of a liquid-membrane cyanide-selective electrode supplied by Amel, Milan, Italy. Potentiometric measurements were converted to CN^- concentration values by means of appropriate calibration plots. When DMF was used as a solvent, the potentiometric method did not give reliable results. Therefore, the occurrence of the photoreaction was looked for by measuring the spectral variations caused by the conversion of $Cr(CN)_6^{3-}$ in $Cr(CN)_5(DMF)^{2-}$.[10]

The emission measurements were performed using the right angle or the frontal illumination method, depending on the absorbance value of the solutions.

Results

Direct Photolysis of $Cr(CH)_6^{3-}$. The photoreaction of $Cr(CN)_6^{3-}$ is a solvation reaction.[10,13,14]

$$Cr(CN)_6^{3-} \xrightarrow[\text{solv.}]{h\nu} Cr(CN)_5(\text{solv.})^{2-} + CN^-$$

The quantum yield is 0.1, independent of the wavelength of excitation, in both water[14] and DMF–water mixtures.[10] In aqueous solutions, we obtained a photoaquation quantum yield of 0.1, in agreement with that previously reported. When a 50% ethanol–water mixture was used as a solvent, the spectral variations on irradiation showed that the same photoaquation reaction occurred as in aqueous solution, but with a quantum yield of 0.04. The quantum yield for the direct photoaquation of $Cr(CN)_6^{3-}$ did not depend on the presence of oxygen in both aqueous and hydroalcoholic solutions.

Sensitization Experiments. A summary of the experimental conditions used in the sensitization and quenching experiments is given in Table I.

Pyrazine. Irradiation of solutions containing pyrazine and $Cr(CN)_6^{3-}$ caused the formation of CN^- ions. After appropriate corrections for the direct photolysis, the apparent quantum yield was obtained. The Stern–Volmer plot for the sensitization of the $Cr(CN)_6^{3-}$ aquation is

(15) F. H. Burstall, *J. Chem. Soc.*, 173 (1936).
(16) V. Balzani, R. Ballardini, N. Sabbatini, and L. Moggi, *Inorg. Chem.*, **7**, 1398 (1968).
(17) C. G. Hatchard and C. A. Parker, *Proc. Roy. Soc., Ser. A*, **235**, 518 (1956).
(18) E. E. Wegner and A. W. Adamson, *J. Amer. Chem. Soc.*, **88**, 394 (1966).

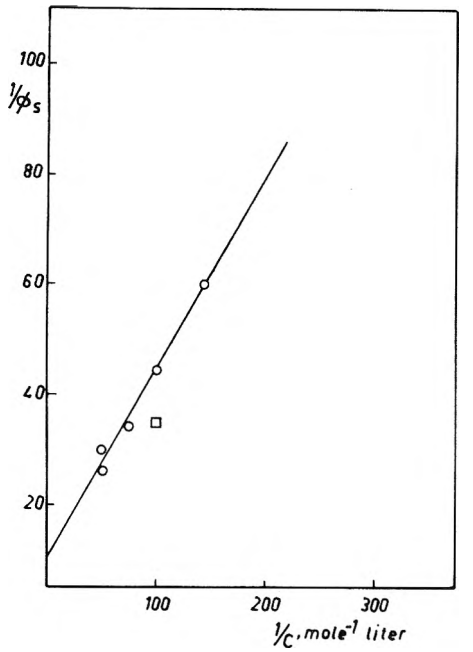

Figure 1. Stern–Volmer plot for the sensitization of the $Cr(CN)_6^{3-}$ photoaquation by pyrazine: O, aerated solutions; □, deaerated solution.

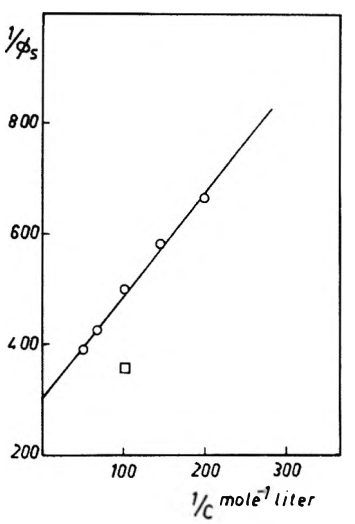

Figure 2. Stern–Volmer plot for the sensitization of the $Cr(CN)_6^{3-}$ photoaquation by xanthone: O, aerated solutions; □, deaerated solution.

shown in Figure 1. From this plot, a limiting quantum yield of 0.1 was obtained. The apparent quantum yield of the sensitized photoreaction was higher for deoxygenated solutions than for the corresponding aerated ones (see Figure 1). The pyrazine fluorescence was not quenched by the complex in the concentration range studied.

Xanthone. Cyanide ions were produced upon irradiation of solutions containing xanthone and $Cr(CN)_6^{3-}$. After appropriate corrections for the direct photolysis, the apparent quantum yield of the sensitized photoreaction was obtained. Figure 2 shows the Stern–Volmer plot for the sensitization of the $Cr(CN)_6^{3-}$ photoaquation. The limiting quantum yield calculated from this plot is 0.003. The apparent quantum yield is higher for deoxygenated solutions than for the corresponding aerated ones (see Figure 2).

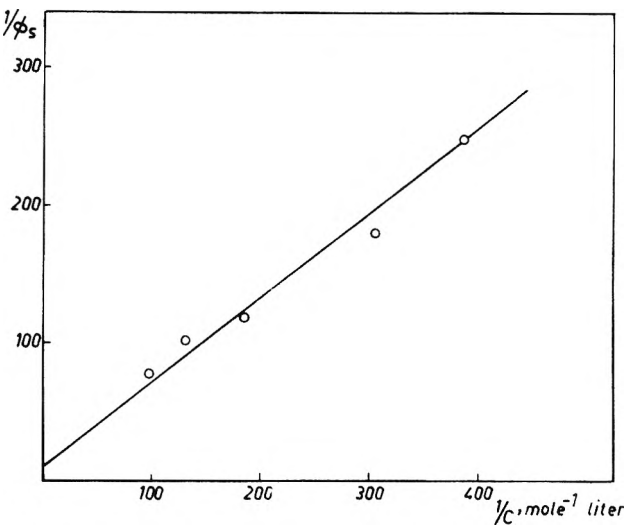

Figure 3. Stern–Volmer plot for the sensitization of the $Cr(CN)_6^{3-}$ photoaquation by acridine.

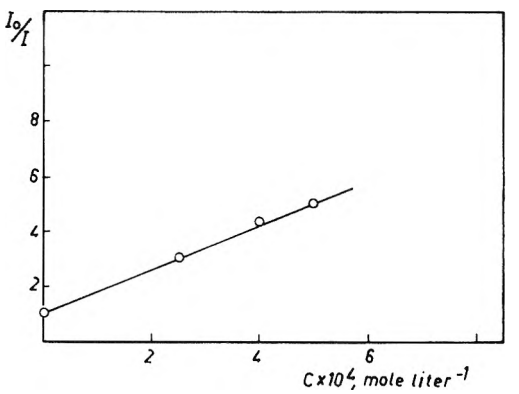

Figure 4. Stern–Volmer plot for the quenching of the $Ru(bipy)_3^{2+}$ phosphorescence by $Cr(CN)_6^{3-}$.

Acridine. Irradiation of solutions containing acridine and $Cr(CN)_6^{3-}$ caused the production of CN^- ions. The Stern–Volmer plot for the sensitization of the $Cr(CN)_6^{3-}$ photoaquation is shown in Figure 3. The limiting quantum yield is 0.01. The apparent quantum yield does not depend on the presence of oxygen in the irradiated solutions. The intensity of the acridine fluorescence was unaffected by the complex.

Naphthalene. Irradiation of solutions containing naphthalene and $Cr(CN)_6^{3-}$ caused the production of CN^- ions. In the same conditions, the naphthalene fluorescence was strongly quenched by the complex.

Michler's Ketone. On irradiating deaerated solutions containing Michler's ketone and $Cr(CN)_6^{3-}$, no cyanide formation was observed other than that due to the direct photoreaction. The sensitized emission of $Cr(CN)_6^{3-}$ could not be looked for, due to the insolubility of Michler's ketone in DMF.

2′-Acetonaphthone. No detectable amount of cyanide was found upon irradiation of deaerated solutions containing 2′-acetonaphthone and $Cr(CN)_6^{3-}$.

$Ru(bipy)_3^{2+}$. On irradiating deaerated aqueous solutions containing $Ru(bipy)_3^{2+}$ and $Cr(CN)_6^{3-}$, no cyanide production was observed other than that due to the direct photoreaction. In the same conditions, the $Ru(bipy)_3^{2+}$ phosphorescence was strongly quenched by $Cr(CN)_6^{3-}$. The Stern–Volmer plot of the quenching of the $Ru(bipy)_3^{2+}$ phosphorescence is shown in Figure 4; from this

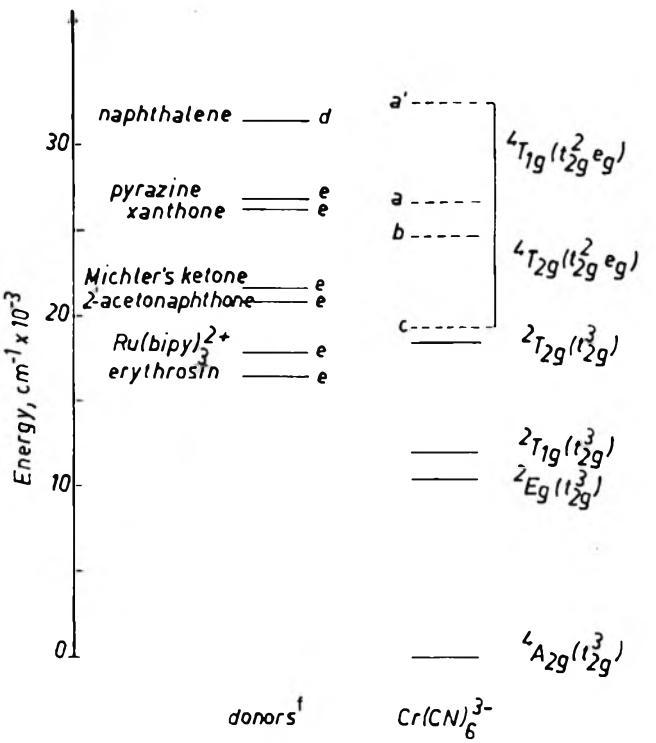

Figure 5. Energy level diagram showing the energies of the electronic excited states potentially involved in the energy transfer from the donors used and $Cr(CN)_6^{3-}$. a and a', energies of the absorption maxima; b and c, upper and lower limit values for the zero vibrational level of $^4T_{2g}$ as deduced from the half-width of the absorption band and the Stokes shift between absorption and emission, respectively; d, energy of the lowest singlet excited state; e, energy of the lowest triplet excited state; f, acridine does not appear in this diagram due to the uncertainty in determining the excited state involved in the energy transfer.

plot, a quenching constant of 8000 mol^{-1} l. was calculated. When DMF was used as a solvent, the quenching of the $Ru(bipy)_3^{2+}$ phosphorescence was accompanied by the appearance of an emission band at about 800 nm, which corresponds to the well-known phosphorescence emission of $Cr(CN)_6^{3-}$.[10,19] The irradiation of deaerated DMF solutions containing $Ru(bipy)_3^{2+}$ and $Cr(CN)_6^{3-}$ did not cause any conversion of $Cr(CN)_6^{3-}$ to $Cr(CN)_5(DMF)^{2-}$.

Erythrosin. The irradiation of deaerated aqueous solutions of erythrosin and $Cr(CN)_6^{3-}$ did not cause cyanide production. The luminescence spectra of deaerated DMF solutions containing erythrosin and $Cr(CN)_6^{3-}$ showed that the excitation of erythrosin caused the appearance of the $Cr(CN)_6^{3-}$ phosphorescence at 800 nm. In such conditions, no quenching of the erythrosin fluorescence by $Cr(CN)_6^{3-}$ was observed. The irradiation of the same system did not cause any conversion of $Cr(CN)_6^{3-}$ to $Cr(CN)_5(DMF)^{2-}$.

Discussion

Our results indicate that naphthalene, pyrazine, xanthone and acridine sensitize the $Cr(CN)_6^{3-}$ photoaquation. The observed sensitized photoreaction most likely occurs as the result of electronic energy transfer since, in our experimental conditions (see Procedures), other processes such as the trivial emission-reabsorption and chemical reaction between the excited donors and the complex do not occur.

The quantum yield of the sensitized photoaquation cannot be calculated from the limiting quantum yields obtained using pyrazine, xanthone, and acridine as donors. In fact, for pyrazine and xanthone, which function as triplet donors, the quantum yield of intersystem crossing in our experimental conditions is not known, and for acridine, the excited state involved in the energy transfer process is not unequivocally determined *(vide infra)*.

The sensitized photoreaction was not observed when Michler's ketone, 2'-acetonaphthone, $Ru(bipy)_3^{2+}$, and erythrosin were used as donors. However, in the $Ru(bipy)_3^{2+}$-$Cr(CN)_6^{3-}$ and erythrosin-$Cr(CN)_6^{3-}$ systems, the sensitization of the $Cr(CN)_6^{3-}$ emission proved that energy transfer from $Ru(bipy)_3^{2+}$ and erythrosin to $Cr(CN)_6^{3-}$ occurred.

As far as the type of donor excited state involved in the energy transfer process to $Cr(CN)_6^{3-}$ is concerned, the results of our sensitization and quenching experiments allow us to infer that pyrazine, xanthone, $Ru(bipy)_3^{2+}$, and erythrosin function as triplet donors. The quenching of the naphthalene fluorescence by $Cr(CN)_6^{3-}$ indicates that, in this case, the energy transfer takes place from the lowest singlet excited state. The results obtained with acridine are quite peculiar. The absence of any oxygen effect on the apparent quantum yield of the sensitized photoreaction allows us to exclude that the lowest π,π^* triplet of acridine,[20] which has a lifetime of 10^{-4} sec,[21] is involved in the energy transfer process. On the other hand, since the acridine fluorescence is unaffected by $Cr(CN)_6^{3-}$, the fluorescent π,π^* singlet[20] cannot be responsible for the observed sensitized photoreaction. Therefore, the acridine excited state involved in the energy transfer to $Cr(CN)_6^{3-}$ cannot be unequivocally identified on the basis of our experimental results. It must be noted, however, that acridine possesses two other excited states, the lowest n,π^* singlet and triplet, which are situated close to the lowest π,π^* singlet.[21-23] One of these states could be responsible for the energy transfer from acridine to $Cr(CN)_6^{3-}$.

In Figure 5, an energy level diagram is reported showing the electronic states of the potential donors and $Cr(CN)_6^{3-}$, which are or could be involved in the energy transfer processes. The energy values of the donor excited states have been taken from the literature.[20,24-26] The energies of the various doublet states of $Cr(CN)_6^{3-}$ are known from absorption and emission studies.[19,27] These states, in fact, since they have the same electronic configuration as the ground state, are not distorted with respect to the ground state, so that the absorption and emission maxima give directly the energy of the zero-vibrational level of the corresponding excited state. On the contrary, the value of the pure electronic energy of the $^4T_{2g}$ state cannot be obtained spectroscopically. In fact, this excited state, since it has a different electronic configuration with respect to the ground state, is expected to have considerably larger chromium-ligand equilibrium distances than the ground state molecule. Consequently, the maximum

(19) H. Gausmann and H. L. Schläfer, *J. Chem. Phys.*, **48**, 4056 (1968).
(20) P. S. Engel and B. M. Monroe, *Advan. Photochem.*, **8**, 245 (1971).
(21) A. Kellmann and J. T. Dubois, *J. Chem. Phys.*, **42**, 2518 (1965).
(22) H. Kokubun, *Bull. Chem. Soc. Jap.*, **42**, 919 (1969).
(23) V. Zanker and G. Prell, *Ber. Bunsenges. Phys. Chem.*, **73**, 791 (1969).
(24) K. K. Innes, J. P. Byrne, and I. G. Ross, *J. Mol. Spectrosc.*, **22**, 125 (1967).
(25) J. N. Demas and A. W. Adamson, *J. Amer. Chem. Soc.*, **93**, 1800 (1971).
(26) T. Ohno and S. Kato, *Bull. Chem. Soc. Jap.*, **42**, 3385 (1969).
(27) R. K. Mukherjee, S. C. Bera, and A. Bose, *J. Chem. Phys.*, **53**, 1287 (1970).

of the absorption band includes a noticeable amount of vibrational energy of the excited state. From the half-width of the absorption band, one can conclude that the zero-vibrational level of the $^4T_{2g}$ state lies at least 2000 cm^{-1} lower than the energy of the absorption maximum. Assuming that the potential energy surface of the $^4T_{2g}$ state has the same curvature as that of the ground state, from the Stokes' shift between the absorption (26,600 cm^{-1}) and the emission (12,000 cm^{-1}) maxima,[28] one could infer that such a level should be at about 12,000 cm^{-1} + (26,600 cm^{-1} to 12,000 cm^{-1})/2, that is about 19,300 cm^{-1}. In reality, since the potential energy surface of the excited state should be flatter than that of the ground state, 19,300 cm^{-1} may well represent a lower limit value of the pure electronic energy of the $^4T_{2g}$ state.

Spin-conservation rules[5] permit energy transfer from both singlet and triplet states of the donor to quartet states of the acceptor, whereas they forbid the transfer from donor singlet states to doublet states of the complex.

From the diagram of Figure 5, one could conclude that, since naphthalene, pyrazine, xanthone, and acridine sensitize the $Cr(CN)_6^{3-}$ photoreaction, whereas Michler's ketone, 2′-acetonaphthone, $Ru(bipy)_3^{2+}$, and erythrosin do not, the energy of the reactive state of $Cr(CN)_6^{3-}$ is higher than 21,000 cm^{-1} (triplet energies of 2′-acetonaphthone and Michler's ketone). However, the results obtained using Michler's ketone and 2′-acetonaphthone as donors are not unequivocal, since no experimental evidence proved that energy transfer to $Cr(CN)_6^{3-}$ really did occur. More significant results are those obtained using $Ru(bipy)_3^{2+}$ and erythrosin as donors. As stated above, these donors were found to sensitize the $Cr(CN)_6^{3-}$ phosphorescence (*i.e.*, in both cases, an energy transfer process involving the population of the ^2E_g state certainly occurred), without causing any sensitized reaction.

These results allow us to conclude that (i) the ^2E_g state is not responsible for the $Cr(CN)_6^{3-}$ photochemistry, and (ii) the photoreactive state of $Cr(CN)_6^{3-}$ lies above 18,000 cm^{-1} (triplet energy of $Ru(bipy)_3^{2+}$). The $^2T_{2g}$ state, which has the same electronic configuration as the ^2E_g state but a shorter lifetime, cannot be responsible for the photoreaction. Therefore, the photoreactive state must be the $^4T_{2g}$ state.

With regard to the energy location of the zero-vibrational level of such a state, our sensitization results prove that it is certainly higher than 18,000 cm^{-1}, but also suggest that it could probably be higher than 21,000 cm^{-1}.

(28) S. N. Chen and G. B. Porter, *J. Amer. Chem. Soc.*, **92**, 2189 (1970).

COMMUNICATIONS TO THE EDITOR

Metal–Ammonia Solutions. X. Single Configuration Coordinate Analysis

Publication costs assisted by The Robert A. Welch Foundation

Sir: The solvated electron in liquid ammonia has been the subject of considerable experimental investigation.[1] Among the more striking physical properties of these solutions is their blue color. This plus the stability of the solvated electron species (under rigorous experimental conditions) has promoted many investigations of the optical absorption spectrum. In general, the spectrum consists of a single absorption band centered near 0.8 eV in the near-infrared. The marked asymmetry of this absorption to higher energy has been cited as the reason for the characteristic blue color. Several suggestions have been made to account for the asymmetric shape of the absorption spectrum. In general these explanations involve the concept of two or more overlapping bands which are attributed either to higher transitions of the solvated electron or to different species. Attempts[2,3] to resolve any overlapping components have met with certain difficulties in the case of metal–ammonia solutions. In this study we assume that the observed asymmetric absorption spectrum is due to a single, bound solvated electron transition.

Several theoretical descriptions of the solvated electron species have been proposed, but no single description can, as yet, account fully for all the observed properties. To account for the optical properties there is, however, one theoretical description[4] formulated in the work of Copeland, Kestner, and Jortner (CKJ) based on the cavity model, which is more successful than the others.

Physically the cavity model is envisioned as a collection of several molecules which are polarized by the presence of an excess electron. These solvent molecules are oriented to form a region of void space in which the excess electron is trapped. For the purposes of the calculations based on the CKJ model, the ensemble of solvent molecules and

(1) J. J. Lagowski and M. J. Sienko, Ed., "Metal-Ammonia Solutions," Butterworths, London, 1970.
(2) R. Lugo and P. Delahay, *J. Chem. Phys.*, **57**, 2122 (1972).
(3) W. H. Koehler and J. J. Lagowski, *J. Chem. Phys.*, **73**, 2329 (1969).
(4) D. A. Copeland, N. R. Kestner, and J. Jortner, *J. Chem. Phys.*, **53**, 1189 (1970).

the trapped, excess electron are considered to be a single species which is referred to as the cavity. It is apparent that this species is best described by a $3N$ coordinate system where N is simply the number of solvent molecules under consideration. To make the calculations more tractable this system is reduced to a single coordinate. Precedents for this reduction in the number of coordinates and the CKJ calculations are numerous, having their origin in the description of trapped electron centers in the solid state when the single coordinate is associated with the radial displacement of a given number of nearest-neighbor ions about the trapped electron center. The motion is concerted and has been called a "symmetric breathing mode," a term which has now been adopted for the liquid state.

It is important to recall at this point the physical significance attached to this symmetric breathing mode. In the solid state the physical reality is certainly more valid than in the liquid state. Actual displacement of ions in a solid lattice is quite small while similar motion in the liquid is probably larger. In addition to this radial displacement, the molecules of the liquid which surround the solvated electron have internal motions of their own[5] (*i.e.*, normal modes of vibrations) whereas simple ions in a solid lattice have not. Thus, one is forced to conclude that the single coordinate description (with its attendant symmetric breathing mode) is at a lower level of approximation in the liquid state than in the solid state.

The object of the calculations using a single coordinate description is configurational diagrams (total energy as a function of the coordinate) which may indicate a stable system. The goal is accomplished both for the solid state and for the case of the solvated electron.[4] From the calculated configurational diagrams it is possible to further calculate the values of experimentally determined quantities such as the optical absorption spectrum. For the case of the solvated electron in liquid ammonia the configurational diagrams have been used to discuss thermodynamic properties[6] of the solvated electron and the observed absorption spectrum.[4] In this discussion we are concerned only with the latter properties.

Calculated values of the optical absorption spectrum parameters of the ammoniated electron, *viz.*, E_{max}, position of maximum intensity; W, width of absorption at half-maximum intensity; $\partial E_{max}/\partial T$, change of E_{max} with temperature, using the CKJ approach are in good agreement with experiment in view of the use of the single configuration coordinate. There are, however, notable discrepancies which require attention. In general, the calculated value of E_{max} is larger than observed; the calculated value of W is a factor of 3 or 4 too small; the values of $\partial E_{max}/\partial T$ calculated from theory are not directly comparable[7] to experimental values.

Since it is possible to calculate these absorption spectrum parameters from the configurational diagrams it would seem plausible that the reverse procedure can be employed. This has been done in several cases. To perform the calculation of the configurational diagrams from the observed optical absorption spectrum it is necessary to make several assumptions. These are, in fact, the same assumptions made when the configurational diagrams are used to calculate the optical absorption spectrum. First, we assume the validity of the single configuration coordinate. Second, we assume that the configurational diagram is accurately represented in the region of importance (*i.e.*, near the energy minima) by the juxtaposition of two parabolas. By further assuming that the ground-state configuration parabola has its minimum at zero on the configuration coordinate the number of parameters necessary to describe the diagram is reduced to five. The last assumption prevents the calculations of the absolute values of the configuration coordinate which correspond to the energy minima. In spite of this last difficulty, valuable information may be obtained.

Values of the configuration coordinate parameters thus obtained surely lie closer to the true values of such a system under the given assumptions. Therefore, these more accurate values may serve to guide future first-principle calculations and future experiments to test the validity of such a model.

A recent report[8] of the calculation of the configurational diagram for the solvated electron in liquid ammonia has prompted us to report our work in this area. Our calculations confirm and extend those which have recently appeared. Recalling that the single configuration coordinate analysis is essentially the same for the solvated electron and the trapped electron center in solids we have adopted the method of Jacobs and Menon[7] (MJ). The actual computation consists of an application of the non-linear least-squares method. Computations have been performed using a large fraction of the optical absorption data in the literature.

Details of the previous calculations (CKJ), Tachiya, (MJ) can be obtained from the cited references. In this report it is our purpose only to briefly describe the parameters calculated and to present preliminary results. The energy of the ground state is given by

$$E_g(R) = 1/2K_gR^2 \quad (1)$$

where R is the configuration coordinate and K_g is the "force constant" for the ground state. The energy of the excited state is given by

$$E_e(R) = \tfrac{1}{2}K_e(R - R')^2 + E_0 \quad (2)$$

where R' is the configuration coordinate offset and E_0 the energy offset of the excited state parabola relative to the ground state parabola. The quantity K_e is the force constant for the excited state. In addition to the four parameters K_g, K_e, R', and E_0 it is also possible to calculate the frequency of vibration ($h\nu$) for the motion of the species described by the single configuration coordinate. The assumption of parabolic configurations diagrams requires that the species is a harmonic oscillator.

The values of the configuration coordinate parameters are given in Table I.[9,10] A configuration coordinate diagram calculated from one set of data is given in Figure 1. As a check on the calculations the value of E_{max} calculated is compared to that reported in the original investigations. Values of $\partial E_{max}/\partial T$ were calculated using the configuration coordinate parameters corrected to constant pressure.[7] In general these values are in good agreement with the experimental, being negative but somewhat smaller in magnitude than the observed.

Several conclusions are immediately apparent from the results. In contrast to the CKJ calculation the force con-

(5) P. F. Rusch and J. J. Lagowski, *J. Phys. Chem.*, **77**, 210 (1973).
(6) G. Lepoutre and J. Jortner, *J. Phys. Chem.*, **76**, 683 (1972).
(7) W. M. Jacobs and A. K. Menon, *J. Chem. Phys.*, **55**, 5357 (1971).
(8) M. Tachiya, *Chem. Phys. Lett.*, **15**, 575 (1972).
(9) R. K. Quinn and J. J. Lagowski, *J. Phys. Chem.*, **73**, 2326 (1969).
(10) M. Gold and W. L. Jolly, *Inorg. Chem.*, **1**, 818 (1962).

TABLE I: Configuration Coordinate Diagram Parameters

Solution	Ref	K_g, eV/Å²	K_e, eV/Å²	E_0, eV	R', Å	$h\nu$, cm⁻¹	E_{max}, eV Calcd	E_{max}, eV Obsd
0.00032 *M* Na −70°	9	0.622	2.046	0.699	0.466	266	0.868	0.860
0.0229 *M* Na −65°	10	0.699	1.984	0.636	0.484	297	0.823	0.806
0.0229 *M* Na −55°		0.672	1.739	0.643	0.484	425	0.798	0.786
0.0229 *M* Na −45°		0.712	2.038	0.597	0.473	231	0.781	
0.008 *M* Na −45°	10	0.720	1.990	0.603	0.478	260	0.786	0.783
0.0105 *M*		0.728	2.033	0.601	0.478	272	0.787	0.780
0.0118 *M*		0.668	1.862	0.598	0.492	267	0.778	0.779
0.0133 *M*		0.698	1.976	0.597	0.480	217	0.783	0.775
0.0295 *M*		0.702	1.978	0.579	0.487	143	0.775	0.770

TABLE II: Temperature Dependence of E_{max} (all Data in cm⁻¹/°C)

Solution	Ref	$(\partial E_{max}/\partial T)_v$[a]	$(\alpha/\beta)(\partial E_{max}/\partial P)_T$[b]	$(\partial E_{max}/\partial T)_p$ Calcd	$(\partial E_{max}/\partial T)_p$ Obsd
0.00032 *M* Na −70°	9	−1.6	4.1	−5.7	−12
0.0229 *M* Na −65°	10	−1.3	4.6	−5.9	
0.0229 *M* Na −55°		−1.1	5.7	−6.8	−14.1
0.0229 *M* Na −45°		−1.3	6.9	−8.2	−11.3
0.008 *M* Na −45°	10	−1.3	6.9	−8.2	
0.0105 *M*					
0.0118 *M*					
0.0133 *M*					
0.0295 *M*					

[a] Calculated from configuration coordinate parameters. [b] Calculated from data of U. Schindewolf, ref 1, p 199.

stant of the excited state is larger than that for the ground state ($K_e > K_g$). Such a conclusion can also be obtained from a simple moment analysis[11] of the observed optical absorption data. The value of R' calculated here is much larger than that obtained by the CKJ calculation. This conclusion, coupled with the value of E_0 and the magnitude of the force constants, indicates that the emission spectrum for these systems would be red-shifted with respect to the absorption spectrum as was proposed earlier. Since the two configurational diagrams do not cross the possibility of radiationless decay seems unlikely. From the data in Table I and Figure 1 this simple configuration coordinate diagram shows that the maximum of the emission spectrum would be expected at about 0.63 eV (1.96 μ) and would be skewed to lower energy. Although this emission may occur from a relaxed 2p state (not calculated here), the energy is not expected to be significantly different. Observation of this emission would be complicated by the intense solvent absorption[5] in the same region.

The value of $h\nu$, the frequency of the normal mode of vibration for the configuration coordinate, is larger than given by previous calculations.[4] Since this vibration is identical with the symmetric breathing mode proposed earlier[4] it would be expected to be Raman active. The observed Raman spectra[12] do not contain a band at the predicted frequency probably for the same reasons cited earlier.[12] The absence of the vibration for the symmetric breathing mode suggests that the single configuration coordinate description of the solvated electron cavity is perhaps not correct. The single configuration coordinate may be some average of coordinates which are not localized in a single mode.

There is, however, a change in the low-energy region of the Raman spectrum of a liquid ammonia solution of solvated electrons relative to the spectrum of the pure solvent. This change is in the region about $h\nu$ predicted by the calculations given here. At this point, we must conclude that any correspondence between these facts and

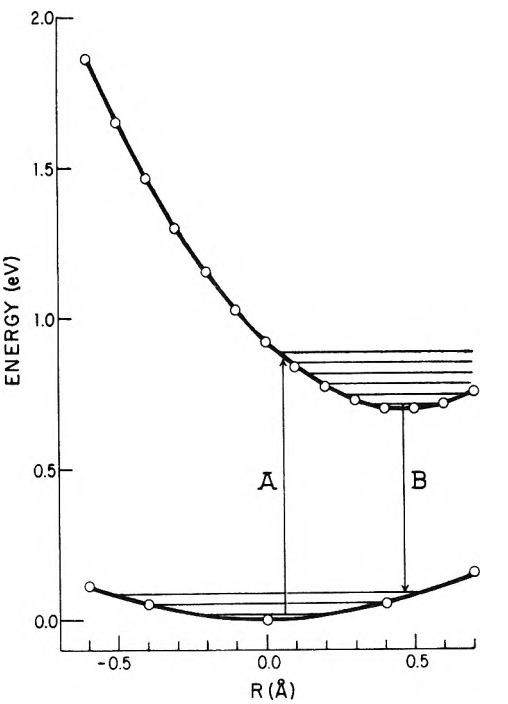

Figure 1. Configuration coordinate diagram from the experimental data in ref 9. Line A corresponds to the maximum in the observed absorption spectrum and line B to the maximum in the predicted emission spectrum.

(11) P. F. Rusch, unpublished results.
(12) (a) W. H. Koehler and B. Smith, *Proc. Int. Conf. Nature Metal-Ammonia Solutions, 3rd, 1972*, in press; (b) M. G. DeBacker, P. F. Rusch, B. de Bettignies, and G. Lepoutre, *ibid.*

the calculations seems to be purely fortuitous. Perhaps more detailed calculations along the lines indicated will reconcile the apparent anomalies.

In addition to the single configuration coordinate calculation there have been several other calculations presented to account for the solvated electron absorption spectrum in liquid ammonia. Perhaps the most recent method[13] is the extension to two coordinates which represent various motions of the solvent molecules in the cavity. Another possibility is to allow for relaxation of the Frank–Condon principle in the system. Such a method was proposed in 1969 and used to show that a distribution of cavity radii[14] (configuration coordinate) could explain the width of the absorption spectrum. A similar method[6] more recently proposed assumes that the observed absorption spectrum is composed of spectra due to cavities with different number of solvent molecules. Using four and six solvent molecules leads to only a small improvement of the calculated absorption spectrum.

Acknowledgment. We should like to acknowledge the generous support of the Robert A. Welch Foundation and the National Science Foundation.

(13) N. R. Kestner, ref 12.
(14) P. F. Rusch, W. H. Koehler, and J. J. Lagowski, ref 1, pp 41–47.

Department of Chemistry **P. F. Rusch**
The University of Texas at Austin **J. J. Lagowski***
Austin, Texas 78712

Received January 5, 1973

Ionic Conductivities and Dielectric Friction

Sir: The results of the theory of ionic mobilities which is based upon the dielectric friction[1] acting on the moving ions have been evaluated for cations in a variety of solvent media.[2,3] It has been shown that the theory accounts adequately for the values of the ionic Walden products ($\lambda_i{}^0\eta$) of tetraalkylammonium ions in dipolar aprotic solvents and (with the introduction of an appropriate correcting factor) also for R_4N^+ in monoprotic solvents.[3]

For alkali metal ions, however, the agreement is poor. The Walden products calculated using the crystal radii of these ions are significantly smaller than the experimental ones. It has been proposed[2] that the dielectric saturation of the solvent dipoles in the vicinity of the moving ion would reduce the dielectric friction acting upon it, thus accounting for the observed discrepancy. This suggestion was based on the calculation of dielectric friction employing a step function for the dependence of the medium permittivity (ϵ) with the distance from the ion. It was assumed[2] that $\epsilon = \epsilon_0$ (ϵ_0 is the static dielectric constant of the medium) for $R > R_0$ and $\epsilon = \epsilon_\infty$ (ϵ_∞ is the optical dielectric constant) for the regions where $R < R_0$. A significant reduction of the discrepancy between experimental and predicted ionic conductivities for alkali metal ions was apparent,[2] and suggested that the use of a more realistic function to express the change of ϵ with distance from the ion might improve further the agreement between calculated and experimental ($\lambda_i{}^0\eta$) for alkali metal ions.

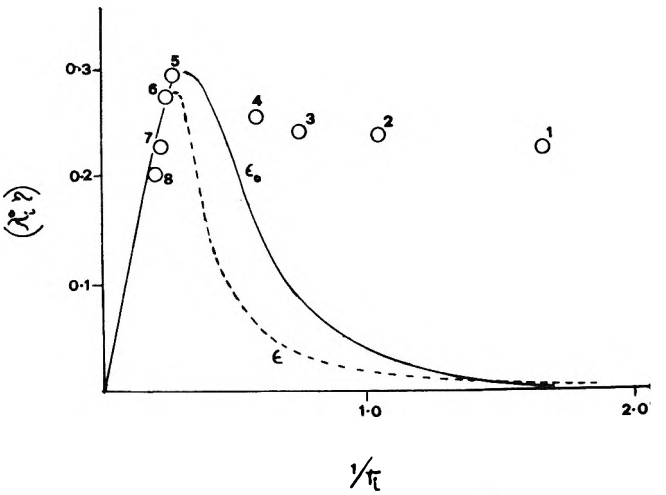

Figure 1. Walden product *vs.* the reciprocal of the ionic crystal radii for monovalent ions in acetone at 25°. Experimental values correspond to the following: (1) Li^+, (2) Na^+, (3) K^+, (4) Cs^+, (5) Me_4N^+, (6) Et_4N^+, (7) Pr_4N^+, (8) Bu_4N^+. The curves are explained in the text.

In the present communication the results of such calculation are reported. The solvent permittivity was considered to vary with the ionic electric field according to Booth's equation,[4] and the differential equations describing dielectric friction were numerically integrated. The calculation was performed for monovalent ions in acetone at 25°. The results are illustrated in Figure 1 where the calculated Walden products, when dielectric saturation is considered (dashed lines) and when there is no dielectric saturation (full line), are compared to the experimental values.[5]

The curves in Figure 1 show that the calculated ionic conductivities, when dielectric saturation is taken into account, are smaller (except for very small ionic size) than in the case when ϵ is made equal to ϵ_0. Thus, the discrepancy between predicted and experimental Walden products for alkali metal ions is *increased* by the effect of dielectric saturation. It now becomes evident that as ϵ decreases due to dielectric saturation the mobility of ions is reduced as if the solvent effectively had a lower dielectric constant. On the other hand, when the value of ϵ is very near ϵ_∞ (very small ions) dielectric friction is considerably reduced because in this case the excess charge due to dielectric relaxation of the solvent dipoles,[1] which is roughly proportional to $(\epsilon - \epsilon_\infty)$, becomes small. In this limiting case the calculated mobilities which result are larger than those predicted for a field independent permittivity. This is the reason why the crude model previously employed[2] seemed to reduce the discrepancy; the step function made $\epsilon = \epsilon_\infty$ in a considerably larger region near the ion which then did not contribute to dielectric friction.

The failure of dielectric friction to explain the values of the ionic conductivities of alkali metal ions may be due to the fact that in its derivation[1] the velocity field of the sol-

(1) R. Zwanzig, *J. Chem. Phys.*, **52**, 3625 (1970).
(2) G. Atkinson and R. Fernández-Prini, *J. Phys. Chem.*, **75**, 239 (1971).
(3) R. Fernández-Prini, *An. Assoc. Quim., Argent.*, **60**, 65 (1972).
(4) F. Booth, *J. Chem. Phys.*, **19**, 391 (1951).
(5) D. F. Evans, J. Thomas, J. A. Nadas, and M. A. Matesich, *J. Phys. Chem.*, **75**, 1714 (1971).

vent in the vicinity of the moving ion is considered to be the same as in the vicinity of a moving uncharged sphere; thus it is assumed not to be affected by the electrostatic interaction of the moving ion with the solvent dipoles. This electrostatic interaction would increase the residence time of oriented solvent dipoles near the ion and, consequently, the friction due to the dielectric relaxation of the solvent would be reduced. The neglect of this electrostatic effect would be particularly important when the electrostatic force is large, *i.e.*, for small and/or polyvalent ions.

Departamento de Fisicoquímica **R. Fernández-Prini**
Facultad de Farmacia y Bioquímica
Universidad de Buenos Aires
Buenos Aires, Argentina

Received November 3, 1972

Raman Spectroscopic Evidence for Contact Ion Pairing In Aqueous Magnesium Sulfate Solutions

Publication costs assisted by Environment Canada

Sir: A number of physiochemical methods[1-5] have been used to study ion association in aqueous $MgSO_4$ solutions. Based on ultrasonic absorption studies, Atkinson and Petrucci[6] have proposed that the following three-step process occurs in aqueous $MgSO_4$ solutions

$$Mg^{2+}(aq) + SO_4^{2-}(aq) \overset{I}{\rightleftharpoons} [Mg(WW)SO_4] \overset{II}{\rightleftharpoons} [Mg(W)SO_4] \overset{III}{\rightleftharpoons} [MgSO_4] \quad (1)$$

Recently Raman spectroscopy has been used to study aqueous $MgSO_4$. Daly, Brown, and Kester[7] have proposed that the only type of ion pairing in $MgSO_4$ solutions consistent with their Raman data is solvent separated ion pairing. Their evidence is based on a Raman study of the effect of Na^+ and Mg^{2+} on the dissociation of the HSO_4^- ion. In the course of Raman work in our laboratory it was observed that the Raman spectrum of aqueous $MgSO_4$ (Figure 1a) is different from that of aqueous Na_2SO_4 (Figure 1b). As Figure 1b shows, the $\nu_1(A_1)$ mode of the sulfate ion, for a Na_2SO_4 solution, is a symmetric band centered around 982 cm^{-1}. For a $MgSO_4$ solution (Figure 1a), the envelope is slightly asymmetric to the high-frequency side and the envelope may be resolved into two bands at 982 (half-width, 14 cm^{-1}) and 995 cm^{-1} (half-width, 25 cm^{-1}). The relative intensity of the band at 995 cm^{-1} increases when $MgCl_2$ is added to the solution. No differences between Na_2SO_4 and $MgSO_4$ solutions were observed in the other frequency regions of the Raman spectrum ($\nu_2(E)$ = 450 cm^{-1}; $\nu_3(F_2)$ = ~1115 cm^{-1}; $\nu_4(F_2)$ = 616 cm^{-1}). Further spectroscopic evidence for an interaction between Mg^{2+} and SO_4^- in aqueous solution is provided by the infrared spectrum, where the normally infrared forbidden $\nu_1(A_1)$ band occurs as a weak band centered around 985 cm^{-1}. In nitrate systems, perturbations in the $\nu_1(A_1)$ region of the Raman spectrum have been shown to occur only when a complex or contact ion pair is formed;[8-10] therefore, it appears that contact ion pairs are formed in aqueous $MgSO_4$ solutions.

The previous Raman study of dilute magnesium sulfate solutions[7] (<0.2 *M*) has been extended to higher concentrations (2.5 *M*) in order to enhance any ion pairing effects. The Raman spectra of several aqueous $MgSO_4$ and Na_2SO_4 solutions were recorded on a Jarrell-Ash Raman spectrometer (Model 25-500) using a Spectra-Physics Model 165 argon ion laser operated at 4880 Å and 800 mW as the excitation source. Band contours were resolved with a Du Pont curve analyzer, and band intensities, relative to the 459 cm^{-1} band of CCl_4, were measured with an accuracy of ±2%. The sum of the relative intensities of the 982- and 995-cm^{-1} bands from $MgSO_4$ solutions fell on the same straight line as the relative intensities of the 982-cm^{-1} band from Na_2SO_4 solutions when they were plotted against sulfate concentration. The relative intensity of the 995-cm^{-1} band was greater than 10% of the total

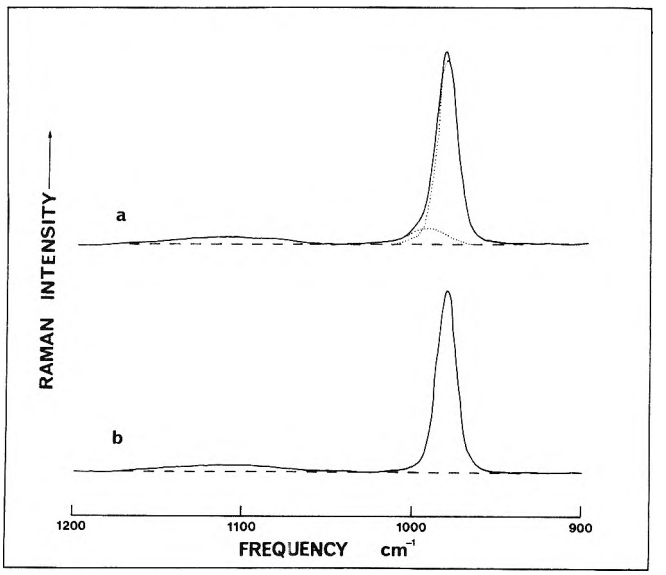

Figure 1. Raman spectrum of (a) 2.0 *M* $MgSO_4$ (900–1200 cm^{-1}) and (b) 1.72 *M* Na_2SO_4 (900–1200 cm^{-1}).

TABLE I: Comparison between the Concentration of Magnesium Sulfate Contact Ion Pairs Measured by the Raman Technique and by the Ultrasonic Technique

$[MgSO_4]$, *M*	Contact ion-paired $[MgSO_4]$ by Raman, *M*	Contact ion-paired $[MgSO_4]$ by ultrasonic, *M*[a]	α, from Raman results[b]
0.10	0.01	0.008	0.10
0.81	0.10	0.08	0.12
1.01	0.13	0.10	0.13
1.41	0.15	0.14	0.11
1.61	0.17	0.16	0.11
2.50	0.28	0.25	0.11

[a] Calculated using equilibrium constants from ref 6; K_1 = 50.1, K_2 = 1.95, K_3 = 0.17. [b] $\alpha = [MgSO_4]/C$.

(1) F. H. Fisher, *J. Phys. Chem.*, **66**, 1607 (1962).
(2) D. R. Kester and R. M. Pytkowicz, *Limnol. Oceanogr.*, **13**, 670 (1968).
(3) W. L. Marshall, *J. Phys. Chem.*, **71**, 3584 (1967).
(4) M. Eigen and K. Tamm, *Z. Elektrochem.*, **66**, 107 (1962).
(5) W. A. Adams and A. R. Davis, *Proc. Electrochem. Soc.*, (1972).
(6) G. Atkinson and S. Petrucci, *J. Phys. Chem.*, **70**, 3122 (1966).
(7) F. P. Daly, C. W. Brown, and D. R. Kester, *J. Phys. Chem.*, **76**, 3664 (1972).
(8) G. J. Janz, K. Balasubrahmanyam, and B. G. Oliver, *J. Chem. Phys.*, **51**, 5723 (1969).
(9) B. G. Oliver and A. R. Davis, *J. Inorg. Nucl. Chem.*, **34**, 2851 (1972).
(10) A. R. Davis and C. Chong, *Inorg. Chem.*, **11**, 1891 (1972).

intensity under the 982 cm^{-1} + 995 cm^{-1} envelope in every $MgSO_4$ solution. The concentration of $MgSO_4$ contact ion pairs was calculated using the following relationship

$$[MgSO_4] = \frac{I_{995}}{I_{982} + I_{995}} C$$

where C is the stoichiometric concentration of $MgSO_4$, determined as magnesium using atomic absorption spectroscopy.

In Table I the concentrations of contact ion-paired $MgSO_4$ found by the Raman technique are compared with those calculated from ultrasonic results.[5] The agreement between the methods is good, and the results support our assignment of the bands at 982 and 995 cm^{-1}.

Our Raman results indicate that it is not possible to distinguish the two types of solvent separated ion pairs in eq 1 from each other or, the sulfate in solvent separated ion pairs from the solvated sulfate ion. The band at 982 cm^{-1} seems to originate from sulfate in all three of these forms, $[SO_4^{2-}(aq)]$, $[MgWWSO_4]$, and $[MgWSO_4]$, whereas the band at 995 cm^{-1} originates only from sulfate in the contact ion pair $[MgSO_4]$.

Water Quality Research Division
Department of the Environment
Ottawa, Ontario

Anthony R. Davis*
Barry G. Oliver

Received January 11, 1973

Thermal Decomposition of Cyclobutanone

Publication costs assisted by the Research Council of Alberta

Sir: A recent article on the thermolysis of cyclobutanone[1] contains a confirmation of the Arrhenius parameters of Das, *et al.*,[2] for the production of ethylene and ketene, but compares rather poorly with the original data of Blades[3] for the minor products, cyclopropane and carbon monoxide. An activation energy for the latter reaction 4.4 kcal mol^{-1} higher than the former is to be compared with the previous value of 6.0 ± 0.5 kcal mol^{-1}, an intrinsically more reliable figure since it was derived from relative rate measurements. It is noteworthy, however, that both sets of data indicate relative rates within 5%.

The computational procedure of O'Neal and Benson[4] which has been used in evaluating the rate parameters for these two modes of decomposition depends on heats of formation of diradicals determined from the independent removal of two H atoms from linear molecules and on the activation energies of geometric and structural isomerizations and decompositions. The heat of formation of the simplest such diradical, trimethylene, has been questioned on interpretational grounds[5] and, since the publication of Hoffmann's[6] theoretical study of trimethylene employing extended Hückel molecular orbital theory, several articles[7-11] dealing with the generation of potential energy surfaces based on semiempirical and *ab initio* quantum mechanical methods for small ring compounds have appeared. Also the correlations of these surfaces with the kinetic behavior of these systems under thermal conditions have been discussed. These calculations predict a small barrier for ring closing, ~1 kcal mol^{-1}, of trimethylene diradical to cyclopropane,[7,9,10] in disagreement with Benson's estimate of 9.3 kcal mol^{-1}. Hence, any definitive pronouncements on the involvement of a particular diradical and/or concerted pathways in more complex systems, such as cyclobutanone, seems premature. These considerations are of particular significance in the possibility of the diradical $\dot{C}OCH_2CH_2\dot{C}H_2$ undergoing a concerted rearrangement to cyclopropane and CO, which was ruled out on the grounds that the activation energy is "likely to be much higher" than "the normal C_4 ring-closing activation energy, 6.6 kcal mol^{-1}."

McGee and Schleifer also carry out a calculation designed to show that the thermal rearrangement of cyclopropane should be negligible under reaction conditions. An alternate source of propylene would be cyclopropane formed in the reaction with energy in excess of the activation energy for its rearrangement (65.1 kcal mol^{-1}).[12] Using 58.0 kcal mol^{-1} as the activation energy for cyclopropane formation,[3] the excitation energy of cyclopropane and CO is 51.4 kcal mol^{-1} plus an amount determined by the "energy distribution of the products" function which is a maximum at $[(s - 1)RT + 51.4]$ where s is the number of oscillators taking part in intramolecular energy transfer. With $s \simeq 15$, this suggests a most probable product energy of 70 kcal mol^{-1} which must be partitioned between cyclopropane and CO. In view of the pressure of the system, $p_i < 40$ Torr,[1] in relation to the effect of pressure on the cyclopropane rearrangement,[12] some propylene should be expected, and, indeed, has been reported.[3] It is interesting to note that the heat of formation of the C_3H_6 entity initially formed will determine the energy partitioned between it and CO, and hence the formation of propylene is, theoretically at least, a key to the preferred mechanism.

It is perhaps worthy of note with regard to reaction mechanisms that activation energies define only the minimum energy path for reaction, but in no way exclude formation of the same products *via* a quite distinct mechanism whose activation energy, if measurable, would be higher. This point is well illustrated by cyclobutanone in the formation of cyclopropane and CO *via* the ground singlet in thermolysis[3] and the triplet in photolysis.[13] Clearly additional thermolysis studies, particularly of substituted cyclobutanones,[14] will be of considerable value in the understanding of reaction mechanisms.

(1) T. H. McGee and A. Schleifer, *J. Phys. Chem.*, **76**, 963 (1972).
(2) M. N. Das, F. Kern, T. D. Coyle, and W. D. Walters, *J. Amer. Chem. Soc.*, **76**, 6271 (1954).
(3) A. T. Blades, *Can. J. Chem.*, **47**, 615 (1969).
(4) H. E. O'Neal and S. W. Benson, *J. Phys. Chem.*, **72**, 1866 (1968); S. W. Benson, "Thermochemical Kinetics," Wiley, New York, N. Y., 1968.
(5) G. R. Freeman, *Can. J. Chem.*, **44**, 245 (1966).
(6) R. Hoffmann, *J. Amer. Chem. Soc.*, **90**, 1475 (1968).
(7) R. Hoffmann, S. Swaminathan, B. G. Odell, and R. Gleiter, *J. Amer. Chem. Soc.*, **92**, 7091 (1970).
(8) R. Hoffmann, C. C. Wan, and V. Neagn, *Mol. Phys.*, **19**, 113 (1970).
(9) P. J. Hay, W. J. Hunt, and W. A. Goddard, III, *J. Amer. Chem. Soc.*, **94**, 637 (1972).
(10) J. A. Horsley, Y. Jean, C. Moser, L. Salem, R. M. Stevens, and J. S. Wright, *J. Amer. Chem. Soc.*, **94**, 279 (1972).
(11) J. S. Wright and L. Salem, *J. Amer. Chem. Soc.*, **94**, 322 (1972).
(12) E. W. Schlag and B. S. Rabinovitch, *J. Amer. Chem. Soc.*, **82**, 5996 (1960).
(13) H. O. Denschlag and E. K. C. Lee, *J. Amer. Chem. Soc.*, **90**, 3628 (1968).
(14) H. A. J. Carless and E. K. C. Lee, *J. Amer. Chem. Soc.*, **92**, 4482, 6682 (1970); **94**, 1 (1972).

Research Council of Alberta
Edmonton, Canada

A. T. Blades*
H. S. Sandhu

Received May 25, 1972

Comment on the Communication, "Thermal Decomposition of Cyclobutanone," by A. T. Blades and H. S. Sandhu

Sir: In the above-mentioned communication Blades and Sandhu indicate a possible discrepancy in previously published data on the activation energy for the formation of cyclopropane in the thermal decomposition of cyclobutanone. In results published by Blades[1] the activation energy for cyclopropane formation obtained from relative rate measurements was determined to be 6.0 ± 0.5 kcal/mol higher than that for the formation of ethylene. The data of McGee and Schleifer[2] indicate activation energies of 51.9 ± 0.8 and 56.3 ± 1.2 kcal/mol for ethylene and cyclopropane, respectively, resulting in a difference of 4.4 ± 2.0 kcal/mol.

The relative rates have been graphed on an Arrhenius type plot (Figure 1) to resolve this problem[3] since such an analysis should be inherently more accurate. A value of 5.5 ± 0.3 kcal/mol for the difference in activation energies is calculated from this plot. We feel that within experimental conditions, this result is in agreement with that previously published by Blades. Along with our reported value of 51.9 kcal/mol for the activation energy for ethylene formation this results in an activation energy of 57.4 kcal/mol for the cyclopropane formation. This slightly revised figure does not alter any of the mechanistic conclusions already published.[2]

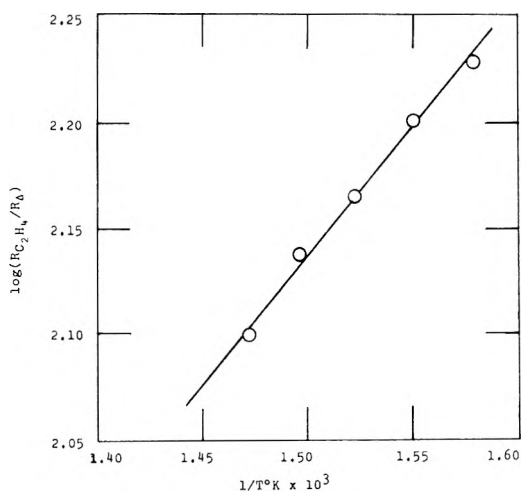

Figure 1. Plot of log $|R(C_2H_4)/R(\Delta)|$ *vs.* the reciprocal of the absolute temperature.

A larger disagreement exists between theoretical and experimental values of the C_3 ring-closing activation energy as discussed above by Blades and Sandhu. These discrepancies are not resolved and clearly additional studies are required in this area. It should be noted, however, that using 1.0 kcal/mol as a lower limit for the C_3 ring-closing activation energy results in a calculated E_a = 69.6 kcal/mol for the formation of cyclopropane *via* the $\cdot COCH_2CH_2CH_2\cdot$ diradical. The observed E_a = 57.4 kcal/mol (as recalculated above) remains significantly lower. Thus, the concerted decomposition of cyclobutanone into c-C_3H_6 and CO is still favored as the dominant reaction mechanism.

Finally, the calculations of McGee and Schleifer indicated that within the experimental conditions employed the rate of propylene formation from cyclopropane is negligible, but not zero. The analysis of Blades and Sandhu supports this in that their results indicate propylene formation to the extent of less than 1% of the cyclopropane.[1] Unfortunately, this amount was not detectable with accuracy under our experimental conditions. The formation of propylene does not conflict with the conclusion that cyclopropane and carbon monoxide are formed in the decomposition of cyclobutanone *via* a concerted mechanism. The formation of propylene to such a small extent substantiates the conclusion that the trimethylene diradical is not formed during the reaction.

(1) A. T. Blades, *Can. J. Chem.*, **47**, 615 (1969).
(2) T. H. McGee and A. Schleifer, *J. Phys. Chem.*, **76**, 963 (1972).
(3) The authors thank Dr. Blades for this suggestion.

York College of The City University of New York Jamaica, New York 11432

T. Howard McGee*
A. Schleifer

Received March 12, 1973

Chemical Relaxation of Aqueous Rhodamine B[1]

Sir: The concentration-jump relaxation method has recently been applied to studying the kinetics of fast reactions[2] and bonding in dye aggregates.[3] In the present work we used the technique to the dimerization of the laser dye rhodamine B in aqueous solution. Knowledge of the spectroscopic properties, as well as the kinetics of the aggregation of the dyes involved, is basic to the understanding of organic dye lasers, since dimer formation is detrimental to laser action in most cases.[4]

The single relaxation times τ of the monomer (M^+)-dimer (D^{2+}) equilibrium

$$2M^+ \underset{{}_0k_{-1}}{\overset{{}_0k_1}{\rightleftharpoons}} D^{2+} \qquad (1)$$

of the dye we measured at 9 and 22°, range from 0.67 to 3.65 msec if the total concentration C_T is between 1.82×10^{-5} and 5.45×10^{-6} M (Figure 1). At larger C_T the relaxation is too fast for the method used, and at smaller C_T the dimer concentration C_D is too low. Due to large OD changes, as well as to sufficiently large perturbations caused by sudden 11-fold dilution, we were able to measure shorter relaxation times than the *ca.* 1.5-msec dead time of our Gibson-Milnes type stopped flow apparatus. In such a case, while the system is far from equilibrium, the nonlinear part of the relaxation occurs during the dead time. The linear end of the relaxation, that would correspond to a small perturbation, is observed after stopping.

The experiments were performed at natural ionic strength of the dye solutions, where the square of the reciprocal relaxation time τ^{-2} of equilibrium 1 is given in terms of total concentration C_T by

(1) Taken in part from M. M. Wong's Ph.D. Thesis, to be submitted at the University of Georgia.
(2) Z. A. Schelly, R. D. Farina, and E. M. Eyring, *J. Phys. Chem.*, **74**, 617 (1970).
(3) Z. A. Schelly, D. J. Harward, P. Hemmes, and E. M. Eyring, *J. Phys. Chem.*, **74**, 3040 (1970).
(4) J. E. Selwyn and J. I. Steinfeld, *J. Phys. Chem.*, **76**, 762 (1972).

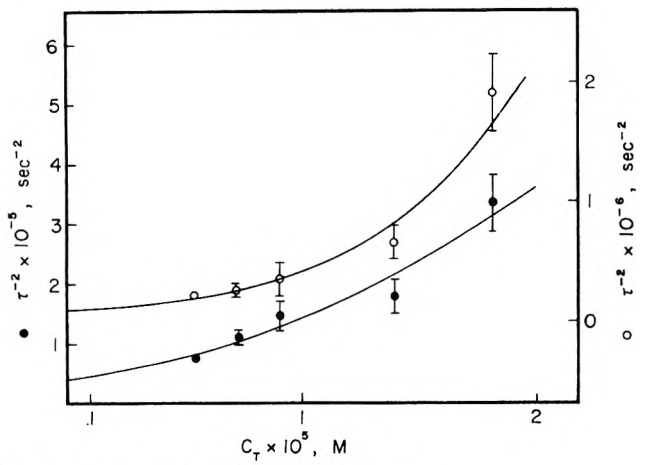

Figure 1. τ^{-2} *vs.* C_T at 9° (●) and 22° (○).

$$\tau^{-2} = {}_0k_{-1}{}^2\left[\frac{f_D}{f_\ddagger}\right]^2 + 8{}_0k_1{}_0k_{-1}C_T\left[\frac{f_M}{f_\ddagger}\right]^2 f_D \qquad (2)$$

Equation 2 is obtained from the expression for the reciprocal relaxation time τ^{-1} of equilibrium 1[5]

$$\tau^{-1} = {}_0k_{-1}\frac{f_D}{f_\ddagger} + 4{}_0k_1\frac{f_M{}^2}{f_\ddagger} \qquad (3)$$

by using the relationships ${}_0k_1/{}_0k_{-1} = C_Df_D/C_M{}^2f_M{}^2$ and $C_T = C_M + 2C_D$. Since the activity coefficients $f_i \to 1$ as $C_T \to 0$, the ionic strength independent forward ${}_0k_1$ and reverse ${}_0k_{-1}$ rate constants were determined from (2) using

$$\lim_{C_T \to 0} \tau^{-2} = {}_0k_{-1}{}^2 \qquad (4)$$

and $K = {}_0k_1/{}_0k_{-1}$, based on non-linear least-squares fitting of the experimental data. The equilibrium constants $K = C_D/C_M{}^2$ were computed from the absorption spectra taken at 9 and 22°,[4] using an iterative method previously described.[6] At the two temperatures, $K_{9°} = 1.55 \times 10^3\ M^{-1}$ and $K_{22°} = 1.44 \times 10^3\ M^{-1}$. At 9° the forward and reverse rate constants are ${}_0k_1 = 3.1 \times 10^5\ M^{-1}\ \text{sec}^{-1}$ and ${}_0k_{-1} = 2.0 \times 10^2\ \text{sec}^{-1}$; at 22° ${}_0k_1 = 4.5 \times 10^5\ M^{-1}\ \text{sec}^{-1}$ and ${}_0k_{-1} = 3.2 \times 10^2\ \text{sec}^{-1}$. The activation energy for association is $E_1 = 4.9$ kcal mol^{-1}, and for the dissociation reaction $E_{-1} = 5.8$ kcal mol^{-1}. These values are in good agreement with $\Delta H° = -935$ cal mol^{-1} of the equilibrium.

Other laser dyes in different solvents are also being studied at the present time, and a comparative analysis will be presented later.

Acknowledgment. This work has been supported in part by the Research Corporation and the National Science Foundation. The authors are indebted to R. Sexton, R. E. Morton, M. W. Williams, and R. J. Krusberg for technical assistance.

(5) Z. A. Schelly, R. D. Farina, and E. M. Eyring, *Monatsh. Chem.*, **101**, 493 (1970).
(6) A. R. Monahan and D. F. Blossey, *J. Phys. Chem.*, **74**, 4014 (1970).
(7) NSF-URP participant.

Department of Chemistry
University of Georgia
Athens, Georgia 30602

M. M. Wong
R. A. Heckman[7]
Z. A. Schelly*

Received February 14, 1973

There's nothing theoretical about the value of I&EC Process Design and Development

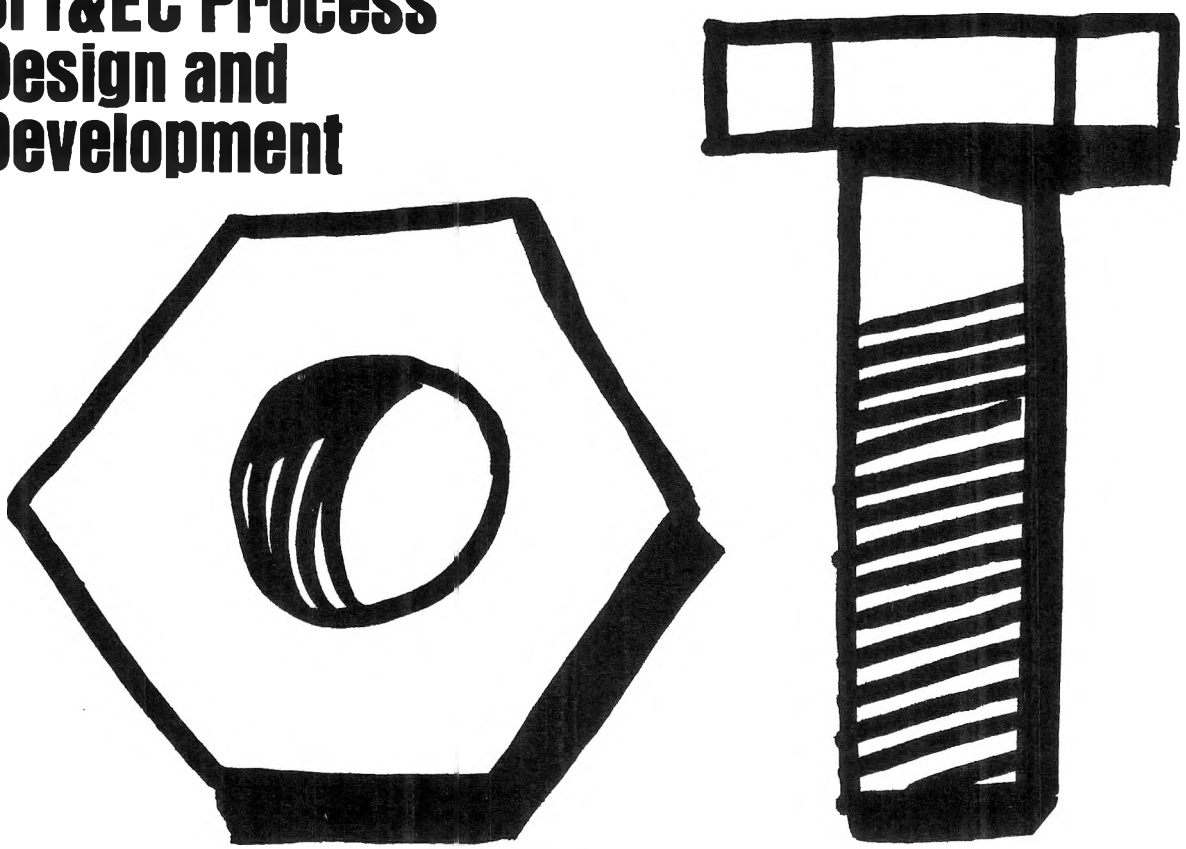

The original papers contained in this quarterly present theoretical and experimental results relating to the development of processes and process equipment—and the value of our publication is a known quantity to our constant readers. Subjects covered include:

- Empirical or Semi-theoretical correlations of data
- Experimental determinations of design parameters
- Methods of integrating systems analysis and process control into process design and development
- Scale-up procedures
- Many other experimental process development techniques.

Put us to the test. Complete and return the order form below today.

. . . another ACS service

I&EC Process Design and Development
American Chemical Society
1155 Sixteenth Street, N.W.
Washington, D.C. 20036

Yes, I would like to receive I&EC PROCESS DESIGN AND DEVELOPMENT at the one-year rate checked below:

	U.S.	*Canada*	*Latin America*	*Other Nations*
ACS Member Personal-Use One-Year Rate	☐ $ 7.00	☐ $10.00	☐ $10.00	☐ $10.50
Nonmember	☐ $21.00	☐ $24.00	☐ $24.00	☐ $24.50

Bill me ☐ Bill company ☐ Payment enclosed ☐

Name _____

Home ☐
Street _____ Business ☐

City _____ State _____ *Zip* _____

O-73

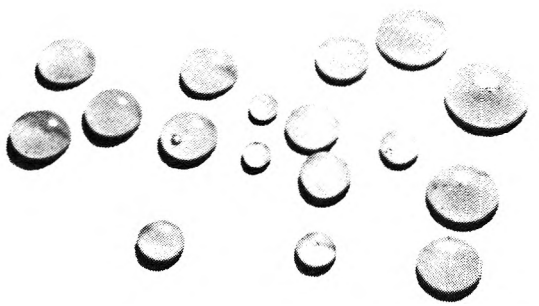

Water
A Comprehensive Treatise

Edited by Felix Franks, Unilever Research Laboratory

Containing contributions written by internationally recognized authorities in the field, this treatise stresses the uniqueness of water by comparing it with more normal liquids. This major, four-volume work will serve as a standard reference in the field.

Volume 1
The Physics and Physical Chemistry of Water
596 pages $37.50

Volume 2
Water in Crystalline Hydrates; Aqueous Solutions of Simple Nonelectrolytes Approx. 640 pages $37.50

Volume 3
Aqueous Solutions of Simple Electrolytes
Approx. 430 pages $37.50

Volume 4
Aqueous Solutions of Macromolecules; Water in Disperse Systems $37.50

This series is eligible for a SPECIAL CHARTER SUBSCRIBER'S DISCOUNT. SPECIAL CHARTER SUBSCRIBERS will receive a special price of $32.50 per volume. For further information, please contact the Publishers. Charter Subscriptions are not available in Japan.

PLENUM PUBLISHING CORPORATION
227 West 17 Street, New York, N.Y. 10011
In United Kingdom: 8 Scrubs Lane, Harlesden, London, NW10 6SE, England